uOttawa

L'Université canadienne
Canada's university

FACULTÉ DES ÉTUDES SUPÉRIEURES ET POSTOCTORALES

uOttawa

L'Université canadienne
Canada's university

FACULTY OF GRADUATE AND POSDOCTORAL STUDIES

Istemi Faruk Ozkan

AUTEUR DE LA THÈSE / AUTHOR OF THESIS

Ph.D. (Civil Engineering)

GRADE / DEGREE

Department of Civil Engineering

FACULTÉ, ÉCOLE, DÉPARTEMENT / FACULTY, SCHOOL, DEPARTMENT

Experimental and Numerical Analysis of Steel Pipes Subjected to Combined Loads

TITRE DE LA THÈSE / TITLE OF THESIS

Magdi Mohareb

DIRECTEUR (DIRECTRICE) DE LA THÈSE / THESIS SUPERVISOR

CO-DIRECTEUR (CO-DIRECTRICE) DE LA THÈSE / THESIS CO-SUPERVISOR

EXAMINATEURS (EXAMINATRICES) DE LA THÈSE / THESIS EXAMINERS

Amir Fam

Hiroshi Tanaka

Hong Khoo

Dan Palermo

Gary W. Slater

Le Doyen de la Faculté des études supérieures et postdoctorales / Dean of the Faculty of Graduate and Postdoctoral Studies

Experimental and Numerical Analysis of Steel Pipes Subjected to Combined Loads

by

Istemi F. Ozkan

Thesis submitted to the Faculty of Graduate and Postdoctoral Studies in partial fulfillment of the requirements for the Ph.D. Degree in Civil Engineering under the auspices of the Ottawa-Carleton Institute for Civil Engineering

Faculty of Engineering
University of Ottawa

Library and
Archives Canada

Published Heritage
Branch

395 Wellington Street
Ottawa ON K1A 0N4
Canada

Bibliothèque et
Archives Canada

Direction du
Patrimoine de l'édition

395, rue Wellington
Ottawa ON K1A 0N4
Canada

Your file Votre référence
ISBN: 978-0-494-41639-6
Our file Notre référence
ISBN: 978-0-494-41639-6

NOTICE:
The author has granted a non-exclusive license allowing Library and Archives Canada to reproduce, publish, archive, preserve, conserve, communicate to the public by telecommunication or on the Internet, loan, distribute and sell theses worldwide, for commercial or non-commercial purposes, in microform, paper, electronic and/or any other formats.

The author retains copyright ownership and moral rights in this thesis. Neither the thesis nor substantial extracts from it may be printed or otherwise reproduced without the author's permission.

AVIS:
L'auteur a accordé une licence non exclusive permettant à la Bibliothèque et Archives Canada de reproduire, publier, archiver, sauvegarder, conserver, transmettre au public par télécommunication ou par l'Internet, prêter, distribuer et vendre des thèses partout dans le monde, à des fins commerciales ou autres, sur support microforme, papier, électronique et/ou autres formats.

L'auteur conserve la propriété du droit d'auteur et des droits moraux qui protège cette thèse. Ni la thèse ni des extraits substantiels de celle-ci ne doivent être imprimés ou autrement reproduits sans son autorisation.

In compliance with the Canadian Privacy Act some supporting forms may have been removed from this thesis.

While these forms may be included in the document page count, their removal does not represent any loss of content from the thesis.

Conformément à la loi canadienne sur la protection de la vie privée, quelques formulaires secondaires ont été enlevés de cette thèse.

Bien que ces formulaires aient inclus dans la pagination, il n'y aura aucun contenu manquant.

Canada

© Istemi F. Ozkan, Ottawa, Canada, 2008

Abstract

A review of previous experimental, analytical, and numerical research conducted on pipe segments subjected to combined loading indicate that very few tests were reported on a) pipes subject to load combinations involving axial tension, internal pressure, and bending, and b) tests involving combinations of torsion, internal pressure, and bending. Within this context, an experimental program consisting of two full-scale test series on a total of eight pipe specimens is conducted. The specimens were made of X65 material (Specified Minimum Yield Strength=448MPa) with 508mm outer diameter (OD), and a nominal diameter-to-thickness ratio (*D/t*) of 80. In the first test series, specimens were subjected to combinations of internal pressure, axial tension, and bending and were aimed at a) quantify the beneficial effect of axial tension on the magnitude of critical buckling strains of pipes and b) determine whether or not the pipes are able to attain their modified plastic moment resistance as predicted by analytically derived plastic interaction relations. In the second test series, pipe specimens were subjected to load combinations involving internal pressure, axial tension, torsion, shear, and bending and were aimed to measure the pipe modified moment capacity. The moment vs. curvature relations, peak moment values, and local buckling behavior of the specimens as obtained from the experiments are documented. The peak moments obtained are compared to the analytically predicted moments. A nonlinear shell finite element model is also developed using the Finite Element Analysis (FEA) simulator ABAQUS in order to predict the moment capacity, critical strains, and the local buckling behavior of pipe specimens. Test results were observed to compare very well with FEA predictions for the moment capacities and buckling modes. Under certain combinations of axial tension and internal pressure, experiments and FEA show that pipes with *D/t*=80 are able to attain their modified plastic moment resistances. The FEA predicted longitudinal compressive strains were fairly good, but less reliable than the FEA predicted moment resistances. After demonstrating the ability of the FEA to reliably predict pipe modified moment capacity in previous and current research programs, a systematic FEA parametric study is conducted to investigate the effect of geometric properties (*D/t*) and loading conditions (torsion, axial force, and internal pressure) on the ability of the pipes to develop their modified plastic moment capacity. As a result of this parametric study, it was observed that the ability of the pipes to develop their plastic moment capacity is strongly dependant on axial force and *D/t* ratio. On the other hand, internal pressure and torsion are relatively less effective on this ability.

Acknowledgements

The author would like to express his most sincere appreciation to his supervisor Dr. Magdi Mohareb for his encouragement and continuous support throughout this research program.

The equipment developed in this program was purchased through a grant from Canada Foundation for Innovation (CFI). Additional support from the Natural Sciences and Engineering Research Council (NSERC) through Dr. M. Mohareb and Ontario Graduate Scholarship (OGS) support to the author are gratefully acknowledged. TransCanada Pipelines is also acknowledged for donating the pipe specimens tested in the first test series.

Special thanks are extended to the University of Ottawa Structural Engineering Laboratory technician and friend Mr. Muslim Majeed for his technical assistance and support for the experimental component of this study. The University of Ottawa Mechanical Engineering machine shop technicians, especially John Perrins, are also acknowledged for their help during this research.

Ayni kaderi paylastigimiz ev arkadaslarim, dostlarim: Cevat Catana ve Isil Toreci; kahve molalari, cok eglendigimiz Cuma/Cumartesi geceleri, Winning Eleven seanslari ve Besiktasimiz olmasaydi bu tez bitmezdi. Yedi yillik mastir ve doktora maceramiza beraber basladigmiz ve bitirdigimiz dostum: Tuncer Baykas, bil ki; gerekirse doktorayi birakirim ama Winning Eleven da mac birakmam.

Bu tezi hayatimin her evresinde oldugu gibi doktora calismalarim sirasinda da benden karsiliksiz desteklerini esirgememis olan Anneme, Babama ve Kardesime adiyorum.

Table of Contents

Appendices

List of Tables

Chapter 2

Chapter 4

Chapter 5

Chapter 6

Chapter 7

Appendix B

List of Figures

Chapter 1

Chapter 2

Chapter 4

Chapter 5

Chapter 6

Chapter 7

Appendix A

Appendix B

Appendix C

Appendix D

List of Symbols

Chapter 1

ε_{cr1}	=	Design buckling strain as a function of D/t and p_r (outcome of previous studies)
ε_{cr2}	=	Design buckling strain as a function of D/t, p_r, and A_r (sought in this study)
τ_r	=	Dimensionless parameter which relates shear and torsion
A	=	Internal axial force
A_r	=	Axial force ratio
A_y	=	Yield axial force resistance
D	=	Measured pipe diameter
D/t	=	Diameter-to-thickness ratio
F_y	=	Measured Yield Strength
L_d	=	Length of the deformed pipe segment
L_i	=	Length of the un-deformed pipe segment
M_p	=	Plastic moment resistance calculated in the absence of other forces
M_{pm}	=	Modified plastic moment capacity
M_r	=	Modified plastic moment capacity-to-plastic moment capacity ratio
M_{rx}	=	Bending moment ratio about x-axis
M_{ry}	=	Bending moment ratio about y-axis
M_x	=	Internal bending moment about x-axis
M_y	=	Internal bending moment about y-axis
OD	=	Nominal outer diameter
p	=	Internal pressure
p_r	=	Internal pressure ratio
p_y	=	Yield internal pressure resistance
r	=	Mean pipe radius
SMYS	=	Specified Minimum Yield Strength
t	=	Pipe wall thickness
T_p	=	Plastic torsion resistance calculated in the absence of other forces
T_r	=	Twisting moment ratio

V_p	=	Plastic shear resistance calculated in the absence of other forces
V_{rx}	=	Shearing force ratio about x-axis
V_{ry}	=	Shearing force ratio about y-axis
V_x	=	Internal shearing force about x-axis
V_y	=	Internal shearing force about y-axis

Chapter 2

α_h	=	Maximum allowed yield to tensile stress ratio in DNV code (Eq. 2.10)
α_{gw}	=	Girth-weld factor in DNV 2000 (Eq. 2.10)
ε_{cr}^{CRC}	=	Critical buckling strain according to Column Research Council Equation (Eq. 2.5)
ε_{cr}^{S}	=	Critical buckling strain according to Sherman Equation (Eq. 2.7)
ε_{cr}^{B}	=	Critical buckling strain according to Battlle Equation (Eq. 2.8)
ε_{c}^{crit}	=	Critical compressive strain according to CAN/CSA Z662-03 (Eq. 2.9)
ε_c	=	Critical compressive strain according to DNV 2000 (Eq. 2.10)
ε_y	=	Yield strain
υ	=	Poisson's ratio
σ_h	=	Hoop stress in DNV 2000 critical strain equation
D	=	Measured outside diameter
D_d	=	Pipe diametric differential
D_e	=	Diametric expansion
D_l	=	Largest outside diameter of the pipe
D_s	=	Smallest outside diameter of the pipe
DSAW	=	Doubly submerged arc weld
ERW	=	Electric resistance weld
E	=	Modulus of elasticity of steel
f_y	=	Yield strength of the pipe material in DNV-2000 critical strain equation (Eq. 2.10)
F_y	=	Yield strength
O_v	=	Ovalization
OD	=	Nominal outside diameter
p_e	=	External pressure CAN/CSA Z662-03 (Eq. 2.9)
p_i	=	Internal pressure as in CAN/CSA Z662-03 (Eq. 2.9)
r	=	Outer pipe radius
SMYS	=	Specified Minimum Yield Strength

t = Wall thickness of the pipe

t_1 = Wall thickness of the pressure containment resistance according to DNV Code

TAPS = Trans-Alaska Pipeline System

Chapter 3

CAN/CSA Z662 (2003)

α_G = Load factor for permanent loads (ranges between 1.00 and 1.25)

α_Q = Load factor for operational loads (ranges between 1.00 and 1.13)

γ = Class factor (ranges between 1.0 and 2.0 depending on the location class and the fluid conveyed)

ε_{cf} = Factored compressive strain in the longitudinal or hoop direction

ε_c^{crit} = Ultimate compressive strain capacity of the pipe wall or weldement (as determined by valid analysis methods or physical tests)

ε_t^{crit} = Ultimate tensile strain capacity of the pipe wall or weldement (as determined from valid fracture mechanics methods or physical tests. In the absence of more detailed information, the standards provide a limiting value for $\varepsilon_t^{crit} = 0.0075$)

ε_{tf} = Factored tensile strain in the longitudinal or hoop direction

ζ = Dimensionless parameter relating length diameter and thickness in shell buckling analysis in circumferential direction

λ = Effective slenderness factor

υ = Poisson's Ratio

ξ = Dimensionless parameter relating length diameter and thickness in shell buckling analysis in longitudinal direction

σ_a = Axial stress

σ_b = Bending stress

σ_{ef} = Maximum factored combined effective stress according to Von Mises criterion

σ_{hf} = Factored hoop stress due to pressure differential (tension positive)

σ_{Lf} = Factored longitudinal stress (tension positive)

σ_θ = Circumferential stress

τ_f = Factored tangential shear stress

$\tau_{z\theta}$ = Shear/torsion stress

ϕ_c = Resistance factor for compressive stability

$\phi_{\varepsilon t}$ = Resistance factor for tensile strain (=0.7)

ϕ_y = Resistance factor for yielding strength (= 0.9)

$\phi_{\varepsilon c}$ = Resistance factor for compressive strain (=0.8)

Δ_θ = Ovalization deformation

Δ_θ^{crit} = Critical ovalization deformation, which can be taken as 0.03 in the absence of detailed information. If it can be shown that premature sectional collapse will not occur under the loads considered, the value can be increased to 0.06, allowing the passage of internal inspection devices

A = Cross-sectional area

D = Outside pipe diameter

$D_{\max}$ = Maximum outside pipe diameter

$D_{\min}$ = Minimum outside pipe diameter

E = Pipe material modulus of elasticity

F_{cr} = Critical buckling stress

F_{ei} = Buckling stress for a given loading (i = a (axial compressive stress), b (bending stress), θ (circumferential stress), υ (shear/torsion stress))

F_y = Effective specified minimum yield strength

f_a = Axial stress (equal to 0 for tensile σ_a, and σ_a for compressive σ_a)

f_b = Bending stress (equal to 0 for tensile σ_b and σ_b for compressive σ_b)

f_θ = Circumferential stress (equal to 0 for tensile σ_θ and σ_θ for compressive σ_θ)

K_i = Dimensionless coefficient depending on the type of the stress (i = a (axial compressive stress), b (bending stress), θ (circumferential stress), υ (shear/torsion stress))

k_i = Buckling coefficient dependent upon loading, geometric proportions, boundary conditions, and imperfections (i = a, b, θ , υ)

L = Pipe length

M_f = Factored bending moment

n = A constant which is 0 where σ_a, σ_b or σ_θ is positive (tensile) and 1 where σ_a, σ_b or σ_θ is positive (compressive)

P_f = Factored axial force

p_e = Minimum external hydrostatic pressure

p_i = Maximum internal design pressure

S	=	Elastic section modulus
t	=	Pipe wall thickness

Det Norske Veritas (DNV 2000)

α_A	=	Anisotropy factor which is equal to 0.95 in axial direction due to relaxed testing requirement in linepipe specifications. It can be taken as 1.00 for other cases
α_c	=	Flow stress parameter accounting for strain hardening (=1.0 for no strain hardening)
α_h	=	Maximum allowable yield strength to tensile strength ratio
α_{gw}	=	Girth weld factor (≤ 1)
α_U	=	Material strength factor, which can be taken as 0.96 or 1.00
γ_m	=	Material resistance factor of either 1.15 or 1.00 depending on the limit state category
γ_p	=	Load effect factor for pressure loads (=1.05)
γ_ε	=	Resistance strain factor ranging between 2.0 to 3.5 depending on the safety classes
γ_{SC}	=	Safety class resistance factor ranging from 1.04 to 1.308 depending on the safety class
ε_c	=	Critical compressive strain
σ_h	=	Hoop stress on the pipe
Δp_d	=	Design differential over pressure
D	=	Outside diameter of the pipe
$f_{u,temp}$	=	Temperature de-rating of the ultimate tensile strength of the pipe material
f_u	=	Characteristic ultimate tensile strength
f_y	=	Characteristic yield stress
$f_{y,temp}$	=	The temperature de-rating of the yield stress of the pipe material
M_d	=	Design bending moment
p_e	=	External hydrostatic pressure
$p_p(t_2)$	=	Burst pressure

p_{ld} = Local design pressure

S_d = Design effective axial force

S_p = Characteristic plastic axial force resistance

SMYS = Specified minimum yield strength

t_2 = Net pipe wall thickness free of possible corrosion

API RP 2A-LRFD-93

ϕ_b = Resistance moment for bending strength (=0.95)

ϕ_c = Resistance factor for axial compressive strength (=0.85)

ϕ_t = Resistance factor for axial tensile strength (=0.95)

λ = Column slenderness parameter

λ_y, λ_z = Column slenderness parameters for member y and z axes, respectively

C_{my}, C_{mx} = Reduction factors corresponding to the member y and z, respectively

D = Nominal outer diameter of the pipe

E = Modulus of elasticity

f_b = M/S bending stress due to factored loads ($M \leq M_p$; when $M>M_y$, f_b is the equivalent bending stress)

F_y = Nominal yield strength

F_{bn} = Nominal bending strength

f_{by} = Bending stress about member y-axis (in-plane) due to factored loads

f_{bz} = Bending stress about member z-axis (out-of-plane) due to factored loads

f_c = Axial compressive stress due to factored loads

F_{cn} = Nominal axial compressive strength

F_{ey}, F_{ez} = Euler buckling strengths corresponding to the member y and z axis, respectively

f_t = Axial tensile stress due to factored loads

F_{xc} = Inelastic local buckling strength

F_{xe} = Nominal elastic buckling strength

K = Effective length factor

L = Un-braced length

M	=	Applied bending moment
M_p	=	Plastic moment
M_y	=	Elastic yield moment
r	=	Radius of gyration
S	=	Elastic section modulus
t	=	Nominal pipe thickness
Z	=	Plastic section modulus

CAN/CSA-S16-01

C_f	=	Axial load on the beam-column
C_y	=	Axial compression capacity
D	=	Pipe Diameter
F_y	=	Yield strength
h	=	Web height
M_p	=	Plastic moment capacity
S	=	Elastic section modulus
t	=	Pipe wall thickness
w	=	Web thickness
Z	=	Plastic section modulus

LRFD Specification for Structural Steel Buildings (1999)

E	=	Modulus of elasticity of the pipe steel
S	=	Elastic section modulus
M_n	=	Flexural capacity
Z	=	Plastic section modulus

CAN/CSA S136-01

ϕ_a	=	Resistance factor (=0.9)
A_e	=	Effective cross sectional area of a member in compression
F_e	=	Euler buckling strength
F_p	=	Compressive limit stress under compression

S_c = Compressive section modulus based on moment of inertia of effective cross-sectional area divided by distance from centroidal axis to the extreme compression fiber

Chapter 4

α	=	Angle of twisting rotation of the test setup
A	=	Axial force applied to the specimens
A_i	=	Net axial tensile force on the pipe due to the effect of internal pressure on pipe ends
b	=	Eccentricity of the hydraulic jack from the pipe centerline in Ozkan and Mohareb Test Series
Bi	=	Bearing frame i=1,2, or 3
D	=	Measured outer diameter of the pipe
D_i	=	Inner diameter of the pipe
e	=	Eccentricity of the hydraulic jack from pipe centerline in the University of Alberta Test Series
H/D	=	Height-to-Diameter ratio
OD	=	Nominal outer diameter of the pipe
p	=	Internal pressure
u	=	Deflection of the test setup about the x-axis
v	=	Deflection of the test setup about the y-axis

Chapter 5

α	=	Angle imaginary line ab makes with the horizontal in un-deformed position of the specimen
δ_T	=	Lateral deflection of the top of the pipe
δ_b	=	Lateral deflection of the location of the buckle
ε	=	Logarithmic strain
ε_{cr}	=	Critical Strain
ε_{cr_a}	=	Critical Strain calculated by Zimmerman (2004) method
ε_{cr_b}	=	Critical Strain calculated by Demec Gages
ε_{crit}	=	Critical strain obtained from other studies
ε_c^{crit}		Critical strain obtained from CAN/CSA-Z662-03
ε_e	=	Engineering Strain
ε_t	=	Tensile Strain at the tension side of the buckle
θ_1	=	Rotation of Actuator 1
θ_2	=	Rotation of Actuator 2
θ_3	=	Rotation of Actuator 3
θ_b	=	Rotation of the bottom of the pipe measured by Clinometer CL4
θ_{bb}		Rotation of the bottom of the buckle
θ_{CL7}	=	Rotation taken by Clinometer CL7
θ_{mb}	=	Rotation of the mid-height of the buckle
θ_p	=	Rotation of the end effect of the internal pressure at the top of the pipe
θ_t	=	Rotation of the top of the pipe measured by Clinometer CL7
θ_{tb}	=	Rotation of the top of the buckle
σ_t	=	True stress
ϕ_{cr}	=	Curvature corresponding to M_{max}
ϕ_g	=	Global curvature

ϕ_L	=	Local curvature
ΔF_1	=	Change of force on Actuator 1
ΔF_2	=	Change of force on Actuator 2
ΔF_3	=	Change of force on Actuator 3
a	=	Length of the imaginary straight line connecting points a and b
A_b	=	Axial force at the location of the buckle including 2nd order effects
A_h	=	Horizontal force at the location of the buckle including 2nd order effects
A_i	=	Axial tensile force induced on the pipe due to internal pressure effect on the closed top and bottom ends
A_r	=	Axial force ratio
A_t	=	Target axial force on the pipe
A_v	=	Vertical force at the location of the buckle including 2nd order effects
A_y	=	Axial yield capacity
CLi	=	Angle measurement device (Clinometer, i=1, 2, 3,…, 7)
D	=	Measured outer diameter
D/t	=	Diameter-to-thickness ratio
E	=	Modulus of Elasticity
F_1	=	Force on actuator 1
F_2	=	Force on actuator 2
F_3	=	Force on actuator 3
F_u	=	Ultimate strength obtained from tension coupon curves
F_y	=	Yield strength of the pipe material
H_{F1}	=	Horizontal distance between point of application of actuator force F_1 and the location of the buckle
H_{F2}	=	Horizontal distance between point of application of actuator force F_2 and the location of the buckle
H_{F3}	=	Horizontal distance between point of application of actuator force F_3 and the location of the buckle
H_a	=	Force on center of the top plate of the pipe along x-axis as measured from the experiments and used as FEA input

L'	=	Distance between the top of the pipe and the mid-height of the buckle
L_1	=	Distance between the demec gages intercepting the buckle in un-deformed configuration
L_2	=	Distance between the demec gages intercepting the buckle in deformed configuration
L_p	=	Pipe specimen length
L_{t-b}	=	Distance between CL7 and CL4 in un-deformed configuration
L_{tb-bb}	=	Vertical distance between top of the buckle and the bottom of the buckle in un-deformed configuration
LVDTi	=	Linear Variable Differential Transducer (i=1, 2,..., 5)
M_b	=	Moment at the location of the buckle including 2nd order effects
M_{bx}	=	Moment at the location of the buckle about x-axis (taken approximately equal to zero)
M_{max}	=	Maximum moment in moment vs. curvature behavior of the specimen
M_p	=	Plastic moment capacity calculated in the absence of other internal forces
M_{pm}	=	Modified plastic moment capacity
M_r	=	Modified plastic moment capacity-to-plastic moment capacity ratio
OD	=	Nominal outer diameter
p	=	Applied internal pressure
p_r	=	Internal pressure ratio
p_y	=	Yield internal pressure capacity of the specimen
PGi	=	Pressure gage (i=1, 2)
S3R	=	3-node reduced integration shell element
S4R	=	4-node reduced integration shell element
SMYS	=	Specified minimum yield strength
t	=	Pipe wall thickness
t_1	=	Time when the internal pressure on the pipe reaches the target internal pressure along the loading history of the pipe
t_2	=	Time when the axial force on the pipe reaches the target force along the loading history of the specimen
V_b	=	Shearing force at the location of the buckle including 2nd order effects

V_{F1} = Vertical distance between the top hinge of the Actuators 1 and the location of the buckle

V_{F2} = Vertical distance between the top hinge of the Actuators 2 and the location of the buckle

V_a = Force on the center of the top plate of the pipe along z-axis as measured from the experiments and used as FEA input

V_r = Shearing force ratio

Chapter 6

β	=	Angle the imaginary line between points A and O is making by the center line of the loading arm
ε	=	Logarithmic strain
ε_{cr}	=	Critical Strain
θ_A	=	Rotation of Actuator A
θ_b	=	Rotation of the bottom of the pipe
θ_B	=	Rotation of Actuator B
θ_p	=	Rotation of the force F_p
θ_{PC}		Angle between line PC and the line of application of force F_p
θ_t	=	Rotation of the top of the pipe
ξ_A	=	In-plane rotation of Actuator A
ξ_B	=	In-plane rotation of Actuator B
σ_e	=	True stress
ν	=	Poisson's Ratio
ϕ	=	Twisting angle of the pipe
$\Delta_i F_A$	=	Change in actuator force F_A in i^{th} iteration
$\Delta_i F_B$	=	Change in actuator force F_B in i^{th} iteration
$\Delta_i D_A$	=	Change in position for Actuator A in i^{th} iteration
Δ_x	=	Deflection of the top of the specimens along x-axis
Δ_y	=	Deflection of the top of the specimens along y-axis
A	=	Axial force applied
A_b	=	Axial Tension at the mid-height buckle location calculated by taking 2nd order effects into consideration
A_r	=	Dimensionless axial force ratio
A_y	=	Yield axial force capacity
CLA	=	Clinometer A

CLB	=	Clinometer B
CLi	=	Clinometer i (i=1, 2, 3, 4)
D	=	Measured outer diameter
D_A	=	Stroke change in Actuator A
D_B	=	Stroke change in Actuator B
D_0	=	Current position of the actuator
D_i	=	Internal diameter
D_t	=	Target position of the actuator
D/t	=	Diameter-to-thickness ratio
E	=	Modulus of elasticity
F_A	=	Force in Actuator A
F_{Ax}	=	Force on Actuator A about the x-axis
F_{Ay}	=	Force on Actuator A about the y-axis
F_B	=	Force in Actuator B
F_{Bx}	=	Force on Actuator B about the x-axis
F_{By}	=	Force on Actuator B about the y-axis
F_u	=	Ultimate yield strength
F_y	=	Measured Yield strength
F_{ylong}	=	Yield strength along longitudinal direction
F_{ytrans}	=	Yield strength along transversal direction
L	=	Distance OP_A or $O'P_A'$
L_p	=	Specimen length
L_t	=	Centerline to centerline distance between the actuators in un-deformed position
LVDT A	=	Linear variable differential transformer A
LVDT B	=	Linear variable differential transformer B
LVDT i	=	Linear variable differential transformer i (i=1, 2, 3, 4, 5)
M_b	=	Bending moment at the mid-height buckle location calculated by taking 2nd order effects into consideration
M_p	=	Plastic moment capacity calculated in the absence of other internal forces
M_{pm}	=	Modified plastic moment capacity
M_r	=	Modified plastic moment capacity-to-plastic moment capacity ratio

n	=	Number of increments to go from D_0 to D_t
n_{long}	=	Plastic exponential along longitudinal direction
n_{trans}	=	Plastic exponential along transversal direction
OD	=	Nominal outer pipe diameter
p	=	Internal Pressure applied
p_r	=	Dimensionless internal pressure ratio
p_y	=	Yield internal pressure capacity
PG i	=	Pressure Gage (i=1, 2)
PT-101-i	=	Position Transducer i (i=1, 2, 3, 4)
SMYS	=	Specified minimum yield strength
t	=	Pipe wall thickness
T	=	Torsion applied
T_b	=	Twisting moment at the mid-height buckle location calculated by taking 2nd order effects into consideration
T_p	=	Plastic torsion capacity
T_r	=	Dimensionless torsion ratio
u_A	=	Displacement of point P_A along x-axis
u_B	=	Displacement of point P_B along x-axis
v_A	=	Displacement of point P_A along y-axis
v_B	=	Displacement of point P_B along y-axis
V_b	=	Shearing force at the mid-height buckle location calculated by taking 2nd order effects into consideration
V_{bx}	=	Component of V_b along the x-axis
V_{by}	=	Component of V_b along the y-axis
V_p	=	Plastic shear capacity
V_r	=	Dimensionless shear force ratio
W	=	Self-weight of the loading arm
x	=	Distance between the centerline of the loading arm to the hinge of the actuators
x_{Fp}	=	Horizontal distance between the application point of force F_p and the mid-height buckle

x_w	=	Horizontal distance between the application point of force W and the mid-height buckle
x_A	=	Length between the hinges of Actuator A in the un-deformed configuration
x_B	=	Length between the hinges of Actuator B in the un-deformed configuration
z	=	Distance between the centerline of the actuators to the location of the buckle in un-deformed position
z_{Fp}	=	Vertical distance between the application point of force F_p and the mid-height buckle

Chapter 7

α	=	Indicator which shows the distance of the moment capacity predicted by FEA to modified plastic moment capacity (M_{pm}) and modified elastic moment capacity (M_{em}) predicted by the interaction relations
A	=	Axial force applied
A_r	=	Ratio of axial force applied-to-yield axial force capacity of the pipe
A_x	=	Component of axial force applied along the x-axis in deformed configuration
A_y	=	Yield axial force capacity of the pipe
A_z	=	Component of axial force applied along the z-axis in deformed configuration
D	=	Measured outer diameter of the pipe
D/t	=	Diameter-to-thickness ratio
E	=	Modulus of Elasticity of the pipe material
F_y	=	Measured yield strength of the pipe material
M_e	=	Elastic moment capacity calculated in the absence of other internal forces
M_{em}	=	Modified elastic moment capacity
M_{FEA}	=	Moment capacity predicted by FEA
M_p	=	Plastic moment capacity calculated in the absence of other internal forces
M_{pm}	=	Modified plastic moment capacity of the pipe
M_r	=	Modified plastic moment capacity-to-plastic moment capacity ratio
M_{test}	=	Moment capacity measured during the tests
OD	=	Nominal outer diameter
p	=	Internal pressure applied
p_y	=	Yield internal pressure capacity
p_r	=	Ratio of internal pressure applied-to-yield internal pressure capacity
SMYS	=	Specified mean yield strength
t	=	Thickness of the pipe

Chapter 8

A_r	=	Ratio of axial force applied-to-yield axial force capacity of the pipe
D/t	=	Diameter-to-thickness ratio
F_y/E	=	Yield strength-to-modulus of elasticity ratio
OD	=	Outer diameter
p_r	=	Ratio of internal pressure applied-to-yield internal pressure capacity

Chapter 1

Introduction and Scope

Pipeline networks are the most economical means to transport large quantities of oil or natural gas over land from the centers of productions to the refineries and to centers of consumption. While buried pipelines are the preferred option in pipeline networks given their reduced construction costs compared to elevated pipelines, engineers resort to elevated pipes in necessary situations (refer to Section 1.1.2).

Massive expansions in the oil and gas networks both buried and elevated are contemplated in the coming decade in Canada in order to convey oil and gas from the northern parts of Canada to the centers of consumptions in the USA. In this context, the present study focuses on the deformation and load capacity of pipe segments subject to complex load combinations inducing bending, axial tension, torsion, and internal pressure. Another line of applications that could potentially benefit from the current study relates to round hollow structural steel (HSS) members subject to complex load combinations. In these applications, internal pressure effects become irrelevant while the other internal forces remain of interest.

1.1 Description of Oil/Gas Pipeline Systems

A pipeline network consists of gathering systems, main trunk lines, and distribution systems. The gathering system transports a mixture of oil, gas, and sometimes water from the production wells to collection points such as gas processing plants or treating facilities where the water is removed and the oil and gas are separated (The Canadian Encyclopedia.com). The trunk or main pipelines move oil or gas at high pressures over long distances through large diameter pipes from the collection points to the market centers. The energy necessary to convey the fluids along the pipeline is supplied by pumping (or compressor stations) spaced at approximately 100 km intervals (The Canadian Encyclopedia.com). In the case of oil, trunk lines supply the refineries, which, in turn, distribute the products to the retailer by truck or product pipelines. Natural gas is withdrawn from the trunk line and is delivered to the consumer via the distribution system. This part of the network is the longest of the three systems. Typically, pipes in this system are of relatively smaller diameter and are operated at low pressure.

Among the three pipeline systems (gathering system, main trunk lines, and distribution system), while the gathering systems and the pipeline systems in the refineries and petrochemical plants are mostly elevated, the main trunk lines can be either elevated or buried. The Trans Alaska Pipeline System (TAPS), which was designed and constructed between 1970 and 1977 between Prudhoe Bay in Northern Alaska and a terminal at the head of the Prince William Sound near Anchorage, is an example of a pipeline system half elevated, half buried. The system has a total of 1280 km with 672 km aboveground and 608 km belowground (tapseis.anl.gov).

1.1.1 Buried Pipelines

The primary loads acting on the buried pipelines include internal pressure caused by the highly pressurized fluids conveyed. These can be associated with axial forces due to Poisson's Ratio effects and temperature differentials between the tie-in temperature and the operating temperature. Secondary loading involve imposed curvatures induced by differential frost heave and thaw settlements, inducing local buckling of pipe segments when the longitudinal strains on the compressive side of the pipe are excessive. Thus, when designing buried pipelines, these phenomena directed researchers to limit the strains on the pipe wall (buckling strain) or other related deformation criteria such as the ovalization of the cross section rather than the stresses, in contrast to design criteria for elevated pipelines, which are stress based.

Design standards provide compressive strain limits as a function of only Diameter-to-thickness ratio (D/t) and internal pressure ratio (p_r). This neglects the possible beneficial effect of axial tension, which may take place as a pipe segment undergoes differential settlements (Section 1.2.1.1).

1.1.2 Elevated Pipelines

Elevated pipes become the preferred design alternative when easier deformation detection, replacement of the damaged parts, and geographical constraints such as river crossings and seismic faults are present. For example, TAPS crosses over 900 rivers and streams and three fault lines. The above ground component of this pipeline system was constructed on specially designed supports, which were 18 m apart (tapseis.anl.gov). Elevated pipelines are also used in pipeline systems in refineries and petrochemical plants.

For elevated pipes in petrochemical plants, in order to relieve the internal axial forces induced by thermal effects, it is common practice to introduce horizontal pipe loops into pipelines at regular intervals. The loops provide flexible axial links between straight pipe segments and allow the pipe to expand or contract longitudinally without inducing excessive internal axial forces. The presence of loops introduces twisting moments in the loop arms of the same order of magnitude as that of the bending moments in the straight section.

Pipes used in these applications are also subject to bending moments and shear forces under common gravity and lateral loads and internal pressure due to the effect of the fluids they convey. Under these load combinations, non-compact pipe sections (pipes with moderate D/t ratio) can be designed according to their elastic resistances using established principles of mechanics in conjunction with metal yield criteria. On the other hand, stockier pipes (pipes with lower D/t ratio) have the ability to develop additional resistance by deforming into the plastic range of the deformation. Current design provisions for pipelines CAN/CSA Z662 (2003) recognize this additional resistance. However, they do not provide general interaction relations for pipe sections under combined loads. These have been formulated in Mohareb (2002 and 2003). Nevertheless, the border delineating compact sections from non-compact sections for a pipe under general loads remains to be determined.

1.2 Objectives

In the above context, the two main objectives of the present study are:

(1) Developing deformation based design criteria (buckling strain limits) for the design of buried pipelines subjected to internal pressure, axial tension, and imposed curvatures. In contrast to most previous studies, the present study aims at quantifying the effect of axial tension on the buckling strain limits. This objective is detailed in Section 1.2.1.

(2) Quantifying the effect of a) D/t ratio, b) internal pressure, c) axial force, and d) torsion on the ability of a pipe to attain its modified plastic moment capacity.

1.2.1 Deformation Based Design Criteria for Design of Buried Pipes

In this section, a discussion of the Catenary Effect, which is commonly associated with the local buckling of buried pipelines is described (Section 1.2.1.1) and the relevant objective of the present study is summarized in Section 1.2.1.2.

1.2.1.1 The Catenary Effect

A deformed buried pipe segment as a result of soil settlements is shown in Fig 1.1. The catenary action is induced as a result of the fact that the deformed pipe segment length L_d in the inclined configuration becomes longer than its originally horizontal length L_i prior to deformation. In most previous experimental investigations and resulting design rules the effect of the catenary action has been neglected, leading to conservative predictions for buckling strains and related deformation limit state criteria. In contrast the present study aims at investigating and quantifying the beneficial effect of axial tensile forces on buckling strain limits for steel pipes.

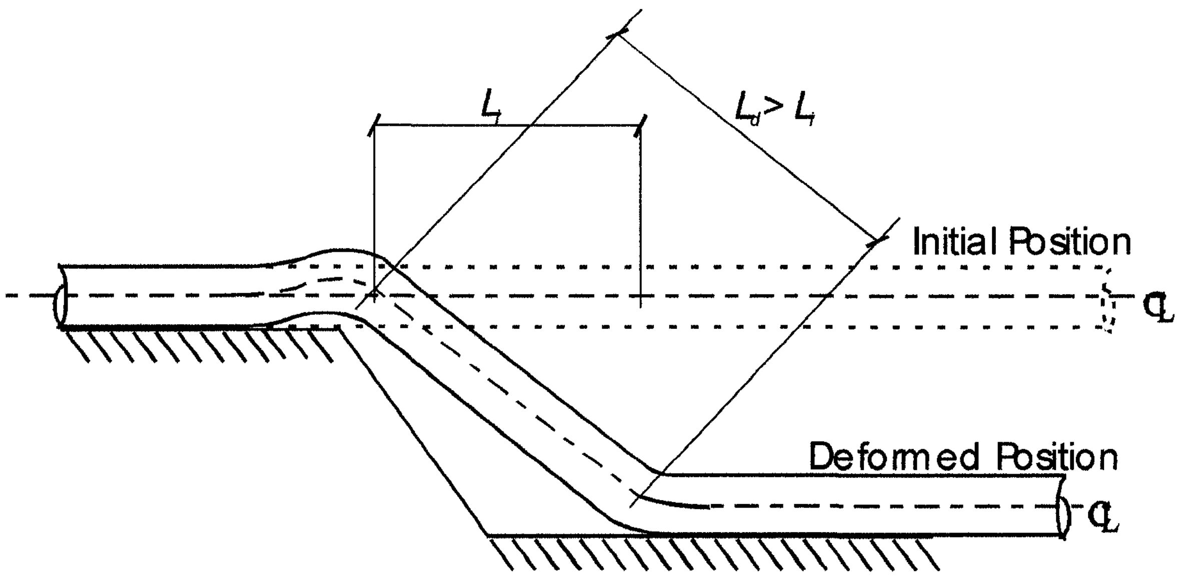

Fig. 1.1 Catenary Action

Local buckling in buried line pipes is normally associated with differential settlements, which is associated with catenary action. Thus, more realistic and possibly less conservative design buckling strain criteria can be obtained by incorporating the effect of the resulting tension on compressive buckling strains. The conventional design buckling strain expressions take the form

$\varepsilon_{cr1} \approx \varepsilon_{cr1}(D/t, p_r)$ (refer to Chapter 2, Section 2.2.1) in which the design buckling strain ε_{cr1} is a function of the pipe diameter to thickness ratio (D/t) and the dimensionless pressure ratio p_r (defined as the ratio of the internal pressure applied to the pressure that yields the pipe wall in hoop direction) and does not recognize the beneficial effect of the tensile force associated with catenary action.

1.2.1.2 Related Objective

A main objective of this study is to lay the foundation for developing better descriptions for design buckling strains by incorporating the effect of the tension force ratio effect A_r (defined as the ratio of the axial force applied to the axial force that yields the pipe wall in longitudinal direction). Specifically, the goal for the proposed study and possible future work is to propose a new description ε_{cr2} for the design buckling strain such that $\varepsilon_{cr2} \approx \varepsilon_{cr2}(D/t, p_r, A_r) \geq \varepsilon_{cr1}$. The new design rules, when consistently applied to the design of new pipeline networks and the assessment of existing pipelines, are expected to realize significant cost savings.

In order to achieve this goal, a test setup was designed and constructed to apply complex load combinations to pipe specimens. Six tests were conducted under combinations of internal pressure, axial tension, and imposed curvatures from which critical strains were measured. An FEA model was developed, which can predict the pipe deformational behavior and calibrated against the tests conducted. Design equations were then proposed based on the critical strain values obtained from the tests.

1.2.2 Developing Classification Rules for Elevated Pipes

In elevated pipes, effects such as bending and torsion become primary load effects in addition to internal pressure. Thus, design standards adopt a stress-based-design methodology when designing elevated pipes. (Refer to Chapter 3, Section 3.3)

1.2.2.1 Background to the Problem

Recently, general interaction relations for pipe sections, which can develop their plastic capacity prior to local buckling when subjected to combinations of axial forces, internal or external pressure, twisting moments, biaxial bending moments, and shearing forces, have been derived (Mohareb 2002 and 2003). These equations are

$$\left(M_{pm}/M_p\right)^2 = M_r^{\,2} = M_{rx}^{\,2} + M_{ry}^{\,2} = \left(1-\frac{3}{4}p_r^{\,2}-\tau_r^{\,2}\right)\cos^2\left\{\frac{\frac{\pi}{2}\left(A_r-\frac{1}{2}p_r\right)}{\sqrt{1-\frac{3}{4}p_r^{\,2}-\tau_r^{\,2}}}\right\} \tag{1.1}$$

$$\frac{V_{rx}^{\,2}+V_{ry}^{\,2}}{\tau_r^{\,2}} = \cos^2\left(\frac{\pi}{2}\frac{T_r}{\tau_r}\right) \tag{1.2}$$

In Eqs. 1.1 and 1.2, M_{pm} is the modified plastic moment capacity of the pipe, $M_p = 4r^2tF_y$ is the plastic moment capacity of the pipe calculated in the absence of other forces, M_{rx} is the ratio of bending moment M_x to the plastic moment resistance M_p, M_{ry} is the ratio of bending moment M_y to the plastic moment resistance M_p, p_r is the ratio of the pressure p (positive for a net internal pressure) to the yield internal pressure $p_y = F_y t/(r-t)$, A_r is the ratio of the axial force A to the axial resistance $A_y = 2\pi rtF_y$, V_{rx} is the ratio of shear force V_x to the plastic shear resistance $V_p = 4rt\left(F_y/\sqrt{3}\right)$, V_{ry} is the ratio of shear force V_y to the plastic shear resistance V_p, and T_r is the ratio of twisting moment T to the plastic twisting moment $T_p = 2\pi r^2 t\, F_y/\sqrt{3}$. The terms r, t, and F_y are the radius, wall thickness, and yield strength of the pipe, respectively. The shear ratio τ_r is a dimensionless parameter that intrinsically relates the twist and shear force ratios (Eq. 1.2) to the moment, axial force, and internal pressure ratios (Eq. 1.1). Equations 1.1 and 1.2 relate the seven loading parameters, M_{rx}, M_{ry}, V_{rx}, V_{ry}, T_r, p_r, and A_r when the section reaches its fully plastic state and can be used to judge whether a given internal force combination is attainable only when the following applicability limits are met.

$$0 \le V_{rx}^{\,2}+V_{ry}^{\,2} \le \tau_r^{\,2},\ 0 \le T_r \le \tau_r,\ \text{and}\ V_{rx}^{\,2}+V_{ry}^{\,2} \le \cos^2\left(\frac{\pi}{2}T_r\right) \tag{1.3a, b, c}$$

$$-2\sqrt{\frac{1-\tau_r^{\,2}}{3}} \le p_r \le 2\sqrt{\frac{1-\tau_r^{\,2}}{3}} \tag{1.4}$$

$$\frac{1}{2}p_r - \sqrt{1-\frac{3}{4}p_r^{\,2} - \tau_r^{\,2}} \le A_r \le \frac{1}{2}p_r + \sqrt{1-\frac{3}{4}p_r^{\,2} - \tau_r^{\,2}} \qquad (1.5)$$

The limits in Eqs. 1.3 through 1.5 are based on geometric constraints (Mohareb 2002). In the absence of shear forces and twisting moments, and under uni-axial moments by taking $M_{ry} = 0$ and $M_r = M_{rx}$, the interaction relations take the simpler form

$$M_r^{\,2} = \left(1-\frac{3}{4}p_r^{\,2}\right)\cos^2\left\{\frac{\frac{\pi}{2}\left(A_r - \frac{1}{2}p_r\right)}{\sqrt{1-\frac{3}{4}p_r^{\,2}}}\right\} \qquad (1.6)$$

Several recent studies (Chapter 2) have assessed the applicability of Eq. 1.6.

1.2.2.2 Related Objective

The validity of interaction relations was experimentally assessed for a database of limited pipe geometries and load combinations (Refer to Chapter 2, Section 2.3.2). However, the conditions under which the interaction relationships are applicable for more general geometries and internal force combinations are yet to be determined. Pipe sections with large *D/t* ratio (non-compact or slender sections) are susceptible to local buckling and the plastic interaction relations in Mohareb (2002 and 2003) are likely to overestimate the resistance of these pipes. In the current design provisions for structural steel codes (CAN/CSA-S16.1-01, and LRFD 1999), the border delineating compact and non-compact pipes is provided only for simple loading (pure bending and pure axial force). For more general loads, it is not well defined (Fig 1.2).

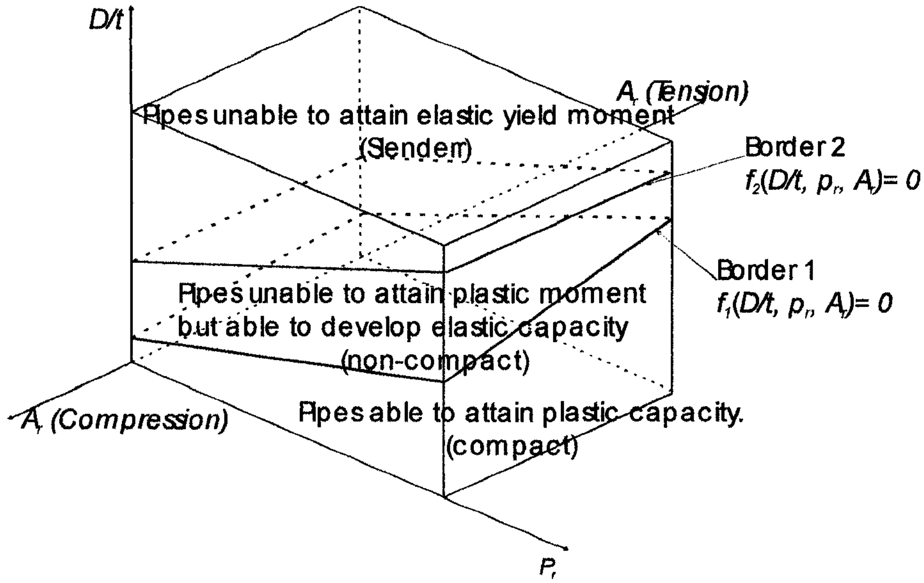

Fig. 1.2 Borders Delineating Pipe Behavior

In this context, the second main objective of this study is to document the effect of the geometric parameter (D/t) and loading conditions (p_r, A_r, and T_r) under which the predicted modified plastic resistance of a pipe as determined by Eqs 1.1 and 1.2. will be attained. Towards this goal, two series of tests were conducted on pipes subject to combinations of internal pressure, axial tension, torsion, shear, and bending (Six specimens under internal pressure, axial tension, and bending moments as presented in Chapter 5 and two specimens under internal pressure, axial tension, torsion, shear, and bending moments as presented in Chapter 6). Additionally, FEA models were developed to predict pipe capacity under combined loads. The results of the models are compared against the test results and subsequently used in a parametric study to study the effect of different variables (D/t, p_r, T_r, and A_r) on the ability of pipes to develop their modified moment capacity. This study is considered as a necessary step towards mathematical description of Border 1 in Fig. 1.2.

1.2.3 Implications of the Study on Structural Applications

A by-product of the present research is the development of classification rules for round Hollow Structural Steel Section (HSS) in various structural applications such as piles of offshore platforms.

Current design provisions for steel structures AISC-LRFD (1999) and CAN/CSA S16 (2001) recognize the additional resistance of stockier tubular sections that can deform into the plastic range of the deformation before buckling locally. They provide classification rules for pipe sections under pure axial force and pure bending, however, they do not provide general classification rules for pipe sections under combined loads involving torsion.

The interaction relationships presented by Eqs. 1.1 and 1.2 are also valid in the design of round tubular HSS sections used in structural applications. When the internal pressure term (p_r), is omitted from Eqs. 1.1 and 1.2, the relations take the form in Eqs. 1.7 and 1.8.

$$M_r^2 = M_{rx}^{\ 2} + M_{ry}^{\ 2} = \left(1-\tau_r^{\ 2}\right)\cos^2\left\{\frac{\frac{\pi}{2}A_r}{\sqrt{1-\tau_r^{\ 2}}}\right\} \tag{1.7}$$

$$\frac{V_{rx}^{\ 2} + V_{ry}^{\ 2}}{\tau_r^{\ 2}} = \cos^2\left(\frac{\pi}{2}\frac{T_r}{\tau_r}\right) \tag{1.8}$$

In order to adopt Eqs. 1.7 and 1.8 in structural design codes, the conditions under which these interaction relations are applicable should be assessed. In this respect, the outcome of the second objective of this study (Section 1.2.2) provides in part this information and can have implications on the design of HSS sections under complex loads.

1.3 Outline of the Thesis

The research encompasses the following tasks:

(1) Reviewing experimental work related to steel pipes under combined loads. Relevant analytical work related to the development of plastic interaction relations is also provided. This is presented in Chapter 2. Also, a review of various standards and codes for the design of buried pipelines, submarine pipelines, elevated pipelines, offshore structures, and tubular HSS sections is presented in Chapter 3.

(2) Conducting two sets of full-scale tests with large D/t ratios (D/t=80), representative of those used in the pipeline industry. In the first set of tests, it is aimed to observe and document the longitudinal compressive buckling strains of pipes under combinations of bending, internal

pressure, and axial tension. The other objective of this test series is to determine maximum moment capacity of pipes. This task is presented in Chapter 5. In the second series of tests, it is aimed to observe and document the maximum load carrying capacity of pipes under combinations of axial force, shear, bending, twist, and internal pressure. This task is presented in Chapter 6.

(3) Developing a Finite Element Model (FEM) for steel pipes including material and geometric non-linearity effects, which is capable of accurately predicting local buckling behavior and pipe capacity under general load combinations (This task is presented in Chapter 5 for the first test series and Chapter 6 for the second test series).

(4) Comparing the results of FEA model in item 3 to those of experimentally observed in item 2. This task is presented in Chapter 5 for the first test series and Chapter 6 for the second test series.

(5) Developing design rules based on critical buckling strains obtained from Test Series 1 for the design of the buried pipelines. This task is presented in Chapter 5.

(6) A comparative review of previous major experimental studies and their FEA counterparts in order to verify the ability of FEA to predict pipe capacity under combined loading. This task is accomplished in Chapter 7.

(7) Conducting a parametric FEA study to determine the effect of D/t ratio, axial force ratio A_r, internal pressure ratio p_r, and torsion ratio T_r on the ability of pipes to develop their modified plastic moment capacity as predicted by interaction relations (Eqs. 1.1 and 1.2). This task is presented in Chapter 7.

(8) A summary of conclusions and recommendations is provided in Chapter 8.

Chapter 2

Review of Previous Research

This chapter presents a review of deformation criteria for buried pipelines (Section 2.1) and overview of studies for buried pipes (Section 2.2). Section 2.3 presents an overview of analytical work on plastic interaction relations. A detailed review of the outcome of experimental studies on pipes is presented in Section 2.4. These studies are separated into two groups; a) experiments aimed at monitoring deformation behavior and b) experiments aimed at determining the moment capacity of pipes

2.1 Deformation Criteria for Buried Pipelines

Since strains are easier to measure or estimate in the field than stresses and since the stress vs. strain relationship of pipe steel is generally flat in the plastic range of the deformation, limiting strain criteria have been suggested in practice by many researchers (Bouwkamp and Stephen 1973, Reddy 1978, Workman 1981, and Kim and Valesco 1988) when designing buried pipelines. Deformation limits can be based on different criteria. These are summarized below.

2.1.1 Buckling Initiation Criterion

The compressive longitudinal strain at onset of local buckling can be considered as a deformation limit state for buried pipeline design. Bouwkamp and Stephen (1973) were the first to measure and document compressive strain values based on this critaria in their full-scale tests on pipes.

2.1.2 Rapid Wrinkle Growth Criterion

In order to set less conservative limits for pipe deformation, Lara (1987) proposed the adoption of a longitudinal compressive strain value after which rapid wrinkle growth was observed. He defined "rapid wrinkle growth" as a rapid change in wrinkling curvature on the compression side of the specimen with respect to the change in the overall curvature of the specimen.

2.1.3 Longitudinal Compressive Strains Corresponding to the Peak Moment Criterion

It was observed by Murphy and Langner (1985) that deformations grew rapidly after the peak moment was reached. Therefore, they suggested the use of longitudinal compressive strain value at which the maximum moment is reached as a limiting deformation limit state. However, since the moment vs. curvature diagram generally exhibits a flat plateau after the elastic range of deformation for pressurized pipes, the point of significant softening (in the moment curvature diagram) can be considered as a better deformation limit state for these types of pipes (Zhou and Murray 1993).

2.1.4 Cross-Sectional Deformation Criteria

Researchers also suggested limiting criterions for the cross-sectional deformation of the pipes in order to allow easy passage of the fluids conveyed and pigging devices. Some of these suggested criteria are presented in this section.

Gresnigt (1986) studied the ovalization of thin pipes under flexural stresses due to the presence of hoop stress components at the extreme compression and tension fibres, which force the pipe wall at these two locations to move towards the centroid of pipe cross section. He proposed limiting the pipe out-of-roundness (O_r) to 0.15, where

$$O_r = \frac{(D - D_s)}{D} \tag{2.1}$$

In which, D is the original outside diameter of the pipe and D_s is the smallest outside diameter of the pipe. The same expression was suggested as a deformation limit state by Price and Barnett (1987). Arbitrary limiting values of O_r of 15% were given for un-pressurized pipes and 6% for fully pressurized pipes by Price and Anderson (1991).

Row et al. (1987) limited the ovalization (O_v) to 7.5%, where

$$O_v = \frac{2(D_l - D_s)}{(D_l + D_s)} \tag{2.2}$$

in which D_l is the largest outside diameter of the deformed cross-section.

Zhou and Murray (1993) suggested the Pipe Diametric Differential (D_d) expression as another limiting criterion for cross-sectional deformation, where

$$D_d = \frac{(D_l - D_s)}{D} \tag{2.3}$$

2.1.5 Maximum Tensile Hoop Strain Criterion

In the outward bulging mode buckle, which is characteristic of pressurized pipes, the diameter of the pipe enlarges, leading to excessive circumferential hoop tensile strains at the crest of the buckle. In order to prevent the pipe from rupturing in these situations, a diametric expansion (D_e) criteria, was also introduced by Zhou and Murray (1993) to limit outward bulge type of buckles, where

$$D_e = \frac{(D_l + D_s)}{D} \tag{2.4}$$

2.2 Studies on Buckling Strains for Buried Pipes

Timoshenko and Gere (1961) derived an expression for the prediction of buckling strain of axially loaded pipes based on the elastic small strain theory. Material plasticity was accommodated by Batterman (1965) in determining critical elastic buckling strains. Schilling (1965) summarized the available information on the local buckling for tubes of moderate length under pure axial force, bending, torsion, shear, and combinations thereof. Bouwkamp and Stephen (1973) conducted a series of seven tests including the combined effect of internal pressure, axial force, and bending moments on 1220 mm diameter pipes to obtain the compressive buckling strain of the pipes that are going to be used in Trans-Alaska Pipeline System (TAPS). Reddy (1978) conducted a series of pure bending tests on aluminum and steel tubes with a diameter of 25 mm and D/t ratio ranging between 30 and 80. The critical buckling strain measured showed a trend relative to D/t ratio similar to that based on Bouwkamp and Stephen (1973) tests. Workman (1981) was able to analytically predict the critical strain values obtained in the tests of Bouwkamp and Stephen (1973) within a margin error ranging from –32.4% to 22.4%. Lara (1987) suggested adopting the longitudinal compressive strains corresponding to rapid wrinkle growth initiation as a critical buckling strain criterion providing less conservative limits. Gresnigt (1986) investigated the pipe deformational behavior and capacity under different load combinations by conducting over 70 small-scale and two full-scale tests, which had a diameter of 610mm with a D/t=95. In his full-scale tests, curvature was applied to the pipes along with external pressure. After the specimen buckled, internal pressure was increased until the specimen ruptured. Based on the tests, Gresnigt (1986) proposed a critical buckling compressive strain expression of pipe D/t ratio, internal and external pressure, and the modulus of elasticity. Later on, Gresnigt equation was adopted by Canadian Steel Line Pipe Code (CAN/CSA Z662 2003). Based on experimental results of Reddy (1979) and Gellins (1980), Ellinas et al. (1987) proposed an inelastic critical bifurcation strain expression for steel cylinders made of with a low strain hardening modulus steel subjected to pure bending. Kim and Valesco (1988) presented an overview of buckling modes of pipes for pipes with different D/t ratios and subjected to various loading conditions. Workman (1988) experimentally documented the difference between pipe material properties in the longitudinal and transversal directions. Zimmerman et al (1995) conducted an experimental and numerical program on pipes with $D/t=87$ to establish a less conservative design limit criteria for buried pipelines subject to internal pressure and bending. One of the tests they conducted was subject to combinations of internal pressure, tension, and bending. Since 1992, experimental, and numerical studies were conducted on plain or girth-welded line pipes under combinations of axial force, bending moments, and internal pressure at the University of Alberta (U of A). This includes the work of Mohareb et al. (1994) who conducted full-scale tests on seven pipe specimens subject to internal pressure, axial force, and bending moments. Yoosef-Ghodsi et al. (1995) extended the study to girth-welded pipes. The FEA conducted by Souza and Murray, (1996) was in good agreement with the experimental observations for girth-welded pipes. Dorey et al. (1999) extended the experimental database on pipe sections under internal pressure, axial force, and bending moments for specimens with D/t=92. By comparing the experimental findings from previous studies at the University of Alberta to available formulations in the literature and existing codes, Dorey et al. (2000) showed that the available expressions for critical strains do not adequately quantify pipe critical buckling strain limits. Das et al. (2000 and 2001) experimentally showed that pipe material does not fracture under monotonically increasing axial strains within operational load conditions. However, strain reversals were shown to create fracture under low cycle fatigue. Dorey et al. (2002) investigated the material grade effects on critical buckling strain. They showed that an increase in the grade of the material decreases the value of the critical buckling strain. They also demonstrated that pipes made of steel having a yield plateau have lower buckling limiting strains compared to pipes made of gradually yielding steel. Zimmerman et al (2004) tested 762 mm diameter spirally welded line pipes with D/t ratios of 82 and 48 and material grades of X70 (483 MPa) and X80 (552 MPa), respectively, under combinations of internal pressure, bending, and axial compressive forces. The tests showed that spirally welded pipes are as good as their longitudinal counterparts in terms of limiting buckling strains. Dorey et al (2006) conducted a finite element analysis (FEA) based parametric study and derived critical buckling strain equations as a function of Diameter-to-thickness (D/t) ratio, internal pressure ratio (p/p_y), material properties (yield strength-to-modulus of elasticity ratio-F_y/E), and initial imperfections. The limiting buckling strain predictions of these new equations were shown to be in good agreement with the ones measured in previous experiments.

2.2.1 Buckling Strain Expressions

The following expressions for critical strains were proposed as a result of the studies outlined in Section 2.2 based on deformational behavior of the pipes:

1) The classical elastic equation for local buckling of tubular shell structures (Column Research Council, 1966) for bending.

$$\varepsilon_{cr}^{CRC} = \left(\frac{1}{\sqrt{3\left(1-\upsilon^2\right)}} \right) \frac{t}{r} \tag{2.5}$$

Where, υ is Poisson's Ratio, r is the radius of the tube, t is the wall thickness of the tube. Since the Poisson's Ratio value for all pipes under consideration ranged from 0.27 to 0.30, by taking $\upsilon \approx 0.30$ as a close approximation, Eq. 2.5 can be simplified as

$$\varepsilon_{cr}^{CRC} \approx 1.2 \frac{t}{D} \tag{2.6}$$

Where D is the outside diameter of the pipe section.

2) The Sherman equation (1976) for bending.

$$\varepsilon_{cr}^{S} = 16\left(\frac{t}{D}\right)^{2} \tag{2.7}$$

3) The Battelle Equation (Stephen et al. 1991) for bending.

$$\varepsilon_{cr}^{B} = 2.42\left(\frac{t}{D}\right)^{1.59} \tag{2.8}$$

4) The Canadian Oil and Gas Pipeline System Code equation (CAN/CSA Z662-03) for the load combinations including axial compression, bending, and internal/external pressure.

$$\varepsilon_{c}^{crit} = 0.5\frac{t}{D} - 0.0025 + 3000\left[\frac{(p_i - p_e)D}{2tE}\right]^{2} \tag{2.9}$$

Where, p_i is the internal pressure, p_e is the external pressure, and E=207,000MPa (the modulus of elasticity of steel). The Canadian code equation is based on Gresnigt Equation (Gresnigt 1986).

5) Det Norske Veritas Offshore Standard for Submarine Pipeline Systems, DNV-OS-F101-2000 equation for the load combinations including bending and internal/external pressure.

$$\varepsilon_{c} = 0.78\left(\frac{t_1}{D} - 0.01\right)\left(1 + 5\frac{\sigma_h}{f_y}\right)\alpha_h^{-1.5}\alpha_{gw} \tag{2.10}$$

Where, t_1 is the wall thickness of the pressure containment resistance, σ_h is the characteristic hoop stress, f_y is the yield strength of the pipe material, α_h is the maximum allowed yield to tensile stress ratio, α_{gw} is the girth weld factor (α_{gw}=1.0 for specimens with no weld present).

2.2.1.1 Assessment of Limiting Buckling Strain Expressions

Dorey et al. (2000) compared the data collected from experimental studies on critical buckling strains, which were conducted at the University of Alberta (Mohareb et al. 1994, Yoosef-Ghodsi et al. 1995, and Dorey et al. 1999) with the critical buckling strain expressions presented previously (Eqs. 2.5 to 2.10).

The following observations were made on the data collected:

- The critical strain values were a function of inverse of *D/t* to a power larger than 1.
- The critical strain values were highly dependant on the internal pressure, therefore, any reliable critical strain formulation should include internal pressure ratio.
- Critical stain values also depend on Yielding Strain $\left(\varepsilon_y = F_y/E\right)$, a factor not recognized in current codes.
- The presence of girth-welds is an important factor which affects the critical strain values

The following observations were made by Dorey et al. (2000) when comparing the experimental data with various models and code equations:

- Equation 2.6 was un-conservative for most load combinations. However, Eqs. 2.7 and 2.8 were conservative for all loading combinations. Since Eqs. 2.6, 2.7, and 2.8 are solely based on the *D/t* ratio, they are not capable of capturing the effect of internal pressure.
- Both Eqs. 2.9 and 2.10 included internal pressure and material property parameters. However, they were providing poor prediction of experimental critical strain values.
- Both Eqs. 2.6 and 2.10 have a linear *D/t* ratio term, which is shown to be inadequate.
- DNV code equation (Eq. 2.10) is the only equation attempting to differentiate between plain and welded specimens.

2.3 Studies on Plastic Interaction Relations

This section presents and overview of studies on plastic interaction relations. Analytical studies are presented in Section 2.3.1 while experimental studies aimed at studying the interaction relationships under combined loads are presented in Section 2.3.2.

2.3.1 Analytical Studies

A summary of early work (Gerald and Becker 1957) provides a number of interaction relations for pipes under various combinations of internal forces. These are limited to pipes with large D/t ratios that undergo local buckling prior attaining their plastic resistance. Lower bound plastic interaction relations for hollow structural sections including thin walled tubular sections were established under combinations of biaxial bending moments, twisting moments, and axial forces by Fenves and Morris (1969). Pillai and Ellis (1971) conducted an experimental study on pipe sections subject to combined axial force and biaxial bending moments and proposed a simplified interaction relation. Chen and Atsuta (1972) formulated lower and upper bound interaction relations for tubular sections under biaxial bending moments and axial forces. The exactness of their solution was demonstrated through the agreement between the two bounds. Their solution also agreed with that developed by Fenves and Morris (1969) when the torque term is omitted. Chen and Sohal (1988) suggested that tubular members under longitudinal force and bending with D/t higher than 35 are susceptible to local buckling on their compressive side before attaining their fully plastic capacity. On the other hand, when tension has a dominant effect on the pipe capacity, it is more likely that pipes can develop their plastic capacity (Haunch and Bai 1999). Mohareb et al. (1994) and Mohareb and Murray (1999) developed interaction expressions including internal pressure, axial force, and bending moments. Their analytical predictions agreed well with experimental results (Mohareb and Murray 1999). Haunch and Bai (1999) modified the solution of Mohareb et al (1994) by incorporating a strength anisotropy factor and revised the equation by including usage/safety factors for design purposes. In Haunch and Bai (2000), the corrosion effect was included. Mohareb (2002) developed a lower bound general plastic interaction relation for pipe sections under normal force, torsion, biaxial bending moments, biaxial shear forces, and internal or external pressure by assuming statically admissible stress fields. Using Lagrange multipliers, the interaction expressions obtained were shown to maximize the lower bound solution (Mohareb 2001). An upper bound solution was developed by Mohareb (2003) by assuming kinematically admissible strain fields. The solution obtained coincided with that based on the lower bound formulation, demonstrating the exactness of the solution within the limitations of the assumptions. It is of interest to note that by omitting the shear and torsion terms from the general expressions, the axial force-bending-internal pressure interaction expressions reported in Mohareb et al. (1994) are recovered.

2.3.2 Experimental Studies

Sherman (1976) experimentally investigated the flexural behavior of the tube sections beyond ultimate moment capacity (bending and shear interaction). Yamaki (1976) conducted tests on fiberglass pipes to investigate the post-buckling behavior of pipe sections under pure torsion. Prion and Birkemoe (1988) conducted a series of tests on large fabricated tubes subjected to combinations of axial compressive load and bending. Obaia et al. (1991) investigated analytically and experimentally the inelastic shear behavior of large diameter pipes subjected to combinations of shear and bending. They proposed an interaction equation for the bending and shear capacities based on regression analysis of their test results. The experimental results in Mohareb and Murray (1999) on pipes bending moment-axial force-internal pressure combinations demonstrate the validity of the interaction relations (Mohareb et al. 1994) for pipes with a diameter to thickness ratio of 51 and 64. Upon full-scale experimental verification, these interaction relations were adopted in limit state design of submarine pipelines by DNV (1996). Ozkan and Mohareb (2003) conducted tests on pipes with D/t ratio of 43 under combinations of bending, shear, and twist. The pipe capacities recorded from the experiments agreed well with the ones predicted by Mohareb (2002 and 2003) for the special case where axial force and internal pressure were omitted.

A summary of experimental studies on pipes is provided in Table 2.1. It is observed that a very limited number of tests involving axial tensile force were performed. Also, pressurized pipes under torsion appear to have not been investigated to detail. The objective of the proposed program is to partially fill these voids by conducting tests on pressurized pipes under combinations of tension, and bending (Test Series 1 in Chapter 5) and pressurized pipes under torsion and bending (Test Series 2 in Chapter 6). The details of the program are provided in the next section.

Table 2.1 Summary of Full-Scale Experimental Studies on Steel Pipes under Combined Loads

Test Series (1)	Number of Tests (2)	Axial Force (3)	Bending (4)	Shear (5)	Internal Pressure (6)	External Pressure (7)	Torsion (8)	F_y (MPa) (9)	*D* (mm) (10)	*D/t* (11)	Objective (12)
Bouwkamp and Stephen (1973)	7	+	+		+			414	1220	104	A
Sherman (1976)	19		+	+				400 and 330	272-274	18 and 102	B
Gresnigt (1986)			+		+*	+		358	610	95	A and B
Prion and Birkemoe (1988)	22	+	+					250 and 450	450	51 and 100	A and B
Obaia et al. (1991)	2		+	+				300	1270	400	B
University of Alberta Test Series (1992-2002)	Over 50	+	+		+			359-483	324-792	51-92	A and B
Zimmerman et al. (1995 and 2004)	9	+	+		+			483-552	610-762	41-87	A
Ozkan and Mohareb (2003)	6		+	+			+	330	406	43	B

* Constant external pressure was applied to the specimens along with increasing bending until the specimens buckled. After buckling, internal pressure was increased until the specimens ruptured

Objectives:

A: Experiments aimed at observing the deformational behavior and measuring critical buckling strains under combined loads

B: Experiments aimed at determining pipe resistance under combined loads

2.4 Detailed Review of Full-Scale Tests

In this section, observations from full-scale tests on pipe sections are presented. These are grouped in two categories based on the goal of the experiments.

(A) Experiments aimed at observing the deformational behavior and measuring critical buckling strains under combined loads, and

(B) Experiments aimed at determining pipe resistance under combined loads

2.4.1 Experiments on Deformational Behavior and Critical Buckling Strains

2.4.1.1 Berkeley Test Series

The first experimental study on pressurized line pipes was conducted by Bouwkamp and Stephen (1973). The goal of the study was to establish the pipe deformation criteria for buried 48in OD (1219mm) line pipes with a D/t=104 under combinations of axial load, bending moments, and internal pressure. The study also investigated the effect of full penetration longitudinal and circumferential welds on the local buckling behavior of pipes. The following observations were made

- The local buckle was confined to a short length of the pipe.
- Under higher levels of internal pressure, the pipe wall exhibited outward buckling over the compression zone. Under lower levels of internal pressure, the compression zone of the pipe wall exhibited an inward diamond buckling shape.
- The failure of the specimen occurred in the pipe wall exhibiting a shear tearing failure around the connection between the test segment and the end zone pipes.
- The displacements at rupture were about 20 times of those during initiation of buckling, showing a highly ductile behavior for the pipe specimens.
- Highly pressurized pipes exhibited more plastic deformations than lowly pressurized pipes.
- The buckling and rupture strains were reported along both the compression and the tension fibers. As the specimen buckled, the neutral axis under bending shifted significantly towards the tension side of the section

2.4.1.2 University of Alberta Test Series

The University of Alberta test series were conducted for the primary purpose to obtain critical buckling strains for pipes with different D/t subjected to combinations of internal pressure, axial force, and imposed curvatures. As a bi-product, the modified plastic moment capacity was obtained on some of the tests. In this section, the outcome of the research on deformational behavior is presented.

Behavior of 508mm OD and 324mm OD Pipes

Mohareb et al. (1994) conducted experiments on seven pipe specimens with *D/t* ratios of to 64 and 51 with outer diameter (*OD*) of 508mm and 324 mm, respectively. The specimens were tested under load combinations involving internal pressure, axial load, and bending moments. The lengths of the specimens were chosen as 1,690 mm (slightly greater than three diameters of the specimens with 508mm diameter, in an attempt to force local buckling to develop in the mid region of the pipes). Other than the cross sectional dimensions and applied load combinations, pipe manufacturing technique, pipe grade, and end conditions were varied as test parameters. Specimens with 508mm *OD* were made of grade X56 steel (*SMYS*=386MPA), manufactured using the doubly submerged arc weld (*DSAW*) technique and those with *OD* 324mm were made of grade X52 steel (*SMYS*=359MPA), manufactured by using the electric resistance weld (*ERW*) technique. Two types of end conditions were studied, namely (1) active condition in which the axial force in the pipe was maintained constant; (2) reactive condition in which the length of the pipe was maintained constant. In both cases, the stroke of the eccentric jack was monotonically increased in order to increase the end rotations of the specimen leading into a displacement controlled loading scheme.

The numerical component of the study was conducted using finite element analysis (FEA) under the finite element simulator ABAQUS for the prediction of the post-buckling response of the specimens. Following are the observations made.

- Local buckling modes vary with internal pressure. An outward bulging mode of buckling took place in fully pressurized specimens while the buckling of the unpressurized specimens can be characterized as diamond-shape mode in agreement with Bouwkamp and Stephen (1973).
- The buckling modes were insensitive to imperfections of the pipe segments.
- The location of the local buckle depends on the second order effect of the axial load and end condition disturbances. Wrinkling took place in the mid region of the specimens when the

second order effects were predominant. On the other hand, when the end effects were predominant, wrinkling occurred in the end region of the pipe segments.

- After initiation of wrinkling, the average curvature was observed to be a function of the length of the specimen considered, Thus, global curvature was concluded to be inadequate to characterize the deformational behavior of the pipe after the occurrence of wrinkling.
- Compressive strain values prior to initiation of wrinkling of importance of buried pipelines with properties similar to the ones tested were documented as part of the study.

Effect of the Circumferential Girth-Welds (OD=508mm and 324mm, D/t=64 and 51)

Yoosef-Ghodsi et al. (1995) conducted a series of full-scale tests on girth welded line pipe segments subjected to combinations of constant axial force, internal pressure, and monotonically increasing curvature. The effects of the girth weld on the local buckling behavior of the pipe segments were experimentally investigated by adopting the experimental setup in Mohareb et al. (1994) to test specimens with girth weld at mid-height.

An FEA under ABAQUS was also conducted for the prediction of the post buckling response of the tested specimens (Souza and Murray, 1996). Observations were as follows.

- The wrinkling configurations observed were similar to those of plain pipe segments with the difference that the wrinkles being located always within 150 mm from the girth welds. This contrasted with plain pipes in which the location of the wrinkle was random along the length of the pipe. It was concluded that the residual stresses generated by welding process and the eccentricities induced when aligning the two cans when forming the specimen were responsible for triggering the buckles near the girth-welds.
- The limiting strains in both series of experiments (plain and girth-welded pipes) were linearly dependant on the internal pressure.
- The initiation of wrinkling for girth-welded pipes took place at strain levels of about 60% of those of plain pipes.
- The buckled configuration in the tests (Yoosef-Ghodsi et al. 1995) and the FEA models (Souza and Murray 1996) of the tests were in good agreement.

Large Diameter Pipes (OD=762 mm and D/t=92)

The test program of Dorey et al. (1999) extended the experimental database to larger diameter pipes (*D/t* ratio of 92, OD = 762 mm) under internal pressure, bending moments, and axial force. The specimens tested were 2700 mm long. The pipe material was grade X70 (*SMYS* = 483 MPa). All specimens were manufactured using *DSAW* (doubly submerged arc weld) process.

- Two different types of buckles were observed, "Diamond-shape" mode for low internal pressure specimens and "bulge" mode for high internal pressure specimens.
- Two types of bulge modes were observed namely (1) mid-height bulge; (2) elephant's foot bulge. The latter one is considered as a type of failure that is governed by the experimental test setup and may not be representative of true pipe behavior.
- Whenever there was a girth weld, the buckle occurs around its vicinity due to perturbations introduced by the weld.
- The pipe specimens soften less rapidly in the post buckling range as the internal pressure is increased.

2.4.1.3 The C-FER Test Series

Large diameter pipes with OD=610mm (D/t=87 and 41) and made of X70 (483MPa) material

Zimmerman et al. (1995) conducted an experimental and numerical study to determine a less conservative limiting strain criteria than those commonly used for the design of buried pipes under bending, axial force, and internal pressure. Five experiments were conducted on 10m long girth welded pipe specimens with *OD*=610mm, *SMYS*=483MPa, and *D/t* of 87 and 41. These five tests were also numerically modeled using the FEA simulator ADINA. After calibrating the FEA model, a parametric study was conducted to expand the experimental database of buckling strains and develop more conservative design criteria. Following were observed:

- All pressurized specimens exhibited "bulge" mode buckling while those with no internal pressure exhibited a "Diamond-shape" mode of buckling.
- The data obtained from the parametric FEA study for the maximum compressive strain value were compared with the available design curves. It was shown that empirical equations resulting from previous research (Sherman 1976, Murphey and Langner 1985, Stephens et al. 1991, and Gresnigt 1986) provided lower bounds while the classical elastic equation provided an upper bound for the data collected. Through curve fitting and linear regression, a

semi-empirical equation for critical strain corresponding to the maximum moment was proposed.

- It was observed that the design criteria for buried pipes available, which limit the compressive strain either by a) the strain corresponding to the maximum moment or b) the strain at the initiation of buckling were overly conservative as they do not reflect the ability of the pipe to deform well into the inelastic range of deformation.
- A less conservative limiting strain criterion was recommended based on limiting the tensile hoop strains at the crest of the wrinkle since it is known that rupture would normally occur at strains between 10% and 38%. A semi-empirical equation for the limit state associated with a maximum 10% tensile hoop strain was proposed.

Spirally Welded Pipes

Zimmerman et al. (2004) conducted a series of experiments consisting of four tests on 762 mm diameter spirally welded pipes with material grades of X70 (483 MPa) and X80 (552 MPa) and D/t ratios of 48 and 82 with a specimen length of 3,200 mm. The experiments were also modeled by the FEA simulator ABAQUS. The compressive strains corresponding to the peak moment capacity were recorded and compared with the FEA predictions. Following were the observations.

- Specimens with no internal pressure showed diamond shape buckle while the fully pressurized specimens buckled in an outward bulge mode.
- Spirally welded pipes were observed to behave identically to longitudinally welded pipes of similar dimensions.
- The results obtained from the FEA model were compared with experimental results. While the FEA successfully predicted pipe buckling modes and peak moment capacities, large discrepancies reaching up to 60% were reported in compressive strain predictions.

2.4.2 Experiments aimed at Determining Pipe Moment Resistance

2.4.2.1 University of Wisconsin Test Series

Sherman (1976) reports tests to investigate flexural behavior of circular steel tubes up to and beyond the ultimate moment capacity subject to combinations of shear and bending. A total of 18 experiments were conducted by using six different D/t ratios (varying from 18 to 35). The end conditions and shearing force ratio were investigated. Also, the effect of manufacturing process of the specimens was investigated. These included hot-formed seamless pipe, with a stress vs. strain curve having a visible yield plateau ($F_y \approx 400MPa$), Electric Weld Resistance (*ERW*), with a gradual yielding stress vs. strain curve ($F_y \approx 290MPa$). Following are Sherman's conclusions based on the tests.

- The fixed ended specimens with *D/t* of 35 and less were able to develop their fully plastic moment capacity for spans up to 22 diameters without significant ovalization at the location of plastic hinge. For the specimens with simple supports, the plastic moment resistance was not attained in the constant moment region. These results were contrary to those from previous work (Schilling 1965) suggesting that a pipe section with a *D/t* smaller than $3{,}300/F_y$ would attain its plastic moment capacity.
- In simply supported and fixed-ended test specimens, shear up to 28% of plastic capacity did not have any significant effect on the hinge development for specimens with *D/t* of 18, 35, and 102.
- In Cantilever specimens with *D/t* of 49, 55, and 77, the presence of shear had a variable influence on strength. While the presence of shear for the section with *D/t* of 49 allowed the plastic moment to be nearly achieved, for the member with *D/t* of 77, the presence of shear prevented the attainment of the plastic capacity. The presence of shear had little influence on the specimen with *D/t* of 55. Sections with *D/t* of 102 buckled after reaching the elastic flexural resistance but prior attaining their fully plastic capacity.
- While in the previous studies (Schilling 1965), it was reported that the critical strain (the strain value in the initiation of buckling) is a function of the parameter $(t/D)(F_y/E)$, the data obtained from Sherman's experimental study appeared to be correlated better with the parameter $(t/D)^2(F_y/E)$.

2.4.2.2 University of Toronto Test Series

Prion and Birkemoe (1987 and 1988) conducted a study on fabricated steel pipes subjected to the combinations of bending moments and axial force. Twenty-two specimens were tested with 450 mm diameter and wall-thicknesses varying between 4.5 mm and 8.8 mm. The measured yield stress varied between 250 MPa and 450 MPa. The lengths of the specimens ranged between 1.5m and 10m.

The load-deflection relationship up to and beyond ultimate load was monitored. Test results were compared with existing and proposed design rules with respect to local buckling, strength, and stability interaction (API 1981, Code 1982, Steel 1984, Plantema 1946, and Sherman 1986). The following conclusions were made based on the experimental observations.

- Three types of local buckles were observed in axially loaded specimens, these are a) single symmetric ring buckle (elephant's foot buckle), b) symmetric buckle, and c) asymmetric buckle.
- Cross-sectional strength interaction relations used in codes and previous research (API 1981; Code 1982, Steel 1984, Plantema 1946, Sherman, 1986) were compared with the experimental results and a more realistic interaction relation was proposed which reflects the observations made in the experiments.
- The stability interaction relations from different specifications (API 1981; Code 1982; Steel 1984) showed reasonable agreement with the experimental results.
- No direct correlation was found between imperfections, which were induced during the fabrication of the specimens, and the ultimate loads.

2.4.2.3 University of Alberta Test Series

Behavior of 508mm OD and 324mm OD Pipes

The observations in Mohareb et al. (1994) test series related to the development of the modified plastic moment capacity of the pipes subject to internal pressure, axial compression, and bending are as following.

- The derived interaction relations reliably predicted the capacity of the pipes.
- The FEA model was able to predict both the post-buckling deformation and moment curvature response of the experiments.

Large Diameter Pipes (OD=762 mm and D/t=92)

In the test series by Dorey et al. (1999), the plastic moment capacity of the specimens were predicted by using previously derived interaction relations (Mohareb et al. 1994) and compared with the experimental moment capacities reached. They observed that the interaction equations overestimated the pipe flexural capacity. An exception was the specimens tested at an internal pressure of 80%, where the ratio between the experimental moment capacity observed and the plastic moment capacity predicted ranged between 95% and 124%.

2.4.2.4 University of Ottawa Test Series

Ozkan and Mohareb (2003) reported a full-scale experimental program consisting of six tests aimed at verifying the validity of the interaction relations (Mohareb 2002 and 2003) under load combinations including shearing force, bending, and twisting moments. All pipes tested had a nominal outside diameter of 406mm and a thickness of 9.5mm with, a *D/t* ratio of 42.7.

The principal conclusions of the work are:

- All specimens exhibited significant deformations in the plastic range of deformation. The onset of local buckling was detected immediately prior the attainment of the peak loads.
- The pipe post buckling behavior is characterized by softening of the resistance curve as a single wrinkle develops and amplifies.
- The local buckling configuration is dependant on the bending, torsion, and shear ratios. For the short specimens with lower bending moments and higher torsion and shear, wrinkling appeared as a diagonal buckle. For medium and tall specimens with lower shear force and higher bending moment and torsion, a wrinkle initiated at the maximum compression fiber and progressed into an un-symmetric mode. For specimens with no torsion but with high bending moments and relatively low shear, an outward bulging local buckle symmetric about the plane of bending was observed. An example of each local buckle type encountered during the experiments can be seen in Fig. 2.1.

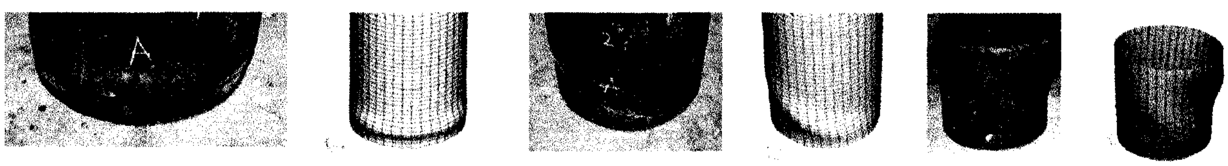

Test FEA Test FEA Test FEA

(a) Outward bulge **(b)** Un-symmetric wrinkle **(c)** Diagonal buckle

Fig. 2.1 Buckled Specimens and FEA Results

- In all tests, the analytical moments predicted by the interaction relations in Mohareb (2002 and 2003) were lower than those measured in tests. The average ratio between the analytical moment predictions and those measured in tests was 94% based on the yield strength determined by extension-under-load method and 91% based on offset method. Strain hardening effects, which were not taken into consideration in the formulation, are believed to be responsible for this difference.

2.5 General Comments

During the review of the literature, it was observed that although there was some experimental and numerical research conducted on pipes under complex load combinations, none of these previous studies investigates the beneficial effect of tensile axial force on the critical stains of line pipes at differential settlement locations except a single test in Zimmerman et al. (1995) and four tests in Dorey (2001) on pipes with D/t=92. It is the aim of the current study to partially fill this void by conducting full-scale tests on pipe segments with D/t=80, under combinations of axial tension, internal pressure, and imposed curvatures. It was also observed that the code equations for critical strains do not recognize the effect of axial tension. Critical strain design equations for pipes with D/t=80 are to be developed by using the critical strain data measured from the experiments as a function of internal pressure and axial tension.

Evidence in the current literature demonstrates that interaction relations can predict the pipe capacity accurately in some cases. However, it is not yet known under which geometric and loading conditions pipes can develop their modified plastic capacity. The development of the plastic capacity is highly dependant on the geometric properties (D/t) of the pipe cross-section and the load combination (internal pressure, axial force, and torsion) on the pipe. It is the objective of this study to investigate the effect of D/t ratio, axial force, internal pressure, and torsion on the ability of a pipe to develop its modified plastic moment capacity as predicted by Eqs 1.1 and 1.2.

Chapter 3

Review of Design Standards for Pipes

The objective of this chapter is to present a comprehensive review of various codes and standards related to the design of pipes. This includes buried pipelines, elevated pipelines, submarine pipelines, and circular hollow structural members.

3.1 Design of the Buried Pipelines

Strain based design criteria are the basis adopted in the design of buried pipelines. The Canadian Standards on Pipelines (CAN/CSA-Z662-03) gives the designer two options when designing buried pipeline design: **a)** working stress design and **b)** Limit states design. In contrast to most structural steel codes (CAN/CSA-S16.1-01, LRFD 1999, etc), limit states design is not a mandatory part of CAN/CSA-Z662 (2003). It is presented as an appendix to the code *"to provide guidance for the design of oil and gas industry steel pipelines, excluding steam distribution pipelines"*. The limit states design option of the code has the advantage of accounting for the variability in resistance and loading by using partial safety and resistance factors determined by probabilistic analysis and is considered advantageous to the more traditional working stress design methodology.

The limit states identified in clause C3.4 of the standard are Ultimate Limit States (ULS) and Serviceability Limit States (SLS). Ultimate limit states are those associated with burst or collapse of the pipe segment. This type of limit state includes rupture, yielding caused by primary loads (i.e., yielding of the pipe wall due to internal pressure), buckling due to primary or secondary loads (i.e., collapse due to external pressure, imposed curvature due to differential soil settlements), and fatigue. Serviceability Limit States are those that restrict normal operations or affect durability, which includes yielding caused by secondary loads and buckling not resulting in collapse (stable local buckling, some upheaval buckling modes).

3.1.1 Ultimate Limit States

Buried pipelines are subject to two types of loading; primary loads and secondary loads. Primary loading is load controlled loading. This includes internal pressure and axial forces due to temperature changes. Secondary loading are deformation controlled loads, which are bending and axial tension due to soil settlements. Under these two loading types, the Canadian Standards on Pipelines (CAN/CSA-Z662-03) identifies the following limits states for buried pipelines:

(1) Rupture limit state

(2) Yielding limit state

(3) Local buckling limit state

(4) Ovalization limit state, and

(5) Global buckling limit state

(1) Rupture Limit State

The tensile strain limit state against rupture due to primary loads, secondary loads, or both, is given in clause C6.3.1, which limits the tensile strains in the vicinity of the local wrinkle or collapse zone in both the longitudinal and hoop directions:

$$\phi_{\varepsilon t}\varepsilon_t^{crit} \geq \varepsilon_{tf} \tag{3.1}$$

where

$\phi_{\varepsilon t}$ = resistance factor for tensile strain (=0.7)

ε_t^{crit} = ultimate tensile strain capacity of the pipe wall or weldement (as determined from valid fracture mechanics methods or physical tests. In the absence of more detailed information, the standards provide a limiting value for $\varepsilon_t^{crit} = 0.0075$)

ε_{tf} = factored tensile strain in the longitudinal or hoop direction

(2) Yielding Limit State

Clause C6.3.2.1 of the code limits the tensile hoop stress due to internal pressure to a fraction ϕ_y of the yielding strength F_y of the pipe material according to the following equation.

$$\phi_y F_y \geq \sigma_{hf} \tag{3.2}$$

where

ϕ_y = resistance factor for yielding strength (= 0.9)

F_y = effective specified minimum yield strength

σ_{hf} = factored hoop stress due to pressure differential = $\dfrac{\gamma(\alpha_Q p_i - \alpha_G p_e)D}{2t}$, where

p_i = maximum internal design pressure

p_e = minimum external hydrostatic pressure

D = outside pipe diameter

t = pipe wall thickness

α_Q = load factor for operational loads (ranges between 1.00 and 1.13)

α_G = load factor for permanent loads (ranges between 1.00 and 1.25)

γ = class factor (ranges between 1.0 and 2.0 depending on the location class and the fluid conveyed)

(3) Local Buckling Limit State

The longitudinal compressive strains ε_{cf} for pipes under primary loads (axial force and internal pressure), secondary loads (imposed bending deformation), or under both effects combined are limited in Clause C6.3.3.2 by

$$\phi_{\varepsilon c}\varepsilon_c^{crit} \geq \varepsilon_{cf} \tag{3.3}$$

where

$\phi_{\varepsilon c}$ = resistance factor for compressive strain (=0.8)

ε_c^{crit} = ultimate compressive strain capacity of the pipe wall or weldment (as determined by valid analysis methods or physical tests). The longitudinal compressive strain can be determined by:

$$\varepsilon_c^{crit} = 0.5\frac{t}{D} - 0.0025 + 3000\left[\frac{(p_i - p_e)D}{2tE}\right]^2$$

in the absence of more detailed information.

A major objective of this study is to develop an experimental database to determine ε_c^{crit} for pipes with D/t=80, subject to bending and tension.

(4) Ovalization Limit State

Cross-sectional ovalization of pipe segments subject to bending should also be limited to prevent sectional collapse, thus, limiting the passage of internal inspection devices. The following limiting condition based on the work of Row et al. (1987) is adopted in CAN/CSA-Z662-03 (C6.3.3.3)

$$\Delta_\theta \leq \Delta_\theta^{crit} \tag{3.4}$$

where

Δ_θ = ovalization deformation defined as $\Delta_\theta = 2\left(\dfrac{D_{\max} - D_{\min}}{D_{\max} + D_{\min}}\right)$,

$D_{\max}$ = maximum outside pipe diameter,

$D_{\min}$ = minimum outside pipe diameter, and

Δ_θ^{crit} = critical ovalization deformation, which can be taken as 0.03 in the absence of more detailed information. If it can be shown that premature sectional collapse will not occur under the loads considered, the value can be increased to 0.06, allowing the passage of internal inspection devices.

(5) Global Buckling Limit State

Clause C6.3.3.4 CAN/CSA Z662 (2003) stipulates designing pipelines against global buckling where such buckling could be detrimental to the pipeline (i.e., upheaval buckling exposing a buried line)

3.2 Design of Submarine Pipelines

Det Norske Veritas (DNV 2000) is a well-detailed set of standards aimed at providing thorough design rules for the design of submarine pipes. Offshore pipes generally have smaller D/t ratios compared to their onshore counterparts due to the presence of external pressure effects in deep water.

The possible limit states as identified in DNV (2000) are classified into four groups. These are: *Serviceability Limit States* (SLS) due to ovalization/ratcheting, accumulated plastic strain. If exceeded, these will cause problems for normal operations of the pipeline.

Ultimate Limit States (ULS) due to bursting, ovalization/ratcheting, local buckling, global buckling, unstable fracture and plastic collapse, impact. If exceeded, these will cause problems related to the integrity of the pipeline,

Fatigue Limit State (FLS): A condition to accommodate cyclic loading patterns (fatigue due to cyclic loading).

Accidental Limit State (ALS): A ULS due to accidental loads (ultimate limit state due to infrequent loading, e.g., gouging due to construction machinery activity).

In the design of the pipes resting on the sea base, similar to the design of buried pipes, strain based design criteria are adopted.

Among these limit states (SLS, ULS, FLS, and ALS), the ULS for longitudinal compressive strain is based on compressive longitudinal bending strain associated with displacements induced by axial force, bending, and net internal pressure when $D/t \leq 45, p_i \geq p_e$, in which p_i is internal pressure and p_e is external pressure. The design compressive strain, ε_d, is given by

$$\varepsilon_d \leq \frac{\varepsilon_c}{\gamma_\varepsilon}, \tag{3.5}$$

where

ε_c = critical compressive strain $0.78\left(\frac{t_2}{D} - 0.01\right)\left(1 + 5\frac{\sigma_h}{f_y}\right)\alpha_h^{-1.5}\alpha_{gw}$ (Also, presented as Eq. 2.10),

t_2 = net wall thickness free of possible corrosion,

D = outside diameter of the pipe,

α_h = maximum allowable yield strength to tensile strength ratio,

α_{gw} = girth weld factor (≤ 1),

$\sigma_h \quad = \Delta p_d\left(\frac{D-t_2}{2t_2}\right),$

in which pressure differential $\Delta p_d = \gamma_p\left(p_{ld} - p_e\right)$

where

p_{ld} = local design pressure,

γ_p = load effect factor for pressure loads (=1.05), and

p_e = external hydrostatic pressure,

f_y = characteristic yield stress given by $f_u = \left(SMYS - f_{y,temp}\right)\alpha_U$ in which $f_{y,temp}$ is the temperature de-rating of the yield stress of the pipe material and α_U is the material strength factor which can be taken as 0.96 or 1.00, and

γ_ε = resistance strain factor ranging between 2.0 to 3.5 depending on the safety classes

In the design of free-spanning submarine pipe segments, stress based design criteria are used similar to the design of elevated pipes (Section 3.3).

The Offshore Pipeline Standard, DNV-OS-F101 (2000) provides a design requirement for pipes with relatively low D/t ratio ($D/t \le 45$) and $p_i > p_e$ under load-controlled deformation subject to combinations of net internal pressure, axial force, and bending:

$$\gamma_{SC}\gamma_m\left(\frac{S_d}{\alpha_c S_p}\right)^2 + \gamma_{SC}\gamma_m\left(\frac{M_d}{\alpha_c M_p}\sqrt{1-\left(\frac{\Delta p_d}{\alpha_c p_b(t_2)}\right)^2}\right) + \left(\frac{\Delta p_d}{\alpha_c p_b(t_2)}\right)^2 \le 1, \tag{3.6}$$

where,

S_d = design effective axial force,

S_p = characteristic plastic axial force resistance,

α_c = flow stress parameter accounting for strain hardening (=1.0 for no strain hardening),

γ_{SC} = the safety class resistance factor ranging from 1.04 to 1.308 depending on the safety class,

γ_m = the material resistance factor of either 1.15 or 1.00 depending on the limit state category,

M_d = design bending moment,

Δp_d = design differential over pressure defined as $\Delta p_d = \gamma_p \left(p_{ld} - p_e \right)$ in which

p_{ld} = local design pressure,

γ_p = load effect factor for pressure loads (=1.05), and

p_e = external hydrostatic pressure

M_p = plastic moment resistance in the absence of axial force and design differential overpressure, and

$p_p(t_2)$ = burst pressure for thickness t_2 given by $Min\left(p_{b,s}(t_2), p_{b,u}(t_2) \right)$ in which

$$p_{b,s}(t_2) = \frac{2t_2}{D - t_2} f_y \frac{2}{\sqrt{3}} \text{ and } p_{b,s}(t_2) = \frac{2t_2}{D - t_2} \frac{f_u}{1.15} \frac{2}{\sqrt{3}}$$

where,

f_u= characteristic tensile strength given by:

$$\left(SMYS - f_{u,temp} \right) \alpha_U \alpha_A$$

in which

$f_{u,temp}$ is the temperature de-rating of the tensile strength of the pipe material,

α_U is the material strength factor which can be taken as either 0.96 or 1.00,

α_A is an anisotropy factor, which is equal to 0.95 in axial direction due to relaxed testing requirements in linepipe specifications. It can be taken as 1.00 for other cases.

3.3 Design of Elevated Pipelines

The Canadian Standards on Pipelines (CAN/CSA-Z662-03) does not include a classification of pipe section according to local buckling under axial compression or flexure. In the design of elevated pipelines, Clause 6.3.2.2.1 of the standards stipulates that *"For pipeline sections where longitudinal stresses are induced by primary loads (e.g. suspended spans), the stresses at all points in the pipe cross section shall be limited by the following requirement"*

$$\phi_y F_y \geq \sigma_{ef} \tag{3.7}$$

where

ϕ_y = resistance factor for yield strength,

F_y = effective specified minimum yield strength, and

σ_{ef} = maximum factored combined effective stress according to von Mises criterion

= $\sqrt{\sigma_{hf}^2 + \sigma_{Lf}^2 - \sigma_{hf}\sigma_{Lf} + 3\tau_f^2}$, in which

σ_{hf} = factored hoop stress (tension positive),

σ_{Lf} = factored longitudinal stress (tension positive), and

τ_f = factored tangential shear stress

In case of combined bending, axial force, and internal pressure, σ_{Lf} can be calculated according to C6.3.2.2 (Eq. 3.8) if the calculated state of stress falls on or within Von Mises Yield Criterion.

$$\sigma_{Lf} = \frac{M_f}{S} + \frac{P_f}{A} \tag{3.8}$$

where

M_f = factored bending moment,

P_f = factored axial force,

S = elastic section modulus, and

A = cross-sectional area

Clause 6.3.3 also provides an alternative stress-based design method, which states *"Pipe sections that are subjected to significant compressive stresses due to primary loads, secondary loads, or both shall be designed to prevent undesirable global or local buckling"*. In order to avoid global or local buckling in the case of significant compressive principal membrane stresses, Clause 8.12 limits the compressive stress on the pipe cross section to a critical buckling stress (Eq. 3.9) based on cylindrical shell analysis.

$$\phi_c F_{cr} \geq \sigma_{ef} \tag{3.9}$$

where

ϕ_c = resistance factor for compressive stability

F_{cr} = critical buckling stress given by $\dfrac{F_y}{\sqrt{1+\lambda^4}}$ in which F_y is taken as the Specified Minimum Yield Strength and effective slenderness factor for shell buckling is given by $\lambda = \sqrt{\left(\dfrac{F_y}{\sigma_{ef}}\left[\dfrac{f_a}{F_{ea}} + \dfrac{f_b}{F_{eb}} + \dfrac{f_\theta}{F_{e\theta}} + \dfrac{\tau_{z\theta}}{F_{ev}}\right]\right)}$

where

f_a = axial stress $(= n|\sigma_a|)$

f_b = bending stress $(= n|\sigma_b|)$

f_θ = circumferential stress $(= n|\sigma_\theta|)$

$\tau_{z\theta}$ = shear/torsion stress

n = 0 where σ_a, σ_b or σ_θ is positive (tensile)

1 where σ_a, σ_b or σ_θ is positive (compressive)

for axial compression, $F_{ea} = k_a \dfrac{\pi^2 E}{12(1-\upsilon^2)}\left(\dfrac{t}{L}\right)^2$, in which axial compression buckling coefficient k_a can be calculated by following in the absence of more detailed information; $k_a = \sqrt{1+(K_a\xi)^2}$, where $K_a = \dfrac{0.36}{\sqrt{1+\dfrac{D}{300t}}}$

for bending, $F_{eb} = k_b \dfrac{\pi^2 E}{12\left(1-\upsilon^2\right)}\left(\dfrac{t}{L}\right)^2$ in which bending compression buckling coefficient k_b can be calculated by following in the absence of more detailed information; $k_b = \sqrt{1+\left(K_b \xi\right)^2}$, where $K_b = \dfrac{0.36}{\sqrt{1+\dfrac{D}{300t}}}$

for shear/torsion, $F_{e\upsilon} = k_\upsilon \dfrac{\pi^2 E}{12\left(1-\upsilon^2\right)}\left(\dfrac{t}{L}\right)^2$ in which shear/torsion buckling coefficient k_υ can be calculated by following in the absence of more detailed information; $k_\upsilon = 5.34\sqrt{1+0.009\zeta^{3/2}}$ for $\dfrac{L}{D} \le 0.963\dfrac{D}{\sqrt{t}}$ or $F_{e\upsilon} = 0.636E\left(\dfrac{t}{D}\right)^{3/2}$ for $\dfrac{L}{D} > 0.963\dfrac{D}{\sqrt{t}}$

for external pressure, $F_{e\theta} = k_\theta \dfrac{\pi^2 E}{12\left(1-\upsilon^2\right)}\left(\dfrac{t}{L}\right)^2$ in which external pressure buckling coefficient k_υ can be calculated by following in the absence of more detailed information; $k_\theta = 4\sqrt{1+0.025\zeta}$ for $\dfrac{L}{D} \le 0.563\dfrac{D}{\sqrt{t}}$ or $F_{e\theta} = E\left(\dfrac{t}{D}\right)^2$ for $\dfrac{L}{D} > 0.563\dfrac{D}{\sqrt{t}}$ where $\zeta = \dfrac{2L^2}{Dt}\sqrt{1-\upsilon^2}$

in which E is the modulus of elasticity, υ is the Poisson's Ratio, t is the pipe wall thickness, and L is the distance between points of supports

σ_{ef} = maximum factored combined effective stress

3.4 Design of Process Piping

Besides the limit states codes, the ASME B31.3 Process Piping Code is based on working stress design and consists of equations to determine the stress levels in a piping system and compares them with allowable stress limits, which are generally determined by multiplying the yield strength of the pipe material with predefined safety factors. The code equations are based on the maximum principal stress failure theory and maximum shear stress failure theory (Tresca). Since the fundamental approach of the code is limiting stresses in the pipe wall within the elastic range of the deformation, no distinction is made between pipes that are capable of developing their fully plastic capacity and those that fail prior to the attainment of the plastic capacity.

3.5 Design of Tubular Members in Offshore Structures

3.5.1 API Code

The American petroleum institute API RP 2A-LRFD-93 code is a recommended practice for construction of offshore platforms. The recommendations given for the design of cylindrical members are valid for cylinders with $t \geq 6$ mm, $D/t \leq 300$, and materials with yield strength less than 414 MPa.

Pipe Sections under Pure Axial Force

According to Clause D.2.1, cylindrical members under axial tensile loads are required to satisfy the requirement.

$$f_t \leq \phi_t F_y \tag{3.10}$$

in which F_y is the nominal yield strength, f_t is the axial tensile stress due to factored loads, and ϕ_t is the resistance factor for axial tensile strength (=0.95). According to Clause D2.2 of the recommended practice, members under axial compression are required to satisfy Eq. 3.11.

$$f_c \leq \phi_c F_{cn} \tag{3.11}$$

where

F_{cn} = nominal axial compressive strength given either by:

$\left[1.0-0.25\lambda^2\right]F_y$ when $\lambda < \sqrt{2}$ or

$\frac{1}{\lambda^2}F_y$ when $\lambda \geq \sqrt{2}$

in which $\lambda = \frac{KL}{\pi r}\left[\frac{F_y}{E}\right]^{0.5}$,

where

λ = column slenderness parameter,

E = modulus of elasticity,

K = effective length factor,

L = un-braced length, and

r = radius of gyration

f_c = axial compressive stress due to factored loads, and

ϕ_c = resistance factor for axial compressive strength (=0.85)

The recommendation does not provide an equation to categorize local buckling and allows the use of thin sections, which would buckle locally before the attainment of the yield strength. However, in the calculation of compressive strength F_{cn}, in order to account for interaction between local buckling and column buckling modes of failure, the standard introduces a modification on F_y. It stipulates the substitution of smaller of nominal elastic buckling strength, F_{xe} or inelastic local buckling strength, F_{xc} for F_y. Stresses F_{xe} and F_{xc} can be calculated by Eqs. 3.12 and 3.13, respectively.

$$F_{xe} = 2C_xE\left(\frac{t}{D}\right) \tag{3.12}$$

$$F_{xc} = F_y \qquad \text{for } D/t \leq 60 \tag{3.13a}$$

$$F_{xc} = \left[1.64-0.23\left(\frac{t}{D}\right)^{1/4}\right]F_y \qquad \text{for } D/t > 60 \tag{3.13b}$$

where

C_x = critical elastic buckling coefficient (The theoretical value is 0.6 but a reduced value of 0.3 is recommended)

Pipe Sections under Pure Bending

The practice recommends the application of Eq. 3.14 in the design of cylindrical members against pure bending.

$$f_b \leq \phi_b F_{bn} \tag{3.14}$$

where

f_b = M/S bending stress due to factored loads ($M \leq M_p$; when $M>M_y$, f_b is the equivalent bending stress),

S = elastic section modulus,

M = applied bending moment,

M_p = plastic moment,

M_y = elastic yield moment,

ϕ_b = resistance moment for bending strength (=0.95), and

F_{bn} = nominal bending strength in stress unit (MPa), which can be calculated as

$(Z/S)F_y$ for $D/t \leq 10340/F_y$,

$\left[1.13 - 2.58\left(F_y D/Et\right)\right](Z/S)F_y$ for $10340/F_y < D/t \leq 20680/F_y$,

$\left[0.94 - 0.76\left(F_y D/Et\right)\right](Z/S)F_y$ ....for $20680/F_y < D/t \leq 300$.

In the above definitions, Z is the plastic section modulus

Pipe Sections under Axial Force and Bending

In the design of fabricated cylindrical members under axial tensile force and bending, the API Practice for Planning and Design of Fixed Offshore Platforms (1993) recommends satisfying Eq. 3.10 and the following interaction equation (Eq. 3.15) at all cross-sections along the length of the member.

$$1-\cos\left[\frac{\pi}{2}\frac{(f_t)}{\phi_t F_y}\right]+\frac{\left[(f_{by})^2+(f_{bz})^2\right]^{0.5}}{\phi_b F_{bn}}\leq 1 \tag{3.15}$$

where

f_{by} = bending stress about member y-axis (in plane) due to factored loads

f_{bz} = bending stress about member z-axis (out-of-plane) due to factored loads

When the cylindrical members are under axial compression and bending Eq. 3.11 along with Eqs. 3.16a and b must be satisfied for all sections of the member along its length.

$$\frac{f_c}{\phi_c F_{cn}}+\frac{1}{\phi_b F_{bn}}\left\{\left[\frac{C_{my}f_{by}}{\left(1-\frac{f_c}{\phi_c F_{ey}}\right)}\right]^2+\left[\frac{C_{mz}f_{bz}}{\left(1-\frac{f_c}{\phi_c F_{ez}}\right)}\right]^2\right\}^{0.5}\leq 1 \tag{3.16a}$$

$$f_c<\phi_c F_{xc} \tag{3.16b}$$

where

C_{my}, C_{mx} = reduction factors corresponding to the member y-axis and z-axis, respectively. They are calculated depending on the bracing conditions as a function of ratio of the smaller end moment to the larger end moment (M_1/M_2) of the section or $f_c/\phi_c F_e$,

F_{ey}, F_{ex} = Euler buckling strengths corresponding to the member y and z axis, respectively given by $F_{ey}=F_y/\lambda_y^2$ and $F_{ez}=F_z/\lambda_z^2$, and

λ_y, λ_z = column slenderness parameters for the member y and z axes, respectively, calculated by $\lambda=\frac{KL}{\pi r}\left[\frac{F_y}{E}\right]^{0.5}$ by taking the properties (K, L, and r) of the member in the direction considered

3.6 Design of Circular Hollow Structural Members

In this section, the approach of North American codes (The Canadian Steel Standards, CAN/CSA-S16-01 and LRFD Specification for Structural Steel Buildings, 1999) in the design of circular HSS members under combined loads is presented.

3.6.1 The Canadian Steel Standards, CAN/CSA-S16-01

Pipe sections under pure axial forces

The Canadian Steel Standards (CAN/CSA-S16-01) categorizes circular hollow structural steel sections into four classes according to their diameter to thickness ratios. These four classes are defined as follows:

(a) **Class 1** sections (plastic design sections) will attain the plastic capacity and subsequent significant redistribution of the load;

(b) **Class 2** sections (compact sections) will attain the plastic capacity but need not to allow for subsequent significant redistribution of the load considered;

(c) **Class 3** sections (non-compact sections) will attain the yield capacity but not the plastic capacity; and

(d) **Class 4** sections will generally undergo local buckling prior attaining yield capacity (Should be designed according to North American Specification for the Design of Cold-Formed Steel Structural Members, CAN/CSA S136-01).

According to the standard, a pipe section under pure axial compression can be considered to meet Class 3 requirements when $D/t \leq 23000/F_y$, which ensures that local buckling will not occur prior attaining the member axial compression capacity as determined by Section 13.3 of the code CAN/CSA S16-01, which takes into consideration the interaction between cross-sectional yielding, global buckling, and residual stresses of the member.

Pipe sections under pure bending

According to CAN/CSA-S16-01, for a circular hollow section under pure flexure, when the condition $D/t \leq 18{,}000/F_y$ is satisfied (Class 2 requirement), the member can be designed according to its plastic moment capacity ($M_p = F_y Z$ in which M_p is the plastic moment capacity, F_y

is the yield strength, and Z is the plastic section modulus). Members satisfying Class 3 requirements ($D/t \leq 66{,}000/F_y$) should be designed according to their elastic moment capacity ($M_y = F_y S$ in which M_y is the elastic moment capacity and S is the elastic section modulus).

Pipe sections under axial force and bending

In the design of wide flange sections, square or rectangular HSS sections or channels, which have webs subjected to compressive axial force and bending (beam columns), CAN/CSA-S16-01 uses different classification equations than pure bending and pure axial force cases. The web of a section is classified as Class 1 if $h/w \leq \left(1100/\sqrt{F_y}\right)\left(1-0.39\left(C_f/Cy\right)\right)$ in which h is the height of the web, w is the thickness, C_f is the axial load on the beam-column, and C_y is the axial compression capacity. It is considered as Class 2 if the web satisfies the condition $\left(1100/\sqrt{F_y}\right)\left(1-0.39\left(C_f/Cy\right)\right) < h/w \leq \left(1700/\sqrt{F_y}\right)\left(1-0.61\left(C_f/Cy\right)\right)$. Class 3 sections should satisfy the condition $\left(1700/\sqrt{F_y}\right)\left(1-0.61\left(C_f/Cy\right)\right) < h/w \leq \left(1900/\sqrt{F_y}\right)\left(1-0.65\left(C_f/Cy\right)\right)$. A set of design equations is provided, which approximates the convex plastic interaction relations for sections under axial force and bending by two straight lines depending on their classification. However, there are no classification rule given for circular hollow sections under combined bending and axial compression.

3.6.2 LRFD Specification for Structural Steel Buildings (1999)

Pipe sections under pure axial forces

LRFD Specification for Structural Steel Buildings (1999) classifies steel sections as follows:

(a) **Compact** sections, which will attain their plastic capacity under the load considered (Class 1 and 2 in CAN/CSA-S16-01) and

(b) **Non-compact** sections, which will attain their yield capacity under the load considered (Class 3 in CAN/CSA-S16-01), and

(c) **Slender** sections, which will buckle locally before the attainment of the yield capacity (Class 4 in CAN/CSA-S16-01).

For a circular hollow section under pure axial force, a section is categorized as minimum non-compact if $D/t \le 0.11E/F_y$ where E is the modulus of elasticity of the pipe steel. The axial compressive capacity of these circular hollow steel columns can be calculated by an equation, which takes into account the interaction between cross-sectional yield strength and global flexural buckling of the member.

Pipe sections under pure bending

For a circular hollow section to qualify as compact under flexure, the requirement $D/t \le 0.07E/F_y$ must be satisfied. The section would be non-compact if $0.07E/F_y < D/t \le 0.31E/F_y$ while a section with $D/t > 0.31E/F_y$ is considered as slender. In LRFD (1999), no distinction is made between Class 1 and 2 sections as both are classified as "compact" sections. For compact circular sections, the flexural capacity, M_n, is taken equal to M_p, where $M_p = F_y Z$ and for non-compact circular sections M_n is calculated by $\{[0.021E/(D/t)] + F_y\}S$.

Pipe sections under axial force and bending

In LRFD (1999), as in Canadian Steel Standards CAN/CSA S16 (2001), classification equations are provided for W sections, channels, and square or rectangular HSS sections depending on the slenderness of their webs. However, no classification rule is given for circular HSS sections under the combined action of bending and axial compression. A bilinear design interaction equation (different from that of CAN/CSA S16-01) is provided in the LRFD (1999).

3.6.3 The Canadian standard on design of cold-formed steel members (CAN/CSA S136-01)

Pipe sections under pure axial forces

CAN/CSA S136-01 requires $C_r = \phi_a A_e F_p$ to be satisfied for tubular sections under axial compression, which satisfy the condition; $D/t < 0.441E/F_y$ in which ϕ_a is the resistance factor (=0.9), A_e is the effective cross sectional area of a member in compression, and F_p is the compressive limit stress under compression (F_p=0.833F_e). In this equation when E is set equal to 200,000MPa, it will take the form $D/t < 88{,}000/F_y$, a condition that is easily met for pipe sections used in the oil and gas industry. An exception takes place when F_y is very high.

For these sections,

when $F_p \le F_y/2$, A_e=A,

when $F_p > F_y/2$ and $D/t \le 0.113E/F_y$, A_e=A,

and when $F_p > F_y/2$ and $0.113E/F_y < D/t \le 0.441E/F_y$, $A_e = A_o + \left[\left(F_y/\left(2F_p\right)\right)\left(A - A_o\right)\right]$.

In these equations A is the unreduced cross-sectional area and $F_e = \pi^2 E/\left(KL/r\right)^2$.

Pipe sections under pure bending

According to CAN/CSA S136-01, pipe sections under bending with D/t not exceeding $0.441E/F_y$ are required to satisfy $M_r = \phi S_c F_c$ in which ϕ is the resistance factor (=0.9), S_c is the compressive section modulus based on moment of inertia of effective cross-sectional area divided by distance from centroidal axis to the extreme compression fiber. The buckling stress F_c is calculated based on D/t ratios.

$$F_c = 1.25F_y \qquad \text{for } D/t \le 0.07\,E/F_y \qquad (3.17a)$$

$$F_c = \left[0.965 + 0.02\left(E/F_y\right)/\left(D/t\right)\right]F_y \qquad \text{for } 0.07\,E/F_y < D/t \le 0.319\,E/F_y \qquad (3.17b)$$

$$F_c = 0.328E/\left(D/t\right) \qquad \text{for } 0.319\,E/F_y < D/t \le 0.441\,E/F_y \qquad (3.17c)$$

Pipe sections under axial force and bending

Two interaction relations are provided by the code. These are to be satisfied by all member types including cylindrical tubular sections. In the interaction relations, the moment and axial compression capacities are calculated as detailed in the previous section on bending moments.

No design rule is given for circular hollow sections under more complex load combinations including twisting moments and shear. The present codes, do not provide the conditions under which pipe sections can develop their plastic capacity when subjected to complex load combinations including torsion, shear, and internal pressure. This issue is addressed in part in the present study.

Chapter 4

Experimental Setup

The first part of this chapter (Section 4.1) presents a review of experimental setups developed in major experimental studies on steel pipes subjected to combined loads. The second part (Section 4.2) presents the details of the test setup designed and constructed as part of the current experimental investigation.

4.1 Experimental Setups in Previous Studies

The test setups used in previous studies includes those of the Berkeley Test Series (Section 4.1.1), the University of Wisconsin Test Series (Section 4.1.2), the University of Toronto Test Series (Section 4.1.3), the University of Alberta Test Series (Section 4.1.4), the University of Ottawa Test Series (Section 4.1.5), and C-Fer Test Series (Section 4.1.6). These are detailed in the following sections.

4.1.1 Berkeley Test Series

A typical test setup for the Berkeley Test Series (Bouwkamp and Stephen, 1973) is shown in Fig. 4.1. The experiments were a four-point bending test with the addition of the internal pressure (p) and axial force (A). The 3,353 mm long test section was fabricated by full-penetration welding of two 1,677 mm long, 1,220 mm OD grade X60 pipes with a Specified Minimum Yield Strength ($SMYS$) of 414 MPa and a nominal wall thickness of 11.7 mm. (D/t = 104). In order to reduce the possibility of premature buckling in the end sections, these parts are fabricated from grade X65 pipe ($SMYS$ = 448 MPa) with a nominal wall thickness of 14.3 mm. The tests are conducted under constant internal pressure, constant axial force, and step-wise increasing lateral deformation which induced pure bending moments along the test section.

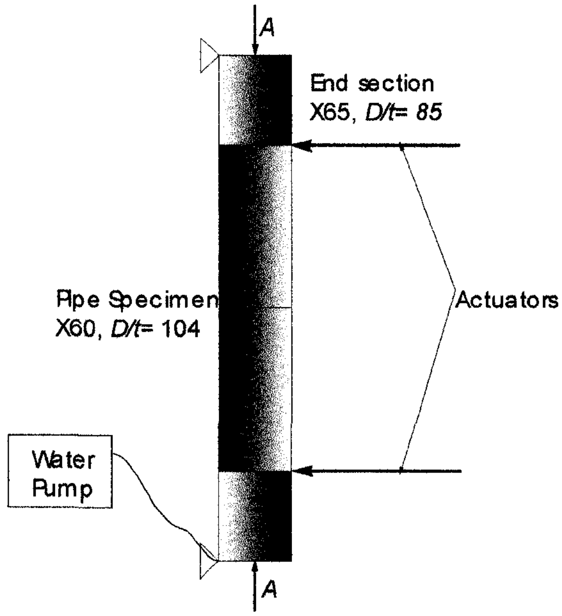

Fig. 4.1 Test Setup of Bouwkamp and Stephen

4.1.2 University of Wisconsin Test Series

Since one of the parameters investigated in the Wisconsin Test Series (Sherman 1976) was the effect of end conditions on pipe behavior, three different test setups with different support conditions were adopted. These setups include a four-point bending setup with simply supported ends (Fig. 4.2a), a four-point load bending with fixed ends (Fig. 4.2b), and cantilevers with end load (Fig. 4.2c).

(a) Four-Point Bending Tests with Simple Supports

(b) Four-Point Bending Tests with Fixed Supports

(c) Cantilever Tests

Fig. 4.2 Test Setup

4.1.3 University of Toronto Test Series

The Toronto Test Series (Prion and Birkemoe 1987) setups used can be seen in Fig. 4.3. Six 10 m long specimens were tested as four-point bending tests with the addition of a horizontally applied axial load A (Fig. 4.3a). The remaining specimens tested were loaded eccentrically (Fig. 4.3b) or concentrically (Fig. 4.3c) depending on the load combination sought.

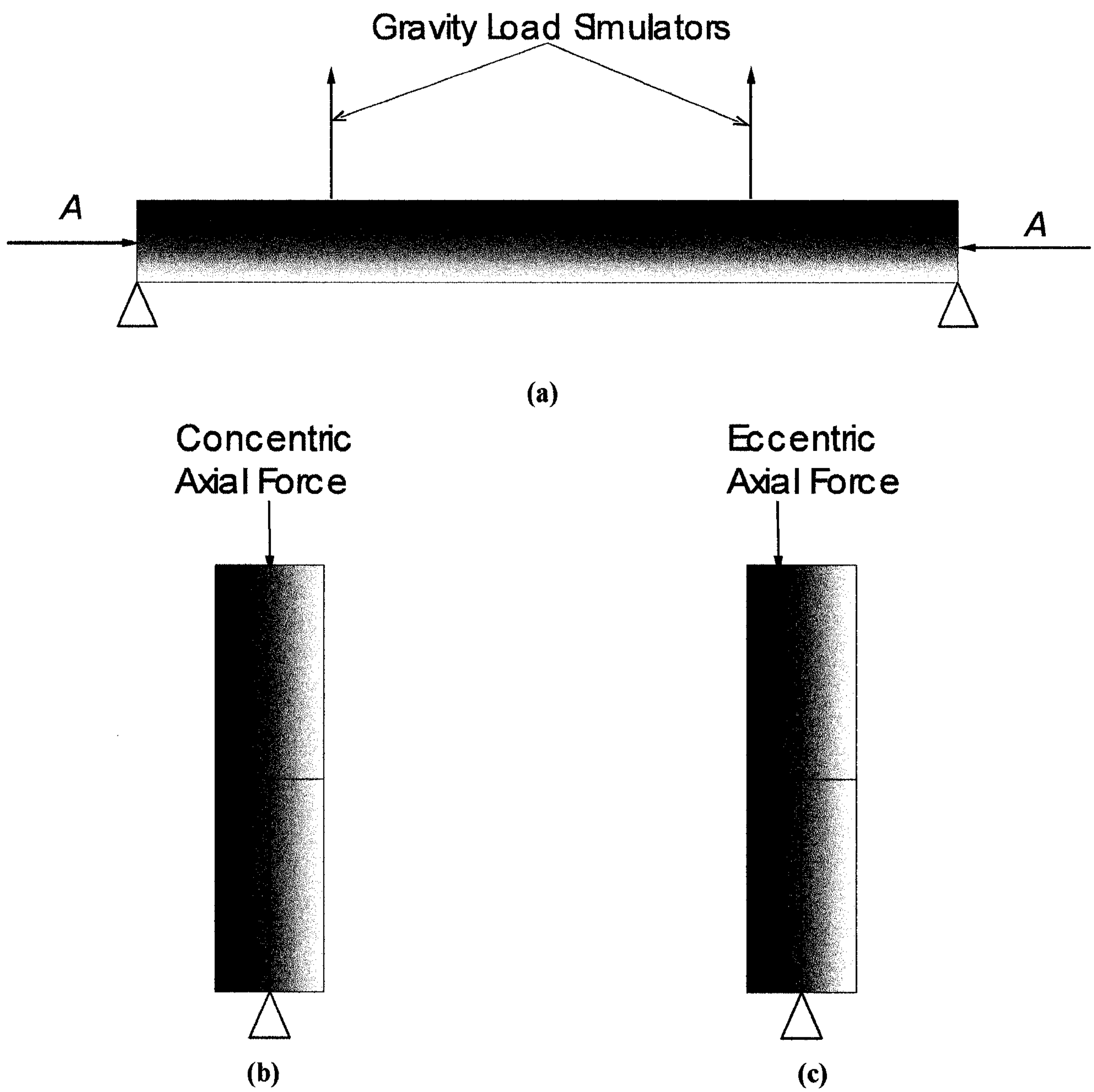

Fig. 4.3 Test Setup (Toronto Test Series)

4.1.4 University of Alberta Test Series

The University of Alberta tests (Mohareb et al 1994, Yoosef-Ghodsi 1995, and Dorey et al. 1999) are conducted as eccentrically loaded beam columns (Fig. 4.4). Specimens are welded between two loading arms through end plates and concentrically located under the head of the universal testing machine, which applies axial loading to the specimen. A hydraulic jack was placed eccentrically between the loading arms in order to apply bending moments and axial load on the specimen, independent of the axial load exerted by the universal testing machine. Internal pressure was applied to the specimen by filling it with pressurized water using a pneumatically operated pump.

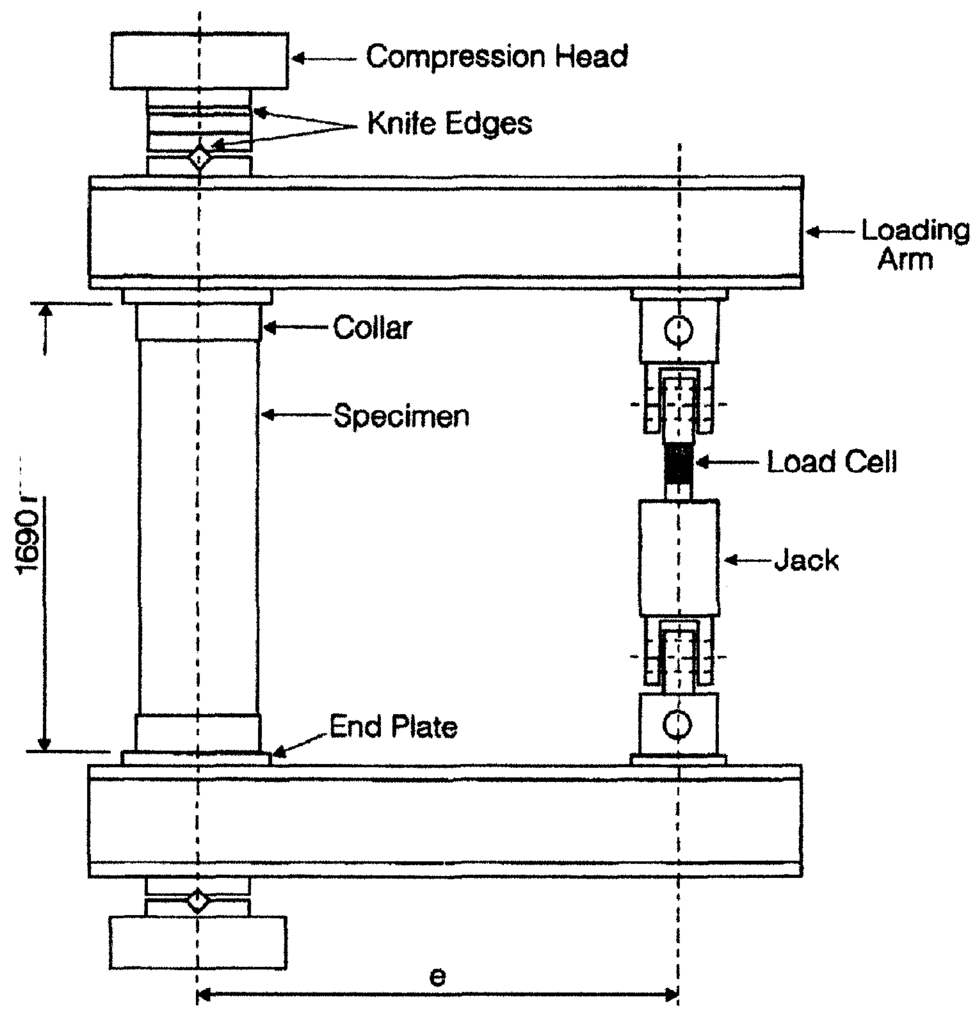

Fig. 4.4 Test Setup of the University of Alberta (from Mohareb et al. 1994)

4.1.5 The C-FER Test Series

The C-Fer Test Series (Zimmerman et al. 1995 and 2004) were conducted under two different setups. Initially, pipes were tested in a four-point bending test setup (Zimmerman et al. 1995) conceptually resembling the one used in Berkeley Test Series. Later on, the setup was changed to a setup resembling the one used in the University of Alberta test series with a pipe specimen located under the head of a universal testing machine which applies a concentric axial forces while bending to the specimen was applied by an eccentrically located actuator (Zimmerman et al. 2004).

4.1.6 University of Ottawa Test Series

The test setup developed (Ozkan and Mohareb 2003) in order to apply combinations of torsion, shear, and bending to pipe specimens is illustrated in Fig. 4.5. The pipe specimen was welded to a thick base plate, which was connected to the thick concrete floor by means of anchor rods. The loading arm welded on the specimen consisted of a built up section, which had three sets of four holes along its length in order to provide three possible attachment locations for the hydraulic jack to vary the eccentricity, *b*, accordingly. An MTS hydraulic actuator was used to provide a horizontal force at an eccentricity, *b*, from the centerline of the specimen. The actuator was pin connected at one end to the loading arm and to a stiff loading frame at the other end. The height of the specimen was varied in order to change the moment arm *a*.

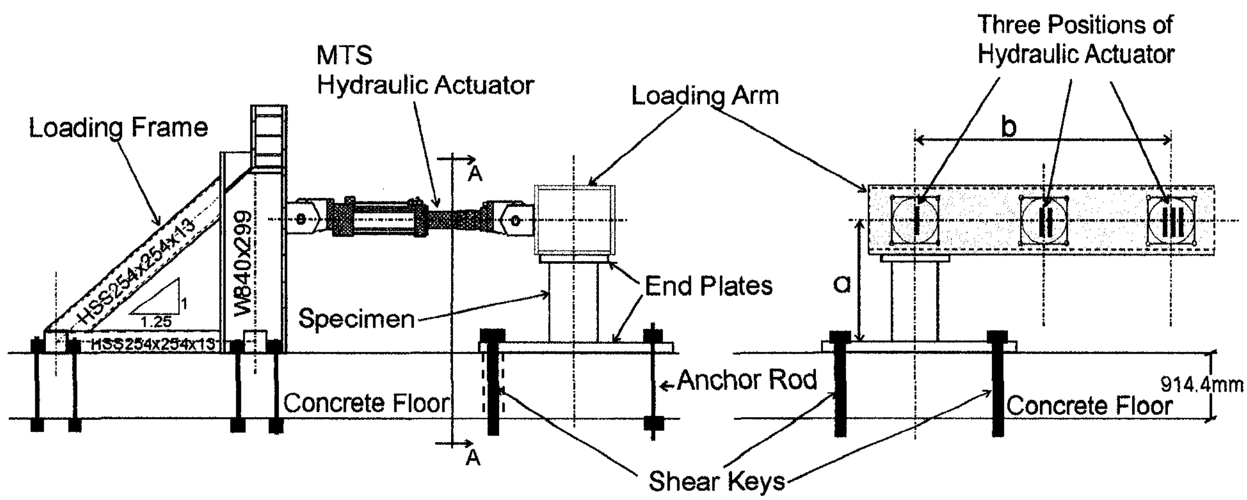

(a) Side view **(b)** Elevation

Fig. 4.5 Test Setup (from Ozkan and Mohareb 2003)

4.2 Setup Developed in the Present Study

The objective of the present study is to test pipes under more general load combinations including axial tension, internal pressure, bending, and torsion to document the pipe local buckling behavior and capacity. In the first series of tests, pipes under internal pressure, axial tension, and bending are tested. In the second series of tests, pipes under internal pressure, axial tension, torsion, and bending are tested. Thus, the test setup developed as part of this study had to be versatile and flexible enough to accommodate these (and other) load combinations. In order to achieve this goal, a new test setup is designed and constructed at the University of Ottawa, Structural Engineering Laboratory.

4.2.1 Main Concepts

The setup is capable of providing complex load combinations to pipe specimens by using multiple MTS actuators. A three dimensional loading arm was designed and constructed as part of the experimental program. The loading arm can be connected to series of horizontal and vertical actuators to achieve the desired load combinations. The potential locations for these actuators are shown by dashed lines in Fig. 4.6. When the horizontal Actuators A, B and C are connected to the loading arm, they are supported by bearing frames (B1, B2, and B3) in their other ends. Base plates and anchor rods are also provided in order to connect the specimen and the vertical Actuators 1, 2, and 3 to the 914mm thick strong concrete floor. A water pump is used to apply the desired internal pressure.

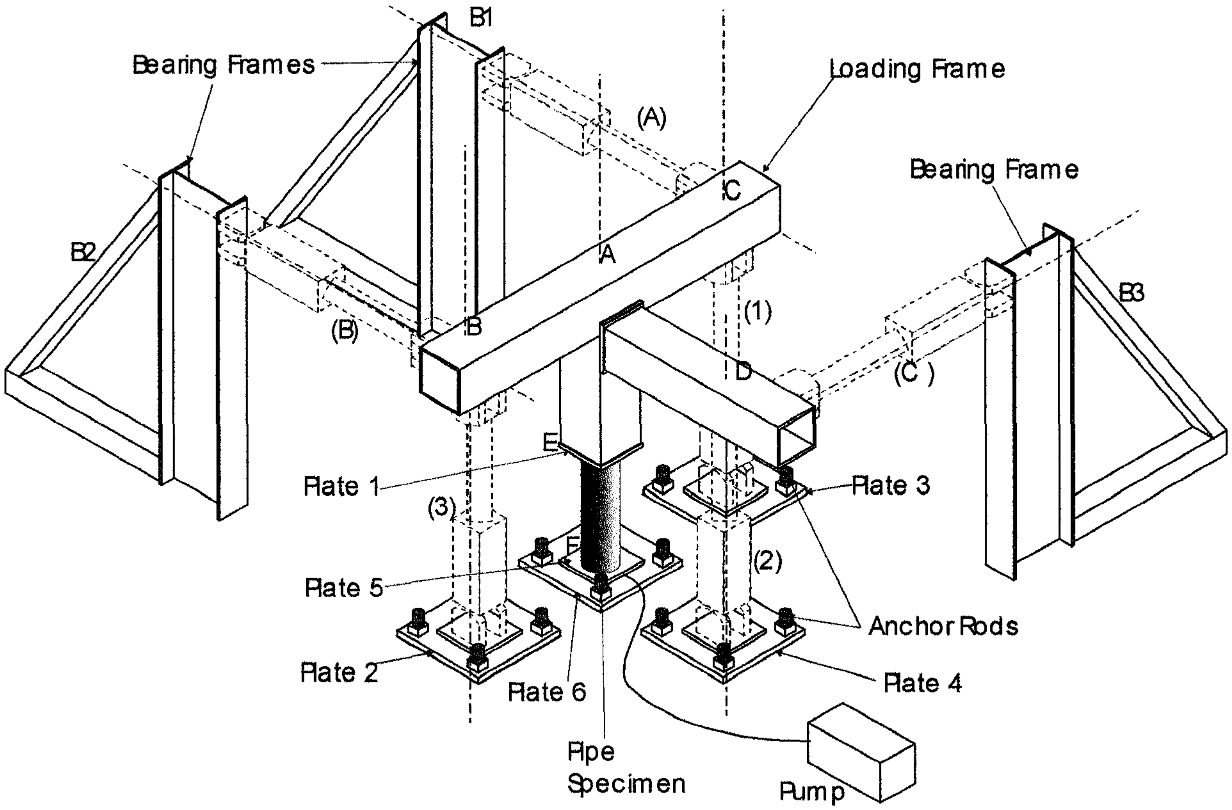

Fig. 4.6 Test Setup and Possible Actuator Positions

4.2.2 Detailed Description

The three-dimensional loading frame is made of four rigidly welded box section arms. Each arm is constructed by welding four 600 mm wide by 25 mm thick steel plates to form a built-up square hollow section. The loading arms are internally stiffened by several transverse plates in order to prevent possible cross-sectional distortions under twisting moments (Refer to Appendix A for the Detailed drawings for the test setup).

In a plan view, the three horizontal arms AB, AC, and AD are arranged in a T shape configuration. Each of the dimensions AB, AC, and AD of the loading arms are 1,828 mm in length. Each arm can be connected to a horizontal and a vertical actuator, as needed. The fourth arm AE is oriented vertically and its bottom end is welded to a 635 mm x 635 mm x 50 mm steel plate (Plate 1 in Fig. 4.6), which is to be welded to the top end of the pipe specimen. The function of the vertical arm AE is to shorten the length, EF of the specimen required for the test, since the dimension AF is dictated by the height of the vertical actuators (1, 2, and 3).

The horizontal arms AB and AC of the loading frame are symmetric with respect to the specimen. By connecting both arms to vertical actuators 1 and 3, and by controlling both actuators to apply equal forces, a pure concentric axial force (compression or tension) can be applied to the specimen. Also, by connecting the two horizontal actuators (A and B) to both arms and controlling their forces to be equal in magnitude and opposite in direction, pure torsion can be applied. The horizontal arm AD can be connected to a third vertical actuator (2), which can be programmed to apply a force eccentric to the specimen in a displacement controlled mode in order to simulate imposed bending deformations to the specimen. For complex loading combinations such as the ones related to the present study, control modules (Ozkan 2007) are developed relating all actuator forces and strokes as desired to control actuators to satisfy any set of user defined constraints.

The top end of the vertical actuators is connected to the loading frame while their bottom end is connected to custom-made spacers concentrically welded to base plates (2, 3, and 4 in Fig. 4.6). The base plates (1219 mm x 1219 mm x 76 mm) are connected to a 915 mm thick strong concrete floor by means of four 75 mm diameter anchor rods.

Each horizontal actuator is connected to the loading frame at one end and to a 3,627 mm high bearing frame at the other end (Figs. 4.6 and 4.7). Intermediate spacers of various geometries are also provided to maximize the use of the available actuator stroke as needed (Fig. 4.7). Each reaction frame is connected to the strong concrete floor through four 75mm diameter anchor rods.

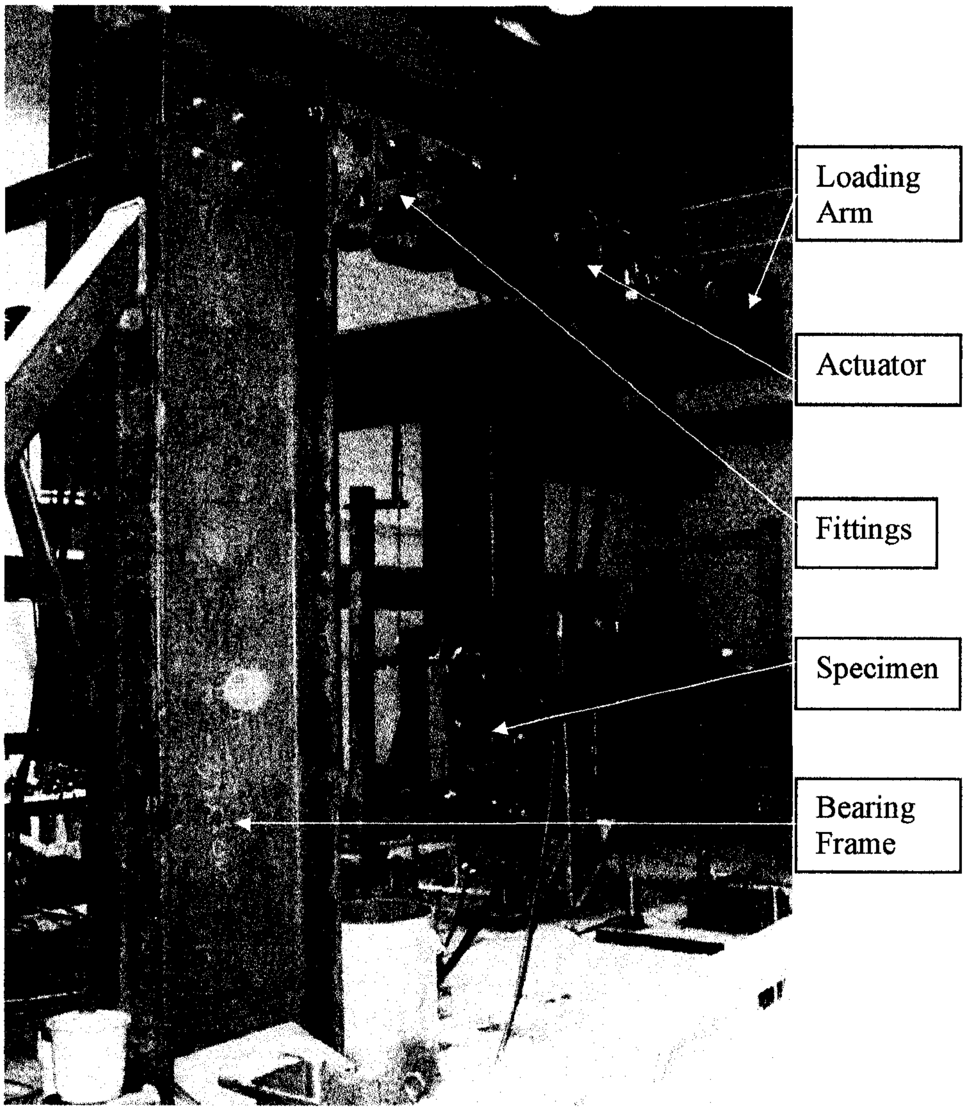

Fig. 4.7 A View from the Test Setup (Bearing Frame + Fittings + Actuator + Loading Arm + Specimen)

At the beginning of a test, the pipe specimen is welded concentrically to plate 5 (635 mm x 635 mm x 50 mm in dimension), which is concentrically welded on plate 6 (1,219 mm x 1,219 mm x 76 mm). The loading arm is inverted so that plane ABCD lies on the floor while plate 1 is oriented upwards. The pipe specimen-plate 6 arrangement is rotated so that the top end of the specimen becomes oriented downwards. The pipe end is then welded to plate 5. The whole plate 6-pipe-loading arm arrangement is then lifted by an overhead crane and rotated though a system of chains and pulleys so that plane ABCD becomes on top again (Fig. 4.8).

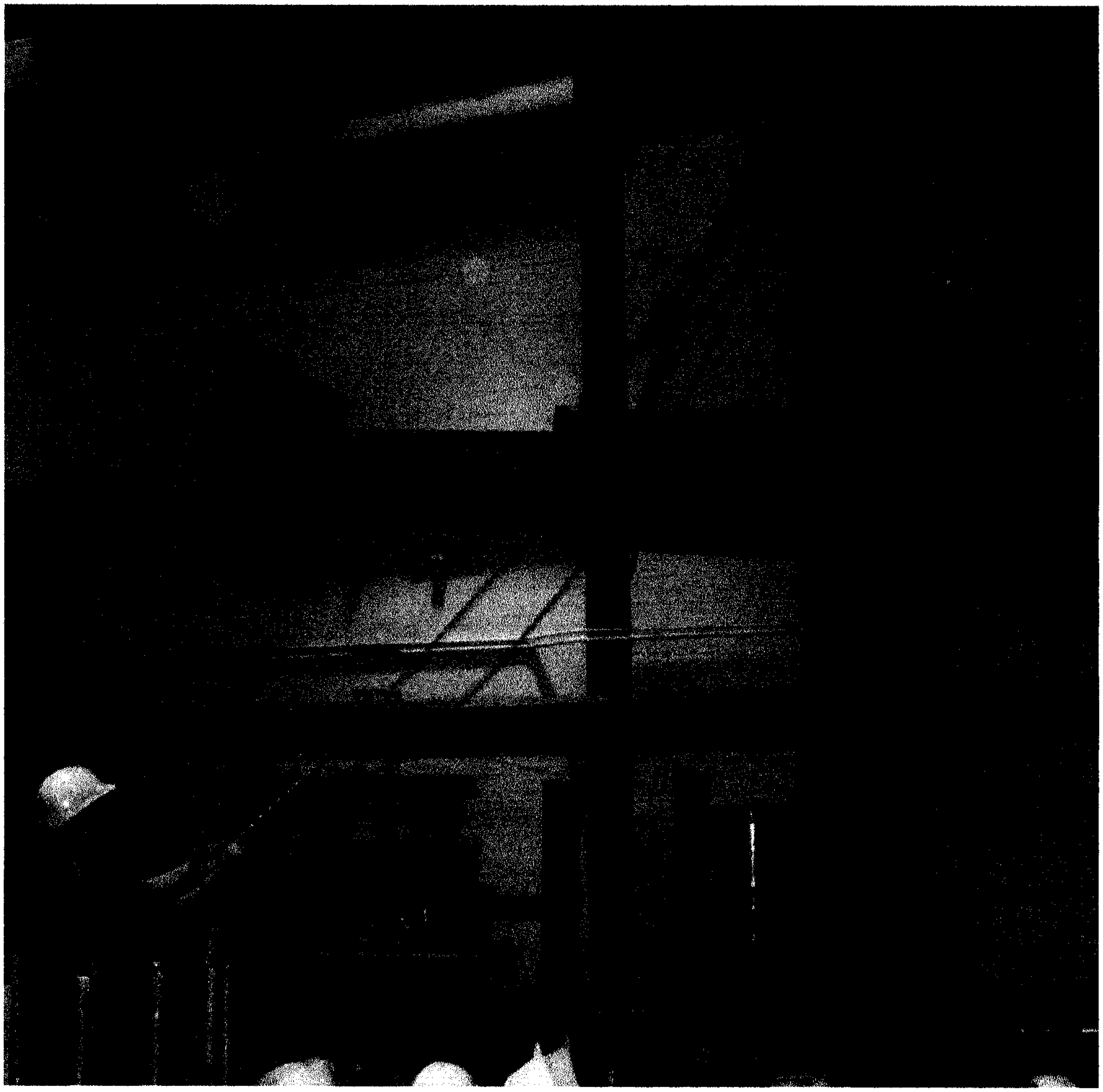

Fig. 4.8 Loading Arm and Welded Specimen are rotated during the Test Setup

Four anchor rods are inserted into plate 6 in order to connect it to the concrete floor. All actuators and necessary spacers are then connected to the loading frame through high-strength bolts.

The internal pressure is applied by filling the inside the specimen with water through an inlet hole located in plate 5. Another bleeding hole in the top plate (Plate 1) allows the dissipation of air as the inside of the pipe is filled with water. The water is then pressurized by an electrically operated water pump until the target pressure value is reached. End forces take place on the bottom of the top plate leading to a net axial tensile force (A_i) in the pipe wall of $(\pi D_i^2/4)\times p$ in which D_i is the inside diameter of the pipe and p is the applied internal pressure. Throughout the test, the volume within the pipe changes as a result of pipe deformations. The internal pressure changes accordingly. Thus, when a pressure change is detected by the pressure gages, it is restored to its target value either by pumping additional water using an electric pump or by releasing water through the bleeding hole in Plate 1.

At the end of each test, all actuators are disconnected and the loading arm is inverted so that plane ABCD rests on the floor while plate 6 is positioned on top. The specimen is flame cut at both ends. The top plate and the bottom plates (plates 1 and 5) are ground smooth. The procedure is then repeated for the next specimen.

By using the actuators in locations (1), (2), and (3), axial load and bending moment combinations can be applied. Also, by using the actuators in locations (A), (B), and (C) bending moment, twisting moment, and shear force combinations can be applied to pipe specimens.

4.2.3 Description of Main Components

In this section, a brief description of different components of the test setup is presented. These components include the actuators, loading arm, bearing frames, fittings, and water pump.

4.2.3.1 Actuators

The actuators available at the U of O structural engineering laboratory are MTS jacks, with a maximum stroke of 508 mm. Three actuators (Type 243.70t) have a capacity of 1,459 kN in compression and 961kN in tension. The fourth actuator (Type 243.60t) has a capacity of 1013 kN in compression and 648 kN in tension. Both ends of actuators are pin connected to swivel ends. Thus, all actuator ends can be considered to be pin-connected about both axes. The swivels are connected to the setup fittings (spacers, loading arms, etc.) by means of four 38 mm diameter bolts. A representative picture of the actuators is presented in Fig. 4.9.

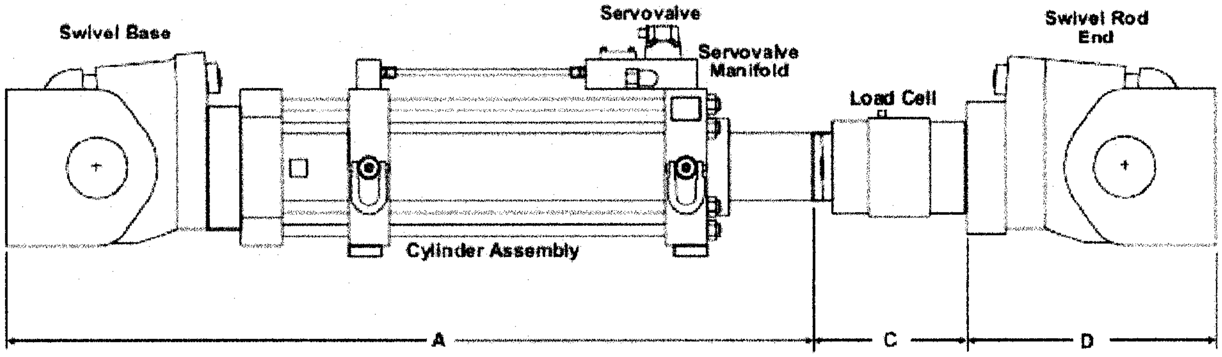

Fig. 4.9 Actuators available at the University of Ottawa Structural Engineering Laboratory

Also, Table 4.1 presents the dimensions of both actuator types available.

Table 4.1 Actuator Dimensions

Type	**Stroke**	**Cylinder w/ Swivel Base *(A)**	**Load Cell & Mounting Hardware Length **(C)**	**Swivel Head Length **(D)**
243.60t	500	1803	489	457
243.70t	500	1943	457	546

*Dimensions are lengths with the actuator positioned at mid-stroke
**Dimensions include spiral washers or other mounting hardware for attachment of the load cell and swivel head assembly

4.2.3.2 Loading Arm

Loading arm is a member of the experiments through which complex load combinations are applied to the pipe specimen (Fig. 4.10). A T-shape from plan view and L-shape from elevation (Fig. 4.10a and Fig. 4.10b, respectively) is selected for the loading arm in order to be able to attach the actuators in different orientations.

During the deformation of the specimen, it is required that the loading arm remains in the elastic range of deformation in order to a) control its deformations throughout the tests and b) to make the loading arm reusable in future tests. Thus, the structural design of the loading arm is undertaken by ensuring this condition is met under the maximum attainable loads of the actuators.

The dimensions of the loading arm were selected to match the foot-print of the actuators, the maximum loads that can be applied on the loading arm, and the spacing of the anchoring mesh available on the thick concrete lab floor. Detailed drawings of the loading arm can be found in Appendix A while a schematic view is presented in Fig. 4.10.

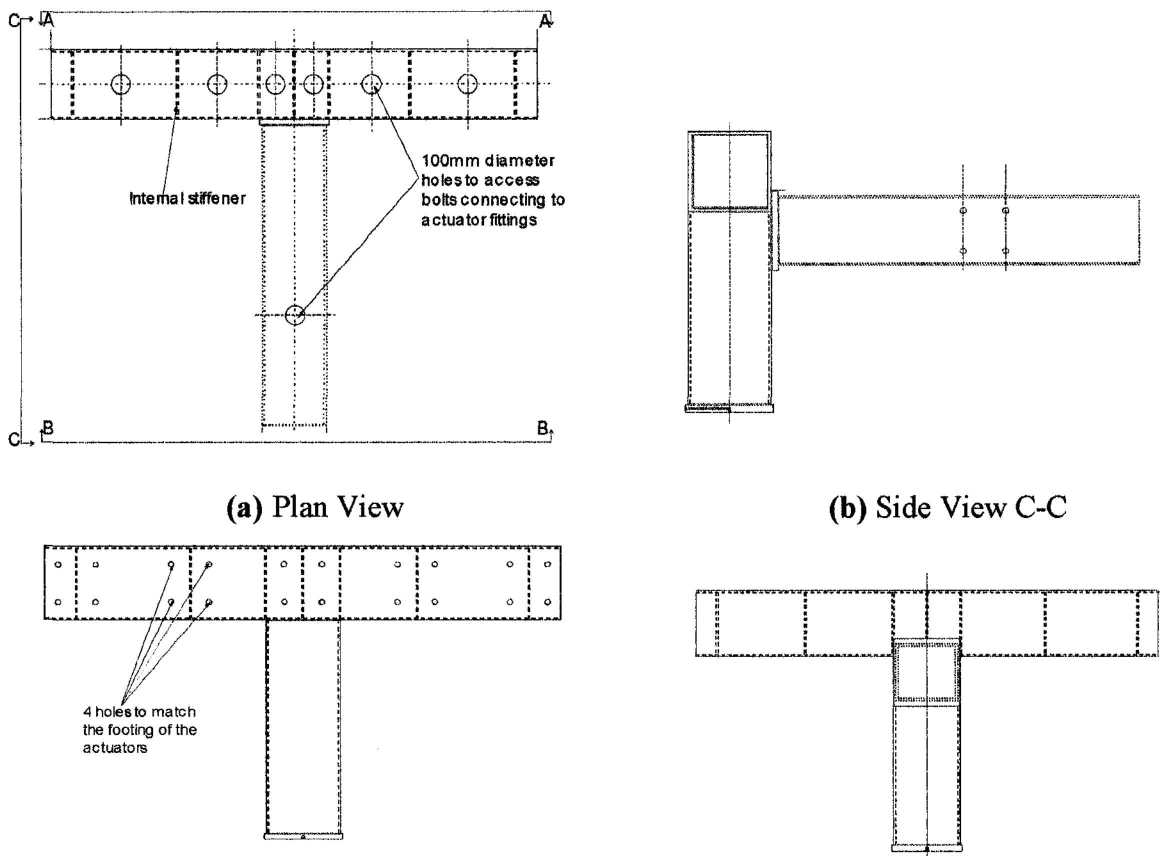

(a) Plan View

(b) Side View C-C

(c) Back View A-A

(d) Front View B-B

Fig. 4.10 Schematic Loading Arm

4.2.3.3 Bearing Frames

Two A-shaped bearing frames were designed and constructed in order to bear the horizontal actuators which were used to apply twisting moments and bending to the pipe specimens (Frames B1 and B2 in Fig. 4.6). The maximum height of the bearing frames were selected to accommodate a 1500mm length pipe specimen welded under the loading arm. The bearing frames were made of a vertical W840x299 section on which actuators are connected by high strength bolts and one diagonal and one horizontal square HSS sections as illustrated in Fig. 4.11. Detailed drawings for the bearing frames are provided in Appendix A.

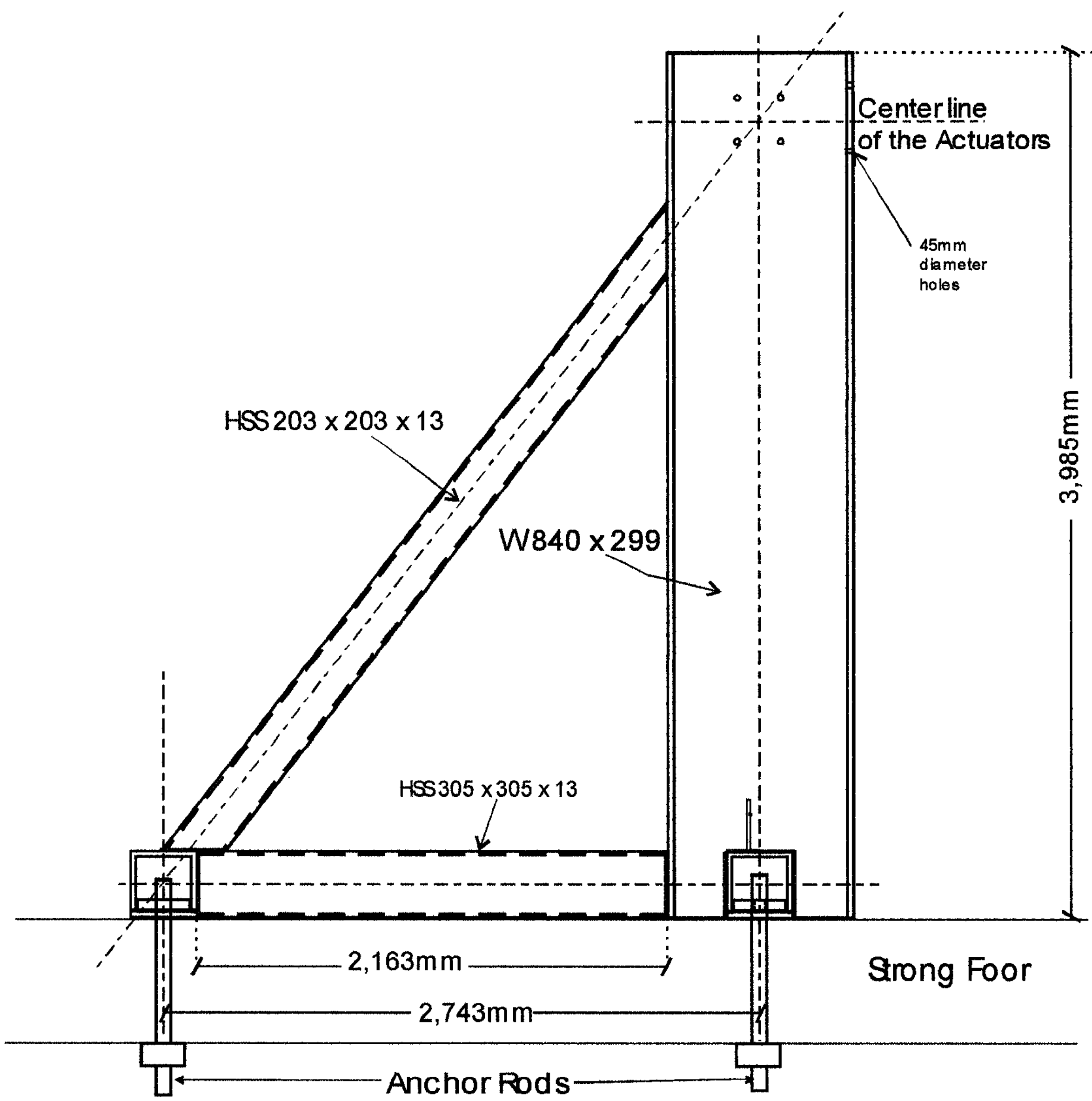

Fig. 4.11 Bearing Frame (Side View)

An existing A-Frame available at the structural engineering lab (Frame B3 in Fig. 4.6) can be used as an additional bearing frame when Actuator C is to be connected. Since the height of this bearing frame is less than that of Frames B1 and B2, the centerline of the arm AD of the loading arm in Fig. 4.6 was placed below that of arm BC in order to position actuators horizontally between arm AD and Bearing Frame B3 (Fig. 4.10b).

4.2.3.4 End Fittings

Spacers, base plates, anchor rods, and a bracing system between the bearing frames are used as part of the test setup. Spacers were used to connect the actuators to the bearing frames (Fig. 4.7) and the base plates, through which the pipe specimen and the actuators are connected to thick concrete floor (Fig. 4.12). Also, in Fig. 6.2 of Chapter 6, the bracings system between bearing frames B1 and B2 is illustrated. The detailed drawings of these items are provided in Appendix A.

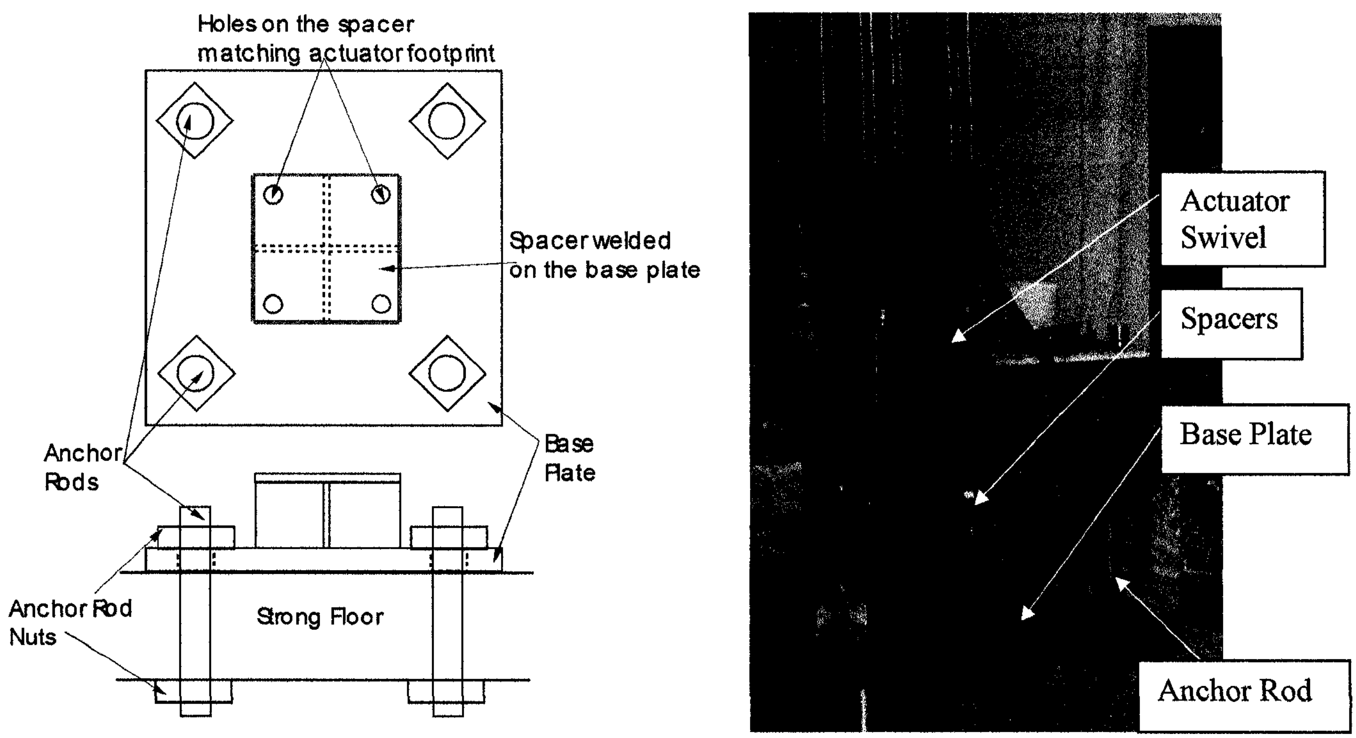

(a) **(b)**

Fig. 4.12 Actuator Swivel, Spacer, Base Plate, and Anchor Rod Arrangement

4.2.3.5 Water Pump

A 15 horsepower electric water pump is used for the application of internal pressure. A picture of the pump with its base saddle can be seen in Fig. 4.13a. The pump is connected to the inlet hole on Plate 5 in Fig. 4.6 through high-pressure hoses and fittings (Fig. 4.13b). During the tests, the pump was operated through an electric toggle switch.

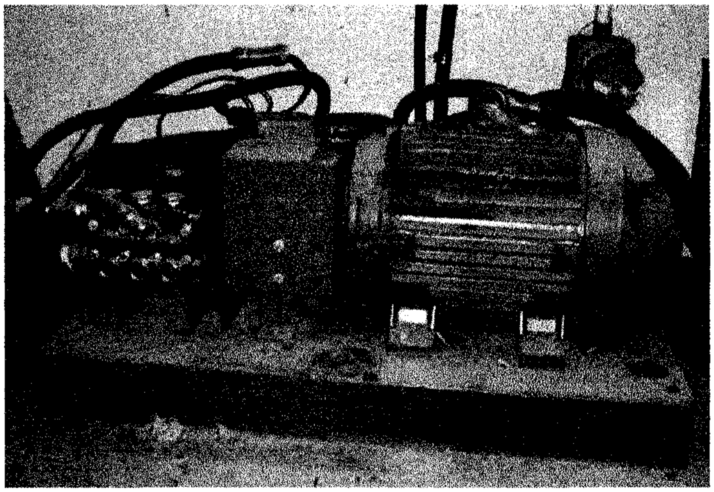

(a) Water Pump

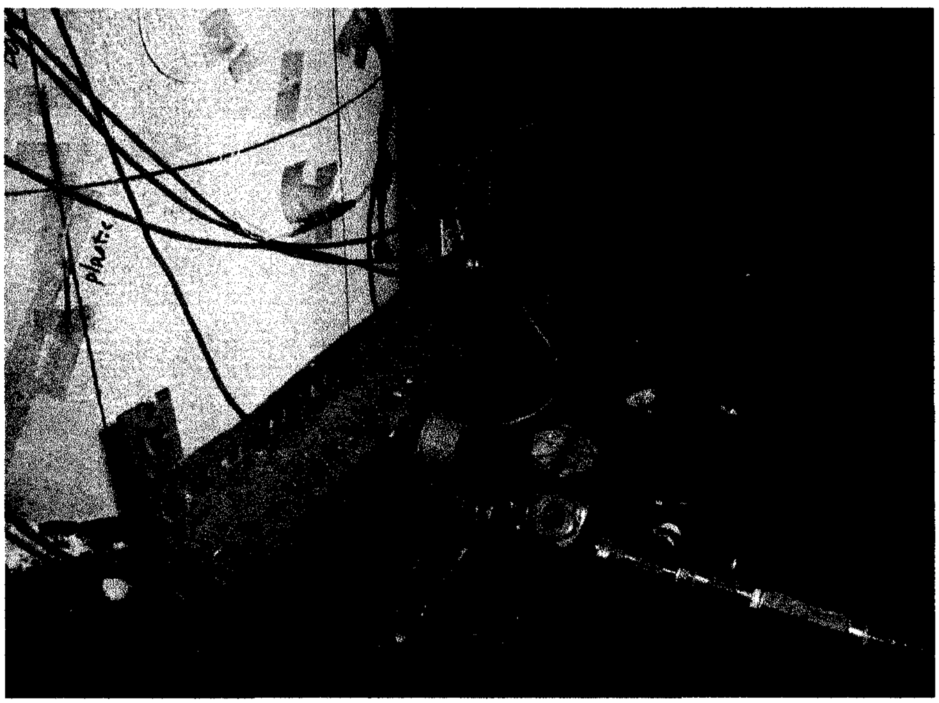

(b) Connection to Plate 5 in Fig. 4.6

Fig. 4.13 Electric Water Pump and Connections

4.2.4 Advantages and Limitations of the Test Setup

The setup described has the advantage of handling complex load combinations including axial forces both compressive or tensile, bending, torsion, shear, and internal pressure. Under the current test configuration, pipe specimens up to 24 in diameters can be tested.

The height of the specimen is dictated to some extent by the dimensions of the vertical actuators (specimen height ranges typically from 1500 mm to 1800 mm). For 20 in OD diameter pipes, this corresponds to a specimen length-to-diameter (L_p/D) ratio of about three. For tests related to local buckling behavior, this ratio has been used by other researchers and is not restrictive.

For loading combinations applying a tensile axial force to the specimen, Actuators 1, 2, and 3 (pin-connected at both ends) will be subjected to high compressive forces. When the pipe specimen is sufficiently stiff, it will tend to preserve the stability of the loading frame, as the lines of action of the three actuators would remain vertical. Conversely, when the pipe softens (through a combination of local buckling and yielding) it is conceivable, under the destabilizing effect of the horizontal components of the forces in the actuators, that the loading arm undergoes in-plane rotation and lateral displacements as depicted in the schematic plan view in Fig. 4.14. Thus, the stability of the loading frame can be a limiting factor in the load magnitudes to be applied to the specimen.

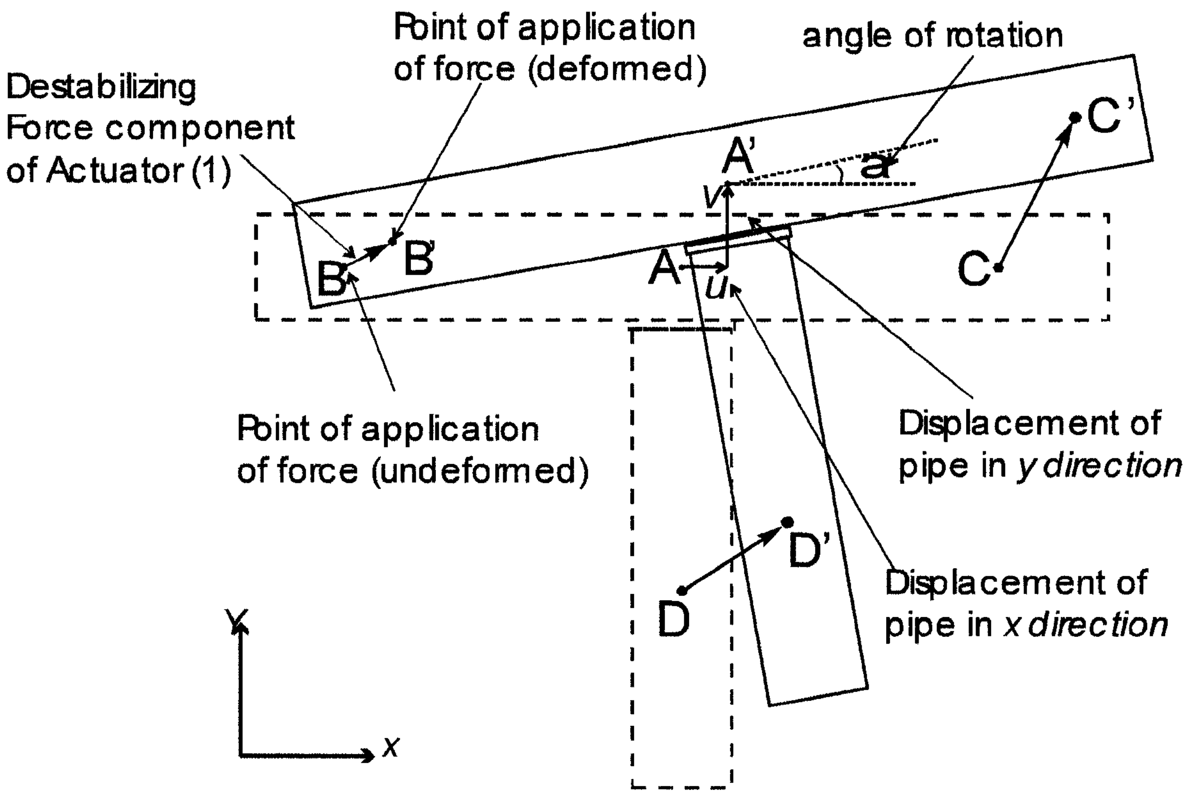

Fig. 4.14 Possible Destabilizing Effects on Loading Frame (Plan View)

While an inherent buckling mechanism is conceivable, it did not take place in the tests conducted within this study.

Chapter 5

Testing and Analysis of Pressurized Pipes under Tension and Bending

In this chapter, the first series of full-scale tests is described. Six tests are conducted on pipe specimens under combinations of internal pressure, axial tension, and monotonically increasing curvatures. The details of the experimental program are presented in Section 5.1. The critical strains and the moment capacity of the specimens are experimentally determined. A nonlinear shell finite element model is also developed using the FEA simulator ABAQUS in order to predict the moment capacity and the local buckling behavior (Section 5.2). The definitions provided and expressions presented in Section 5.3 are necessary to interpret the results and comparisons presented in Section 5.4. The chapter conclusions are presented in Section 5.5. These include the moment vs. curvature relations (Section 5.4.1), critical strain values measured from the tests, their comparison with similar tests from previous studies, and design recommendations (Section 5.4.2), local buckling behavior of the specimens (Section 5.5.3), and a comparison between the peak moments (Section 5.5.4).

5.1 Testing of Steel Pipes

This section presents the details on selection of the pipe specimens (Sub-section 5.1.1), selection of load combinations applied (Sub-section 5.1.2), the specifics of the experimental setup (Sub-section 5.1.3), the load sequence and control (Sub-section 5.1.4), the data acquisition instrumentation (Sub-section 5.1.5), and determination of material properties (Sub-section 5.1.6).

5.1.1 Selection of Pipes

The size of the pipes selected is representative of those typically used in the oil/gas industry. Most oil and gas pipelines in current practice have a D/t ranging between 30 and 100 (Kim and Velasco, 1988). A common pipe size used in the pipeline industry in Alberta which lies within the above limits, is 508mm OD with a thickness of 6.35mm and a corresponding D/t ratio of 80, made of X65 grade steel (SMYS=448MPa). The measured average wall thickness for the specimens tested is 6.26mm and the measured OD is 508mm, corresponding to D/t=81.2.

The local buckling behavior of a pipe segment is generally independent of the specimen length. Therefore, specimens with a length L_p=1,740mm were selected. This length corresponds to about 3.5 pipe diameters.

5.1.2 Load Combinations

Six specimens were tested under combinations of internal pressure, axial tension, and bending. Internal pressure corresponding to hoop stress of 0%, 40%, and 80% of the SMYS were selected. Also, axial tensile forces corresponding to 0%, 20%, and 40% of the longitudinal yield capacity (A_y) are targeted. The loading combinations selected are presented in Table 5.1.

Each specimen is assigned a designation of the form Pxx-Ayy-Mzz in Column 1, in which the descriptors P, A, and M denote the ratios of internal pressure p_r, axial tension A_r, and modified plastic moment ratio $M_r = M_{pm}/M_p$, respectively. The descriptor xx is the target pressure as a percentage ratio to the pressure value that would cause the hoop stresses to attain SMYS in the absence of other internal forces. The xx descriptor takes the values 00, 40, and 80, respectively corresponding to the cases of no internal pressure, internal pressure causing a hoop stress of 40% of SMYS, and 80% of SMYS. Also, the yy descriptor takes the values 00, 20 and 40, denoting the cases of zero axial tension, an axial tensile force of 20% of the yield tensile force (based on SMYS), and 40% of the yield tensile force, respectively. Finally, the zz descriptor denotes the moment capacity as predicted based on the plastic interaction equation (Eq. 1.6) as a percentage ratio the plastic moment capacity of the pipe section in the absence of other internal forces. For example, specimen P40-A40-M89 is initially pressurized until a hoop stress in the pipe wall of 40% SMYS. The target tension force for the specimen is 40% of the pipe axial yield capacity. Under these applied forces, the modified moment capacity M_{pm} of the specimen as predicted by the interaction relation (Eq. 1.6) is 89% of its plastic moment capacity M_p calculated in the absence of other internal forces. Hence, the final descriptor zz takes the value 89. It is noted that all three descriptors xx, yy, and zz, are based on the nominal diameter, nominal thickness, and SMYS as opposed to their measured values.

Table 5.1 Test Load Ratios (all ratios are provided as percentages)

	Target Load Ratios based on SMYS=448MPa			Load Ratios applied in the test based on F_y=541MPa			
Test Identifier (1)	p_r (2)	A_r (3)	$M_r^{\#}$ (4)	p_r* (5)	A_r* (6)	V_r* (7)	$M_r^{\&}$ (8)
P00A0M100	0.00	0.00	1.00	0.00	-0.01	0.00	1.00
P00A20M95	0.00	0.20	0.95	0.00	0.16	0.01	0.97
P40A00M89	0.40	0.00	0.89	0.34	-0.01	0.00	0.92
P40A20M94	0.40	0.20	0.94	0.34	0.16	0.02	0.96
P40A40M89	0.40	0.40	0.89	0.34	0.33	0.06	0.92
P80A40M72	0.80	0.40	0.72	0.67	0.33	0.07	0.81

*Load applied during the experiments

Calculated by interaction relations based on nominal properties

& Calculated by interaction relations based on measured properties in the absence of shear

5.1.3 Experimental Setup

The experimental program was carried out at the Structural Engineering Laboratory of the University of Ottawa. The general test setup illustrated in Fig. 4.6 is employed by using only the vertical actuators (Actuators 1, 2, and 3) for the application of axial tension and bending. The modified version of the test setup is illustrated in Fig. 5.1. The detailed sketches of the test setup are presented in Fig. 5.2 in which the actuators are represented by solid lines.

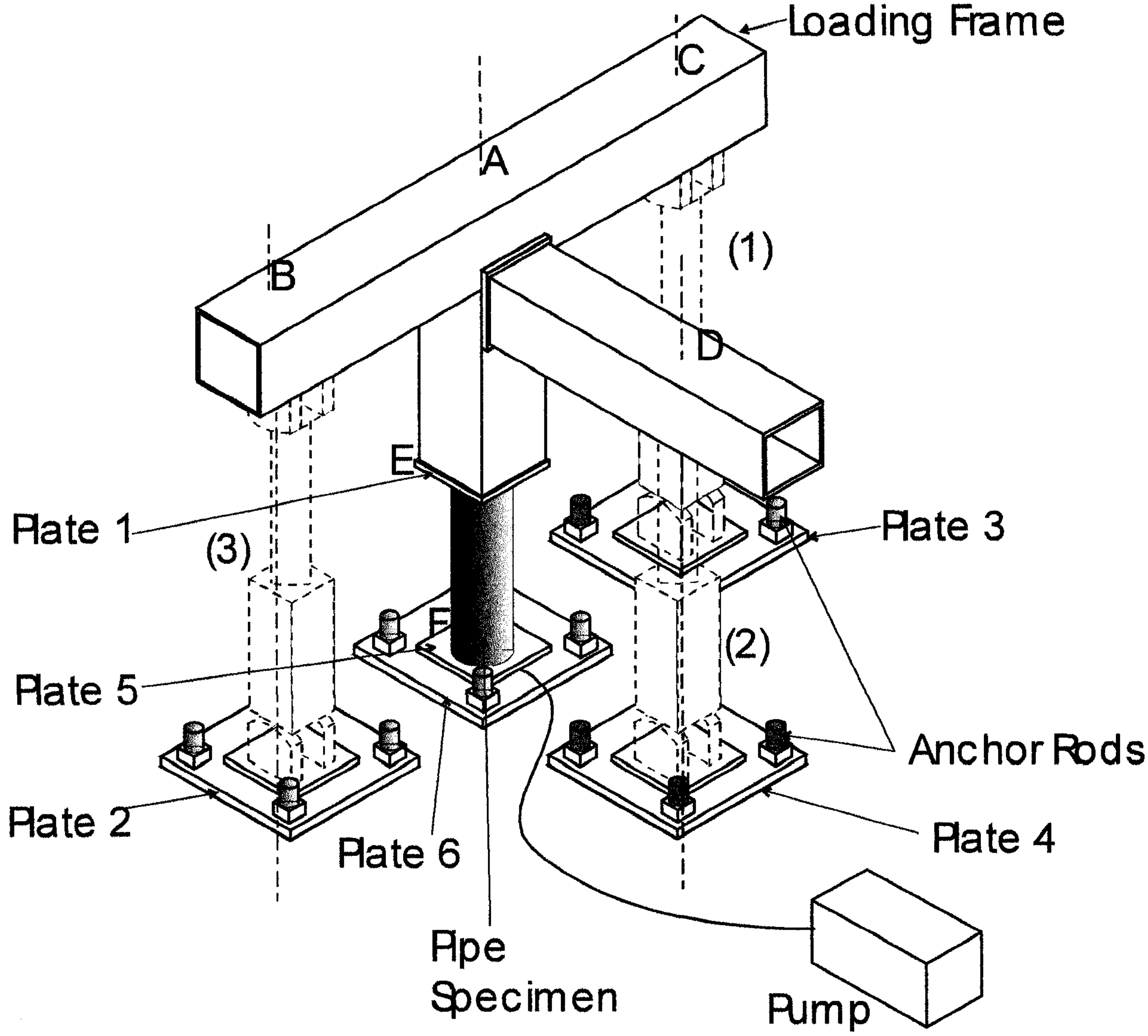

Fig. 5.1 Test Setup (Internal pressure + Axial Tension + Bending)

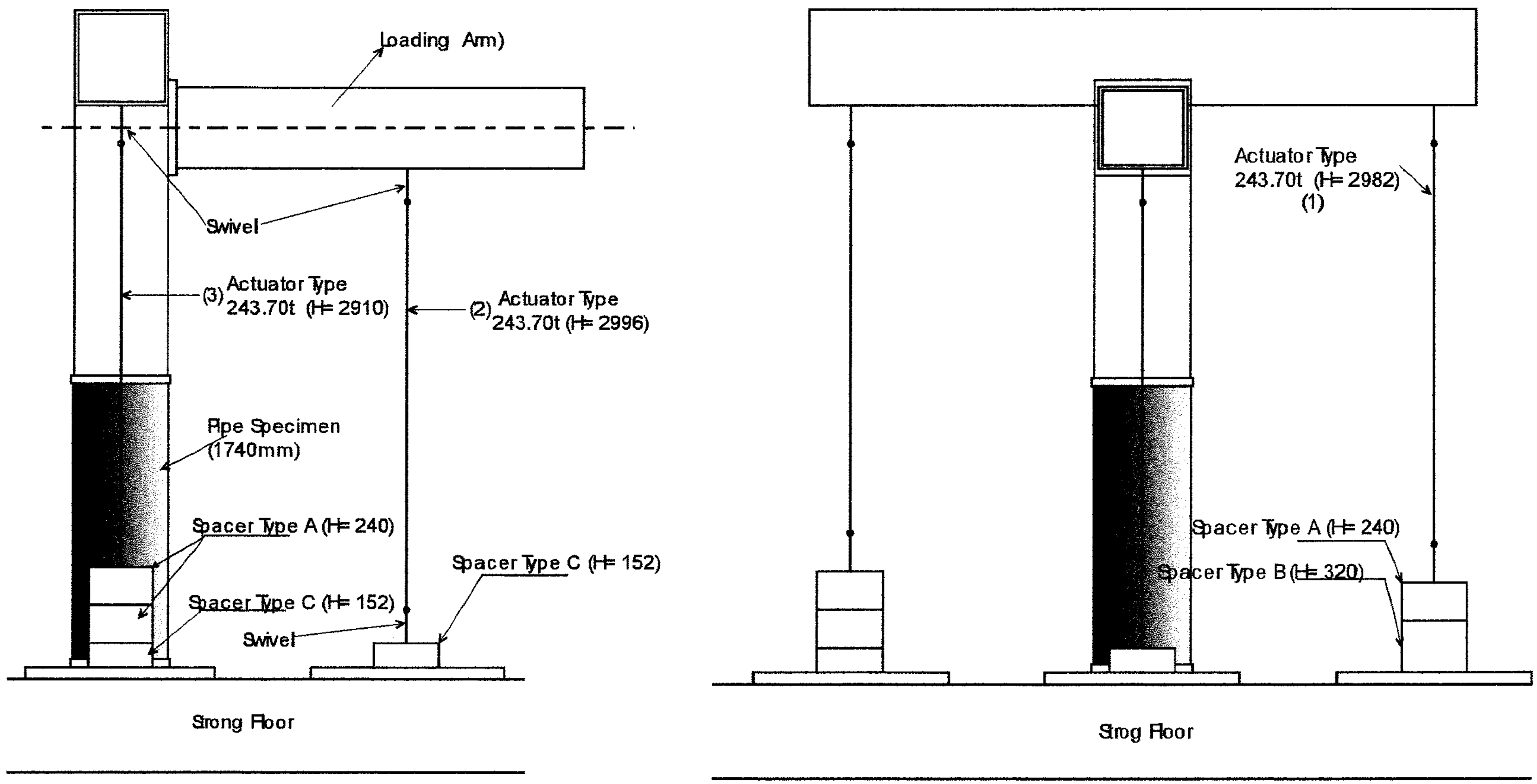

(a) Side View

(b) Front View

Fig 5. 2 Test Setup (Internal Pressure + Axial Tensile Force + Bending)

5.1.4 Load Sequence and Control

Figure 5.3 schematically shows the loading sequence to be achieved during the test. First, water is pumped into the pipe and pressurized to the target pressure value using an electric pump. As the pressure is increased, its effects on the closed top and bottom end plates induce an axial tensile force A_i at time t_1 as shown in Fig. 5.3b. In general, the magnitude of this axial force is different from the target axial force A_t (as specified in the identifier yy of the specimen in Table 5.1). The target value is attained by controlling the magnitude of the forces in Actuators 1 and 3 in Fig. 5.1, to satisfy the relation $F_1 + F_3 + A_i = A_t$ at time t_2. Throughout the ramping process $(time \geq t_1)$, the forces applied by Actuators 1 and 3 are maintained equal, i.e., $F_1 = F_3$.

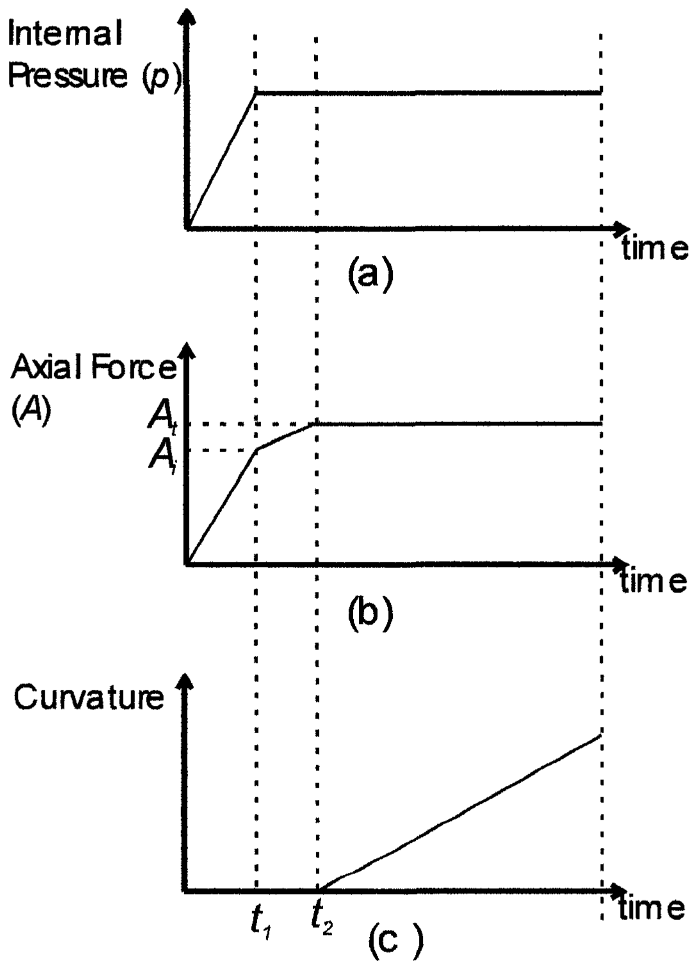

Fig. 5.3. Loading Scheme; (a) internal pressure, (b) axial force, and (c) curvature

Lastly, monotonically increasing imposed bending deformations are subsequently applied to the specimen by ramping (decreasing) the stroke of Actuator 2 in the range $time \geq t_2$. This change in stroke will induce a change in the axial force applied to the pipe specimen. In order to maintain the net axial force A equal to the target tensile force A_t throughout the test, a control program, developed under Labview VII, is used to iteratively satisfy the condition $A = F_1 + F_3 + A_i + F_2 = A_t$ or $\Delta F_1 + \Delta F_3 + \Delta F_2 = 0$. Further details related to the control program can be found in Ozkan (2007).

5.1.5 Instrumentation

The instrumentation for the experiments is shown in Fig. 5.4 in which the centerlines of the actuators are depicted as solid lines. Clinometers (electronic rotation measurement sensors), Linear Variable Differential Transformers (LVDTs), pressure gages, load cells, and temposonics are used in order to measure the rotations, deflections, water pressure, actuator forces, and actuator strokes, respectively. Assuming ideal test conditions and no pipe imperfections, the top end of the specimen is expected to undergo three types of deformations: (a) an axial displacement along the z-axis (measured by LVDTs 3, 4, and 5), (b) a horizontal displacement along the x-axis (measured by LVDTs 1 and 2 (hidden), and (c) a rotation in the vertical plane about y-axis. The rotation of the vertical Actuators), 2, and 3 were measured by three Clinometers CL1 (hidden), CL2, and CL3, respectively in order to capture second order effects of the actuators as they undergo rotations throughout the test. The angles of rotation of the pipe at different heights were measured by four Clinometers CL4, CL5, CL6, and CL7, which were mounted on the pipe wall at approximately 65mm, 580mm, 1,160mm, and 1,675mm from the bottom end plate of the pipe for specimens P00-A00-M100 and P00-A20-M95 (Clinometer CL3 is located at 0mm from bottom for this specimen) and 65mm, 573mm, 1,167mm, and 1,675 mm from the bottom end plate for the rest of the specimens. The angles of rotation can be subsequently processed to determine the curvature of the pipe based on various gage lengths as needed.

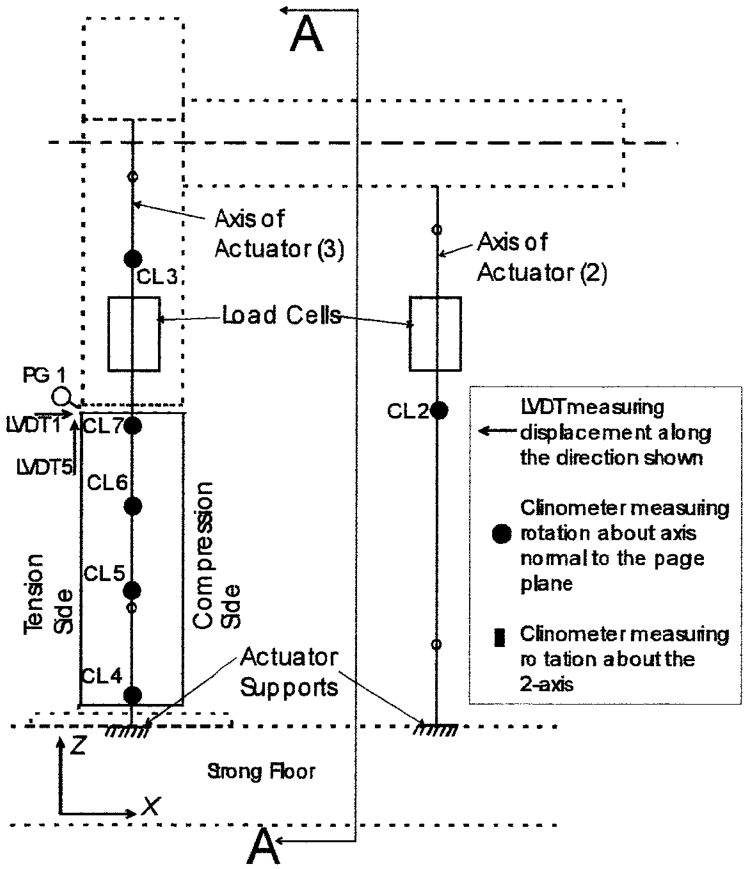

(a) Side View

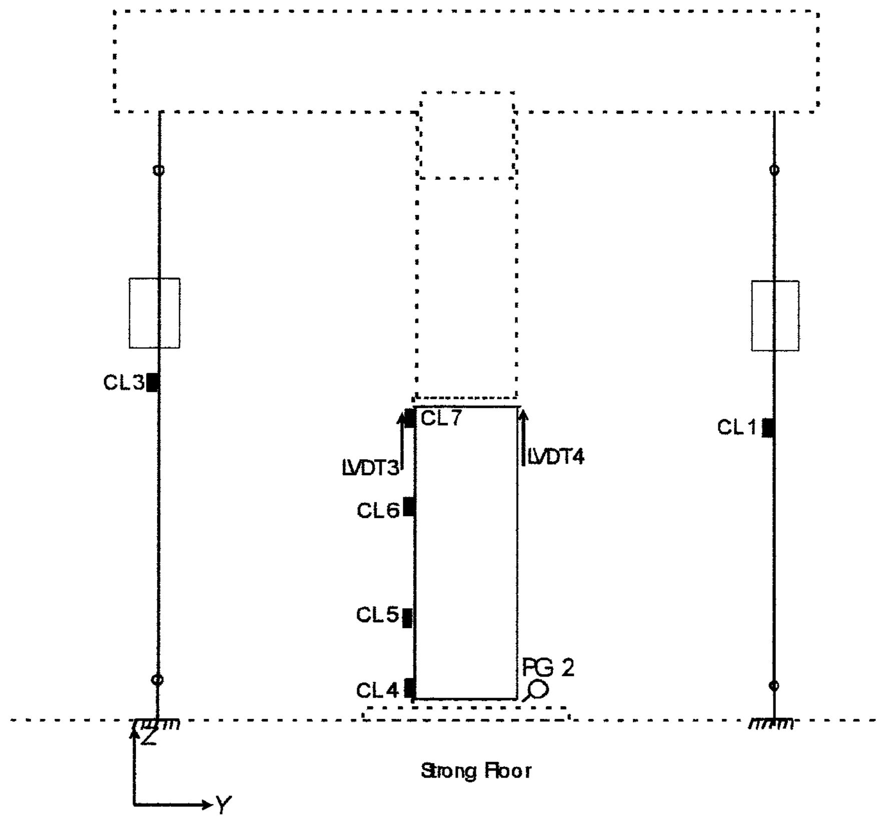

(b) Sectional Elevation A-A (looking from compression side)

Fig. 5.4. Instrumentation

As a result of slight imperfections in the test setup or specimen, the top of the pipe may undergo a displacement along the y-axis and a rotation with respect to the z-axis, which can be measured by LVDTs 1 and 2. The measurement of LVDTs 4 and 5 also provide an indication of the rotation of the loading arm about the x-axis.

The loads applied by the actuators are measured by load cells, which were internally mounted within each actuator. Stroke readings of the actuators were also measured by temposonics embedded in the actuators. The pressure of the water inside the specimen was measured by pressure gages, PG1 and PG2, which were mounted to the holes available on the top and the bottom plates welded to the pipe.

Strain gauges were mounted on different locations on the specimens. These locations are shown in Fig. 5.5. They were attached to the extreme compressive and tensile fibers of the specimens. Two different strain gage arrangements were used for un-pressurized and pressurized tests. Strain gages were located uniformly over the length of the pipe for un-pressurized specimens (Fig. 5.5a). On the other hand, for pressurized specimens, as it was observed in previous research that the local buckle generally tends to occur close to one of the ends of the pipe (Mohareb 1994). Thus, the strain gauges were concentrated within a height of one diameter of the pipe from the ends of the specimen (Fig. 5.5b). Also, at the pipe mid-height, around the specimen circumference, strain gauges were located at 45 degree intervals along the pipe circumference in order to detect any eccentricity of the applied axial load with respect to the pipe centerline.

Besides the strain gages, Brillouin fiber optic sensors were applied along the extreme compression and tension fibers of the specimens in order to have a better understanding of the strain distribution at these locations. The details regarding to the application of Brillouin fiber optic sensors and measurements collected by these sensors can be found in Zhang et al. (2007).

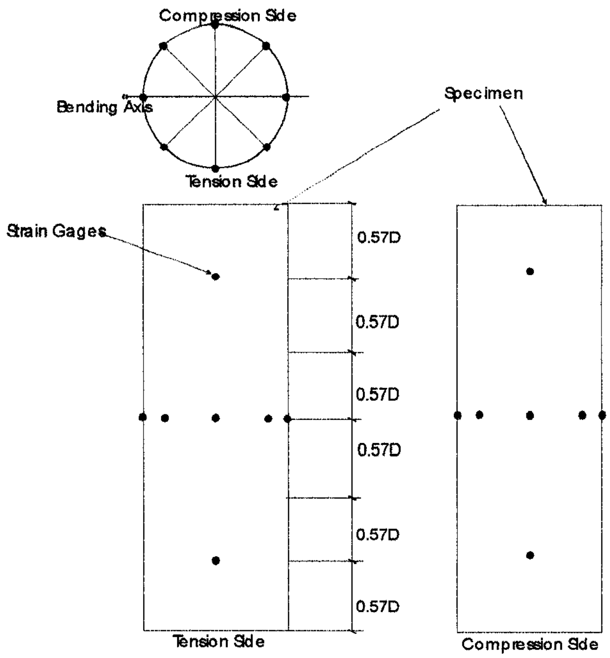

(a) Strain Gage arrangement for Specimens P00-A00-M100 and P00-A20-M95

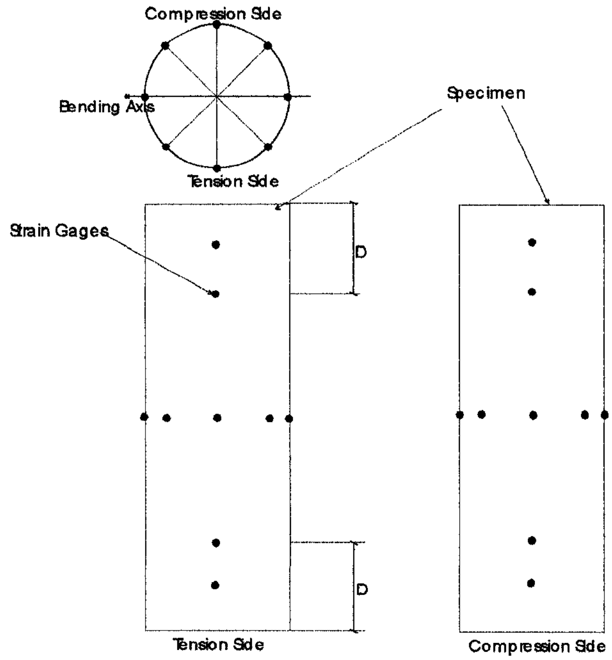

(b) Strain Gage arrangement for Pressurized Specimens

Fig. 5.5 Strain Gage Arrangements on the Specimens

5.1.6 Material Properties

The engineering stress vs. engineering strain relationship of the pipe material was determined by testing 14 longitudinal tension coupons with dimensions according to ASTM-E8 (2001) specifications. The locations of these specimens around Pipe Cross-Section are shown in Fig. 5.6a.

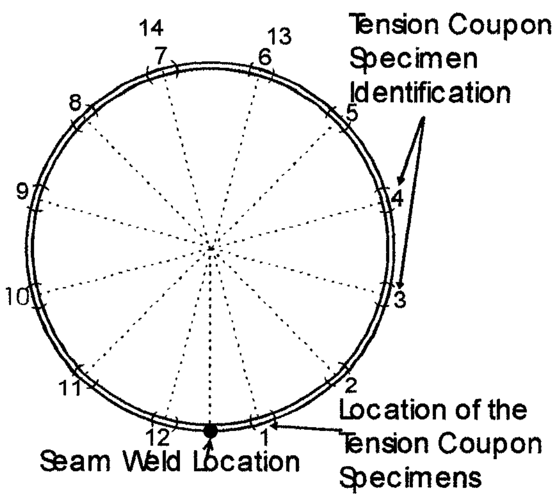

(a) Tension Coupon Locations around Pipe Cross-Section

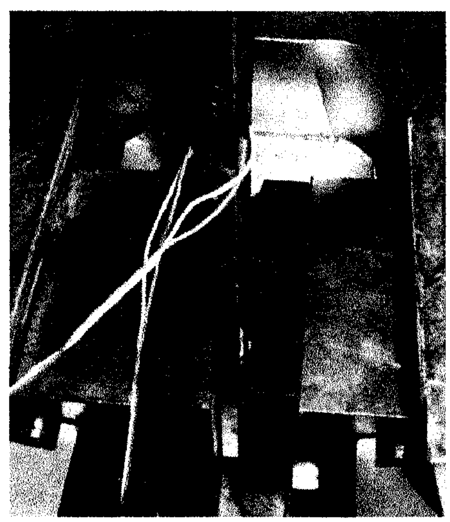

(b) Curved Grips used

Fig. 5.6. Tension Coupon Tests

Since the specimens were cut from the curved pipe surface, they had a slight curvature. Curved grips (Fig. 5.6b) with an OD identical to those of the pipes were used in order to ensure that the line of action of the tensile force for the machine coincided with the center of area of the coupon cross-section.

Stress vs. strain values representative of those measured are tabulated in Table 5.2. These were used in the finite element model. The extension-under-load method corresponding to a specified total strain of 0.005 was used to determine the yield strength of the pipe material (according to ASTM E 8M-01), which was found as 541MPa. This value is 21% higher than the specified value (448MPa). The ultimate strength (F_u) was found as 587MPa. The modulus of elasticity (E) of the pipe was 209,000 MPa with a proportional limit of 415MPa. The Poisson's ratio was measured as 0.26 and the measured rupture strain was 0.31 corresponding to a rupture stress of 387MPa.

Table 5.2 Stress vs. Strain Readings

Engineering Stress (MPa) (1)	**Engineering Strain** (2)	**True Stress (MPa)** (3)	**Logarithic Strain** (4)
415	0.00198	415	0.00198
459	0.00224	460	0.00224
501	0.00250	502	0.00249
541	0.00377	543	0.00377
541	0.00604	544	0.00602
570	0.04004	593	0.03926
584	0.06004	619	0.05831
587	0.08708	638	0.08350
583	0.13461	661	0.12629
568	0.17829	669	0.16406
496	0.22648	608	0.20415
472	0.23409	582	0.21033
387	0.30804	506	0.26853

Appendix B includes the data obtained from 14 tension coupon tests conducted.

5.2 Numerical Analysis

In this section, a finite element study for the tests is conducted for the prediction of the pipe deformational behavior and capacity. Section 5.2.1 introduces the finite element program (ABAQUS) employed in this study. In Section 5.2.2, a general description on the shell element selected for the modeling of the pipe is presented. The material model idealization employed under ABAQUS is described in Section 5.2.3. Section 5.2.4 presents the finite element mesh selected for the model while Section 5.2.5 provides the modeling details of the boundary conditions. In Section 5.2.6, the application sequence of the loads is presented.

5.2.1 Finite Element Program

The FEA simulator ABAQUS, was selected since it includes features that are important in predicting the pipe deformational behavior as it includes a) an elastoplastic, isotropic hardening constitutive material model suitable for the modeling of the pipe material, b) capabilities of accounting for geometric non-linear effects, c) the shell element S4R, which is reliable for the large displacements, large rotation, and finite membrane strain analysis, d) various capabilities of accurately modeling complex boundary conditions, e) a feature for modeling of the internal pressure as a follower force, and f) load control and displacement control capabilities as well as post-processing capabilities to view deformed configurations, contour lines for different variables and ability to plot selected variables.

In previous studies (Mohareb 1994, Yoosef-Ghodsi 1995, Souza 1996, Mohareb et al. 2001), it was shown that by using ABAQUS, the moment vs. curvature behavior were accurately predicted for the pipes with various *D/t* ratios subjected to combinations of axial compressive force, bending moment, and internal pressure.

5.2.2 Shell Element Features

In order to model the required conditions for pipe local buckling, the shell element type S4R was used from ABAQUS Shell Element Library. Element S4R is a four-node shell element. Each node has five degrees of freedom. These are three orthogonal translations and the change in the direction cosines of a unit vector normal to shell surface. Two of the three direction cosines are independent quantities and the third one is obtained from the condition that the normal vector is equal to unity.

Each of the independent degrees of freedom is linearly interpolated. Externally, the user has access to three translational and three rotational degrees of freedom per node. The S4R element uses a mixed plate bending formulation. In this formulation, neither the pure Kirchoff nor the pure Mindlin theory is used. A transverse shear strain field is assumed, which is similar to that of the Bathe-Dvorkin plate element (1985). The transverse shear strain is defined as the change in the projection of a vector initially normal to the reference surface onto the tangent to the reference surface of the shell (Hibbit et al. 2006).

5.2.3 Material Model Idealization

Although Workman (1988) recognized that the pipe material properties are slightly different in the longitudinal and circumferential directions, it is assumed in the model that the pipe material is isotropic and follows the properties in longitudinal direction. A piecewise linear isotropic hardening stress-strain model is used. The stress vs. engineering strain data points are input to ABAQUS as true stresses σ_t, and logarithmic strains ε. These are related to the engineering strain ε_e and the engineering stress σ_e through the formulas $\sigma_t = \sigma_e(1+\varepsilon_e)$ and $\ln(1+\varepsilon_e)$ respectively (Hibbit et al. 2006). The stress vs. strain values measured from coupon tests modified as logarithmic strain and true stress (Table 5.2) were input to the FEA model.

5.2.4 Finite Element Mesh

The finite element model generated for the prediction of test results can be seen in Fig. 5.7. The model consists of two main parts: (1) the pipe specimen, which is modeled by S4R shell elements (32 elements in the circumferential direction x 35 elements along the height of the pipe. Further mesh refinements for Specimen P40A40M89 to 4480 elements (64 x 70) were observed not to cause any change in the predicted moments, the deformed configurations in the pre-peak range of deformation, and the general buckling configuration, on the other hand, the finer mesh resulted in a slightly more negative slope in the post peak range of curvature), (2) the top plate, modeled by S3R shell elements (a degenerated 3-node form of the S4R element), which is modeled as rigid body by the Rigid Body option of ABAQUS. Within this option, a group of nodes and elements can be defined as rigid body whose motion is governed by the motion of a single node (rigid body reference node). In this application, the center node of the numerical model of the top plate is selected as the reference node. The nodes and elements of the top plate move as a rigid body throughout the simulation.

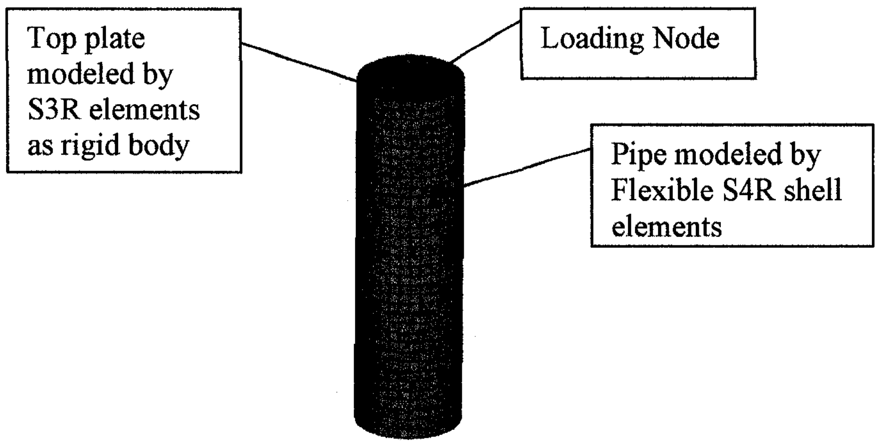

Fig. 5.7 Finite Element Model

5.2.5 Boundary Conditions

The kinematics of the test require that each end of the pipe specimen remains perfectly circular after deformation since the specimen ends are welded to thick end plates with nearly infinite in-plane and out of plane rigidities. The bottom end of the pipe specimen is welded on a thick base plate, which is firmly connected to the floor. In order to model this condition, all six degrees of freedom of the bottom nodes of the pipe model were restrained. Also, all points of the top end should remain in a single plane, which is allowed to undergo rigid body displacements and rotations under the imposed loads. In order to accomplish that, the nodes at the top plate are coupled to those of the rigid plate. The in-plane rigidity of the top plate ensures that the top of the specimen remains circular.

5.2.6 Sequence of Load Application in Analysis

The load magnitude time history input in the numerical analysis is prepared by calculating the horizontal component (H_a) and vertical component (V_a) of the resultant force acting on the top plate of the pipe specimen at its center due to actuator forces, axial tension due to internal pressure, and self-weight of the loading arm corresponding to each rotation reading of Clinometer CL7 (Fig. 5.4). Also, the internal pressure time history consistent with the tests is prepared for each specimen. These load amplitudes are then applied to the Loading Node (Fig. 5.7) of the numerical model along with the internal pressure, which is applied to the pipe wall as a follower pressure load.

5.3 *Key Definitions and Expressions*

In this section, various definitions and expressions used in the comparison of experimental and numerical results are presented. These include an expression for moments accounting for second order effects (Section 5.3.1), an expression for shearing and axial forces (Section 5.3.2), global curvature definition (Section 5.4.3), local curvature definition (Section 5.4.4), and critical strain definition (Section 5.4.5).

5.3.1 Expression for Moments

After the initiation of a local buckle in a specimen, the loading arm was observed to undergo gradual sway (Fig. 5.8). The free-body diagram of the test specimen in the deformed state is illustrated in Fig. 5.9 where the loading arm was considered to undergo rigid body displacement and rotation.

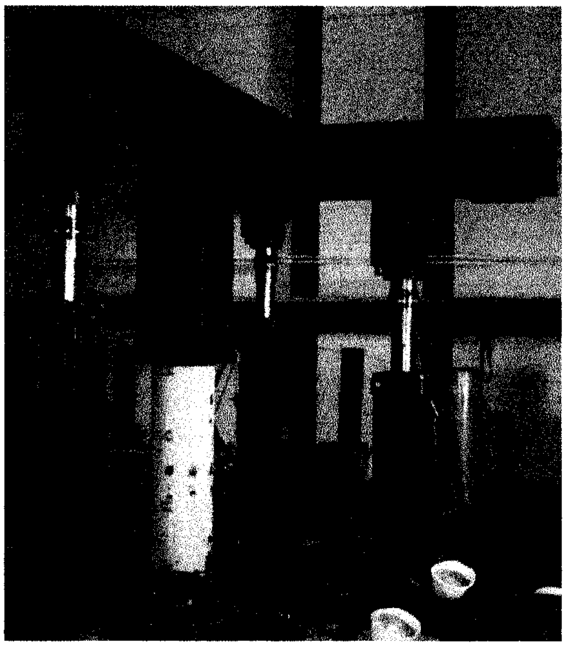

(a) Beginning of the test

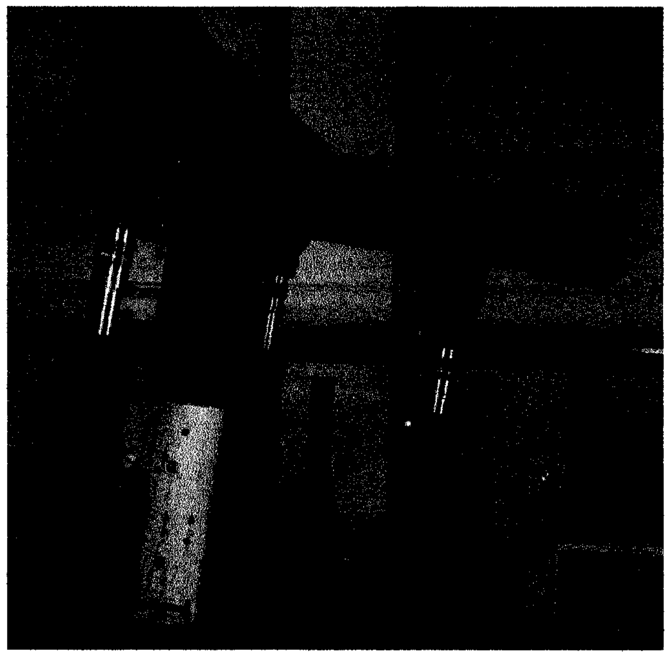

(b) End of the test

Fig. 5.8 Test setup (Specimen P40-A40-M89)

The figure shows forces F_2 and F_3 (note that the force F_1, is hidden behind the specimen and its line of action is approximately parallel to that of Actuator 3). As the specimen deforms throughout the test, the lines of action of Actuators 1, 2, and 3 rotate through angles θ_1, θ_2, and θ_3, respectively (Fig. 5.9), which were measured by clinometers CL1, CL2, and CL3 in Fig. 5.4.

The reactions on the pipe at the location of the buckle consists of a bending moment (M_b), an axial tension force (A_b) as well as a second order shear force (V_b), which arises from the horizontal component of the actuator forces and end effect of the internal pressure undergoing rotations.

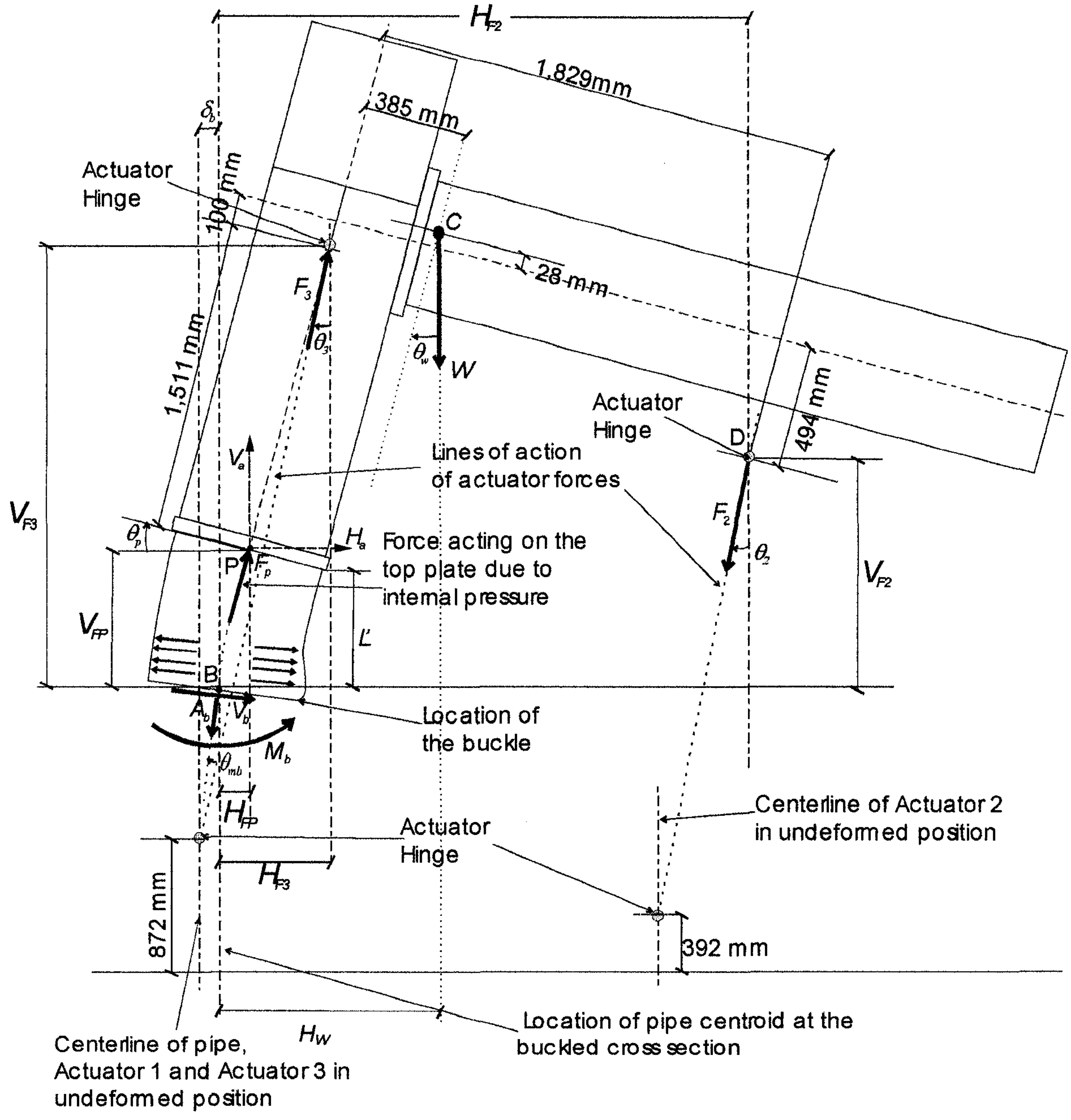

Fig. 5.9 Free-body Diagram of the Test in Deformed State of the Specimen

The reaction moment (M_b) at the location of the buckle including second order effects due to the rotation of the actuators and the specimen is calculated by

$$\begin{aligned} M_b = & -F_1 H_{F1} \cos\theta_1 + F_1 V_{F1} \sin\theta_1 + F_2 H_{F2} \cos\theta_2 - F_2 V_{F2} \sin\theta_2 \\ & - F_3 H_{F3} \cos\theta_3 + F_3 V_{F3} \sin\theta_3 - F_p H_{Fp} \cos\theta_p + F_p V_{Fp} \sin\theta_p + W H_w \end{aligned} \qquad (5.1)$$

In Eq. 5.1, distances H_{F1}, H_{F2}, H_{F3}, H_{Fp}, and H_w are the respective horizontal distances from the centerline of the specimen at the buckling section mid-height to points of application of actuator forces F_1, F_2, F_3, the force that is applied on the top plate of the pipe due to internal pressure F_p, and the self-weight W of the loading arm. In the same equation, the distances V_{F1}, V_{F2}, V_{F3}, and V_{Fp} are the vertical distance between points of application of forces F_1, F_2, F_3, and F_p, to the centerline of the specimen at the buckling section. Table 5.3 gives the definitions and expressions of the variables used in Eq. 5.1.

Table 5.3 Definitions and the Calculations of the Variables in Eq. 5.1

Variable	Definition	Calculation
H_{F1}	Horizontal distance between point of application of actuator force F_1 and the location of the buckle	$1{,}511\sin(\theta_{CL7})+\delta_T-\delta_b$
H_{F3}	Horizontal distance between point of application of actuator force F_3 and the location of the buckle	$1{,}511\sin(\theta_{CL7})+\delta_T-\delta_b$
H_{F2}	Horizontal distance between point of application of actuator force F_2 and the location of the buckle	$a\cos(\alpha-\theta_{CL4})+\delta_T-\delta_b$
a	The length of an imaginary straight line connecting points a and b	$a=\sqrt{(1{,}511+100-494)^2+1{,}829^2}$
V_{F1}	Vertical distance between the top hinge of the Actuators 1 and the location of the buckle	$1{,}511\cos(\theta_{CL7})+L'$
V_{F2}	Vertical distance between the top hinge of the Actuators 2 and the location of the buckle	$1{,}511\cos(\theta_{CL7})+L'$
L'	Distance between the top of the pipe and the location of the mid-height the buckle	Measured in the end of Each experiment.
α	The angle the imaginary line ab makes with the horizontal in un-deformed position of the specimen	$\alpha=\tan^{-1}\left[(1{,}511+100-494)/1{,}829\right]$
θ_{CL7}	Rotation of the top of the pipe measured by Clinometer CL7	Rotation measurement taken by Clinometer CL7 in Fig. 5.4
θ_p	Rotation of the end effect of the internal pressure at the top of the pipe	$\theta_p\approx\theta_{CL7}$
δ_T	Lateral deflection of the top of the pipe	Measured by LVDTs 1 and 2 (Fig 5.4)
δ_b	The lateral deflection of the location of the buckle	Taken as zero when the buckling location is in the bottom of the pipe and taken as $\delta_b=\delta_t-L'\tan\theta_{CL7}$ when the local buckle is close to the top of the pipe specimen

Equation 5.1 predicted a nearly uniform moment along the height of the pipe specimens with a local buckle occurring at specimen mid-height. This is the case for Specimen P00-A00-M100 for which the peak moment at the top of the specimen was 783kNm while the moment at the bottom was 778kNm. Also, for Specimen P00A20M95, the top moment was 771kNm while the bottom moment was 787kNm. For these two specimens, the average of bottom and top moment values was used to estimate the moment at the location of the buckle, which occurred around specimen mid-height.

Since the location of the buckle was either at the bottom or top of the rest of the specimens, the determination of the moments at the location of the buckle was simpler. When calculating the internal forces (M_b, V_b, and A_b) at the location of the buckle for specimens that buckled close to their bottom ends, it was assumed that the lateral deflection of the pipe centerline of the location of the buckle was approximately equal to zero. For the specimen with a local buckle close to its top end (P40-A00-M89), a linear deflected shape is assumed between the location of Clinometer CL7 and the location of the buckle with a slope equal to the rotation measured by Clinometer CL7 and the lateral deflection of the location of the buckle is calculated accordingly

5.3.2 Expressions for Shearing and Axial Forces

The shear (V_b) (Fig. 5.9) at the location of the buckle can be calculated as

$$V_b = A_h \cos\theta_{mb} + A_v \sin\theta_{mb} \tag{5.2}$$

Also the axial force (A_b) (Fig. 5.9) is calculated as

$$A_b = -A_h \sin\theta_{mb} + A_v \cos\theta_{mb} \tag{5.3}$$

In Eqs. 5.2 and 5.3 the definitions $A_h = F_2 \sin\theta_2 - F_3 \sin\theta_3 - F_1 \sin\theta_1 - F_p \sin\theta_p$ and $A_v = -F_2 \cos\theta_2 + F_3 \cos\theta_3 + F_1 \cos\theta_1 + F_p \cos\theta_p - W$ were adopted. Angle θ_{mb} is the rotation at the mid-height buckle.

In the sixth and seventh columns of Table 5.1, the shear and axial force ratios for each specimen as calculated by Eqs., 5.2, and 5.3 based on measured material yield strength (F_y) and measured cross-sectional properties (D, t) are tabulated. (The comparison of the moment capacity predicted by the interaction relation (Eqs. 1.1 and 1.2) in the presence of shear (V) coincide with that based on neglecting the shear force (Eq. 1.6) within a maximum difference of 0.02% for the Specimen P80-A40-M72, which had the largest shear force).

Besides moment, axial force, and shear, there also exist out of plane bending moment (M_{bx}) and torsion at the location of the buckle. For all of the tests, M_{bx} was negligible when compared to the magnitude of M_b. For the tests P00-A20-M95 and P40-A40-M89, when the specimens reached their maximum bending capacity, torsion values of 9kNm and 18kNm were observed, respectively, corresponding to 1% and 2% of the plastic torsion capacity of the pipes calculated in the absence of other forces. This amount of torsion was judged negligible.

5.3.3 Global Curvature

The global curvature ϕ_g is the average curvature measured along the distance $L_{t\text{-}b}$ between the two clinometers placed at the top and bottom of the pipe in the un-deformed configuration of the pipe specimen as illustrated in Fig. 5.10 and is obtained by

$$\phi_g = \frac{\theta_t - \theta_b}{L_{t-b}} \tag{5.4}$$

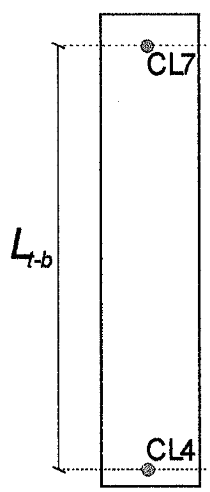

(a) Un-deformed Specimen

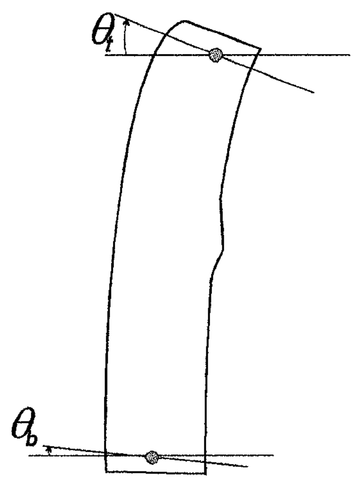

(b) Deformed Specimen

Fig. 5.10 Global Curvature

in which, θ_t is the rotation of the top of the pipe specimen as measured by the Clinometer CL7 (Fig. 5.4), θ_b is the rotation of the bottom of the pipe specimen as measured by the Clinometer CL4 (Fig.

5.4), and $L_{t-b} = 1{,}610mm$ for all of the specimens except P00-A20-M95 for which the clinometers were spaced by a distance $L_{t-b} = 1{,}675mm$.

Post-buckling curvatures determined by Eq. 5.4 are dependent upon the gage length $L_{t\text{-}b}$. Thus, they are not a reliable indicator of local buckling deformations. A better indicator is the local curvature values as discussed in the following section.

5.3.4 Local Curvature

Local curvature (ϕ_l) is the average curvature based on a specified gage length L_{tb-bb}. The conventional gage length taken by the pipeline industry is as one diameter $L_{tb-bb} = D$, which intercepts the local buckle (Fig. 5.11). Thus, in each of the tests, a gauge length of one diameter is targeted, whenever possible. The actual gauge lengths taken for each specimen are presented in Column 2 of Table 5.4.

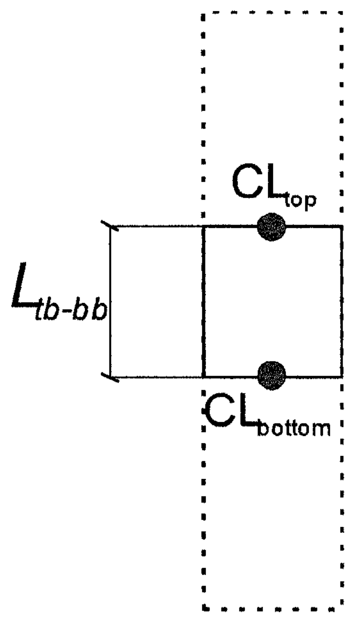

(a) Un-deformed Specimen

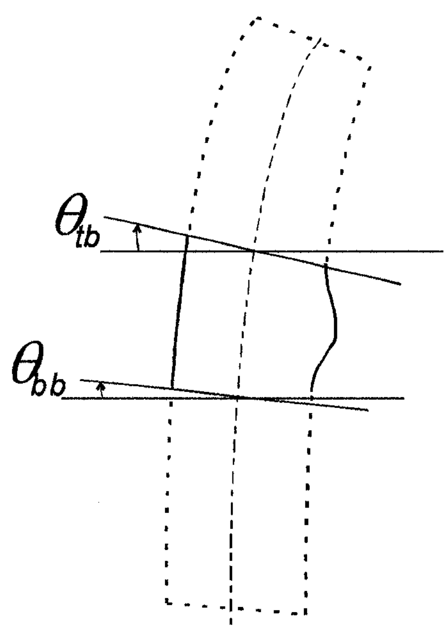

(b) Deformed Specimen

Fig. 5.11 Local Curvature

The average local curvature (ϕ_l) is expressed as

$$\phi_l = \frac{\theta_{tb} - \theta_{bb}}{L_{tb-bb}} \tag{5.5}$$

where θ_{tb} is the rotation measured by the Clinometer CL_{top} located at the top of the gage length L_{tb-bb}, θ_{bb} is the rotation measured by Clinometer CL_{bottom} located at the bottom of the gage length L_{tb-bb}, and L_{tb-bb} is the distance between these two clinometers.

In pressurized tests, L_{tb-bb} was taken as 1.0D. For Specimen P00-A00-M00, the buckle occurred between two clinometers spaced at 1.14D while for Specimen P00-A20-M95, the buckle took place at the location of one of the clinometers. Thus, a longer gauge length of 2.29D was adopted in order to properly intercept the buckle.

5.3.5 Critical Strains

In this study, the critical strain ε_{cr} is defined as the average strain on the compression side of the specimen corresponding to a local curvature value (critical curvature, ϕ_{cr}) associated with the maximum moment, M_{max} (Fig. 5.12) as determined from moment M_b (as defined in section 5.3.1) vs. local curvature ϕ_l (as defined in section 5.3.3) diagram.

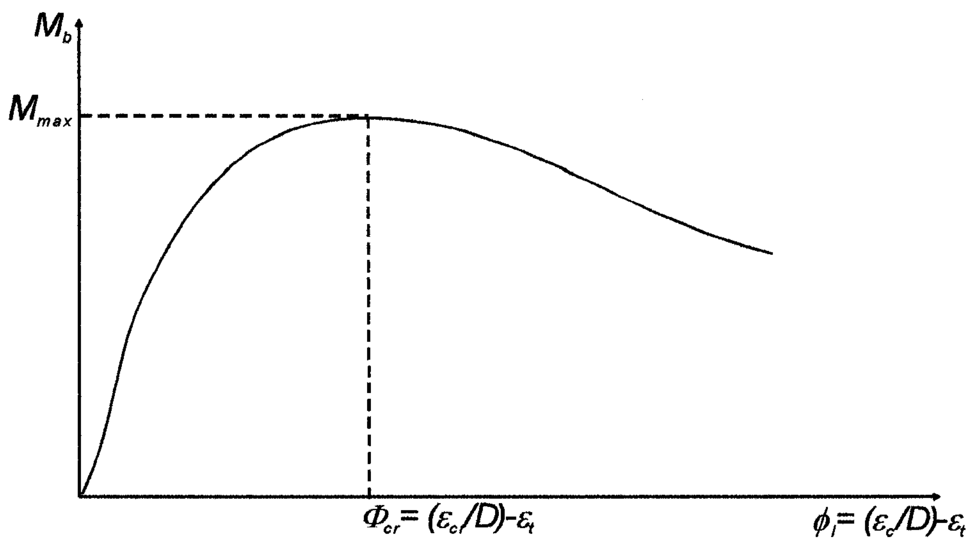

Fig. 5.12 Definition of Critical Curvature

In the literature review conducted, it was also found that critical curvature ϕ_{cr} could be obtained from Local Curvature ϕ_l vs. Global Curvature ϕ_g relations. As previously mentioned, since after the initiation of buckling, local curvatures deviates from global curvatures, the Local Curvature ϕ_l vs. Global Curvature ϕ_g have distinct behaviors in pre-buckling and post-buckling regions. The point where the slope changes in Local Curvature ϕ_l vs. Global Curvature ϕ_g relations could be considered as a point of initiation of buckling and the local curvature value corresponding to this point can be regarded as the critical curvature (Dorey et al. 2000). Appendix C illustrates the plots for Local Curvature ϕ_l vs. Global Curvature ϕ_g relations for each of the tests conducted.

Two methods are used in extracting the critical strain values. Both methods were found to agree reasonably well.

5.3.5.1 Clinometer/Strain Gage Readings

The method documented in Zimmerman et al. (2004) was used to obtain average compressive strains $\left(\varepsilon_{cr_a}\right)$. In the experiments of Zimmerman et al. (2004), the tensile strains $\left(\varepsilon_t\right)$ were measured using strain gauges. In contrast to longitudinal strains on the compression side, those on the tension side are expected to be uniform. Thus, the tensile strains measured by strain gauges tend to be reliable.

The local curvature $\left(\phi_l\right)$ intercepting the local buckle is calculated by Eq. 5.5. Knowing the local curvature, the critical strain $\left(\varepsilon_{cr_a}\right)$ is calculated from

$$\varepsilon_{cr_a} = \varepsilon_t - \phi_l D \tag{5.6}$$

Equation 5.6 is based on the "plane sections remain plane" assumption at both ends of the gage length $L_{tb\text{-}bb}$=D, which is approximately valid away from the local buckle.

5.3.5.2 Demec Gage Readings

Average compressive strains for pressurized specimens were also determined through Demec gauges intercepting the buckle on the extreme compression fiber of the specimen (Fig. 5.13).

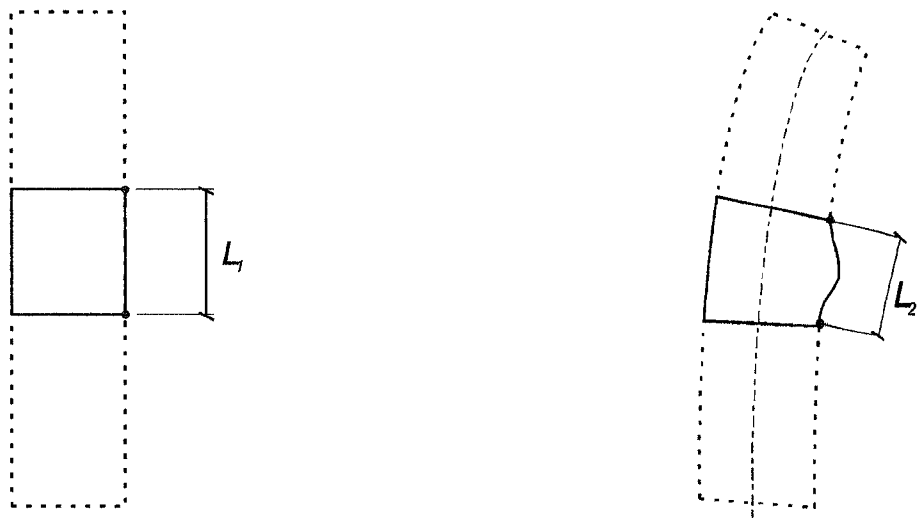

(a) Un-deformed Pipe **(b)** Deformed Pipe

Fig. 5.13 Demec Gages

The average compressive strain values based on Demec gages were calculated by Eq. 5.7

$$\varepsilon_{cr_b} = \frac{L_1 - L_2}{L_1} \tag{5.7}$$

in which L_1 is the distance between the Demec points in the un-deformed configuration (taken as $L_1 = D$) and L_2 is the distance between the same Demec points after local deformation.

5.4 Results

This section presents the results as obtained from the tests and FEA. These include: Comparisons between moment vs. local curvature diagrams (Section 5.4.1), critical strains (Section 5.4.2), buckling patterns and location (Section 5.4.3), and moment capacity (Section 5.5.4).

5.4.1 Moment vs. Local Curvatures

The effects of axial tension on the Moment-Local curvature results are illustrated in Fig. 5.14. On the same figure, the FEA predictions of the moment-Local curvature results are overlaid for a) comparison with experimental results and b) to augment the experimental database where no tests were conducted.

Figure 5.14a illustrates the behavior of non-pressurized specimens (Specimens P00-A00-M100 and P00-A20-M95) while Figure 5.14b relates to specimens with 40% internal pressure (Specimens P40-A00-M89, P40-A20-M94, and P40-A40-M89), and in Fig. 5.14c, the moment curvature of Specimen P80-A40-M72 is provided.

As a general observation, the presence of axial tensile force increased the ability of the specimens to deform into the plastic range of the deformation prior buckling. It is also observed that the increase in the axial tensile force increases the post peak stiffness (characterized by the mild negative slope of the moment vs. curvature relationship) of the pipe.

The FEA model was able to predict the magnitude of the peak moments with reasonable accuracy. Also, the Moment vs. Curvature behavior of the experiments was reasonably well predicted. (An increase in axial tensile force was found to increase (a) the ability of the specimens to deform into the plastic range of the deformation prior buckling and (b) the stiffness of the pipes in the post-buckling range of the deformation for the specimens). However, the post-peak moment curvature response was found somewhat different. Similar observations were made in the single specimen subjected to tension in Zimmerman et al. (1995).

Figures 5.14(d) through 5.14(f) provide the bending moments normalized with respect to the modified plastic moments for all tests. A peak normalized bending moment with a ratio of unity indicates that the experimental moment (or an FEA moment) is equal to the modified plastic moment predicted by the interaction relations (Eq. 1.1 and 1.2) in the presence of tensile force and internal pressure. A peak ratio less than unity indicates that the FEA or the pipe in the test was unable to attain the modified plastic moment while a peak ratio more than a unity indicates that the pipe was able to exceed the modified plastic moment.

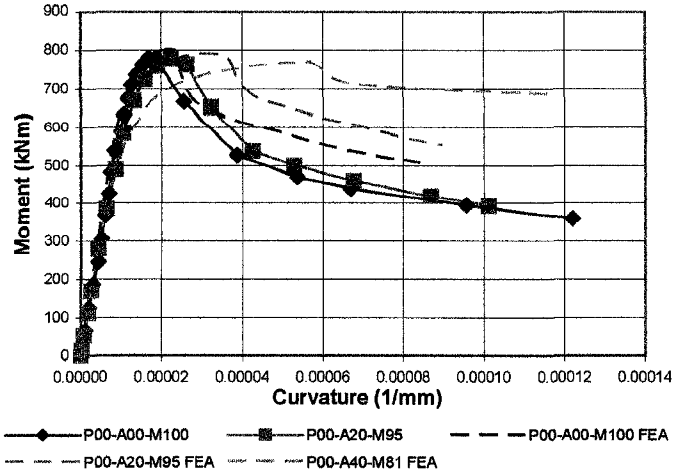

(a) Moment vs. Curvature (p_r= 0%)

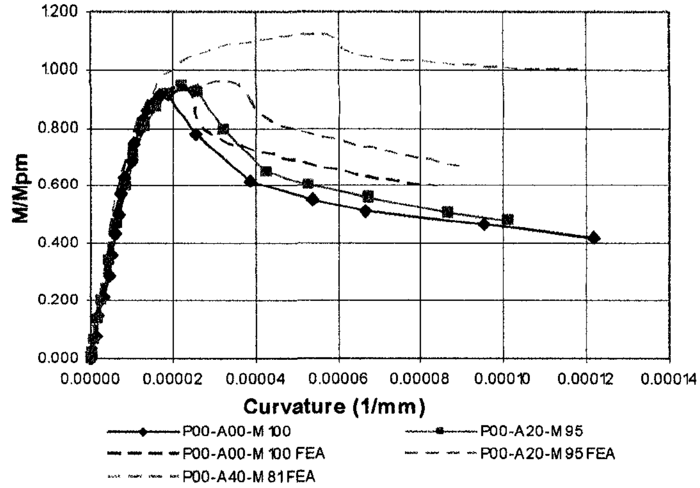

(d) Normalized Moment vs. Curvature (p_r = 0%)

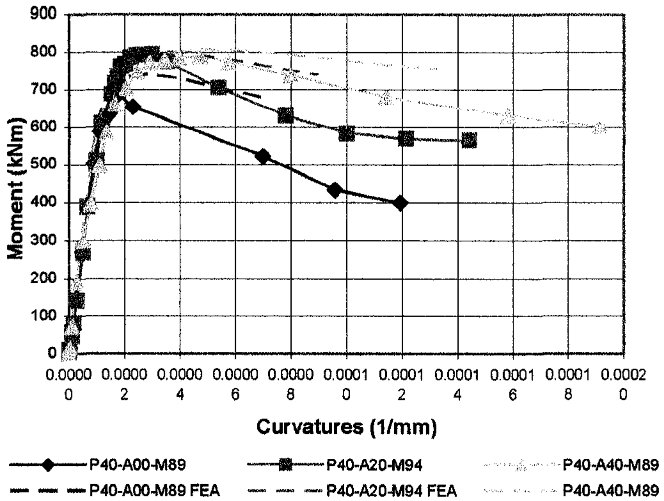

(b) Moment vs. Curvature (p_r = 40%)

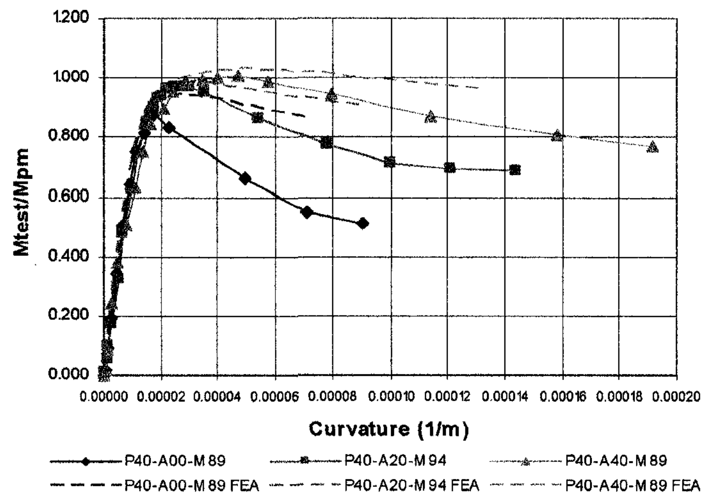

(e) Normalized Moment vs. Curvature (p_r = 40%)

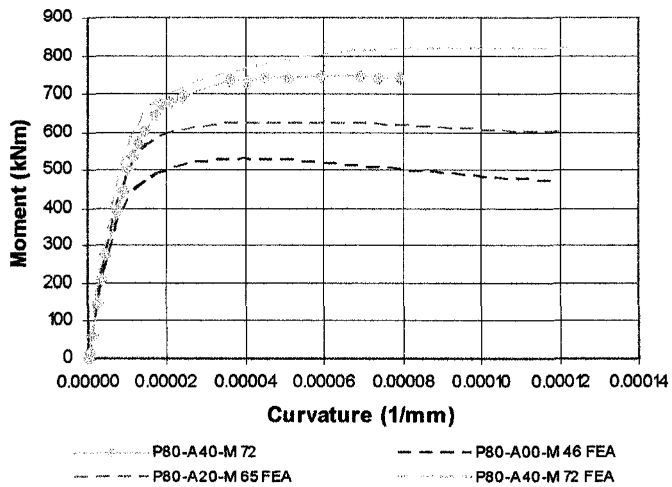

(c) Moment vs. Curvature (p_r = 80%)

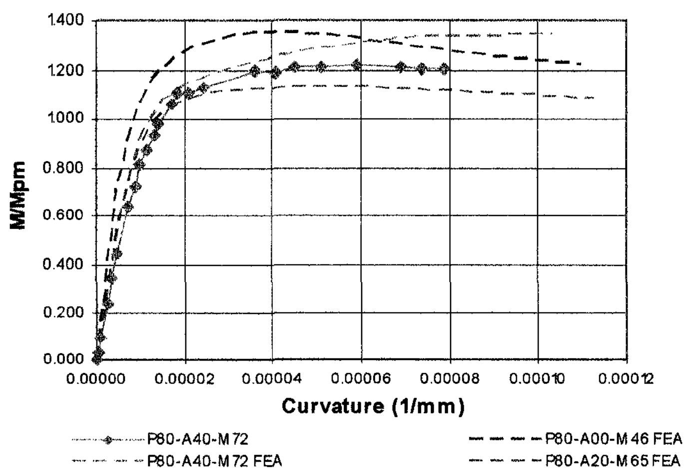

(f) Normalized Moment vs. Curvature (p_r = 80%)

Fig. 5.14 Moment vs. Curvature Relationships

All specimens were able to preserve their integrity until the end of the test except for Specimen P40-A40-M89, which was deformed significantly and eventually ruptured on the tension side after a curvature of 1.92×10^{-4} 1/mm was attained. The location on the rupture on this specimen is presented in Fig. 5.15.

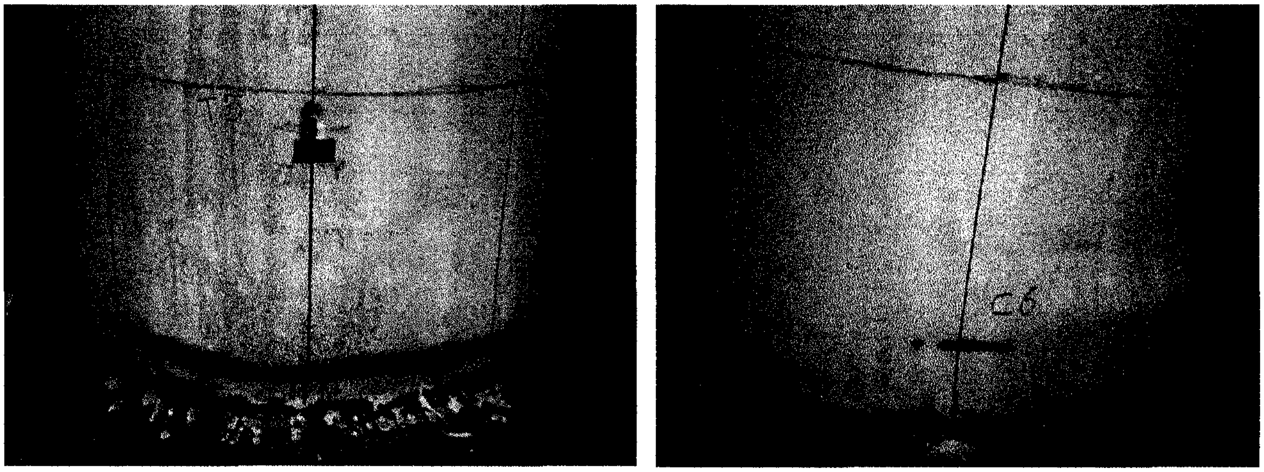

(a) Tension Side **(b)** Bending Axis

Fig. 5.15 Rupture Location of the Specimen P40-A40-M89

5.4.2 Critical Strain Values

The critical strain values as obtained based on Clinometer/Strain gages, Demec gauges, and as predicted by the code equation (Can/CSA Z662 2003) are shown in Table 5.4. Comparisons with FEA predicted strains are also presented.

Table 5.4 Critical Strains

		Based on Clinometers					Based on Demec Gage Readings		
Test ID	Gage Length	Test	FEA	Test/ FEA	Code*	Test/ Code	Test	FEA	Test/ FEA
P00-A00-M100	1.14D	0.48%	0.68%	0.70	0.37%	1.30	-	-	-
P00-A20-M95	2.29D	0.53%	1.09%	0.49	-		-	-	-
P40-A00-M89	1.00D	0.63%	0.96%	0.66	0.61%	1.03	0.54%	1.17%	0.46
P40-A20-M94	1.00D	0.86%	0.98%	0.88	-	-	0.67%	1.22%	0.55
P40-A40-M89	1.00D	0.93%	0.91%	1.02	-	-	>0.53%	1.19%	-
P80-A40-M72	1.00D	1.52%	3.03%	0.50	-	-	1.52%	3.05%	0.50

*Critical Strain Values Calculated According to CAN/CSA-Z662-03

The critical strain values based on the Demec gauges were found to be slightly less than those based on the clinometers, with an average ratio of 0.88 between both methods.

5.4.2.1 Comparison with Code Predictions

In the absence of tension, Clause 6.3.3.3 of Oil and Gas Pipeline Systems Code CAN/CSA-Z662-03 provides limiting compressive strains ε_c^{crit} through the equation

$$\varepsilon_c^{crit} = 0.5\frac{t}{D} - 0.0025 + 3{,}000\left(\frac{pD}{2tE}\right)^2 \qquad (5.8)$$

in which E is Young's modulus. Equation 5.6, based on the work of Gresnigt (1986), was applied for Specimens P00-A00-M100 and P40-A00-M89, which have zero axial force. For Specimen P00-A00-M100, the critical strains based on CAN/CSA Z66 (2003) were 0.37%. This compares to a test value of 0.48%, which is 30% larger. For Specimen P40-A00-M89, the critical strain based on the standard is 0.61% and the measured critical strain is 0.63%, which is 3% larger than the code value.

5.4.2.2 Comparison with Other Experimental Results

In order to assess the validity of the test results reported, comparisons with critical strain measurements in other studies are presented in this section. Only those tests with reasonably close D/t, p/p_y, F_y/E, and A/A_y ratios to the ones tested in this program are selected for the comparison.

Specimen P00-A00-M100

Tables 5.5 presents experimentally determined critical strain as obtained from different tests in the literature along with the specimen properties (material properties F_y/E, internal pressure ratios p/p_y, D/t ratios, axial tension ratios A/A_y, an indication of whether the pipe section tested includes a girth-weld or not, and percentage imperfections reported). These include a specimen in Sorenson et al. (1970), a specimen in Bouwkamp and Stephen (1974), and a specimen in Zimmerman et al. (2004). The data for Specimen P00-A00-M100 is also provided at the bottom of the table for comparison. Even though the specimens have slightly different F_y/E values, imposed material imperfections, and internal pressure for the first three tests, the critical compressive strain values for all four specimens were reasonably close. As expected, the critical compressive strain value for Specimen P00-A00-M100 tested in this series is within the range of those reported by Sorenson et al. (1970), Bouwkamp and Stephen (1974), and Zimmerman et al. (2004).

Table 5.5 Comparison of Critical Strain of the Specimen P00-A00-M100 with other Experimental Results

Reference	D/t	p/p_y	F_y/E	A/A_y	Girth Weld/Plain	% Imperfections	ε_{crit}
Sorenson et al. (1970)	80.9	0.00	0.21%	0.00	Plain	11	0.42
Bouwkamp and Stephen (1974)	82.1	0.08	0.25%	0.00	Plain	11	0.48
Zimmerman et al. (2004)	82.0	0.00	0.24%	0.00	Spirally welded	-	0.52
P00-A00-M100	**81.2**	**0.00**	**0.26%**	**0.00**	**Plain**	-	$\varepsilon_{cr_a} = 0.48$

***Specimen* P80-A40-M72**

The closest test to Specimen P80-A40-M72 is the one specimen from Zimmerman et al. (1995) test series. Table 5.6 provides the material properties loading conditions, and the critical strain of this specimen along with those of Specimen P80-A40-M72 of the present study.

Table 5.6 Comparison of Critical Strain of the Specimen P80-A40-M72 with other Experimental Results

Reference	D/t	p/p_y	F_y/E	A/A_y	Girth Weld/Plain	% Imperfections	ε_{crit}
Zimmerman et al. (1995)	87	0.80	$\approx$ 0.22%	0.40	Girth-weld	Less than 0.5% of the diameter	0.72
P80-A40-M72	**81.2**	**0.80**	**0.26%**	**0.40**	**Plain**	-	$\varepsilon_{cr_a} = 1.52$

Both tests have reasonably close D/t, p/p_y, F_y/E, and A/A_y, ratios. The major difference is related to the presence of a girth-weld in Zimmerman et al. (1995) while for P80-A40-M72 the pipe tested was plain.

For 12" and 20" OD pipes with D/t=51 and 64, respectively, Yoosef-Ghodsi et al. (1995) observed that the critical strain for girth-welded pipes were about 60% of those for plain pipes. A ratio of critical strain between the specimen of Zimmerman at al. (1995) and Specimen P80-A40-M72 tested in this program is found to be 47%. A likely reason for this small ratio (compared to 60% value reported in Yoosef- Ghodsi et al., 1995) is the fact that the specimen of Zimmerman et al. (1995) had a higher D/t ratio.

5.4.2.3 Critical Strains based on Current Study

The critical compressive strain vs. axial tension for the six specimens tested is presented in Fig. 5.16. Since code equations provide critical strain values for the case of only zero axial force, three critical strain values as predicted by the code for internal pressure levels of p=0.0p_y, p=0.4p_y, and p=0.8p_y are overlaid on the figure. With only one experimental critical strain value available for the case p=0.8p_y, a linear critical strain vs. axial tension relationship is generated by using the code prediction for 80% internal pressure and 0.0% axial force and experimental measurement for 80% internal pressure and 40% axial force ratio. For p=0.0, a constant critical strain vs. axial force relationship is adopted for axial force values higher than 20% axial force ratio, which assumes the critical strain value of Specimen P00-A20-M95 since there is no experimental data available in this range.

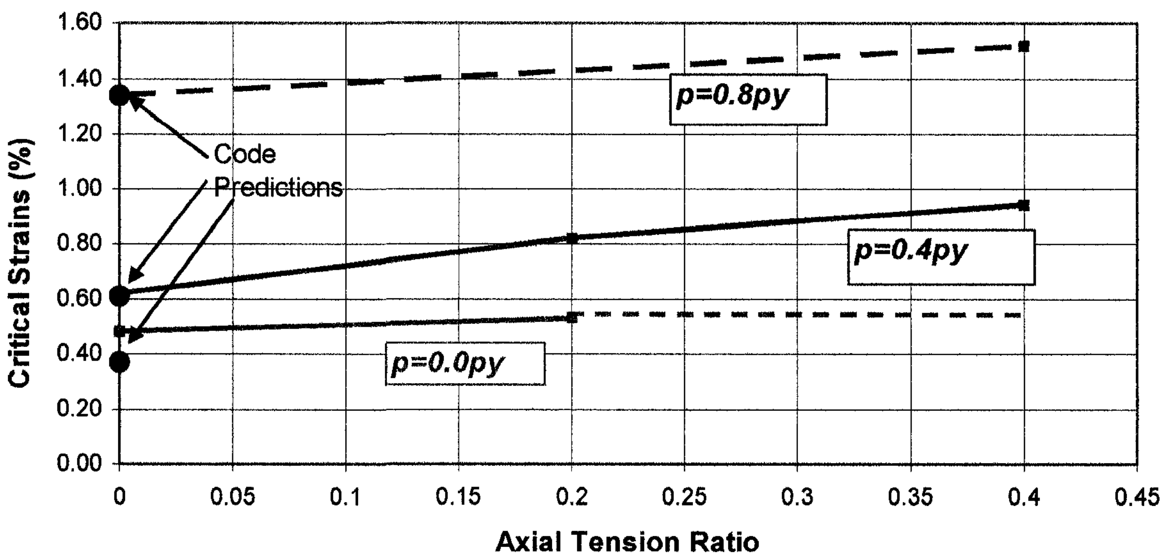

Fig. 5.16 Critical Strain vs. Axial Tension Ratio (Experimental)

As a general observation, the experimental results consistently demonstrate an increase in critical strain values by increasing axial tension. When Specimens P00-A00-M100 and P00-A20-M95 are compared, a 20% increase in axial tension, increased the critical strain capacity by 10%. The same amount of increase in axial tension, increased the critical strain capacity of Specimen P40-A00-M89 by 36.5%. When the specimens P40-A00-M89 and P40-A40-M89 are compared, 40% increase in axial tension, increased the critical strain capacity by 48%.

5.4.2.4 Critical Strains based on FEA

The critical strains as predicted by FEA were tabulated in Table 5.4. Also, Fig. 5.17 provides a plot of critical strains versus axial tension ratio based on FEA predictions overlaid on those from the tests.

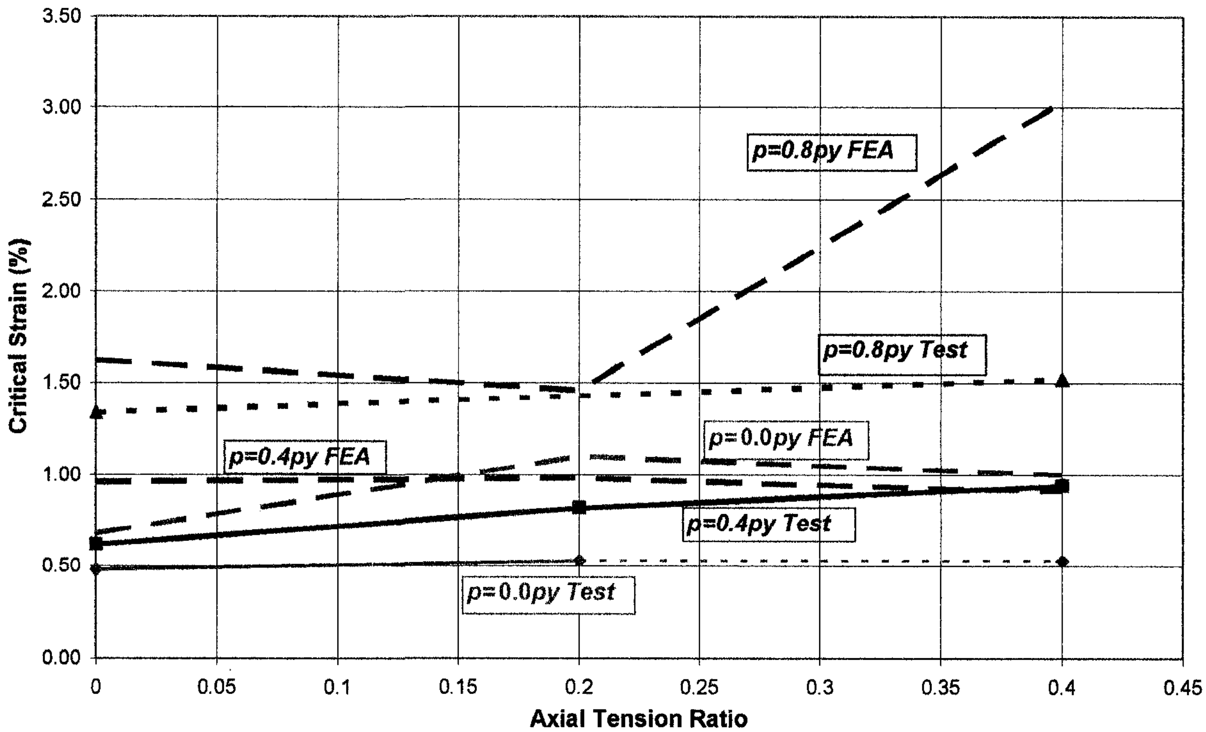

Fig. 5.17 Comparison of Critical Strain vs. Axial Tension Ratio based on FEA and Experiments

As a general observation, FEA results over-predicted critical strains. On the average, the FEA predicted critical strain-to-test measured critical strain ratio was found to be 1.41. Also, a comparison of Figs. 5.16 and 5.17 suggests that the FEA model yields unreliable results when predicting critical strains.

A possible reason for the discrepancy is the presence of the residual stresses within the specimens, which are not modeled in FEA model.

5.4.2.5 Design Recommendations

Based on the rather limited experimental data provided in this study, the proposed limits for critical strains are:

For $p = 0.0$

$\varepsilon_{cr} = 0.25A_r + 0.48$	$0 \leq A_r < 0.2$	5.7a
$\varepsilon_{cr} = 0.53$	$A_r \geq 0.2$	5.7b

For $p = 0.4p_y$

$\varepsilon_{cr} = 1.15A_r + 0.63$	$0 \leq A_r < 0.2$	5.7c
$\varepsilon_{cr} = 0.35A_r + 0.79$	$0.2 \leq A_r < 0.4$	5.7d
$\varepsilon_{cr} = 0.93$	$A_r \geq 0.4$	5.7e

For $p = 0.8p_y$

$\varepsilon_{cr} = 0.45A_r + 1.34$	$0 \leq A_r < 0.4$	5.7f
$\varepsilon_{cr} = 1.52$	$A_r \geq 0.4$	5.7g

In Eqs. 5.7a to 5.7g, all critical strains are provided as a percentage, A_r is the axial force ratio, which is positive (i.e., all equations are valid for tensile forces only). Also, linear interpolation is recommended for internal pressure values different from 0, $0.4p_y$, and $0.8p_y$.

5.4.3 Buckling Patterns and Location

Figure 5.18 shows the final buckled configurations of the specimens and their FEA simulations. The buckles for all specimens initiated at the extreme compressive fiber. As the curvature was increased, they spread in the circumferential direction symmetrically with respect to the plane of bending. The un-pressurized specimens exhibited a diamond shape local buckle within the middle third region of the specimen on the compression side. While the buckle of specimen P00-A00-M100 was confined within a length of 0.5*D*, the buckle in specimen P00-A20-M95 was spread over a longer segment of the pipe of about 0.75*D*, suggesting that the presence of a tensile force tends to increase the length of localization of the pipe. Specimens with 40% internal pressure exhibited an outward bulge local buckle near their bottom ends, except for the Specimen P40-A00-M89, which buckled near its top end. All outward bulge buckles occurred within a length of 0.25*D*. For the fully pressurized Specimen P80-A40-M72, the deformation patterns observed near the peak moment consisted of three outward bulges with small amplitudes on the compression side. As the deformations progressed during the test, the bottom outward bulge was amplified while the amplitudes of the other two buckles dampened and eventually disappeared. The finite element model was able to predict the buckling modes accurately. However, the location of the predicted buckles for the specimens (P40-A00-M89, P40-A20-M94, and P40-A40-M89) did not match the ones observed in the test.

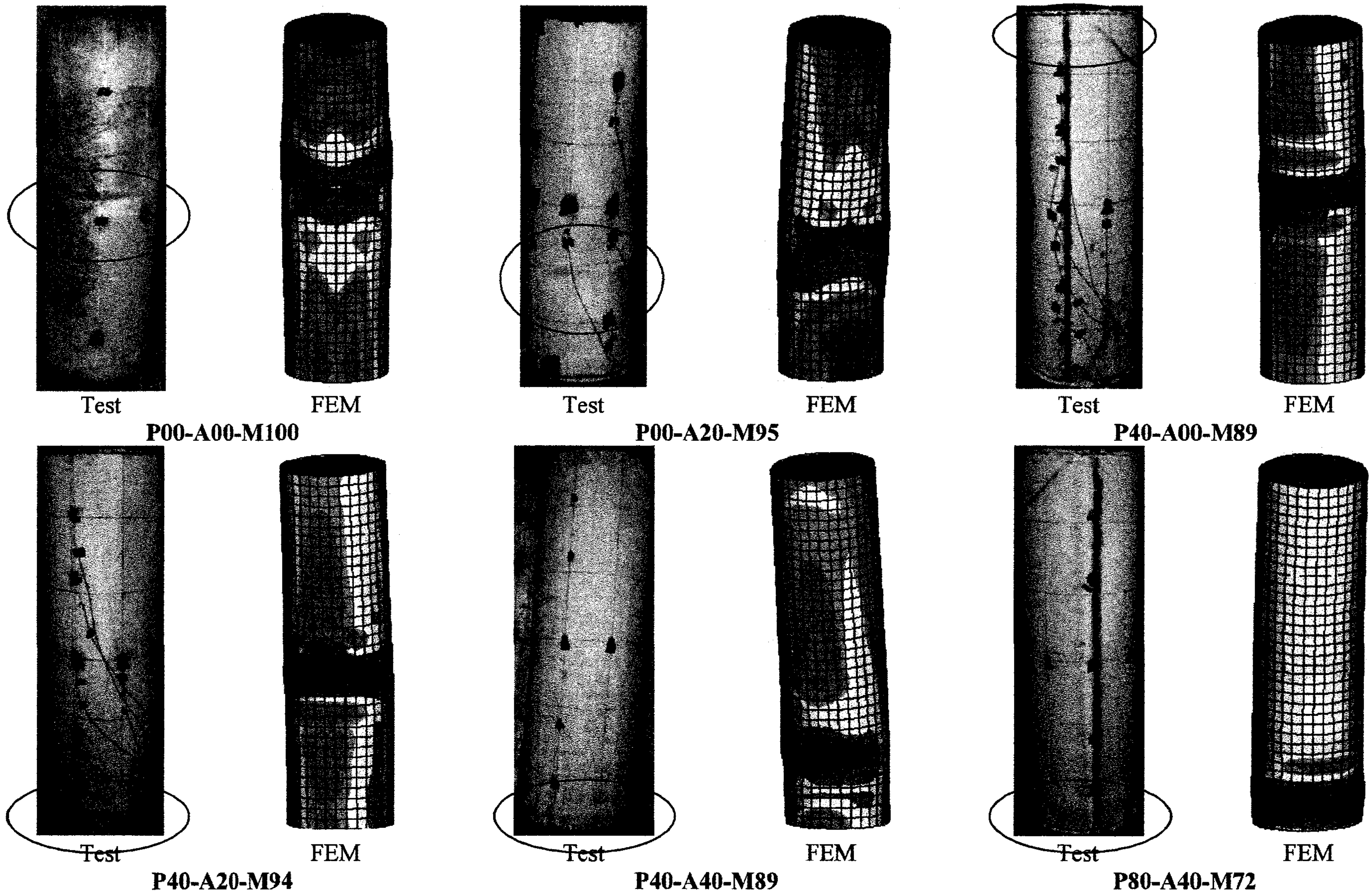

Fig. 5.18 Buckled Shapes

Numerical experimentation with the FEA has shown that the location of the buckle is highly sensitive to material properties, which have shown little variability in the tension tests conducted $\left(F_y = 541\text{MPa} \pm 7.78\text{MPa}\right)$. By varying the material yield within this range, the buckles in the FEA model were successfully triggered at the locations observed in the test. Similar results were observed by slightly varying the thickness of the pipe. An example is demonstrated in Fig. 5.19. By decreasing the thickness of the elements to 6.13mm (98% of average measured thickness 6.26) at the location of the buckle in the test, the buckle was triggered at this location for Specimen P40-A00-M89. It is thus believed that the difference in the location of the buckle between the test and FEA could be attributed to possible variability of material properties and/or geometric imperfections (Measured specimen thickness values are tabulated in Table 5.7).

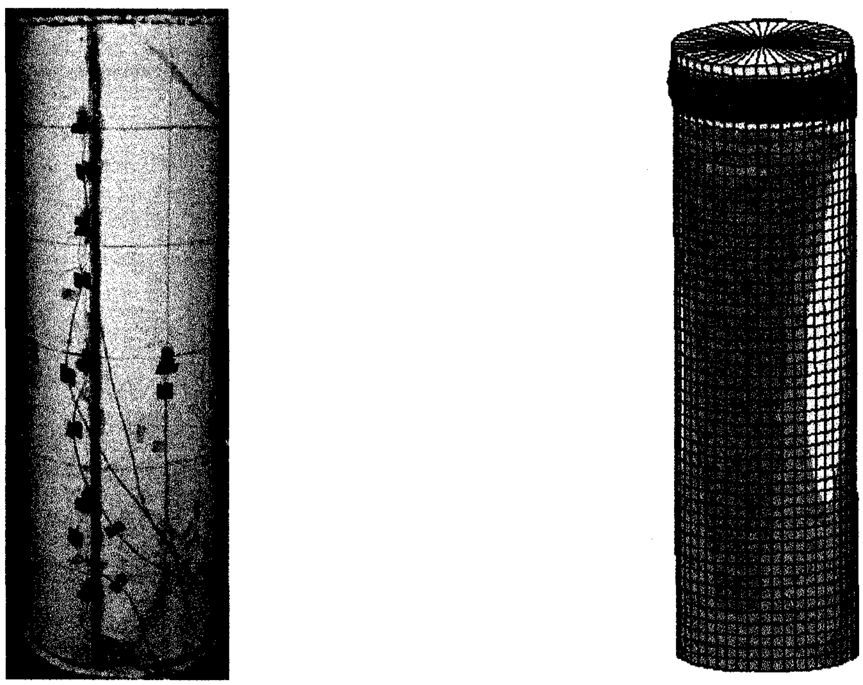

(a) Test **(b)** FEA

Fig. 5.19 Local Buckle Triggered at the Location observed during the Test for Specimen P40-A00-M89 by decreasing the Thickness of the Elements at the Buckling Location

For specimen P80-A40-M72, five outward bulges were observed in FEA model compared to the three outward bulges observed in the test. As in the test, the bottom bulge amplified while the others disappeared when the global curvature was further increased.

Table 5.7 Measured Thickness Values

Measured Thickness (mm)	
6.13	6.27
6.23	6.30
6.27	6.25
6.35	6.30
6.27	6.25
6.35	6.17
6.30	6.27
6.21	6.25
6.30	6.23
6.27	6.28
6.27	6.26
6.30	6.19
6.32	6.26
6.30	6.26
6.32	6.23
6.21	6.25
6.09	6.29
6.20	6.30
6.30	6.31
6.23	6.25
6.30	6.21
6.26	6.19
6.27	
Average	6.26
Standard Deviation	0.052

5.4.4 Moment Capacity

Table 5.8 summarizes the analytical moment capacity predictions, the FEA moment capacity predictions, and experimentally measured moment capacity of the specimens.

The experimental and FEA results were in good agreement with an average moment ratio of 0.96 and a standard deviation of 3.2%. It is concluded that the FEA model is capable of predicting pipe moment capacity when the pipes are subject to the combinations of internal pressure, axial tension, and bending.

Table 5.8 Moment Capacity

Test Identification (1)	Local Moment Capacity (kNm) Test (2)	FEA (3)	Analytical (4)	Moment Capacity Ratios Test/FEA (5)	Test/Analytical (6)
P00A00M100	780	802	853	0.97	0.91
P00A20M95	779	791	826	0.98	0.94
P40A00M89	687	739	784	0.93	0.88
P40A20M94	794	802	818	0.99	0.97
P40A40M89	788	806	784	0.98	1.01
P80A40M72	748	820	690	0.91	1.08

A comparison between the analytical moment capacity with the predicted from the tests (Column 6 of Table 5.8) shows that Specimens P40-A40-M89 and P80-A40-M72 show a test-to-analytical ratio higher than unity. For other tests, the ratio was less than unity. Thus only, Specimens P40-A40-M89 and P80-A40-M72 were able to develop their modified plastic capacities due to the fact that the biaxial state of tension induced by internal pressure and axial tension in these specimens delayed the point of onset of local buckle.

5.5 Conclusions

In this chapter, the critical buckling strains and moment capacity of pipe sections with D/t=81.2 and F_y=541MPa under internal pressure and axial tension are experimentally and numerically determined. The principal conclusions of the work are provided in the following.

5.5.1 Conclusions related to Critical Buckling Strains

1. As a general observation, specimens under axial tension exhibited significant deformations in the plastic range of deformation reaching higher curvature values when compared to specimens with zero or lower levels of axial tension. The FEA was able to predict this behavior along with the buckling modes reasonably well. However, it over-predicted critical curvatures and strains when compared to the tests.
2. Compressive strain limits were observed to increase significantly with axial tension for specimens tested under internal pressure, on the other hand, the increase was not as

significant for un-pressurized specimens. Design equations accounting for this beneficial effect were proposed.

3. The local buckling configuration is dependant on load combination acting on the pipe. Un-pressurized pipes exhibited a diamond shape mode buckle. The presence of internal pressure induced outward bulging buckles. The FEA provides very good predictions of the local buckling mode. Nevertheless, the predicted locations of the buckle were found to be very sensitive to the input stress-strain relationships and pipe cross-sectional properties.
4. Un-pressurized specimens with higher axial tensile forces experienced a more distributed local buckle along their length, for instance, while the buckle for specimen P00-A00-M100 was confined within a length of $0.5D$, the buckle in specimen P00-A20-M95 was spread over a longer segment of the pipe of about $0.75D$.

5.5.2 Conclusions related to Moment Capacity

5. The interaction equations in Mohareb (2002 and 2003) predicted a higher capacity than those recorded in the tests for four out of six specimens tested. Specimens P40-A40-M89 and P80-A40-M72 were able to develop their plastic capacities.
6. Based on the experimental program, it is judged that the ability of the pipes to develop their plastic capacity is dependant on the load combinations acting on the pipe. The stabilizing effect of internal pressure and axial tension is beneficial for pipes to develop their modified plastic moment capacity.
7. The FEA provides very good predictions of the bending moment capacity and FEA model developed in the study can be used for the capacity prediction of pipes subject to combinations of internal pressure, axial tension/compression, and bending in the absence of experimental data.

Chapter 6

Testing of Pressurized Pipes under Tension, Torsion, and Bending

6.1 Scope

In this chapter, two full-scale tests on pipes subject to combinations of internal pressure, axial tension, torsion, shear, and bending are presented. As mentioned in Chapter 3, although pipeline standards (CAN/CSA Z662 2003) recognize the ability of stocky pipe sections to develop their plastic capacity prior to local buckling in the design of elevated pipelines, they do not include general classification rules for these sections under complex load combinations including torsion. Previous experimental work (Chapter 2) has focused on testing pipes under internal pressure, axial force (mainly compression), and bending. The experiments presented in Chapter 5 extended the experimental database to pipes under tension. It is the objective of this chapter to further extend the existing experimental database by testing pipes under more complex loading involving axial tension, internal pressure, shear, torsion, and bending. An FEA model is also developed as part of the study. It is shown for both pipes tested that FEA is a reliable tool in predicting moment capacity for pipes under complex loads. The FEA model validated in this chapter and in Chapter 5 will be used in Chapter 7 in order to expand the database numerically and systematically assess the effect of various parameters on the ability of pipes to attain the modified plastic resistance.

6.2 Design of Experiments

A description of the specimens selected is presented in Section 6.2.1. The test setup specifics are presented in Section 6.2.2. Section 6.2.3 presents the loading protocol while Section 6.2.4 presents the instrumentation.

6.2.1 Specimen Geometry and Material Properties

Two pipe specimens with 508mm OD with a thickness of 6.35mm and a corresponding D/t ratio of 80 and made of X65 grade steel (SMYS=448MPa) are tested. The pipes have the same nominal material and geometric properties as the first test series. However, the supplier of the specimens of this series of tests (LaBarge Pipe & Steel) is different from that of specimens described in Chapter 5.

Thus, another set of geometric measurements and material properties were taken. The measured average wall thickness (t) of the specimens was found to be 6.37mm and the measured diameter D is 508mm, corresponding to D/t=79.7. The length L_p of the specimens was selected as 1,500mm, which corresponds to about 3.0 pipe diameters.

6.2.2 Description of the Test Setup

The general test setup in Fig. 5.1 was modified for the requirements of this test series. The figure for the modified test setup is schematically illustrated in Figs. 6.1 and a photo of the test setup is presented in Fig. 6.2. Among the six possible actuator locations, only horizontal Actuators A and B were used in order to apply the desired load combinations of torsion and bending to pipe specimens.

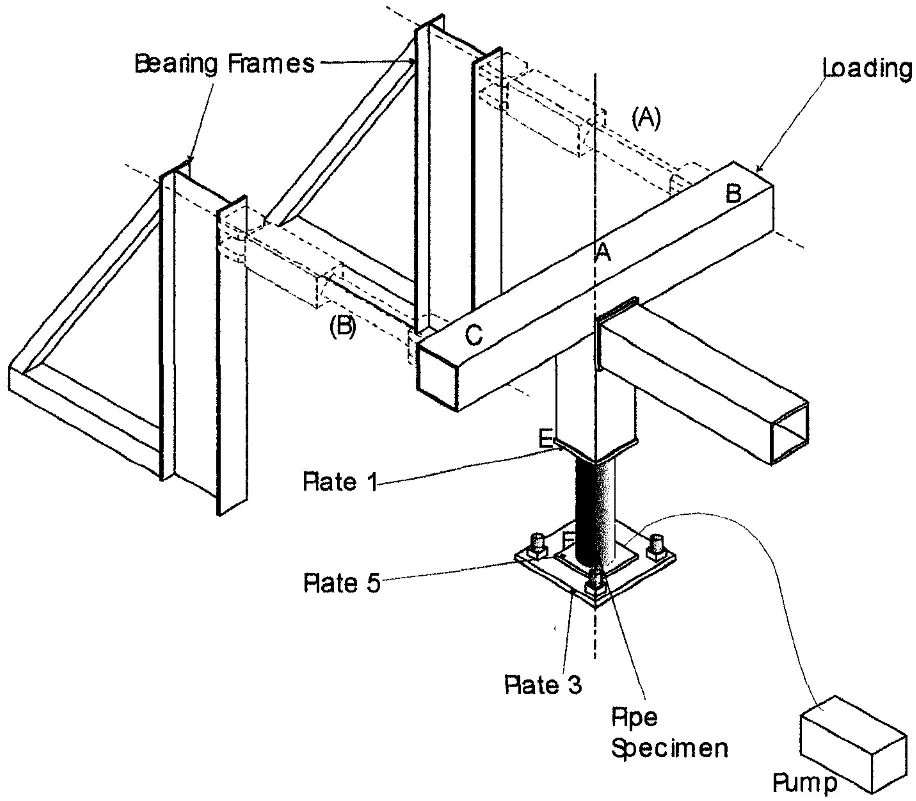

Fig. 6.1 Test Setup for the Test Series 2 (Internal Pressure + Axial Tension + Torsion + Shear + Bending)

Actuators A and B were connected to the loading arm through high strength bolts at one end and to the bearing frames (B1 and B2) at the other end. The bearing frames were anchored to the strong floor by means of anchor rods (Fig. 6.2). Also, a K-truss bracing system (not shown on Fig. 6.1 for clarity but depicted in Fig. 6.2) made of a horizontal square HSS 152x152x13 and two diagonal angles L152x152x16 between the two bearing frames were provided to prevent potential lateral torsional buckling of the vertical members as the actuators are ramped against the loading arm (Fig. 6.2). An electric water pump was used in order to provide the internal pressure and axial tension on the specimen. At the beginning of the test, the pipe was filled with water. The water was then pressurized to the desired level by means of an electric switch, which controls the water pump. Throughout the test, the pressure was monitored through two pressure gages located at the top and bottom plates (Plates 1 and 5 in Fig. 6.1). The water pressure acting on the top and bottom plates also provided an axial tensile force on the specimen. Torsion was then applied to the specimen by ramping the actuator forces by equal amounts in opposite directions. Subsequently, the stroke of both actuators was ramped in the same direction, thus inducing bending moments and an associated shearing force.

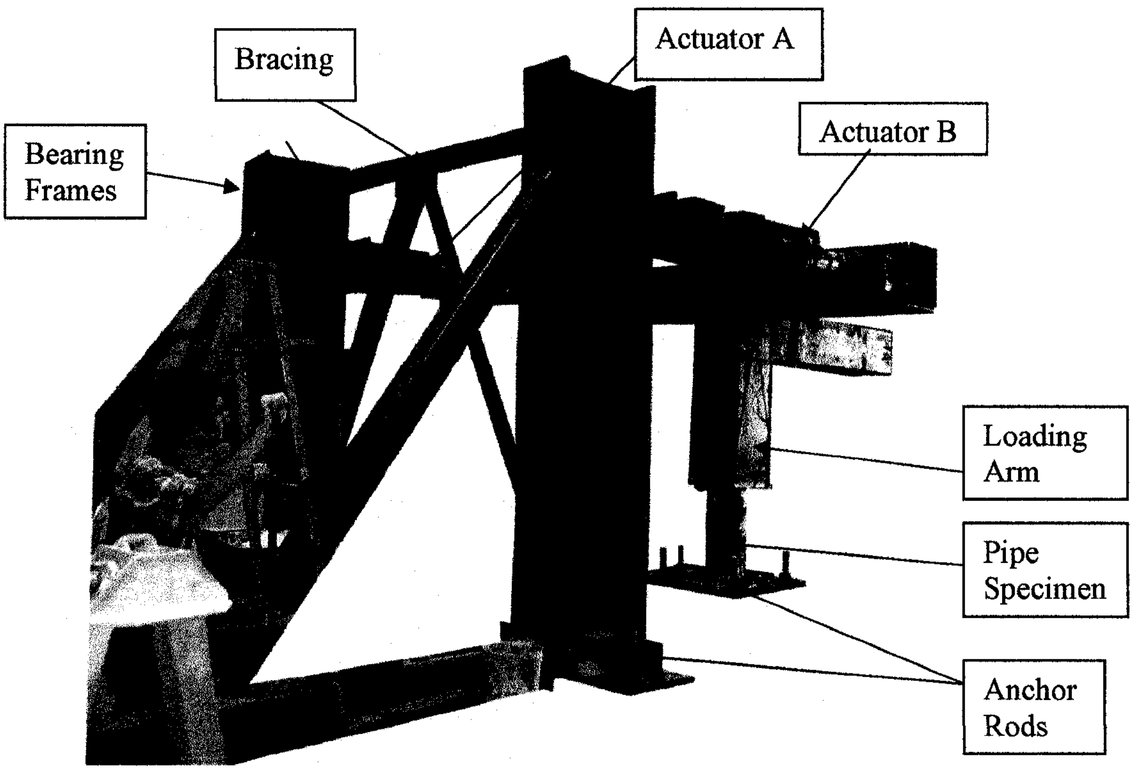

Fig. 6.2 Test Setup

6.2.3 Loading Protocol

Both specimens were tested under the same combination of internal pressure and axial tension while the torsion, shear, and bending combination was different. The load ratios applied to both specimens are presented in Table 6.1.

Table 6.1 Test Load Ratios (all ratios are provided as percentages)

Test ID	Target Load Ratios based on SMYS=448MPa					Load ratios applied in the test based on F_y=464MPa				
	p_r	A_r	T_r	$V_r^{\#}$	$M_r^{\#}$	p_r^*	A_r^*	T_r^*	Vr^*	$M_r^{\&}$
(1)	(2)	(3)	(4)	(5)	(6)	(7)	(8)	(9)	(10)	(11)
Test-1	40	20	50	9	75	39	18	48	11	76
Test-2	40	20	75	6	50	39	18	72	9	54

*Load applied during the experiments
#Predicted by interaction relations based on nominal properties (Eqs. 1.1 and 1.2)
&Predicted by interaction relations based on measured properties (Eqs. 1.1 and 1.2)

For both tests, an internal pressure corresponding to a hoop stress of 40% of the SMYS was applied. An associated axial tensile force corresponding to 20% of the longitudinal yield capacity (A_y) was applied through the action of the pressurized water on the end of the pipe. The twisting moment applied was different in both tests. For Test-1, 50% of the plastic torsion capacity of the pipes (calculated in the absence of other internal force components) was applied to the specimen. In Test-2, this value was increased to 75%. After the application of torsion, lateral displacements were applied to the top of the specimen by the actuators leading to a constant shear and linear moment along the specimen height (the details are discussed in Section 6.3). When second order effects resulting from the deformation of specimen are ignored, shearing force V_b and bending moment M_b at the location of the buckle can be related through.

$$M_b = V_b z \tag{6.1}$$

where z is the vertical distance between the point of application of the actuators and the mid-height of the local buckle on the pipe. For Test-1, distance z was 3,449mm and for Test-2 z=3,386mm. By substituting the applied load ratios for internal pressure (p_r), axial tension (A_r), and torsion (T_r) given in Table 6.1, and expressing the moment ratio M_b/M_p in terms of shear from Eq. 6.1, one obtains $M_b/M_p = V_b z/M_p$. Further substitutions into interaction relations (Eqs. 1.1 and 1.2) yield to the modified moment ratio M_{pm}/M_p. Based on this procedure, one obtains predicted shear ratios of 9% and 6% of the plastic shear capacity (V_p) and modified moment ratios M_{pm}/M_p of 75% and 50% for specimens 1 and 2, respectively. The shear ratios predicted are tabulated in Column 5 of Table 6.1 while the bending ratios predicted were tabulated in Column 6.

6.2.4 Instrumentation

The instrumentation for the experiments is shown in Fig. 6.3. In the figure, the centerlines of both actuators are depicted as solid lines.

Assuming ideal conditions, the top section of the specimen is expected to undergo four types of displacements. These are: (1) axial displacement along the z-axis, (2) angle of twist about the z-axis, (3) angle of rotation about the y-axis, and (4) horizontal displacement along the x-axis. Because of possible imperfections (such as any slight asymmetry of the test setup, eccentricity of the pipe, out-of-straightness, etc.) and second order effects, there could be some minor displacements along the *y*-axis and rotations about the *x*-axis, respectively, which increase the number of degrees of freedoms at the top section to six.

As illustrated in Fig. 6.3, Clinometers CLA and CLB are mounted on Actuators A and B in order to measure their rotation about the y-axis (Fig. 6.3c) throughout the test. Clinometers CL1, CL2, CL3, and CL4 are mounted at 500mm intervals along of the specimen to obtain the rotations about the y-axis (Fig. 6.3a). LVDTs A and B are located on the loading arm along the centerline of the actuators in order to measure the deflections along the x-axis (Fig. 6.3a). LVDTs 1 through 5 are located at the top of the specimen in the directions shown to measure the deflections at this level (Figs 6.3a and 6.3b). Position transducers (PT101-1, 2, 3, and 4) are used to measure the horizontal deflection of the actuators from which the rotation of the actuators about the z-axis (vertical) can be calculated (Fig. 6.3c).

The loads applied by the actuators are measured by load cells, which were internally mounted within each actuator. Stroke readings of the actuators were also measured by temposonics embedded in the actuators. The pressure of the water inside the specimen was measured by pressure gages PG1 and PG2 (Fig. 6.3b), which were mounted on holes located on the top and the bottom plates.

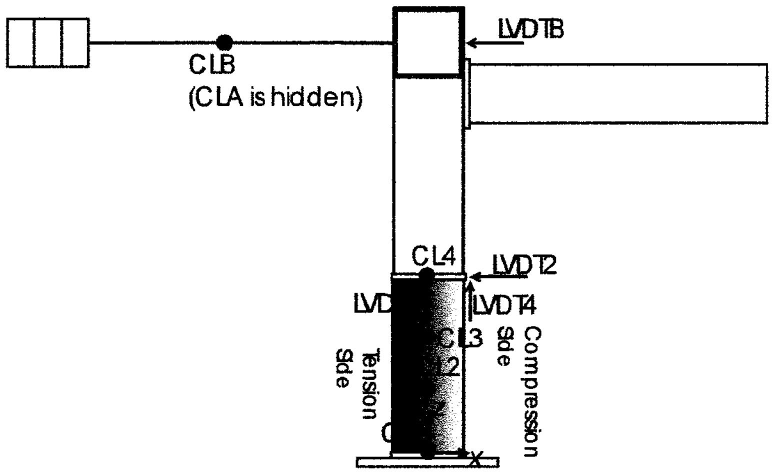

(a) Side View

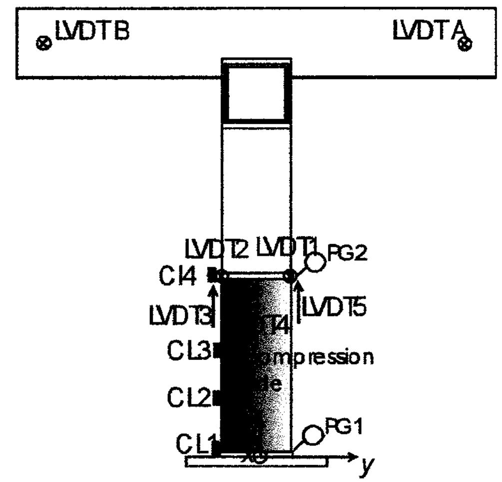

(b) Front View

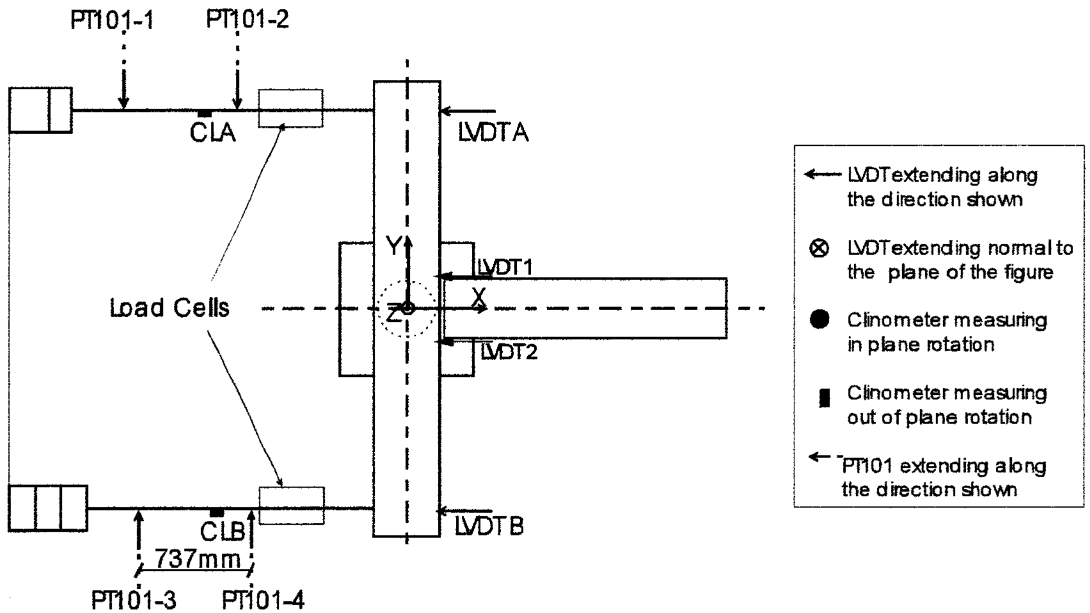

(c) Plan View

Fig. 6.3 Instrumentation

6.3 Load Sequence and Control

Water is pumped into the inside of the pipe using an electric pump and pressurized until the hoop stress reaches 40% of the nominal yield stress i.e., $pD_i / 2t = 0.4F_y$. The internal pressure acting on plates 1 and 5 induces a tensile force of 20% of the pipe axial tensile yield capacity.

The loading scheme described in Fig. 6.4 was implemented through a control program developed under Labview VII. The program consists of two modules. Module 1 applies a pure twisting moment to the specimen through a user input target force magnitude for Actuators A and B, both forces being equal and apposite, while Module 2 preserves the previously attained twisting moment magnitude while increasing the displacement of Actuator A by a user specified amount.

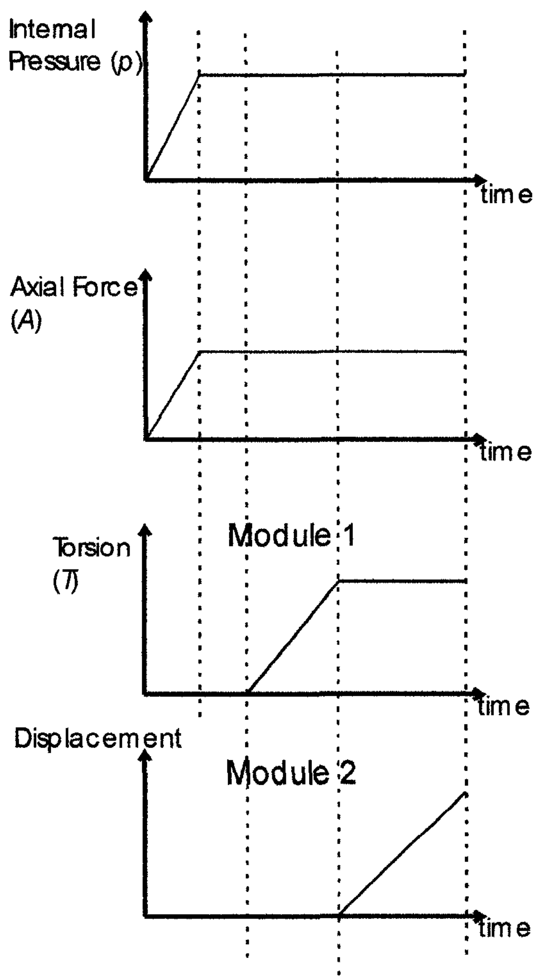

Fig. 6.4 Load Application Sequence

Module 1 starts by increasing the force F_A in Actuator A, by a small increment $\Delta_1 F_A$ specified by the user. As a result of the increment force $\Delta_1 F_A$ of Actuator A, the force F_B on Actuator B is increased by an equal amount in the opposite direction ($\Delta_1 F_B = -\Delta_1 F_A$). The change in force of Actuator B initiates another incremental change ($\Delta_2 F_A$) in force F_A. The force in Actuator B is readjusted by an amount $\Delta_2 F_B = -\Delta_2 F_A$. The process is repeated until the force change in Actuator A, $\Delta_i F_A$, drops below a prescribed tolerance value, say 0.5 kN. The procedure is repeated for the next load increment automatically until the specified target force (or twisting moment) is attained. When this condition is reached, the procedure stops and the user is prompted to initiate Module 2. When Module 2 is started, the current position (D_0) of Actuator A is read and its target position (D_t) is input to the program by the user. The process of going from D_0 to (D_t) is performed incrementally by applying a number (n) of displacement increments $\Delta_1 D_A$ to Actuator A such that $\Delta_1 D_A = (D_t - D_0)/n$.

During an applied stroke increment ($\Delta_1 D_A$), the force in Actuator A is recorded and the corresponding force change $\Delta_1 F_A$ is determined. The force in Actuator B is increased by an equal amount ($\Delta_1 F_A$) in the same direction. This preserves the initial magnitude of the torsion. The change in force in Actuator B causes an additional incremental change $\Delta_2 F_B$ in force of Actuator A, which is recorded. Again, the force in Actuator B is changed by an equal amount ($\Delta_2 F_A$). A third cycle of iteration is started, and the iterations stop when the change $\Delta_i F_A$ drops below a user specified tolerance, say 0.5 kN.

When the above condition is achieved, the following displacement increment is automatically applied. The procedure is repeated until the target displacement D_t is achieved. In each applied displacement increment, a linearly varying moment along with constant shearing force is applied to the pipe specimen. Further details related to the control program can be found in (Ozkan 2007).

6.4 Ancillary Tests

The engineering stress vs. engineering strain relationship of the pipe material was determined by testing three longitudinal tension coupons with dimensions according to ASTM-E8 (2001) specifications. Figure 6.5 shows the locations where these coupons were taken from the pipe cross-section.

Very little material variation between the three tension coupon tests was observed. Thus, the stress vs. strain values measured from the maximum compression fiber (Coupon 2 in Fig. 6.5) is selected as a representative relationship of the material properties in the longitudinal direction. These values were also used in the finite element model (Section 6.6). Table 6.2 presents the stress-strain values measured from these coupons.

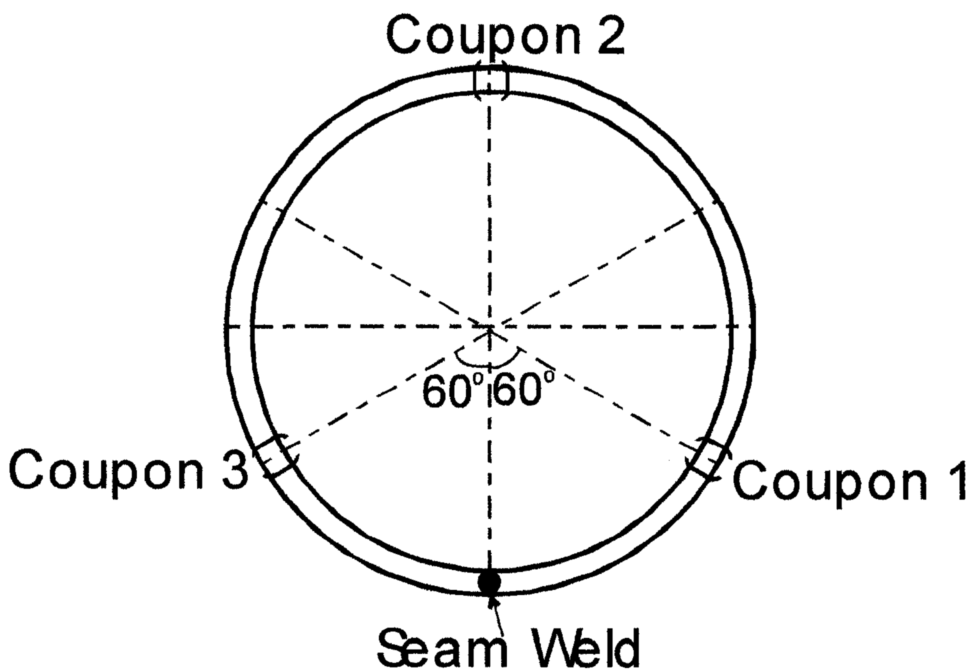

Fig. 6.5 Location of the Tension Coupon Specimens

Table 6.2 Stress vs. Strain Data

Engineering Stress (MPa)				True Stress (Mpa)	
Coupon			Engineering Strain	Coupon	Logarithmic Strain
1	2	3		2	
0	0	0	0.0000	0	0.0000
70	76	76	0.0004	76	0.0004
103	116	117	0.0006	116	0.0006
140	154	156	0.0008	155	0.0007
180	193	197	0.0009	193	0.0009
220	232	236	0.0011	233	0.0011
241	252	257	0.0013	253	0.0013
267	277	282	0.0014	277	0.0014
301	309	320	0.0016	310	0.0016
322	330	335	0.0018	331	0.0018
340	347	352	0.0019	348	0.0019
377	385	388	0.0022	386	0.0022
412	422	423	0.0027	423	0.0027
431	445	437	0.0031	446	0.0031
461	464	464	0.0047	466	0.0047
467	465	475	0.0095	469	0.0095
471	468	478	0.0123	474	0.0122
502	503	507	0.0357	520	0.0351
513	513	517	0.0504	539	0.0492
522	521	524	0.0655	555	0.0634
528	528	529	0.0850	573	0.0816
532	531	533	0.1175	594	0.1111
532	531	533	0.1258	598	0.1185
532	531	533	0.1377	604	0.129
532	532	532	0.1386	606	0.1298
531	531	532	0.1601	616	0.1485
531	531	531	0.1826	627	0.1677
516	516	516	0.2608	650	0.2318
476	476	476	0.2957	617	0.2591
372	372	372	0.4000	521	0.3365

The extension-under-load method corresponding to a specified total strain of 0.005 was used to determine the yield strength of the pipe material (ASTM E 8M-01), which was found as 464 MPa. This value is 3.6% higher than the specified value (448 MPa). The ultimate strength (F_u) was found as 532 MPa. The modulus of elasticity (E) of the pipe was 208,968 MPa with a proportional limit of 193 MPa. The Poisson's ratio was measured as 0.27 and the measured rupture strain was 0.40 corresponding to a rupture stress of 372MPa.

6.5 Internal Forces Obtained from Experiments

The calculation of internal force components including the second order effects is presented in this section. These internal forces include torsion (Section 6.5.1), bending moment (Section 6.5.2), and axial tension and shear (Section 6.5.3).

The plan view of the test setup in the deformed configuration can be seen in Fig. 6.6. Also, the free-body diagram in an elevation view for the deformed test specimen is illustrated in Fig. 6.7. In these figures, the loading arm was assumed to undergo rigid body displacements and rotation.

In the deformed configuration in Fig. 6.6, Point O of the loading arm undergoes displacement Δ_x and thus moves to O'. Also, the four corner points of the loading arm C, D, E, and F move to C', D', E', and F', respectively. Points P_A and P_B, located at the hinges of the swivel of Actuators A and B, respectively, move to positions P_A' and P_B' after the deformation. Throughout deformation, the line of action of actuator forces F_A and F_B undergo in-plane rotation angles ξ_A and ξ_B, respectively. As a result of the asymmetry of the buckling modes due to torsion, it was observed that the top of the specimens underwent a displacement along y-axis (Δ_y) after the initiation of the buckle, which coincides with the peak moment. However, no instruments were used to measure this deflection. Finite element model of the tests predicted a deflection of 0.30 mm along y-axis for Test 1 at the peak moment. This value increased to about 1.97 mm at the end of the deformation history. Deflection along y-axis was 1.14 mm at the peak moment for Test 2. This value demonstrated a rapid increase after the initiation of buckle and reached to 5.63 mm at the end of the deformation history. As a conclusion, it was judged that the deflection along y-axis results in very small rotations of Actuators A and B and was ignored in the calculation of torsion.

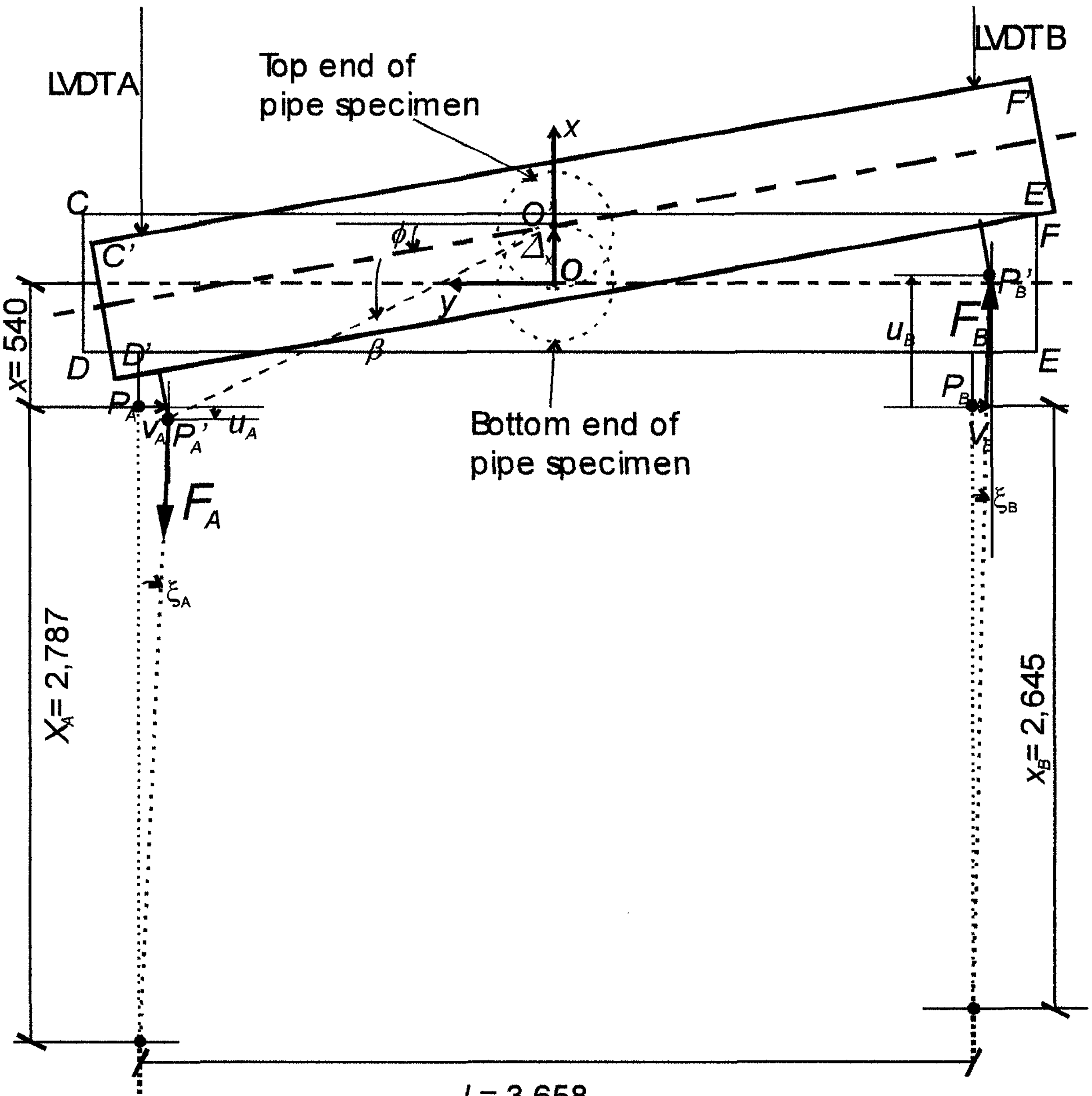

Fig. 6.6 Plan View of the Deformed Test Setup after the Application of Internal Pressure, Torsion, Axial Tension, and Bending (all dimensions are in mm)

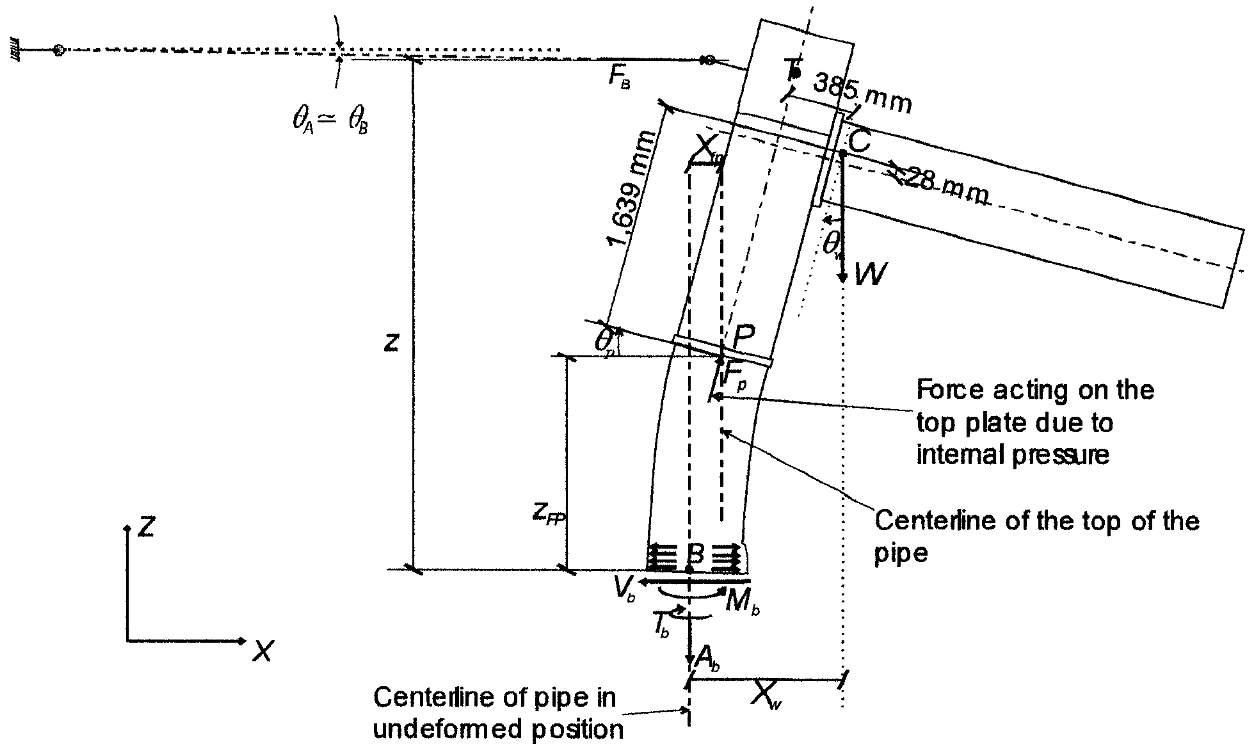

Fig. 6.7 Elevation after the Application of the Displacements

Figure 6.7 shows force F_B (note that force F_A, is hidden behind the line of action of force F_B and is approximately parallel to that of Actuator B). As the specimen deforms throughout the test, the lines of action of Actuators A, and B rotate through angles θ_A and θ_B, respectively (Fig. 6.7), which were measured by clinometers CLA and CLB in Fig. 6.3. It was observed that rotations θ_A and θ_B reach a maximum of around 0.65 degrees at the end of the tests, which is judged to be negligible. Thus, second order effects that arise from rotations θ_A and θ_B are disregarded.

6.5.1 Expression for Torsion

In the deformed position, the twisting moment acting at the bottom section of the pipe can be calculated by taking the moments of the inclined forces F_A and F_B about Point O in Fig. 6.6.

$$T_b = F_{Ax}L\cos(\phi+\beta) - F_{Ay}(x+u_A) + F_{Bx}L\cos(\beta-\phi) + F_{By}(x-u_B) \tag{6.2}$$

in which $F_{Ax} = F_A \cos\xi_A$, $F_{Ay} = F_A \sin\xi_A$, $F_{Bx} = F_B \cos\xi_B$, and $F_{By} = F_B \sin\xi_B$. The definitions of other variables appearing in Eq. 6.2 are given in column 2 of Table 6.3. Column 3 of Table 6.3 provides either the equation used to determine the variables or identifies the instrument used to measure it

6.5.2 Expression for Bending Moments

The reactions at the buckle mid-height, (close to bottom of the pipe in both tests) consist of a bending moment (M_b) as calculated by Eq. 6.3, an axial tension force (A_b) as calculated by Eq. 6.6, shearing forces (V_{bx} and V_{by}) as calculated by Eqs. 6.4 and 6.5, and a twisting moment (T_b) as calculated by Eq. 6.1.

The reaction moment (M_b) at the location of the buckle including second order effects due to the rotation of the specimen and the loading arm is calculated by summing the moment about point *B*.

$$M_b = F_{Ax} z + F_{Bx} z - F_p x_{Fp} \cos\theta_p + F_p z_{Fp} \sin\theta_p + W x_w \tag{6.3}$$

In Eq. 6.3, we recall that $F_{Ax} = F_A \cos\xi_A$, $F_{Ay} = F_A \sin\xi_A$, $F_{Bx} = F_B \cos\xi_B$, and $F_{By} = F_B \sin\xi_B$. Distance z_{Fp} is the vertical projection of the distance between top plate centerline and the buckle mid-height. It takes the values 1,398mm and 1,335mm for Test-1 and Test-2, respectively. Length x_w is the horizontal distance between the center of gravity of the loading arm to the centerline of the pipe in its un-deformed position and is calculated by $L_{PC} \sin\left(\theta_{PC} + \theta_p\right) + x_{Fp}$ in which L_{PC} is distance PC ($L_{PC} = \sqrt{1{,}639^2 + 385^2} = 1{,}684$) and angle θ_{PC} is the angle between line PC and the line of application of force F_p. In the same equation, distance z is the vertical distance between the point of application of forces F_{Ax} and F_{Bx}, and the centerline of the specimen in its un-deformed position. Angle θ_p is the rotation of the top of the specimen as measured by Clinometer CL4 (Fig. 6.3).

Table 6.3 Definition of the variables in Eq. 6.2

Variable (1)	Definition (2)	Calculation (3)
F_A	Force on Actuator A	Measured by Load Cell A on Actuator A
F_B	Force on Actuator B	Measured by Load Cell B on Actuator B
L	Distance OP_A or $O'P_A'$	$\sqrt{x^2+(L_t/2)^2}=\sqrt{540^2+1{,}829^2}=1{,}907mm$
u_A	Displacement of point P_A along x-axis	Obtained from LVDT A
u_B	Displacement of point P_B along x-axis	Obtained from LVDT B
ϕ	Twisting angle of the pipe	$\arctan\left[(u_B-u_A)/L_t\right]$
L_t	Centerline to centerline distance between the actuators in un-deformed position	3,658mm
β	Angle the imaginary line between points A and O is making with the center line of the loading arm	$\arctan\left[x/(L_t/2)\right]=\arctan(540/1{,}829)=16.4^o$
v_A	Displacement of point P_A along y-axis	$(L_t/2)-\left[L\cos(\phi+\beta)\right]$
v_B	Displacement of point P_B along y-axis	$\left[L\cos(\beta-\phi)\right]-(L_t/2)$
D_A	Stroke change in Actuator A	Measured by Temposonic A of Actuator A
D_B	Stroke change in Actuator B	Measured by Temposonic B of Actuator B
ξ_A	In-plane rotation of Actuator A	$\arcsin\left[v_A/(x_A+D_A)\right]$
x_A	Length between the hinges of Actuator A in the un-deformed configuration	2,787mm
ξ_B	In-plane rotation of Actuator B	$\arcsin\left[v_B/(x_B+D_B)\right]$
x_B	Length between the hinges of Actuator B in the un-deformed configuration	2,645mm
x	Distance between the centerline of the loading arm to the hinge of the actuators	540mm

6.5.3 Expressions for Shearing and Axial Forces

The shearing force components (V_x and V_y) at the bottom of the pipe are calculated by

$$V_{bx}=F_{Ax}+F_{Bx}+F_p\sin\theta_p \tag{6.4}$$

$$V_{by} = F_{Ay} + F_{By} \tag{6.5}$$

Since V_{by} is very small compared to V_{bx}, it was ignored in the calculations of modified plastic ratio.

Also the axial force (A) is calculated as

$$A_b = F_p \cos\theta_p - W \tag{6.6}$$

Columns 7, 8, 9, and 10 of Table 6.1 provide internal pressure ratio p_r, torsion ratio T_r, shear ratio $V_r = V_{bx}/V_p$, and axial force ratio A_r for each specimen as calculated by Eqs. 6.2, 6.4, and 6.6 corresponding to the maximum moment observed in the experiments based on measured material yield strength (F_y) and measured cross-sectional properties (D and t). The modified bending ratio M_{pm}/M_p is calculated by the interaction relations (Eqs. 1.1 and 1.2).

6.6 Description of the FEA Model

The finite element model generated for the prediction of test results can be seen in Fig. 6.8. The model consists of three main parts: (1) the pipe specimen, which is modeled by using 40 S4R shell elements in the circumferential direction and 38 S4R shell elements along the height of the pipe (The features of element S4R have been discussed in Section 5.2.1), (2) the top plate, modeled by using S3R shell elements (a degenerated 3-node form of the S4R element), which is modeled as rigid body through the Rigid Body option of ABAQUS, and (3) loading arm, modeled as a rigid body through two beam elements (element type B31) through the Rigid Body option of ABAQUS, thus, assuming the deformation of the loading arm is negligible compared to that of the pipe specimen.

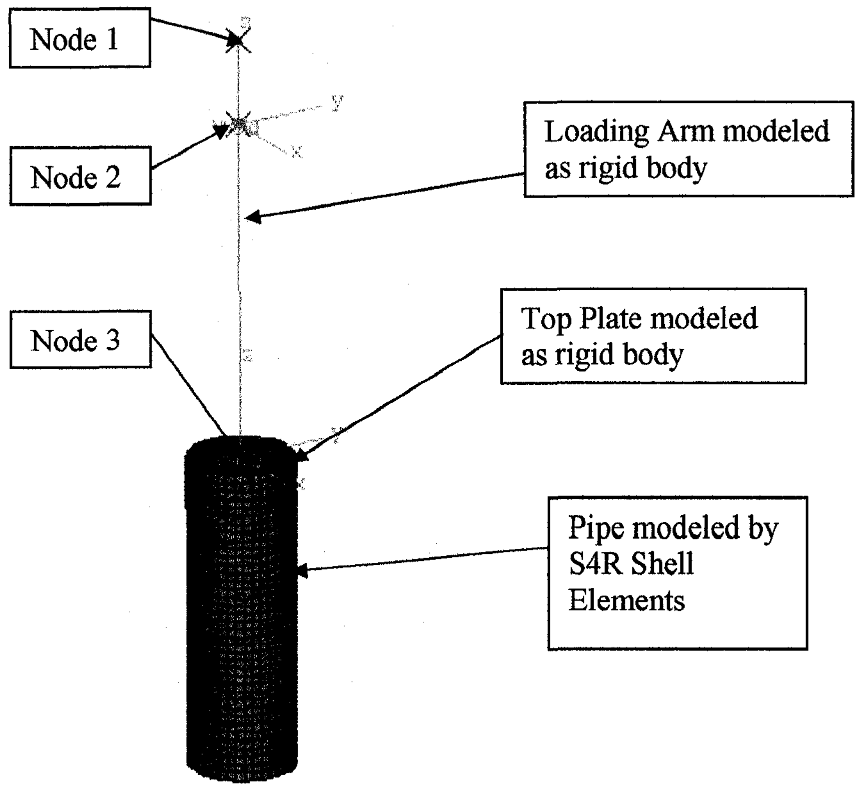

Fig. 6.8 Finite Element Model

The loads and deformations are applied to the model through the nodes of the loading arm as follows: Firstly, the self-weight of the loading arm along with the moment it creates about the centerline of the pipe is applied to node 2 of the loading arm (Fig. 6.8). Secondly, internal pressure is applied as a follower pressure normal to the shell elements. Also, the axial force on the pipe ends due to the internal pressure is applied as follower force at node 3 of the top plate (Fig. 6.8). Lastly, the average displacements recorded, based on the readings of LVDTs A and B (Fig. 6.3), are applied to the FEA model through node 1 along the x-axis (Fig. 6.8).

6.7 Results

This section presents a comparison between the experimental and FEA results. They include the plastic moment capacity (Section 6.7.1), the buckled pipe configurations (Section 6.7.2), Moment vs. Curvature relations (Section 6.7.3), and buckling strains (Section 6.7.4)

6.7.1 Plastic Moment

Table 6.4 provides the moment capacity based on the tests (column 2), FEA (column 3), and analytical predictions as provided by Eqs. 1.1 and 1.2 (Column 4). In Column 5, the Test-to-FEA ratio is provided

Table 6.4 Moment Capacity

	Moment Capacity (kNm)			Moment Capacity Ratios	
Test (1)	**Test (2)**	**FEA (3)**	**Analytical (4)**	**Test/FEA (5)**	**Test/Analytical (6)**
Test-1	601	597	568	1.01	1.06
Test-2	457	471	402	0.97	1.13

The proximity of this ratio to unity is an indication of the excellent ability of the FEA to predict test results in terms of moment resistance.

Recalling the Canadian Steel Code (CAN/CSA S16-01), classification for circular hollow sections subject to pure flexure, pipes, which satisfy the requirement $D/t \le 13{,}000/F_y$ are considered Class 1 sections and can be designed against bending by plastic design requirements. Pipes that satisfy the requirement $D/t \le 18{,}000/F_y$ are considered Class 2 (compact) sections and can also be designed based on their plastic resistances. Pipes that satisfy the requirement $D/t \le 66{,}000/F_y$ are considered Class 3 (sub-compact) sections and can be designed against bending by elastic design requirements. Pipes, which cannot satisfy Class 3 requirements are considered as Class 4 (slender) sections.

According to the classification rules of Canadian Standards for steel structures (CAN/CSA S16-01), if the specimens tested in this test series were subjected to pure bending moment, they are expected to develop their elastic moment capacity (M_e), however, they would undergo local buckling prior to the attainment of their plastic moment capacity (M_p) (Class 3 section). In contrast to this prediction of CAN/CSA S16-01, Column 6 of Table 6.4 indicates that the test-to-analytical ratio for both specimens are slightly higher than unity indicating that in both tests, both pipes attained their modified plastic moment resistance. A possible reason for the fact that plastic moment resistance is higher than test results is the moment gradient along the specimen. The validity of this hypothesis is assessed in the following section.

6.7.1.1 Effect of Moment Gradient

In order to assess the validity of the above hypothesis, two finite element runs were performed. The FEA model used for these runs can be seen in Fig. 6.9. In the first run, the specimen was initially loaded by internal pressure (p_r=40%), axial tension (A_r=30%), and torsion (T_r=50%). Then, Node 1 of top plate of the FEA model was displaced along the x-axis, which leads into a moment gradient along the length of the pipe associated with constant shear. The resulting maximum moment capacity predicted by FEA-to-moment capacity predicted by interaction relationships (Eqs. 1.1 and 1.2) ratio was 1.26. In the second run, the specimen was again initially loaded by internal pressure (p_r=40%), axial tension (A_r=30%), and torsion (T_r=50%). Then, Node 1 of the top plate of the FEA model was rotated about the y-axis, which led to an approximately constant moment along the length of the pipe. The resulting moment capacity predicted by FEA-to-moment capacity predicted by interaction relationships (Eqs. 1.1 and 1.2) ratio was only 0.99. The comparison of results shows that constant moment along the length of the pipe is a more severe loading case than that of a moment gradient.

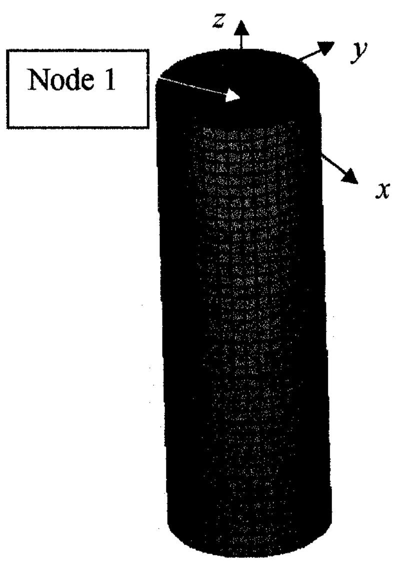

Fig. 6.9 The FEA used to quantify the Effect of Linear Moment Gradient vs. Constant Moment along the Length of the Pipe

6.7.2 Buckled Configuration

Figure 6.9 illustrates the local buckles obtained from the tests and FEA model. The local buckles occurred at the bottom of the pipes as a result of the maximum moment at that location. Unsymmetric outward bulge buckles were observed with an inclination of about 20 degrees for Test-1 and about 30 degrees for Test-2. The FEA model predictions agreed very well with the buckling modes observed during the tests. The modes observed are similar to those observed in tests of Ozkan and Mohareb (2003) on un-pressurized pipes (D/t=41) under torsion, shear , and bending.

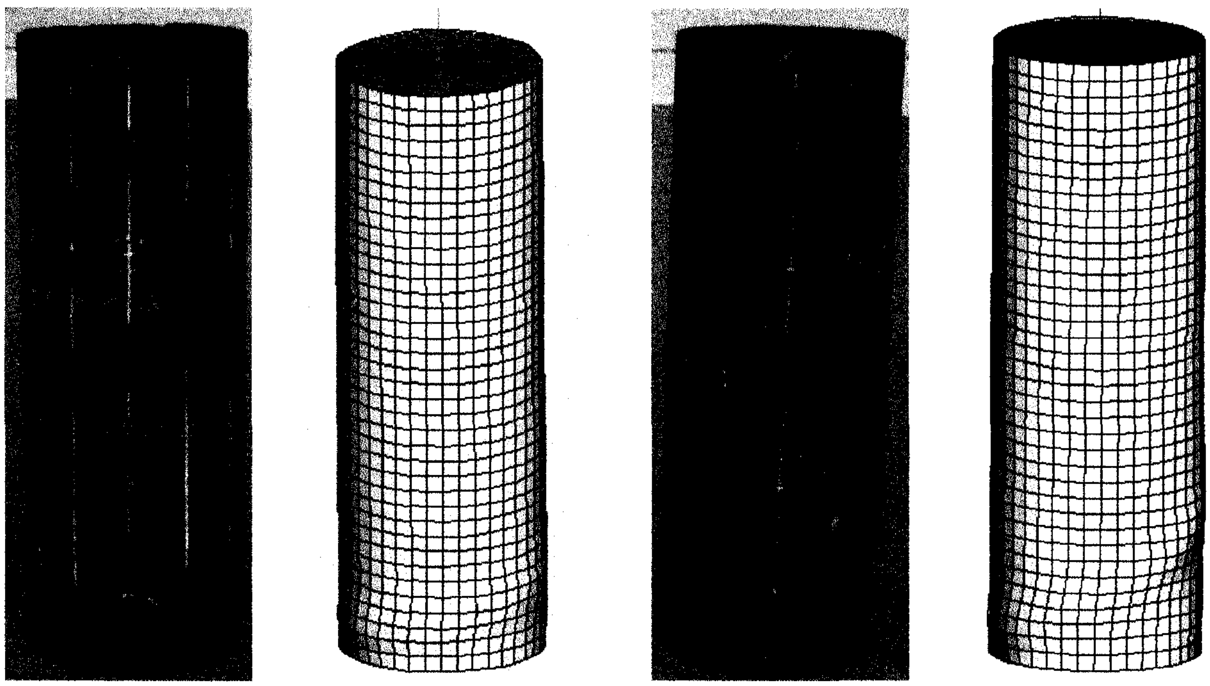

Test FEA Test FEA

(a) Test-1 **(b)** Test-2

Fig. 6.10 Buckling Modes

6.7.3 Moment vs. Global Curvature Relations

The moment at the location of the buckle (M_b) as calculated by Eq. 6.3 vs. Global Curvature (as defined by Eq. 5.4) for both specimens tested and their FEA simulation are presented in Fig. 6.11. When using the definition in Eq. 5.4 for global curvature for the tests, the rotation at the top of the pipe θ_t is taken equal to that measured by Clinometer CL4. The rotation of the bottom of the pipe θ_b is taken equal to that rotation measured by Clinometer CL1 in Fig. 6.3 (NOTE: since Clinometer CL1 was detached at the beginning of Test-1, θ_b was not available. As a result, the global curvatures for this specimen was calculated by taking $\theta_b = 0$ leading to a slight underestimation of the stiffness of the specimen in the elastic range of deformation). The corresponding FEA values are presented for two tests for comparison. The slight difference in initial slope for Test-1 between experiment and FEA is apparent.

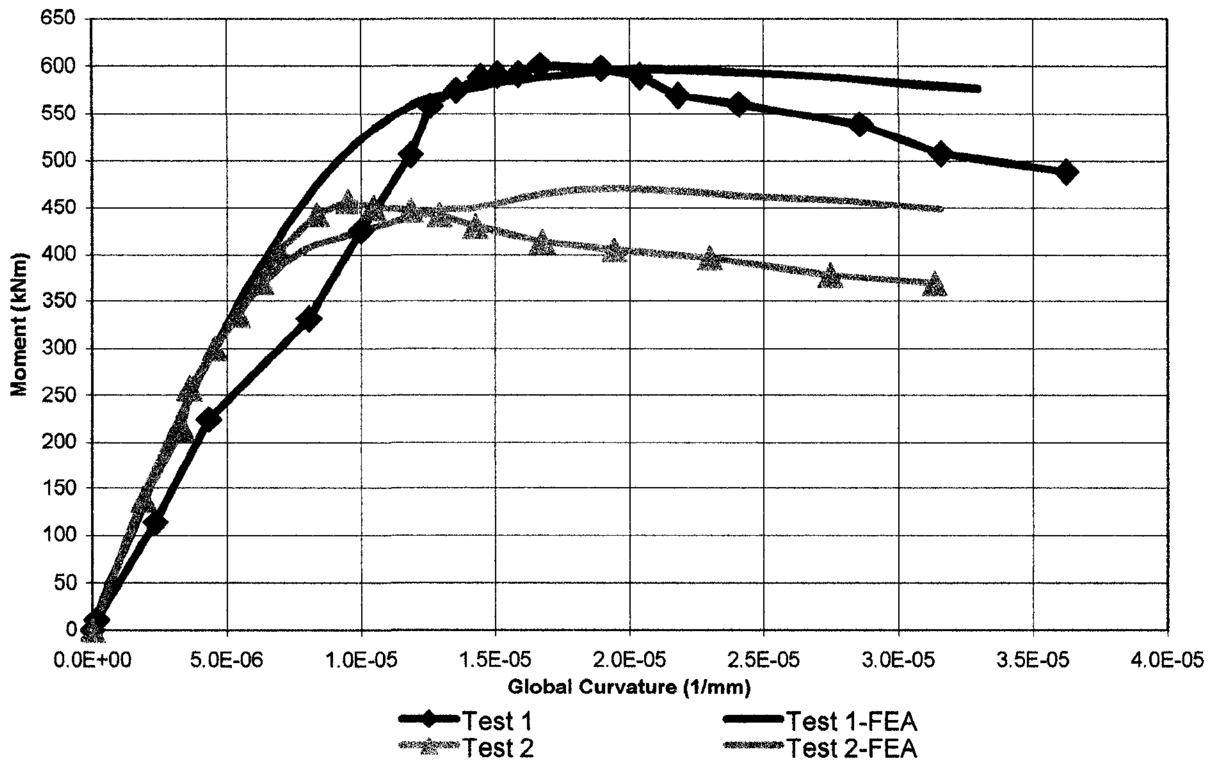

Fig. 6.11 Moment vs. Global Curvature Relationships

In Fig. 6.11, the FEA predicted peak moments agree well with the experimental peak moments. However, the Moment vs. Global Curvature relations exhibit a stiffer post-peak response. A possible reason for the difference is the difference of material properties of the pipe steel in longitudinal from the transversal directions as suggested by Workman (1988). According to Workman (1988) the pipe material in the longitudinal direction has a lower yield strength F_{yl} and plastic exponent value n_l than the yield strength F_{yt} and the plastic exponent value n_t in the transversal direction ($F_{yl}<F_{yt}$ and $n_l< n_t$). Representative true stress vs. logarithmic strain curves for longitudinal and transversal directions are presented in Fig. 6.12. Workman (1988) also suggests that pipe material with higher plastic exponent (e.g., pipe material in transversal direction n_t) causes the initiation of the buckling of the pipe earlier than pipe material with lower plastic exponent. Thus, pipes with higher plastic exponent reach their maximum load carrying capacity at earlier deformation levels.

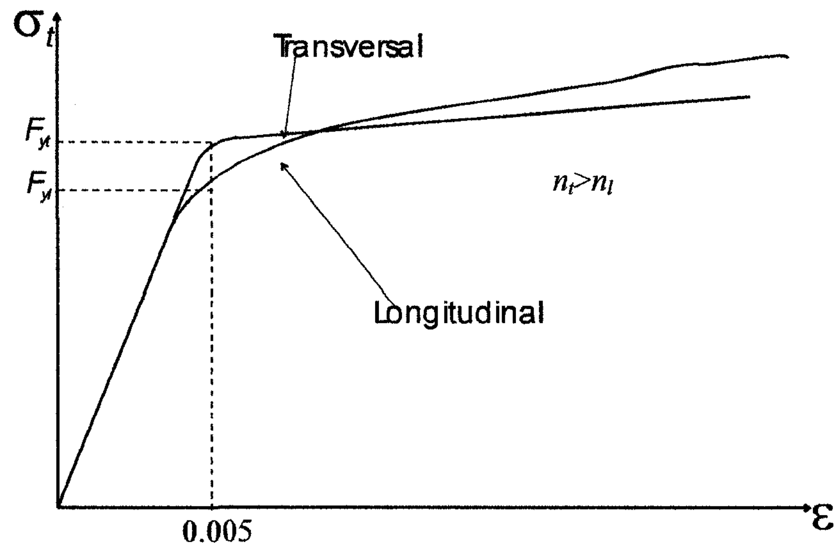

Fig. 6.12 Longitudinal vs. Transversal Stress-Strain Curves

6.7.4 Critical Strains

In most practical cases, since the pipes are laid horizontally (layout A in Fig. 6.13), torsion does not appear in buried pipelines. On the other hand, according to Gresnigt (1986), it can be considered as a loading type against which pipeline should be designed when the buried pipes is laid in a curved format (layout B in Fig. 6.13).

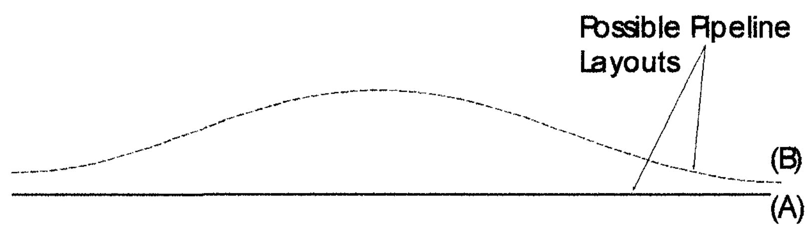

Fig. 6.13 Plan View of Two Possible Crossings of a Pipeline Layout (Gresnigt 1986)

Critical strains ε_{cr} for the two tests conducted under torsion are calculated as outlined in Section 5.3.2.1. The critical strains were found as 0.67% for Test 1 and 0.65% for Test 2. Based on both tests, an increase in torsion ratio T_r from 50% to 75%, reduced the critical strain very slightly. Given the number of the samples tested, no definite trends can be inferred.

6.8 Conclusions

In this chapter, two tests on pipes made of X65 material (SMYS=448MPa) with D/t=80 subjected to general load combinations including internal pressure, axial tension, shear, torsion, and bending were presented. Finite Element Models were also developed. The principal conclusions of the work are:

1. The FEA moment predictions of moment capacities were in very good agreement with the test results leading into a conclusion that FEA is a reliable tool in predicting moment capacity for pipes under complex load combinations.
2. The buckled shapes as obtained from the tests and FEA were also in excellent agreement. The local buckles occurred at the bottom of the pipes since the maximum moments along the pipes occurred at this location.
3. The specimens were able to develop a higher modified moment capacity than those predicted by interaction relations (Eqs. 1.1 and 1.2). The FEA shows that this is due to the moment gradient along the length of the pipe, which is a less severe case than a constant moment along the length of the pipe.
4. Some differences were observed between the experimental Moment vs. Global Curvature curves and those based on FEA. It was postulated that that the difference is due to varying material properties of pipes in longitudinal and transverse directions, which cannot be modeled by the constitutive model available within ABAQUS.
5. The very good agreement between the moment capacity and buckling configuration of the pipes obtained from the tests and FEA provide confidence in employing the FEA model in a parametric study through which the effect of different parameters on the ability of a pipe to develop its modified plastic moment capacity can be quantified. This will be presented in Chapter 7.

6. An increase in torsion ratio T_r, reduced the critical strain very slightly. Given the number of the samples tested, no definite trends can be inferred.

Chapter 7

Parametric Study

In this Chapter, the FEA model developed and verified in Chapters 5 and 6 is used in a parametric study to assess the effect of the cross-sectional geometric property (*D/t*) and loading conditions (internal pressure, axial force, and torsion) on the ability of a pipe to develop its modified plastic moment capacity as predicted by Eqs. 1.1 and 1.2 and the modified elastic moment capacity as developed in Appendix D. In the FEA study conducted, both material and geometric non-linear effects are modeled using the FEA simulator ABAQUS.

In Section 7.1 of this chapter, a review of major studies involving full-scale testing and finite element analysis of pipe segments under combined loads is provided. The finite element mesh employed in the present parametric study is introduced in Section 7.2. A discussion of the parameters studied is presented in Section 7.3. The assumed material properties, boundary conditions, and load application sequence are presented in Sections 7.4, 7.5, and 7.6, respectively. Section 7.7 provides a discussion of the results of the parametric study.

7.1 Comparative Review of Pipe Moment Capacity

This section presents a comparative summary between experimentally measured moment resistances and FEA predicted moments in previous studies (Section 7.1.1) as well as the current study (Section 7.1.2).

7.1.1 Previous Experimental Studies

In this section, emphasis is placed on research programs which have two components: a) a recent full-scale testing program on pipes subjected to combined loads, b) an FEA finite element analysis based on shell elements, including material and geometric non-linear effects. Table 1 summarizes results from test series of Prion and Birkemoe (1988) (The FEA modeling of the tests were conducted by Hu at al. (1992)), Mohareb et. al (1994), Yoosef-Ghodsi et al. (1995) (The FEA modeling of the tests were conducted by Souza and Murray (1994)), Zimmerman et al. (1995), Dorey (2001), and Zimmerman et al. (2004). Column 1 of Table 7.1 cites the main publication in which the test series is documented. Column 2 assigns a serial number for each specimen. Column 3 provides test descriptors as used in the relevant publication. Columns 4, 5, and 6 respectively provide the nominal outer diameter OD, D/t ratio, and Specified Mean Yield Strength (SMYS). Column 7 provides the internal pressure ratio p_r (i.e., the applied internal pressure to the pressure causing hoop the yield stress) maintained throughout the test and the axial force ratio A_r (i.e., the applied axial force to the axial yield resistance). Ratio A_r is positive for tension. Column 8 is the moment resistance as measured in the tests while Column 9 provides the ratio of the moment resistance measured (M_{test}) to the moment resistance as predicted by FEA (M_{FEA}).

Table 7.1 Experimentally measured and FEA predicted moment capacity comparison of previous studies

Reference	**No**	**Test Descriptor**	**OD (mm)**	***D/t***	**SMYS (MPa)**	**Loading Conditions (7)**		M_{test} **(kNm)**	M_{test}/M_{FEA} [(d)]
(1)	**(2)**	**(3)**	**(4)**	**(5)**	**(6)**	p_r [(b)]	A_r [(c)]	**(8)**	**(9)**
Prion and Birkemoe (1988)[(a)]	1	ST-6	455	70	304	0.00	0.94	64.9	0.93
	2	ST-12	450	100	266	0.00	0.81	68.0	0.98
	3	ST-7	450	100	266	0.00	1.04	0.00	0.94
	4	ST-13	511	70	450	0.00	0.98	0.00	0.99
Mohareb et al. (1994)[(e)]	5	UGA508	508	64	391	0.00	-0.27	685	1.00
	6	UGR508	508	64	391	0.00	-0.27	769	1.10
	7	DGA508	508	64	391	0.80	-0.03	416	1.00
	8	DLR508	508	64	391	0.80	+0.24	579	0.92
	9	UGA324	324	51	378	0.00	-0.29	211	1.08
	10	HGA324	324	51	378	0.36	-0.19	192	1.10
	11	DGA324	324	51	378	0.72	-0.08	146	1.12
Yoosef-Ghodsi et al. (1995)[(f)]	12	UGA20W-1	508	63	391	0.00	-0.27	460	0.87
	13	UGA20W-2	508	63	391	0.00	-0.27	640	1.21
	14	HGA20W	508	63	391	0.40	-0.15	595	1.11
	15	DGA20W	508	63	391	0.80	0.00	440	1.10
	16	UGA12W	324	50	378	0.00	-0.29	210	1.10
	17	HGA12W	324	50	378	0.36	-0.18	190	1.06
	18	DGA12W	324	50	378	0.72	-0.08	142	1.08
Zimmerman et al. (1995)	19	B1	610	87	440	0.80	0.00	774	0.99
	20	B2	610	87	440	0.00	0.00	1,086	0.99
	21	B3	610	87	400	0.80	+0.39	997	0.98
	22	B4	611	87	470	0.80	0.00	1,869	1.00
	23	B5	611	41	470	0.00	0.00	2,421	1.08
Dorey (2001)	24	CP0W-2	762	92	483	0.00	-0.22	1,684	1.00
	24	CP20W	762	92	483	0.20	-0.26	1,910	1.05
	26	CP40W	762	92	483	0.40	-0.30	1,833	1.06
	27	CP80W	762	92	483	0.80	-0.37	1,626	1.16
	28	CP20N-2	762	92	483	0.20	-0.26	1,924	1.02
	29	CP40N-2	762	92	483	0.40	-0.30	1,805	0.97

Table 7.1 Continued

	30	CP80N-2	762	92	483	0.80	-0.37	1,547	1.02
	31	T20P40W	762	92	483	0.40	+0.20	2,315	1.02
	32	T20P40N	762	92	483	0.40	+0.20	2,350	1.04
	33	T20P80W	762	92	483	0.80	+0.20	1,920	1.04
	34	T20P80N	762	92	483	0.80	+0.20	1,861	1.01
Zimmerman et al. (2004)	35	1	762	82	483	0.00	0.00	2,667	0.98
	36	2	762	82	483	0.80	0.00	1,845	1.01
	37	3	762	48	552	0.80	0.00	3,718	1.03
	38	4	762	48	552	0.00	0.00	5,198	0.99
								Average	1.03
								Stand. Dev	0.068

(a) The FEA modeling was conducted by Hu at al. (1992)
(b) Ratio of Internal pressure applied (p)-to-yield internal pressure capacity (p_y)
(c) Ratio of Axial force applied (A)-to-Yield axial force capacity (A_y) (positive when A is tensile)
(d) Ratio of Moment capacity measured in the tests (M_{test})-to-Moment capacity predicted by FEA (M_{FEA}).
(e) Moment capacity predicted by FEA (M_{FEA}) values are approximated from the Moment vs. Curvature relations provided in the document
(f) Moment capacity measured in the tests (M_{test}) and Moment capacity predicted by FEA (M_{FEA}) values are approximated from the Moment vs. Curvature relations provided in Souza and Murray (1994)

The average M_{test}/M_{FEA} for all 38 tests reported in Table 7.1 is 1.029 with a standard deviation of 0.068.

7.1.2 Present Study

The descriptions of Columns (1) through (9) are similar to those of Table 7.1. The ratio of the moment resistance measured from the tests-to-FEA moment capacity predictions from the current study is presented in the Table.

While the previous studies have focused mostly on pipes under internal pressure, axial force (compression for the most part), and bending, the present study has expanded the experimental database to include the pipes subjected to tensile forces and torsion in addition to internal pressure and bending.

Table 7.2 Experimentally measured and FEA predicted moment capacity for the present study

Reference (1)	No (2)	Test Descriptor (3)	OD (mm) (4)	D/t (5)	SMYS (MPa) (6)	Loading Conditions (7)		M_{test} (kNm) (8)	M_{test}/M_{FEA}[c] (9)
						p_r[a]	A_r[b]		
Chapter 5	39	P00A00M100	508	80	448	0.00	0.00	780	0.97
series	40	P00A20M95	508	80	448	0.00	+0.20	779	0.98
	41	P40A00M89	508	80	448	0.40	0.00	687	0.93
	42	P40A20M94	508	80	448	0.40	+0.20	794	0.99
	43	P40A40M89	508	80	448	0.40	+0.40	788	0.98
	44	P80A40M72	508	80	448	0.80	+0.40	748	0.91
Chapter 6	45	Test-1	508	80	448	0.00	+0.20	601	1.01
series	46	Test-2	508	80	448	0.00	+0.20	457	0.97
								Average	0.97
								Stand. Dev	0.032

(a) Ratio of Internal pressure targeted p_r-to-yield internal pressure capacity p_e

(b) Ratio of Axial force targeted A_r-to-Yield axial force capacity A_e (positive when A_t is tensile)

(c) Ratio of Moment capacity measured from the tests M_{test}-to-Moment capacity predicted by FEA M_{FEA}.

The average M_{test}/M_{FEA} of the eight tests in Table 7.2 is 0.97 with a standard deviation of 0.032. For the 46 specimens in Tables 7.1 and 7.2, the average ratio M_{test}/M_{FEA} is 1.018 with a standard deviation of 0.067, indicating the reliability of FEA in predicting the modified moment capacity of pipes subject to general combined loading.

7.2 Finite Element Model

A finite element model resembling the one generated for Test Series 1 (Chapter 5, Section 5.2.4) is used for the parametric study in this chapter. It is recalled that the model consists of two main parts: (1) the pipe specimen, which is modeled by S4R shell elements (40 elements in the circumferential direction x 38 elements along the height of the pipe), (2) the top plate, modeled by S3R shell elements (a degenerated 3-node form of the S4R element), which is modeled as a rigid body by means of the Rigid Body option of ABAQUS. The material non-linear effects on the pipe elements (S4R elements) are modeled according to idealized material properties (Section 7.4). Geometric non-linearity was also modeled.

7.3 Parameters Investigated

The OD of the numerical pipe model was selected as 508mm. The length of the pipe model was taken as 1,500mm, which corresponds to about three pipe diameters. The diameter-to-thickness ratio (D/t), internal pressure ratio (p_r), axial force ratio (A_r), and Torsion ratio (T_r) were selected as the varying parameters. Diameter-to-thickness ratio (D/t) ratio was taken as 60, 80, and 100 by varying the thickness of the pipe model. The internal pressure ratio was taken as 0%, 20%, and 40%. The axial force ratio on the pipe was taken as –30% (compression), 0%, and 30% (tension), and the torsion ratio was taken as 0%, 25%, and 50%. Each of the four parameters identified had three different values, leading to a total of 81 combinations. For pipes with D/t=80, three additional runs with a torsion ratio T_r=75% were conducted in order to observe and assess trends which were not clear in the initial 81 runs. Thus, the total number of FEA runs was 84.

An identifier system similar to that introduced for Test Series 1 (Chapter 5) is adopted for each finite element simulation in the present parametric study. For example, finite element run Dt60P40A-30T25 represents an FEA analysis for a pipe with a D/t=60 subjected to internal pressure of 40% of SMYS, 30% of the yield axial compression capacity (compression is negative), and 25% of the plastic torsion. After the application of these forces, imposed bending rotation was applied to the top end of the pipe and the analysis was conducted past the peak moment capacity.

7.4 Idealized Material Properties

An idealized isotropic elastic-perfectly plastic Engineering Stress vs. Engineering Strain constitutive model is assumed for the pipe material. The initial elastic region had a modulus of elasticity of 207,000 MPa and a yield strength of F_y=448MPa (similar to an X65 pipe) and a Poisson's Ratio of 0.3. The plastic region consisted of a flat yielding plateau (Fig. 7.1). The stress-strain idealization leads to conservative results compared to a real Engineering Stress vs. Engineering Strain relationship, which includes strain-hardening effects. The bilinear model is input to the FEA model in terms of the true stress vs. logarithmic strain (Fig. 7.1).

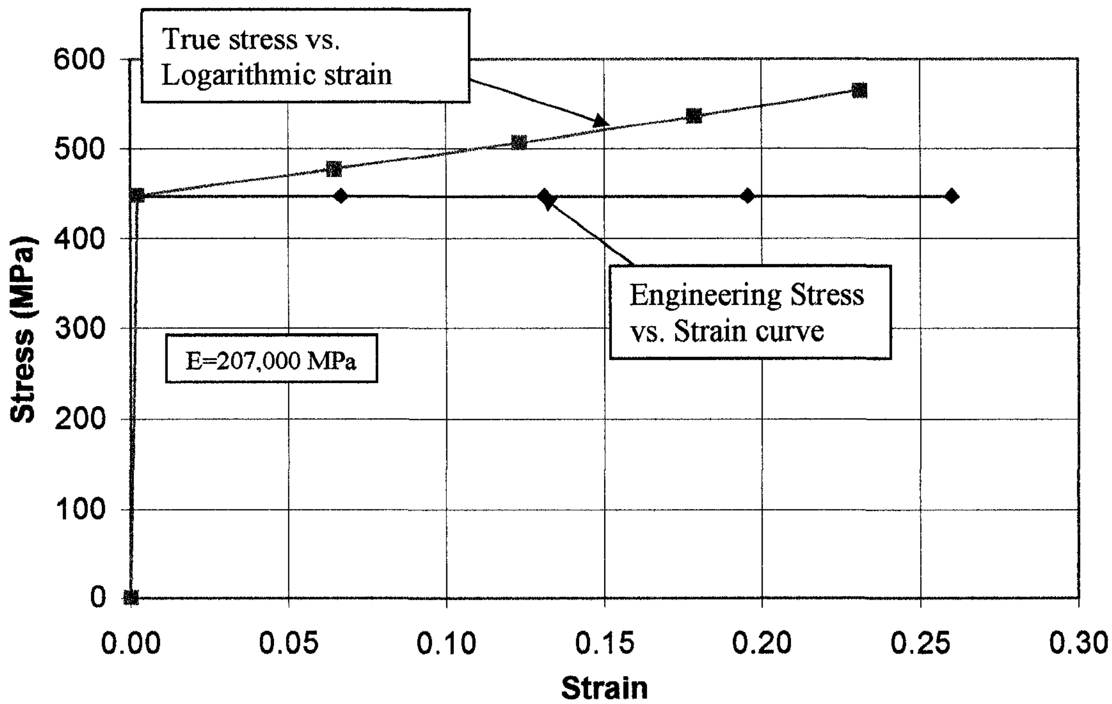

Fig. 7.1 Idealized Stress vs. Strain Curve used in the Parametric Study

7.5 Boundary Conditions

All six degrees of freedom of the bottom nodes of the pipe model were restrained (Fig. 7.2) and the top of the pipe was kept circular throughout the deformation by the rigid top plate.

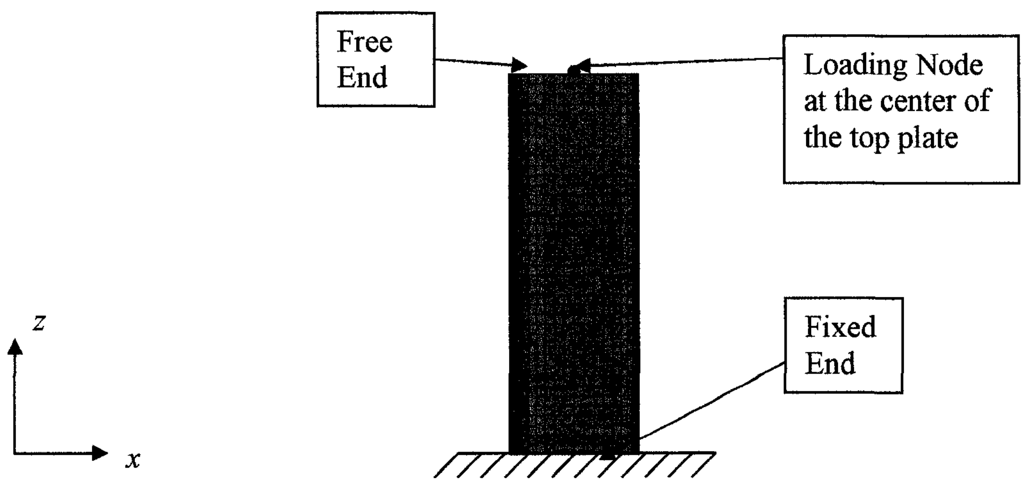

Fig. 7.2 FEA Model

7.6 Load Application Sequence

The load application sequence is illustrated in Fig. 7.3. Firstly, internal pressure was applied as a follower force normal to the shell elements surface forming the pipe. Secondly, the axial force effect was introduced by applying a follower force to the center node of the top plate (loading node in Fig. 7.2) initially acting along the z-axis direction. Thirdly, the desired twisting moment was applied to the loading node as a concentrated moment about the z-axis. Fourthly, by rotating the loading node, imposed curvatures were applied until the pipe model reached its peak moment capacity. The analysis was continued slightly past the peak moment.

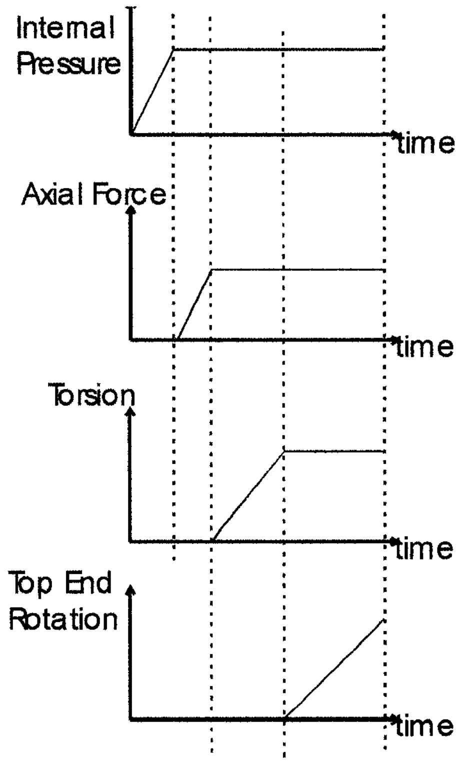

Fig. 7.3 Load Application Sequence

7.7 Results

In this section, the effect of each of the parameters investigated on the ability of a pipe to develop its plastic moment capacity is assessed.

7.7.1 General

Figure 7.4 illustrates the free-body diagram of the FEA model after the buckle formed on the pipe. Point P is the center node of the top plate (loading node in Fig. 7.2). Force A is the applied follower axial force. Forces A_x and A_z are the components of axial force A_a along the x and z directions, respectively. Moment M_{top} is the reaction moment at Point P and Point B is the centroid of the cross-section at the buckle mid-height in the deformed configuration. Its coordinates were calculated by averaging the coordinates of the nodes obtained from ABAQUS corresponding to the buckle mid-height (i.e., $(x_b, z_b) = \left(\sum x_i/n, \sum z_i/n\right)$ in which n=40 is the number of the nodes around the circumference, x_i is the x coordinate of the i^{th} node of the model in the deformed state, and z_i is its z coordinate.

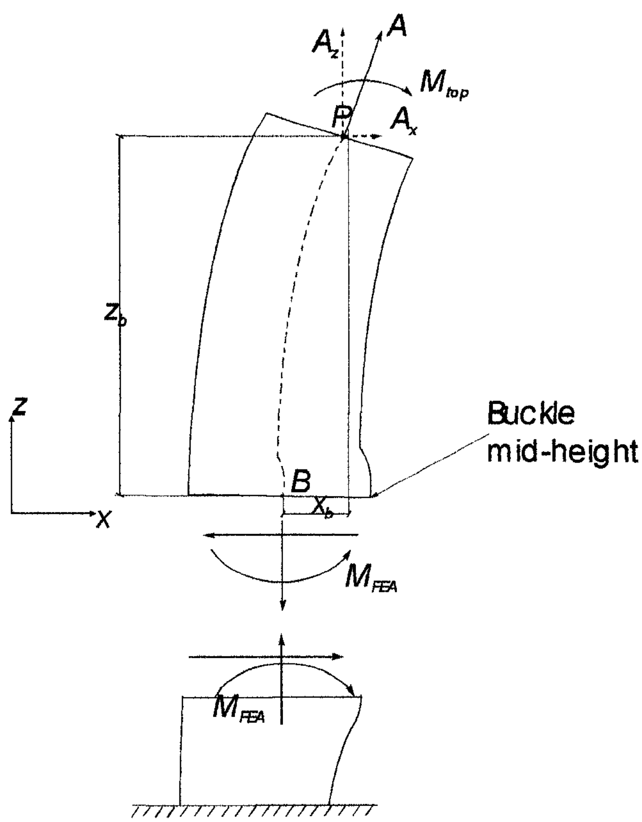

Fig. 7.4 FEA Model in Deformed State

The peak moment (M_{FEA}) at Point B (Fig. 7.4) is calculated by taking into consideration second order effects, which arise as a result of the rotation and displacement of the top of the pipe under the applied rotations, i.e.,

$$M_{FEA} = M_{top} + A_x z_b - A_z x_b \tag{7.1}$$

Tables 7.3, 7.4, and 7.5 provide the parametric run results for pipes with D/t ratios of 60, 80, and 100, respectively. Column 1 in all there tables provides the identifier of the parametric run conducted. The FEA peak moments (M_{FEA}) are tabulated in Column 2 of of Tables 7.3 through 7.5. In the same tables, Column 3 provides the modified plastic moment M_{pm} as predicted by the plastic interaction relations in Mohareb (2003) while Column 4 provides the modified elastic moment capacity (M_{em}) as predicted by elastic interaction relations, which are developed in Appendix D. Column 5 provides the ratio M_{FEA}/M_{pm}, which is a measure indicating whether or not the pipe model was able to develop the modified plastic moment capacity. This ratio exceeds unity when the pipe is able to develop its modified plastic moment capacity as provided in Column 3 (i.e., the pipe section can be considered as "Compact" according to LRFD 1999 terminology). On the other hand, this ratio is less than unity when the pipe is unable to develop its modified plastic moment capacity predicted for the load combination considered. Column 6 provides the ratio of the elastic modified moment to the modified plastic moment M_{em}/M_{pm}. When the ratio M_{FEA}/M_{pm} is greater than M_{em}/M_{pm}, the pipe is able to develop its modified elastic moment capacity and can be considered to meet the non-compactness requirement (according to LRFD 1999 terminology). On the other hand, in the event the ratio M_{FEA}/M_{pm} is less than M_{em}/M_{pm}, the pipe is unable to develop its modified elastic moment capacity (and thus the section can be classified as "slender" according to LRFD 1999 definitions). This was not the case in any of the parametric runs performed in this study, but could conceivably occur to pipes with D/t greater than 100. Column 7 provides a parameter $\alpha = \left(M_{FEA} - M_{em}\right)/\left(M_{pm} - M_{em}\right)$, which is an indicator of the proximity of the moment M_{FEA} is from the limiting value M_{pm}. When $\alpha \geq 1.00$, the moment capacity as predicted by FEA $M_{FEA} \geq M_{pm}$, which signifies that the pipe is able to develop its modified plastic moment capacity, under the load combination considered. Conversely, when $1 > \alpha \geq 0.00$, the moment capacity predicted by FEA $M_{pm} > M_{FEA} \geq M_{em}$ i.e., the pipe is able to develop its modified elastic moment capacity but buckles prior to the attainment of its modified plastic moment capacity.

Table 7.3 Finite Element vs. Plastic Interaction Moment Predictions for D/t=60 and SMYS=448MPa (M_p=947kNm and M_e=731kNm)

	Moment Capacity predicted by FEA, Plastic, and Elastic Interaction Relations (kNm)			Moment Ratios Normalized w.r.t. Modified Plastic Moment			
FEA ID	M_{FEA} [(a)]	M_{pm} [(b)]	M_{em} [(c)]	M_{FEA}/M_{pm}	M_{em}/M_{pm}	α [(d)]	Class[(e)]
(1)	(2)	(3)	(4)	(5)	(6)	(7)	(8)
Dt60P00A-30T00	758	844	512	0.898	0.61	0.741	NC
Dt60P00A-30T25	721	814	489	0.885	0.60	0.713	NC
Dt60P00A-30T50	599	701	414	0.855	0.59	0.645	NC
Dt60P00A00T00	911	947	731	0.962	0.77	0.833	NC
Dt60P00A00T25	884	919	708	0.962	0.77	0.836	NC
Dt60P00A00T50	784	824	633	0.952	0.77	0.791	NC
Dt60P00A+30T00	826	843	512	0.980	0.61	0.949	NC
Dt60P00A+30T25	795	814	489	0.976	0.60	0.940	NC
Dt60P00A+30T50	708	701	414	1.010	0.59	1.025	C
Dt60P20A-30T00	667	748	428	0.892	0.57	0.747	NC
Dt60P20A-30T25	632	710	404	0.890	0.57	0.744	NC
Dt60P20A-30T50	502	593	328	0.847	0.55	0.657	NC
Dt60P20A00T00	882	920	647	0.958	0.70	0.859	NC
Dt60P20A00T25	851	890	623	0.956	0.70	0.853	NC
Dt60P20A00T50	760	790	547	0.962	0.69	0.877	NC
Dt60P20A+30T00	900	885	574	1.016	0.65	1.047	C
Dt60P20A+30T25	871	853	550	1.021	0.64	1.059	C
Dt60P20A+30T50	767	749	474	1.024	0.63	1.065	C
Dt60P40A-30T00	524	595	320	0.881	0.54	0.743	NC
Dt60P40A-30T25	480	553	296	0.868	0.54	0.716	NC
Dt60P40A-30T50	353	413	215	0.855	0.52	0.697	NC
Dt60P40A00T00	804	839	540	0.958	0.64	0.883	NC
Dt60P40A00T25	774	805	515	0.962	0.64	0.893	NC
Dt60P40A00T50	665	694	434	0.958	0.63	0.888	NC
Dt60P40A+30T00	900	877	613	1.026	0.70	1.087	C
Dt60P40A+30T25	870	844	588	1.031	0.70	1.103	C
Dt60P40A+30T50	767	737	507	1.041	0.69	1.132	C

(a) Moment capacity Calculated by Eq. 7.1 based on FEA predictions
(b) Moment capacity predicted by Plastic Interaction Relations (Eqs. 1.1 and 1.2)
(c) Moment capacity predicted by Elastic Interaction Relations (Appendix D)
(d) Calculated by $\alpha = (M_{FEA} - M_{em})/(M_{pm} - M_{em})$
(e) NC=Non-compact section and C=Compact section

Table 7.4 Finite Element vs. Plastic Interaction Moment Predictions for D/t=80 and SMYS=448MPa (M_p=716kNm and M_y=555kNm)

FEA ID	Moment Capacity predicted by FEA, Plastic, and Elastic Interaction Relations (kNm)			Moment Ratios Normalized w.r.t. Modified Plastic Moment			
	M_{FEA}[(a)]	M_{pm}[(b)]	M_{em}[(c)]	M_{FEA}/M_{pm}	M_{em}/M_{pm}	α[(d)]	Class[(e)]
(1)	(2)	(3)	(4)	(5)	(6)	(7)	(8)
Dt80P00A-30T00	531	637	389	0.83	0.61	0.572	NC
Dt80P00A-30T25	503	616	371	0.83	0.60	0.539	NC
Dt80P00A-30T50	423	530	314	0.80	0.59	0.504	NC
Dt80P00A00T00	667	716	555	0.93	0.78	0.696	NC
Dt80P00A00T25	654	695	538	0.94	0.77	0.742	NC
Dt80P00A00T50	583	623	481	0.94	0.77	0.720	NC
Dt80P00A00T75	443	473	367	0.94	0.78	0.717	NC
Dt80P00A+30T00	621	637	389	0.97	0.61	0.935	NC
Dt80P00A+30T25	595	616	371	0.97	0.60	0.915	NC
Dt80P00A+30T50	531	530	314	1.00	0.59	1.005	C
Dt80P20A-30T00	458	566	325	0.81	0.57	0.553	NC
Dt80P20A-30T25	432	537	307	0.80	0.57	0.544	NC
Dt80P20A-30T50	354	448	249	0.79	0.56	0.527	NC
Dt80P20A00T00	648	696	491	0.93	0.71	0.766	NC
Dt80P20A00T25	624	673	473	0.93	0.70	0.755	NC
Dt80P20A00T50	550	597	415	0.92	0.70	0.741	NC
Dt80P20A+30T00	675	669	436	1.01	0.65	1.024	C
Dt80P20A+30T25	633	645	418	0.98	0.65	0.947	NC
Dt80P20A+30T50	573	566	360	1.01	0.64	1.032	C
Dt80P20A+30T75	410	403	243	1.02	0.60	1.044	C
Dt80P40A-30T00	367	450	243	0.82	0.54	0.600	NC
Dt80P40A-30T25	336	418	225	0.80	0.54	0.575	NC
Dt80P40A-30T50	246	312	163	0.79	0.52	0.556	NC
Dt80P40A00T00	589	634	410	0.93	0.65	0.798	NC
Dt80P40A00T25	565	609	391	0.93	0.64	0.800	NC
Dt80P40A00T50	476	525	330	0.91	0.63	0.750	NC
Dt80P40A+30T00	660	663	465	1.00	0.70	0.985	C
Dt80P40A+30T25	635	638	446	1.00	0.70	0.985	C
Dt80P40A+30T50	554	557	385	0.99	0.69	0.982	NC
Dt80P40A+30T75	405	388	257	1.04	0.66	1.130	C

(a) Moment capacity Calculated by Eq. 7.1 based on FEA predictions

(b) Moment capacity predicted by Plastic Interaction Relations (Eqs. 1.1 and 1.2)

(d) Moment capacity predicted by Elastic Interaction Relations (Appendix D)

(d) Calculated by $\alpha = (M_{FEA} - M_{em})/(M_{pm} - M_{em})$

(e) NC=Non-compact section and C=Compact section

Table 7.5 Finite Element vs. Plastic Interaction Moment Predictions for D/t=100 and SMYS=448MPa (M_p=576kNm and M_y=438kNm)

FEA ID	Moment Capacity predicted by FEA and Plastic and Elastic Interaction Relations (kNm)			Moment Ratios Normalized w.r.t. Modified Plastic Moment			
	M_{FEA}[(a)]	M_{pm}[(b)]	M_{em}[(c)]	M_{FEA}/M_{pm}	M_{em}/M_{pm}	α[(d)]	Class[(e)]
(1)	(2)	(3)	(4)	(5)	(6)	(7)	(8)
Dt100P00A-30T00	400	513	314	0.78	0.61	0.572	NC
Dt100P00A-30T25	396	493	300	0.80	0.61	0.539	NC
Dt100P00A-30T50	319	427	254	0.75	0.59	0.504	NC
Dt100P00A00T00	522	576	448	0.91	0.78	0.696	NC
Dt100P00A00T25	512	559	434	0.92	0.78	0.742	NC
Dt100P00A00T50	452	501	388	0.90	0.77	0.720	NC
Dt100P00A+30T00	494	513	314	0.96	0.61	0.935	NC
Dt100P00A+30T25	478	495	300	0.96	0.60	0.915	NC
Dt100P00A+30T50	414	426	254	0.97	0.60	1.005	NC
Dt100P20A-30T00	351	455	262	0.77	0.58	0.553	NC
Dt100P20A-30T25	327	432	248	0.76	0.57	0.544	NC
Dt100P20A-30T50	263	361	201	0.73	0.56	0.527	NC
Dt100P20A00T00	505	560	397	0.90	0.71	0.766	NC
Dt100P20A00T25	486	541	382	0.90	0.71	0.755	NC
Dt100P20A00T50	424	480	335	0.88	0.70	0.741	NC
Dt100P20A+30T00	523	539	352	0.97	0.65	1.024	NC
Dt100P20A+30T25	504	519	337	0.97	0.65	0.947	NC
Dt100P20A+30T50	444	456	290	0.97	0.64	1.032	NC
Dt100P40A-30T00	280	361	196	0.78	0.54	0.600	NC
Dt100P40A-30T25	268	336	181	0.80	0.54	0.575	NC
Dt100P40A-30T50	183	251	132	0.73	0.52	0.556	NC
Dt100P40A00T00	452	510	331	0.89	0.65	0.798	NC
Dt100P40A00T25	434	490	316	0.89	0.64	0.800	NC
Dt100P40A00T50	361	422	266	0.86	0.63	0.750	NC
Dt100P40A+30T00	517	533	376	0.97	0.70	0.985	NC
Dt100P40A+30T25	498	513	360	0.97	0.70	0.985	NC
Dt100P40A+30T50	437	448	311	0.98	0.69	0.982	NC

(a) Moment capacity Calculated by Eq. 7.1 based on FEA predictions
(b) Moment capacity predicted by Plastic Interaction Relations (Eqs. 1.1 and 1.2)
(e) Moment capacity predicted by Elastic Interaction Relations (Appendix D)
(d) Calculated by $\alpha = \left(M_{FEA} - M_{em}\right)/\left(M_{pm} - M_{em}\right)$
(e) NC=Non-compact section and C=Compact section

7.7.2 Classification of Pipes under Pure Bending

Table 7.6 provides the section classification rules according to Canadian Steel Code CAN/CSA S16-01 and American Steel Code LRFD (1999) and under pure bending.

The equivalent rule in CAN/CSA S16-01, circular hollow sections subject to pure bending, which satisfy the requirement $D/t \le 18{,}000/F_y$ are considered as Class 2 sections and can be designed based on their plastic resistance M_p.

According to CAN/CSA S16-01, pipe sections subject to pure bending are classified as Class 2 sections (i.e., attain their plastic moment resistance M_p prior buckling locally) when $D/t \le 18{,}000/F_y$. For $F_y = 448$ MPa, the requirement becomes $D/t \le 40.2$. When pipes meet the requirement $18{,}000/F_y < D/t \le 66{,}000/F_y = 147.3$ they are classified as Class 3 sections and are designed based on their elastic resistance M_e.

According to LRFD (1999), pipe sections subject to pure bending are classified as compact (i.e., attain their plastic moment resistance M_p prior to buckling locally) when $D/t \le 0.07E/F_y = 31.2$. For E=200,000Mpa and $F_y = 448MPa$, the requirement becomes $D/t \le 31.2$. When pipes meet the requirement $0.07E/F_y < D/t \le 0.31E/F_y = 138.4$ they are classified as non-compact and are designed based on their elastic resistance M_e.

In the present study, all runs were based on pipes with D/t=60, 80, and 100. Thus, they are expected to behave as Class 3/non-compact sections and thus, are expected to develop their elastic moment capacity M_e and buckle locally before reaching their plastic moment capacity M_p when subjected to pure bending. This is indeed the case in Tables 7.3, 7.4, and 7 5 for runs Dt60P00A00T00, Dt80P00A00-T00, and Dt100P00A00T00 (which involve the case of pure bending) which developed their elastic moment capacity M_e but not their plastic moment capacity M_p. The M_{FEA}-to-M_{pm} ratios are less than unity (0.96, 0.93, and 0.91, respectively) but higher than M_{em}-to-M_{pm} ratios. Also, the indicator α takes the respective values of 0.83, 0.70, and 0.58. The moment capacity for specimen with D/t=60 was closest to the plastic moment capacity ($0.96M_p$) since its D/t is closer to lower classification limit $D/t \le 31.2$ according to LRFD (1999) and $D/t \le 40.2$ according to CAN/CSA S16 (2001). As expected, as *D/t* increases, the value of indicator α reduces. For the run with the largest diameter-to-thickness ratio of 100, (Dt100P00A00T00), it is observed that the predicted finite element moment is only 0.91 of the plastic moment M_{pm} as predicted by the plastic interaction equation. The above discussion shows that the FEA results are consistent with the classification rules in LRFD 1999 and CAN/CSA S16 (2001).

Table 7.6 Section Classification Rules according to Canadian and American Codes

Section Class	Can/CSA S16-01	LRFD Specification*	Classification (F_y=448MPa)		
			***D/t*=60**	***D/t*=80**	***D/t*=100**
Class 2 (Compact)	$\frac{D}{t} \le \frac{18,000}{F_y} = 40.2^{**}$	$\frac{D}{t} \le \frac{14,000}{F_y} = 31.2$			
Class 3 (Non-Compac)	$\frac{18,000}{F_y} = 40.2 < \frac{D}{t} \le \frac{66,000}{F_y} = 147.3$	$\frac{14,000}{F_y} = 31.2 < \frac{D}{t} \le \frac{62,000}{F_y} = 138.4$	+	+	+
Class 4 (Slender)	$\frac{D}{t} > \frac{66,000}{F_y} = 147.3$	$\frac{D}{t} > \frac{62,000}{F_y} = 138.4$			
M_{FEA}/M_p			0.96	0.93	0.91
α			0.83	0.70	0.58

*In LRFD Specification, the section classification equations are a function of Modulus of Elasticity (*E*). The equations presented in this table are calculated by setting *E*=200,000MPa

**Based on F_y=448MPa

A principal objective of the present study is the to assess whether the concept of section classification used in structural steel codes could be extended to steel pipes which are subject to more general load combinations by assessing whether a pipe under a given load combination (torsion, internal pressure, and axial force) is able to attain its modified plastic (or elastic) capacity.

7.7.3 Effect of Loads and Geometry

Figures 7.5, 7.6, and 7.7 depict moment ratio as a function of torsion and internal pressure ratios for *D/t* ratios of 60, 80, and 100, respectively, for axial force ratios of –30%, 0, and 30%. In the figures, Surface 1 represents moment ratio M_{em}/M_{pm}=1.0 as a function of internal pressure ratio and torsion ratio, Surface 2 represents the moment ratio M/M_{pm} is intended to represent the limiting case where the moment capacity is equal to the modified plastic moment capacity, and Surface 3 is moment ratio M_{FEA}/M_{pm} as a function of internal pressure ratio and torsion ratio (Fig. 7.5a). Surface 3 is above Surface 2 ($M_{FEA}/M_{pm} \geq 1$) when the specimen is able to develop its modified plastic moment capacity and thus meets the compactness requirement. Surface 3 stays below Surface 2 but above Surface 1 when the specimen is unable to develop its modified plastic moment capacity but is able to develop its modified elastic moment capacity and thus, is classified as a non-compact section. In Figs. 7.5a and b, Surface 3 stays below Surface 2 meaning that pipes with D/t=60 and F_y=448MPa, were unable to develop their modified plastic moment capacities for axial force ratios of –0.30 and 0, respectively. On the other hand, in Fig. 7.5c, where the axial force ratio is 0.30 (tensile), for some combinations of torsion and internal pressure ratios, pipes were observed to develop their modified plastic moment capacity (Surface 3 is above Surface 2) i.e., compact section behavior. Within the rest of the domain pipe exhibited a sub-compact behavior. The border delineating these two behaviors is illustrated in the same figure.

Figures 7.5 to 7.7 indicate that effect of internal pressure and torsion ratios on the ability of the pipes to develop their plastic moment capacity is not very significant. This is characterized by the nearly horizontal shape of Surface 3.

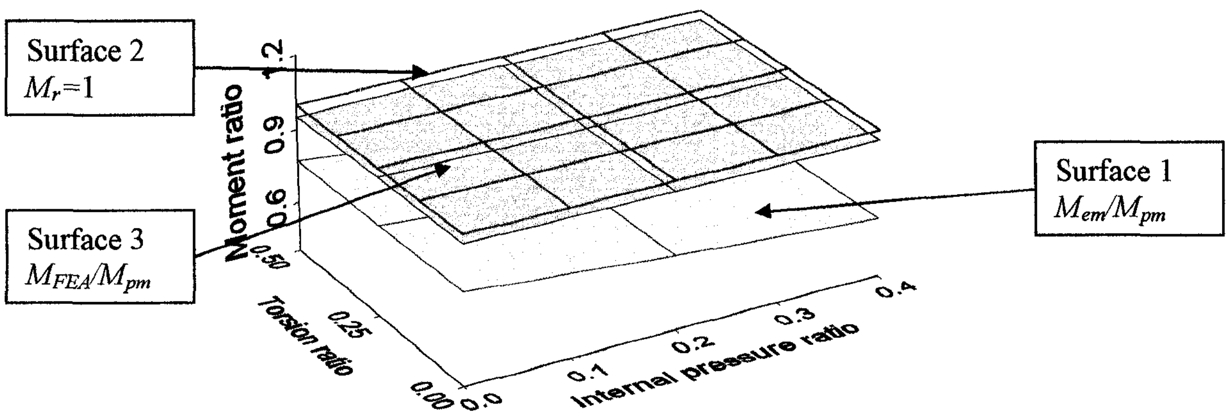

(a) Axial Force Ratio A_r=-0.30

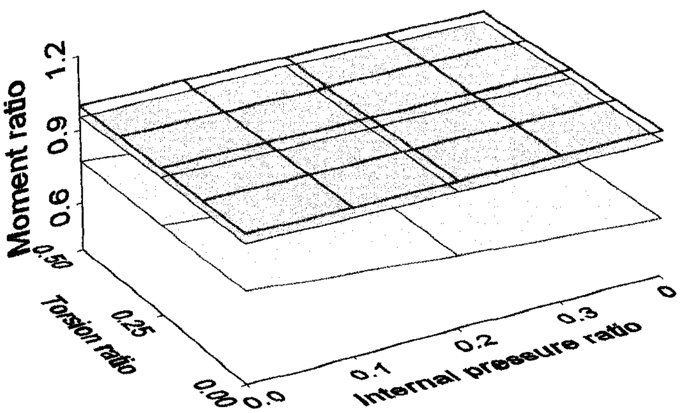

(b) Axial Force Ratio A_r=0.00

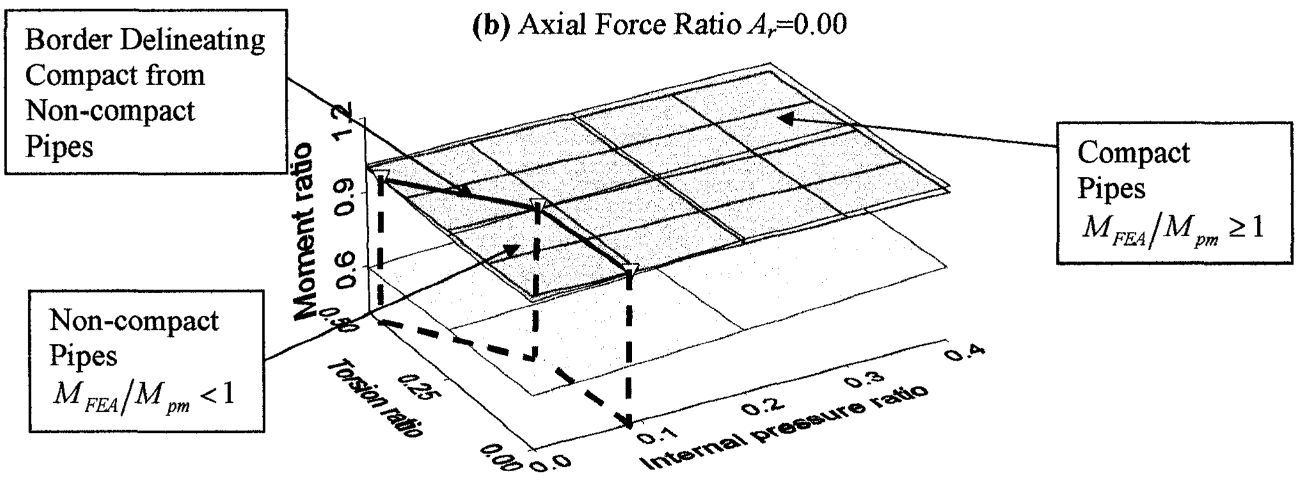

(c) Axial Force Ratio A_r=0.30

Fig. 7.5 Moment Ratio as a Function of Torsion and Internal Pressure Ratios for D/t=60

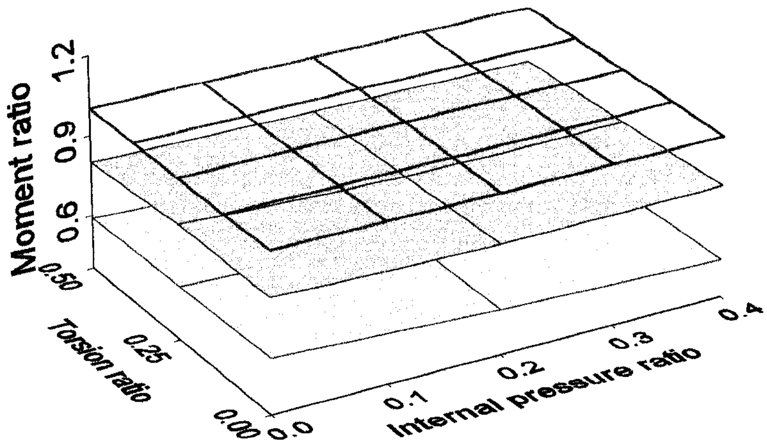

(a) Axial Force Ratio A_r=-0.3

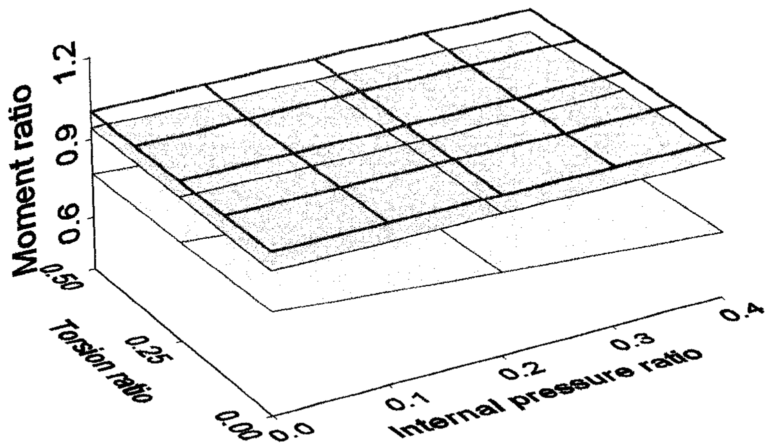

(b) Axial Force Ratio A_r=0.0

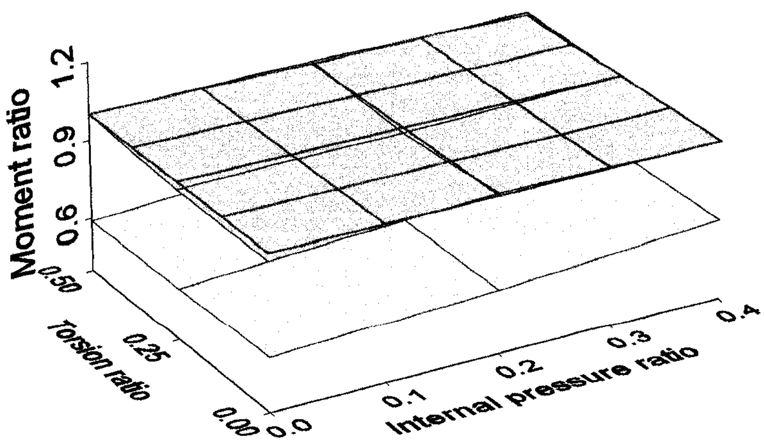

(c) Axial Force Ratio A_r=0.3

Fig. 7.6 Moment Ratio as a Function of Torsion and Internal Pressure Ratios for D/t=80

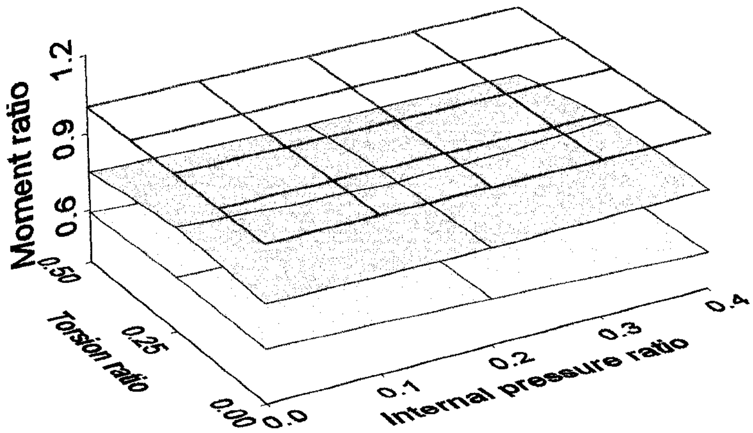

(a) Axial Force Ratio A_r=-0.3

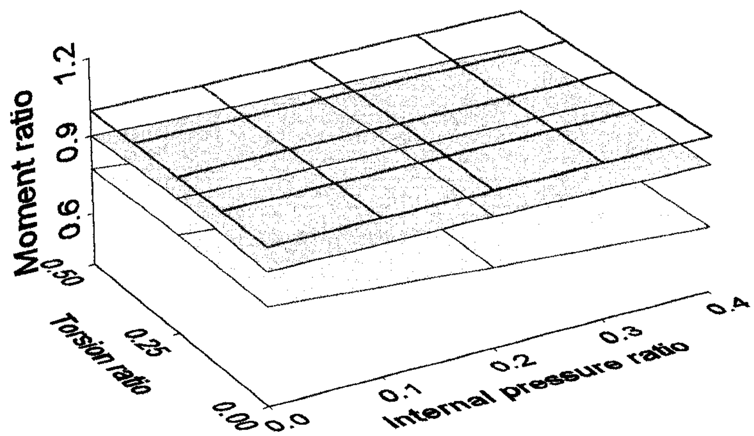

(b) Axial Force Ratio A_r=0.0

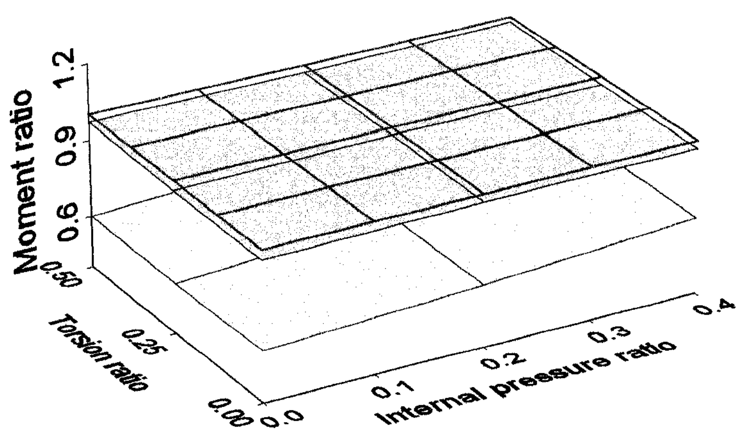

(c) Axial Force Ratio A_r=0.3

Fig. 7.7 Moment Ratio as a Function of Torsion and Internal Pressure Ratios for D/t=100

7.7.3.1 Effect of Torsion

From Columns 5 of Tables 7.3 to 7.5 and Figures 7.5, to 7.7, one can observe that the gradient $\partial\left(M_{FEA}/M_p\right)/\partial T_r$ takes slightly negative values with axial compression (A_r=-30%), becomes almost zero for zero axial force (A_r=0%), and takes slightly positive values with axial tension (A_r=30%). This suggest that an increase in torsion decreases the ability of the pipe to develop its modified plastic moment capacity in the presence of axial compression, has almost no effect for zero axial force, and slightly increases the ability of the pipes to reach their modified plastic moment capacity when subject to tension. For practical purposes, when determining the ability of a pipe to attain its modified plastic moment capacity, the effect of torsion can be neglected $\left(\partial\left(M_{FEA}/M_p\right)/\partial T_r \approx 0\right)$. Thus, in subsequent plots in Fig. 7.8, the torsion ratio is omitted.

7.7.3.2 Effect of Internal Pressure

From Columns 5 of Tables 7.3 to 7.5 and Figures 7.5, to 7.7, one can draw the following conclusions.

1) For pipes subjected to axial compression, the presence of internal pressure had a detrimental effect on the ability of a pipe to develop its modified plastic moment capacity. This is evidenced by the negative moment gradient $\partial\left(M_{FEA}/M_p\right)/\partial p_r < 0$.
2) For pipes with D/t=60 subject to zero axial load, internal pressure was observed to essentially have no effect $\left(\text{i.e., } \partial\left(M_{FEA}/M_p\right)/\partial p_r \approx 0\right)$ on the ability of a pipe to develop its modified plastic moment capacity. On the other hand, while internal pressure had a slight detrimental effect on the development of the modified plastic moment capacity for pipes with D/t=80 $\left(\text{i.e., } \partial\left(M_{FEA}/M_p\right)/\partial p_r \leq 0\right)$, this detrimental effect was more pronounced for pipes with D/t=100 and zero axial force.
3) For pipes with D/t=60 and 80, combinations of internal pressure and axial tension had a beneficial effect $\left(\text{i.e., } \partial\left(M_{FEA}/M_p\right)/\partial p_r > 0\right)$ and these pipes were able to develop their modified plastic moment capacity. Internal pressure had no effect with D/t=100 pipes subject to axial tension $\left(\text{i.e., } \partial\left(M_{FEA}/M_p\right)/\partial p_r \approx 0\right)$.

The effect of internal pressure can be characterized as mild though more pronounced than the effect of torsion.

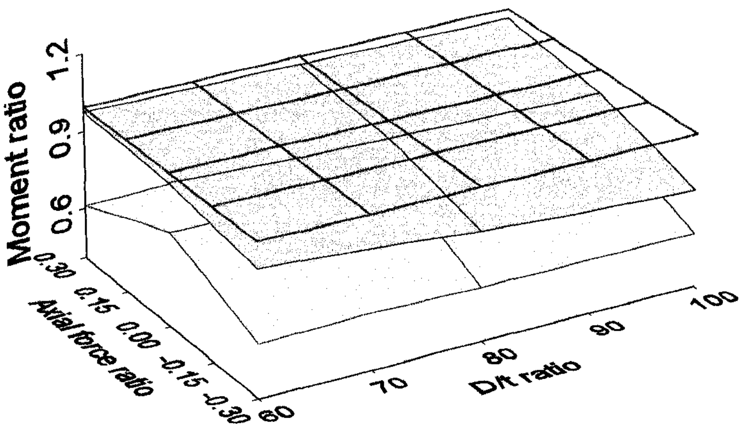

(a) Internal Pressure Ratio p_r=0.0

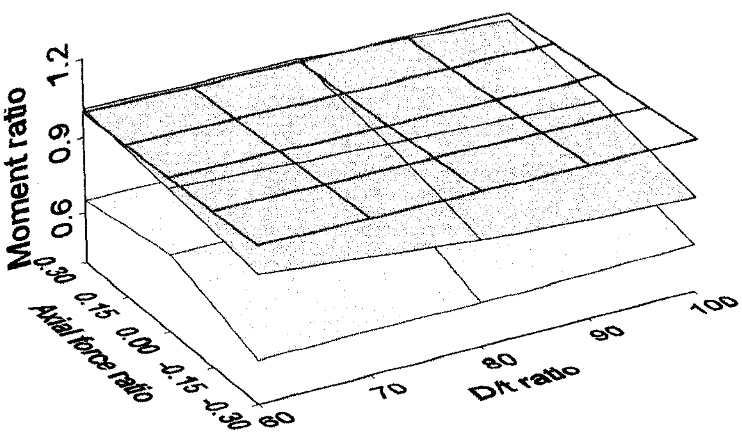

(b) Internal Pressure Ratio p_r=0.2

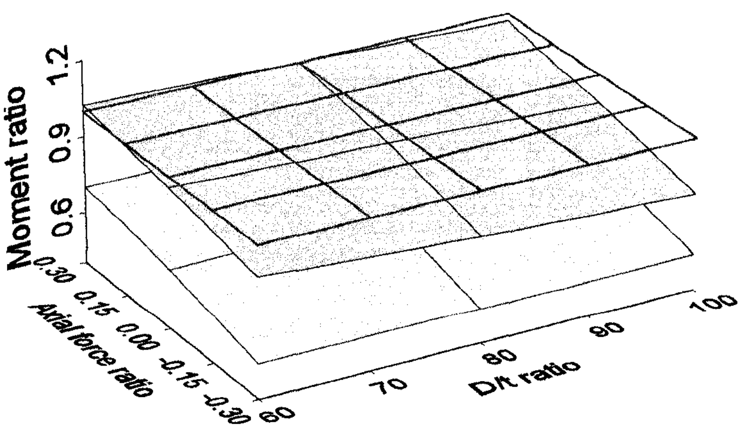

(c) Internal Pressure Ratio p_r=0.4

Fig. 7.8 Moment Ratio as a Function of D/t and Axial Force Ratios

7.7.3.3 Effect of *D/t* Ratio

Figure 7.8 illustrates the moment ratio as a function of *D/t* and axial force ratios for each internal pressure ratio (p_r=0, 0.2, and 0.4). The diameter-to-thickness ratio is observed to have a significant effect on the ability of the pipes to develop their plastic moment capacity. An increase in *D/t* ratio is observed to significantly decrease the M_{FEA}/M_P. This is clear by the negative sign of the gradient $\partial\left(M_{FEA}/M_p\right)/\partial\left(D/t\right)$.

7.7.3.4 Effect of Axial Force Ratio

Figure 7.8 also shows that the axial force has a significant effect on the ability of a pipe to develop its modified plastic moment capacity ($\partial\left(M_{FEA}/M_p\right)/\partial A_r > 0$). The FEA runs conducted indicates the presence of axial compression accelerates local buckling and triggers it before the pipes reach their modified plastic moment capacity. On the other hand, the presence of axial tension is observed to delays local buckling and allows the pipes to develop their modified plastic capacity in some cases (Figs 7.8b and c). Relatively thin-walled pipes with *D/t*=100 were able to develop around 97% of their modified plastic moment capacity in the presence of axial tension (A_r=30%).

7.7.4 Buckled Configurations

The buckling modes obtained in the FEA study are illustrated in Fig. 7.9. Pipes under axial compression, zero torsion, and zero internal pressure exhibited a symmetric diamond-shape buckle (Fig. 7.9a). This type of buckle was also experimentally observed in previous studies for pipes under axial compression and bending (Mohareb 1994, Zimmerman 1995, Zimmerman 2004, etc.) and pipes under axial tension and bending in this study (Chapter 5).

Pipes tested under axial compression, zero internal pressure, and 25% of their plastic torsion capacity exhibited asymmetric diamond shape buckle (Fig. 7.9b).

Regardless of the amount of axial force on them, pipes under 50% of their plastic torsion capacity and zero internal pressure exhibited a diagonal buckle (Fig. 7.9c). A buckle type resembling the one in Fig. 7.9c was observed in Ozkan and Mohareb (2003) in experiments on short pipes subjected to bending, shear, and torsion.

Some of the pipes tested under zero axial force or 30 % axial tension, zero internal pressure, and zero torsion exhibited a slightly different diamond shape buckle with a major depression in the middle of the buckle and four small depressions around the major depression (symmetric diamond buckle-2 in Fig. 7.9d). It was observed that this type of buckle was spread along a greater pipe length than symmetric diamond buckle (Fig. 7.9d) possibly due to the presence of axial tension.

Pipes under internal pressure, axial force, and zero torsion exhibited symmetric outward bulging buckle (Fig. 7.9e), which is the characteristic buckle type for this kind of loading (Bouwkamp and Stephten 1973, Mohareb 1994, Zimmerman 1995 etc.). Some of the pipes tested under internal pressure, axial tension, and zero torsion exhibited outward bulging buckle at the bottom (characterized as elephant foot buckle in Dorey 1999) as illustrated in Fig. 7.9f.

Pipes tested under internal pressure, axial force, and torsion exhibited asymmetric outward bulging buckle (Fig. 7.9g), which was also observed as the buckling modes of the specimens of test series 2 of this study (Chapter 6).

Pipe Dt80P20A-30T00 exhibited two symmetric outward bulging buckles (Fig. 7.9h). Pipe Dt80P20A30T25 exhibited two asymmetric outward bulge buckles (Fig. 7.9i).

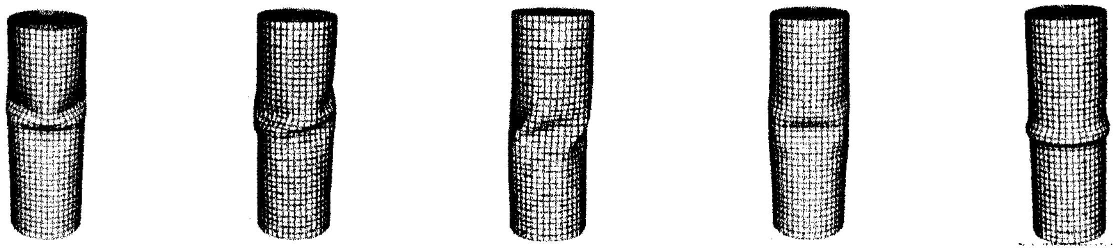

(a) Symmetric Diamond Buckle of Dt60P00A-30T00

(b) Asymmetric Diamond Buckle of Dt60P00A-30T25

(c) Diagonal Buckle of Dt60P00A-30T50

(d) Symmetric Diamond Buckle-2 of Dt60P00A00T00

(e) Symmetric Outward Bulging Buckle of Dt60P20A-30T00

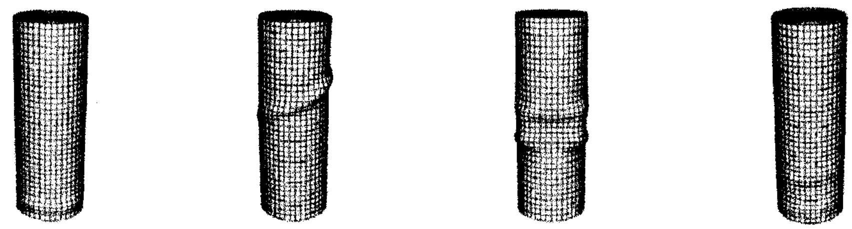

(f) Elephant foot buckle of Dt80P20A30T0

(g) Asymmetric Outward Bulging Buckle of Dt80P20A-30T50

(h) Two Symmetric outward bulging buckles of Dt80P20A-30T00

(i) Double Asymmetric Outward Bulging Buckle Dt80P20A30T25

Fig. 7.9 Sample Buckling Modes

7.8 Conclusions

The effects of torsion, internal pressure, axial force (compression/tension), and *D/t* on the ability of the pipes to develop their modified plastic moment capacity were systematically assessed by FEA parametric study documented in this chapter. Following are the main conclusions of the work.

1) While torsion had a slight detrimental effect on the ability of the pipes to develop their modified plastic moment capacity in the presence of axial compression, its effect can be considered as practically negligible.
2) Combinations of compression and internal pressure cause a slight decrease in M_{FEA}/M_{pm} ratio. In contrast, combined axial tension and internal pressure, has a favorable effect on M_{FEA}/M_{pm} ratio. However, the effect of internal pressure up to 40% is observed to be small.
3) An increase in *D/t* ratio has a pronounced detrimental effect on the ability of the pipes to develop their modified plastic moment capacity.

4) Among the parameters investigated, the most effective on the ability of the pipes to develop their modified plastic moment capacity is the axial force. While the axial compression had a detrimental effect in attaining the modified plastic moment, axial tension had a beneficial effect in attaining the modified moment ratio. In both cases, the moment attained was always smaller than the fully plastic moment M_p.

5) It is possible to extend the concept of classification rules adopted in structural steel codes for hollow sections under bending to the design of elevated pipelines, which involve complex loads. The classification rules for elevated pipes would depend on D/t and F_y/E similar to structural steel codes but also on A_r, p_r and weakly dependent on T_r.

6) In summary, the ability of a pipe to develop its modified plastic moment capacity is dependent on the following parameters.

   - Axial force ratio (most important parameter)
   - D/t ratio (strong dependence)
   - Internal pressure (weak dependence)
   - Torsion (negligible)

Chapter 8

Summary and Recommendations

In this chapter, a summary of the research conducted and the outcome is presented in Section 8.1. Recommendations for future research are provided in Section 8.2.

8.1 Summary

As a result of the comprehensive literature review conducted on previous experimental studies on steel pipes, it was observed that a very limited number of full-scale tests was conducted on pipes subjected to complex load combinations including internal pressure, axial tension, torsion, shear, and bending. In order to partially fill this void, an experimental program consisting of two full-scale test series on pipe specimens made of X65 material with OD=508mm and nominal D/t=80 were undertaken. Experiments were conducted under an innovative test setup, which was developed at the Structural Engineering Laboratory of the University of Ottawa. The setup is capable of accommodating complex load combinations.

The first test series (Chapter 5) consisted of testing six pipes under combinations of axial tension, internal pressure, and imposed curvatures. The main aim of the tests was to document the beneficial effect of axial tension on critical buckling strains of pipes, which are used in the design of buried pipelines. The moment capacities of pipe specimens were also measured in order to investigate whether or not relatively thin pipes (D/t=80) are able to attain their modified plastic moment capacity as predicted by analytically derived interaction relations (Mohareb 2002 and 2003). The study was also successful in obtaining deformation limit states of interest in designing buried pipes. An FEA model of the pipe specimens was developed under the FEA simulator ABAQUS in order to predict test results. Following is the outcome of the work.

1. As characterized by Moment vs. Local Curvature relationships of the pipe specimens tested, pipes under high axial tension were able to reach higher curvature values prior buckling locally when compared to specimens with lower levels of axial tension. The FEA was able to predict this behavior reasonably well. However, it over-predicted critical curvatures and strains when compared to the tests.

2. Compressive strain limits were observed to increase with axial tension. Design equations accounting for this beneficial effect were proposed. The new compressive strain limits are s functions of axial tension ratio A_r and internal pressure ratio p_r.
3. Pipe local buckling configurations are dependant on load combinations. Un-pressurized pipes exhibited a diamond shape mode buckle. The presence of internal pressure induced outward bulging buckles. The FEA provides very good predictions of the local buckling modes. Nevertheless, the predicted locations of the buckle were found to be very sensitive to the input stress-strain relationships and pipe cross-sectional properties. The location of the buckle in the FEA model could be initiated where it took place in the tests by introducing slightly different stress-strain relationship. The same results can also be obtained by slightly decreasing the thickness of the pipe elements at that location.
4. The interaction equations in Mohareb (2002 and 2003) predicted a higher resistance than those recorded in the tests except for specimens P40-A40-M89 and P80-A40-M82, which were able to develop their plastic capacities as predicted by the relations in Mohareb (2002 and 2003). Based on the experimental program, it is judged that the ability of the pipes to develop their plastic capacity is dependant on the load combinations acting on the pipe. The combined stabilizing effect of internal pressure and axial tension is beneficial for pipes to develop their modified plastic moment capacity.
5. The FEA provides very good predictions of the bending moment capacity and FEA model developed in the study and can be reliably used for the capacity prediction of pipes subject to combinations of internal pressure, axial tension/compression, and bending in the absence of experimental data.

The aim of the second test series (Chapter 6) was to extend the experimental database to specimens tested under more complex load combinations and also to demonstrate that FEA model of the specimens were able to predict the pipe moment capacity reasonably well. In this respect, two pipe specimens were subjected to combinations of torsion, internal pressure, axial tension, shear, and bending. Their FEA model using ABAQUS Simulator was also developed to predict the test results. Following are the outcome of the work.

1. The FEA predictions of moment capacities were in very good agreement with the test results. The buckled shapes as obtained from the tests and FEA were also in excellent agreement.
2. Although the presence of torsion is of importance only in fewer situations in the design of buried pipelines, critical strains of the specimens were measured. An increase in torsion ratio appears to very slightly reduce the critical strain. No definite trends could be inferred from the tests given the rather small sample size.

As a last step of the research program, a comprehensive study based on FEA was conducted. Previous full-scale experimental studies on steel pipes under combined loading along with their FEA simulations were summarized. It was observed that FEA moment capacity predictions were in excellent agreement with experimental measurements. The quality of the agreement obtained in this program also gave confidence to apply the FEA model developed in a parametric study in order to investigate the effect of geometric property D/t and different load types (internal pressure, axial tension, and torsion) on the ability of the pipes to develop their modified plastic moment capacity as predicted by the interaction relationships (Mohareb 2002 and 2003). It was observed that the axial force ratio was the most important parameter affecting the ability of the pipes to develop their modified plastic moment capacity. This ability also showed strong dependence on the D/t ratio. While internal pressure had slight effect on the ability of the pipes to develop their modified plastic moment capacity, the effect of torsion was judged negligible.

8.2 Recommendations for Future Research

8.2.1 Recommendations for Critical Buckling Strains

As a result of the experimental program conducted, it was observed that axial tension has a beneficial effect on limiting buckling strains. Given the small sample tested, it is recommended to undertake more tests in order to yield more reliable and possibly less conservative design rules.

The FEA model developed was observed to overestimate the critical strain values. One reason for the discrepancy could be the presence of residual stresses in the pipes induced during the production process, which was not measured nor modeled in the FEA. It is recommended to measure the residual stress distribution in the pipe wall and develop an FEA model, which models residual stresses. The introduction of residual stresses to the FEA model is likely to improve the prediction of critical buckling strains and possibly achieve a better agreement between the experimental measurements and the FEA predictions.

8.2.2 Recommendations for Moment Capacity

The present study investigated the effect of D/t ratio and loading such as internal pressure, axial force, and torsion on the ability of pipes to develop their modified plastic and elastic moment resistance. An extension of work to incorporate the effect of yield strength-to-Modulus of elasticity ratio (F_y/E) is a logical extension of the work and could generalize the result for material strength.

Although it was shown that for some combinations of D/t, axial force, internal pressure, and torsion, pipes were able to develop their modified plastic moment capacity while for some other combinations they were not, the border delineating these two behaviors is yet to be mathematically defined. The definition of this border together with verified interaction relations could form a complete set of design rules to be incorporated in pipeline codes.

In the second test series, bending was applied to the specimens by displacing the top of the specimen, which led into a moment gradient along the height of the pipe associated with constant shear. Further numerical experimentation in Chapter 6 showed that constant moment along the length of the pipe is a more severe case than that of a moment gradient. It is of interest to experimentally verify this hypothesis by applying combinations of internal pressure, axial tension, torsion, and constant moment along the length of the pipe.

REFERENCES

AISC. (1999). *Load and resistance factor design specification for structural steel buildings*, American Institute of Steel Construction, Chicago.

API (1981) *Recommended Practice for Planning Designing and Constructing Fixed Offshore Platforms. API RP 2A*, 12^{th} Ed., American Petroleum Inst., Washtington, D.C., 30-47.

ANSI/API (1993) *Recommended Practice for Planning Designing and Constructing Fixed Offshore Platforms- Load and resistance factor design*, American National Standard, Washington.

ASME B31.3 (1999) *Process Piping*, Edmonton, Alberta.

ASTM (2001), *American standard test methods for tension testing of metallic materials [Metric]*[1], designation E 8M-01, USA.

Bath KJ, Dvorkin EN (1985) "A four-node plate bending element based on a mixed interpolation." *International Journal for Numerical Methods in Engineering*, Vol. 21: 367-383.

Batterman, S.C. (1965). "Plastic buckling of axially compressed cylindrical shells." AIAA J., 3(2), 316-325.

Bouwkamp, J. G., and Stephen, R. M. (1973). "Large diameter pipe under combined loading." *Transp. Engrg. J.*, ASCE, 99(3), 521-536.

Bouwkamp, J. G., and Stephen, R. M. (1974). "Full Scale Studies on Structural Behavior of Large Diameter Pipes under Combined Loading." Report No. UC-SESM 74-1, University of California, Berkeley

CAN/CSA S136 (2001), "Design of cold-formed steel members", Candian Standards Associantion, Rexdale, Ont.

CAN/CSA S16 (2001). "Limit States Design of Steel Structures", Canadian Standards Association, Rexdale, Ont.

CAN/CSA Z662 (2003) "Oil and Gas Pipeline Systems" Canadian Standards Association, Rexdale, Ont.

Chen, W. and Atsuta, T. (1972). "Interaction equations for biaxially loaded sections." *J. Struct. Engrg.*, ASCE, Vol. 98 (ST5), 1035-1051.

Chen, W. F. and Sohal, I.S. (1988). "Cylindrical members in offshore structures", *Thin-walled Structures,* Vol. 6, 1988. Special Issue on Offshore Structures. Elsevier Applied Science.

Code of Practice for Fixed Offshore Structures, Part 3: Steel (1982), BS62345, British Standards Inst., London, England, 612-615.

Column Research Council (1966). "Guide to Stability Design Criteria for Metal Structures.

Das, S., et al. (2000). "Laboratory Study of Local Buckling, Wrinkle Development, and Strains for NPS12 Line Pipe" Proc. of International Pipeline Conference (IPC2000). ASME (OMAE Division), Calgary, Alberta, Oct.1-5, 2000, pp 909-915. Paper IPC00-0006.

Das, S., et al. (2001). "Wrinkle Behavior under Cyclic Strain Reversal in NPS12 Pipe" Proc. of International Conference on Offshore Mechanics and Arctic Engineering. ASME (OMAE Division), Rio de Janeiro, Brasil, June.3-8, 2001. Paper OMAE01-4010.

Det Norske Veritas. (1996). "Rules for Submarine Pipelines." Oslo, Norway.

Det Norske Veritas, DNV-OS-F101. (2000). "Rules for Submarine Pipelines." Oslo, Norway.

Dorey, A.B., Murray, D.W., Cheng, J.J.R., Grondin G.Y., and Zhou, Z.J. (1999). "Testing and Experimental Results for NPS30 Line Pipe under combined Loads" *Proc. of the 18th inter. Conf. on OMAE*, ASME, St. John's, Newfoundland. Paper No. OMAE99/PIPE-5022.

Dorey, A., B., Murray, D., W., Cheng, J., J., R. (2000) "An Experimental Evaluation of Critical Buckling Strain Criteria." Proc. of International Pipeline Conference (IPC2000). ASME (OMAE Division), Calgary, Alberta, Oct.1-5, 2000, pp 71-77. Paper IPC00-0157.

Dorey (2001) "Prediction of wrinkling behavior of girth welded line pipe" University of Alberta, Dept. of Civil. Eng. Structural Engineering Report No:197.

Dorey, A., B., Murray, D., W., Cheng, J., J., R. (2002) "Material Property Effects on Critical Buckling Strains in Energy Pipelines" Proc. of IPC'02, 4th Int. Pipeline Conf. ASME, Calgary, Alberta, Sep. 3-Oct. 29, pp 475-484. Paper IPC2002-27225.

Dorey, A., B., Murray, D., W., Cheng, J., J., R. (2006) "Critical Buckling Strain Equations for Energy Pipelines-A Parametric Study" *J.Offshore Mech. and Arctic Eng.* 128, August 2006, pp248-255.

Ellinas C. P., Raven, P. W. J., Walker, A. C., and Davies, P. (1987) "*Limit State Philosophy in Pipeline Design*" ASME, Proceedings of the 6th International Offshore Mechanics and Arctic Engineering Symposium, January.

Gellin, S. (1980). "The plastic buckling of long cylindrical shells under pure bending." *Int. J. Solids and Struct.*, 16, 397-407.

Gerald, G. and Becker, H., (1957), "Handbook of Structural Stability, Part III-Buckling of Curved Plates and Shell", *National Advisory Committee for Aeronautics, Tech. Note* No. 3783.

Gresnigt, A. M. (1986). "Plastic design of buried steel pipelines in settlement areas." *Heron*, 31(4).

Hauch, S. and Bai, Y. (1999) “Bending Moment Capacity of Pipes”, Offshore Mechanical and Arctic Engineering, OMAE’99, July 11-16, 1999.
Hauch, S. and Bai, Y. (2000) “Bending Moment Capacity of Groove Corroded Pipes”, ISOPE200.

Hibbit, H.D., Karlson, B.I., and Sorensen, P., (2006), “ABAQUS Version 6.3-Theory Manual”, Pawtucket, RI.

Hu, S Z; Birkemoe, P C; Prion, H G L (1992), “Finite element modeling of imperfections and residual stresses in fabricated tubular columns”, Design of Marine and Offshore Structures., Computational Mechanics Publications/Elsevier Applied Science, Southampton (UK), 1992, pp. 709-720.

Kim, H. O. and Valesco P. (1988) “Review of Pipe Buckling for Arctic Pipeline Design” The Seventh International Conference on Offshore Mechanics and Arctic Engineering, Houston, Texas, February.

Labview User Manual (2005). National Instruments. Austin, Texas, USA.

Lara, P. F. (1987) “Revisiting Failure Criteria of Buried Pipelines” ASME Engineering Symposium, ETCE, Dallas, Texas.

Mohareb, M. (2001). “Exact yield hyper surface for thin pipes.”, *Int. J. of Pressure Vessels and Piping*, 78(7), 507-514.

Mohareb, M. (2002). “Plastic interaction relations for pipe sections”, *J. Eng. Mech.*, ASCE, Jan. Vol.128(1), 112-120.

Mohareb, M. (2003) Plastic Interaction Relations for Pipe Sections- An upper bound solution, *Journal of Engineering Mechanics*, ASCE, Jan. Vol.128(1), 112-120.

Mohareb, M. and Murray, D. W. (1999). “Mobilization of fully plastic moment capacity for pressurized pipes subjected to axial loading” *ASME J. Offshore Mech. Arct. Eng.*, 121 (4), 237-241.

Mohareb, M., Elwi, A., Kulak, G. L., and Murray, D. W. (1994). “Deformational behavior of line pipe.” *Struct. Eng. Rep. No. 202*, Dept. of Civ. Engrg., University of Alberta, Edmonton, Alberta, Canada.

Morris, G. and Fenves, S. (1969). “Approximate yield surface equations”, *J. Eng. Mech Division*, ASCE, Vol. 95 (EM4), 937-954.

Murphy, C. E. and Langner C. C. (1985) “Ultimate Pipe Strength under Bending, Collapse, and Fatigue” ASME, Proc. 4th International Offshore Mechanics and Arctic Symposium, Dallas, February.

Obaia, K. H., Elwi, A., Kulak, G. L. (1991). "Inelastic transverse shear capacity of large fabricated steel tubes" *Struct. Eng. Rep. No. 170*, Dept. of Civ. Engrg., University of Alberta, Edmonton, Alberta, Canada.

Ozkan, I. F. (2007). "Control modules for testing of steel pipes under complex loads" Report submitted to the Department of Civil Engineering at the University of Ottawa.

Ozkan, I. F., Mohareb, M. (2003). "Testing of Steel Pipes under Bending, Twist, and Shear", Journal of Structural Engineering, American Society of Civil Engineering (ASCE), Vol. 129, No. 10, p. 1350-1357.

Pillai, S. U., and Ellis, J. S. (1971). "Hollow tubular beam-columns in biaxial bending." *J. Struct. Eng.*, ASCE, 97(ST5), 1399-1406.

Plantema, F.J. (1946). "Collapsing stresses of circular cylinders and round tubes." Report S. 280, Nat. Luchtvaartlaboratorium, Amsterdam, the Netherlands.

Price, P. St. J. and and Barnett, J. A. (1987) "Pipeline Codes and Structural Criteria for Pipelines in Arctic and Earthquake Regions" Sixth International Symposium and Exhibit on Offshore Mechanics and Arctic Engineering, Houston, March 1-6.

Price, P. St. J. and Anderson, H., A. (1991). "Intergrity Monitoring and Maintanence Criteria for New and Existing on Land or Marine Pipelines", Proceedings on the First International Offshore and Polar Engineering Conference, Edinburgh, United Kingdom, 11-16 August.

Prion, H. and Birkemoe, P. (1988) "Experimental Behavior of Un-stiffened Fabricated Tubular Steel Beam-Columns", University of Toronto, Department of Civil Engineering, Publication No. 88-03, ISBN 07-7727-7096-4.

Prion, H. and Birkemoe, P. (1992). "Beam-Column behavior of fabricated steel tubular members." *J. of Struct. Engineering*, Vol. 118, No. 5, pp. 1213-1232.

Reddy, B. D. and Calladine, C.R. (1978). "Classical buckling of thin-walled tube subjected to bending moment and internal pressure". *Int. J. Mech. Sci.* Vol. 20, pp. 641-650.

Reddy, B. D. (1979). "An experimental study of the circular cylinders in pure bending." *Int. J. Solids and Struct.*, 15(9), 669-683.

Row, D. G., Powell, C. H., and Morris, G. R. (1983) "Local Buckling Analysis of Pipelines", Proceedings of the second International Offshore Mechanics and Arctic Engineering Symposium, ASME.

Schilling, C. G. (1965). "Buckling Strength of Circular Tubes", *J. of Struct. Division*, ASCE, Vol.102, No. ST11, pp.2181-2195.

Sherman, D. R. (1976), "Tests of Circular Steel Tubes in Bending", *J. of Struct. Division*, ASCE, Vol.91, No. ST5, pp.325-348.

Sherman, D. R. (1986) "Inelastic Flexural Buckling of Cylinders" *Steel Structures-Recent Research Advances and Their Applications to Design*, M. N. Pavlovic, ed., Elsevier Applied Science Publishers, London, England, 339-357.

Sorensen, J., et al. (1970), "Buckling strength of offshore pipelines", Battelle Report to Offshore Pipeline Group Columbus, OH.

Souza, L., T. and Murray, D., W. (1994) "Prediction of wrinkling behavior of girth-welded line pipe" University of Alberta, Dept. of Civil Engineering, Structural Engineering Report No:197.

Souza, L., T. and Murray, D., W. (1996) "Analysis for Wrinkling Behavior of Girth-Welded Line Pipe", International Pipeline Conference-Volume 2, ASME 1996.

"Steel Structures for buildings-Limit States Design" (1984), *CAN 3-S16.1-M84*, Canadian Standards Assoc., Ottawa, Ontario, Canada.

Timoshenko, S. P. and Gere, J. M. (1961) "Theory of Elastic Stability", Second Edition, McGraw-Hill.

The Canadian Encyclopedia.com "Pipeline" 4 July 2007 http://www.thecanadianencyclopedia.com/ Path: Pipelines; Structure of the System.

Tapseis.anl.gov "What is Taps?" 4 July 2007 http://tapseis.anl.gov/ Path: TAPS Guide; What is TAPS?

Workman, G. H. (1981) "Pipe Wall Stability Analysis of 12.75 in O.D. x 0.25 W.T. Grade 52 Pipe", Summary Report to Canuck Engineering Ltd., March.

Workman, G. H. (1988) "Manufacturing Residual Stress Effects on Buried Pipeline Structural Response", the Seventh International Conference on Offshore Mechanics and Arctic Engineering, Houston, Texas, February 7-12.

Yamaki, H., (1976) Experiments on the Post-Buckling Behavior of Circular Cylindrical Shell under Torsion, *Proc. IUTAM, Symp. Buckl. of Struct., Springer-Verlag*, Heidelberg, pp.312-330

Yoosef-Ghodsi, N., Kulak, G.L., and Murray, D.W.(1995). "Some Tests Results on Wrinkling of Girth-Welded Line Pipe" *Proc. of the 14th inter. Conf. on OMAE*, Vol. V-Pipeline Technology, ASME, Copenhagen, pp. 379-388.

Zhang, C., Bao, X., Ozkan, I. F., Mohareb, M., Ravet, F., Du., M., DiGiovanni, D., J. (2007). "Prediction of the pipe buckling by using broadening factor with distributed Brillouin fiber sensors", Optical Fiber Technology, to appear Feb. 2008

Zhou, Z. and Murray, D. (1993) "Behaviour of Buried Pipelines under Imposed Deformations", *OMAE,* Vol. V, Pipeline Technology.

Zimmerman, T.J.E., Stephens, M.J., DeGeer, D.D., and Chen Q. (1995). "Compressive Strain Limits for Buried Pipelines" *Proc. of the 14th inter. Conf. on OMAE* Copenhagen, June.

Zimmerman, T.J.E., Xie, J., Timms, C., Asante, J. (2004). "Buckling Resistance of Large Diameter Spiral Welded Line Pipe" *Proc. of International Pipeline Conference (IPC2004).* ASME, Calgary, Alberta, Oct.4-8, 2000,. Paper IPC04-0364.

Appendix A-Detailed Drawings of the Test Setup Equipment

Appendix A consists of following sections.

Section A1: Detailed drawings of Loading Arm.

A key drawing for the loading arm is provided in Fig. A1 while the detailed views are illustrated in Figs A2 through A7.

Section A2: Detailed drawings of Bearing Frames and Bracings

A key drawing for the bearing frames and bracings is provided in Fig. A8 while the detailed views are illustrated in Figs A9 through A13.

Section A3: Detailed drawings of Fittings (Base plates, Spacers, and Anchor Rods)

Drawings for Spacer types A, B, and C are provided in Figs. A14, A15, and A16, respectively. Figure A17 illustrates the base plates and Fig. A18 is the drawing for anchor rods and bottom plate.

A1 Detailed Drawings of Loading Arm

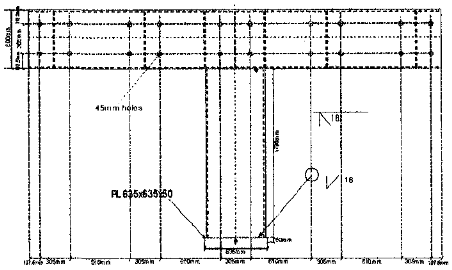

Fig. A5 Back View A-A

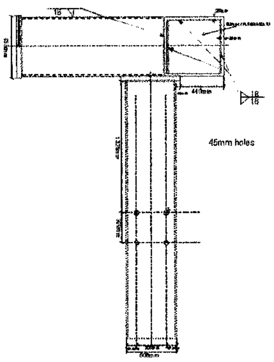

Fig. A 4 Side View C-C

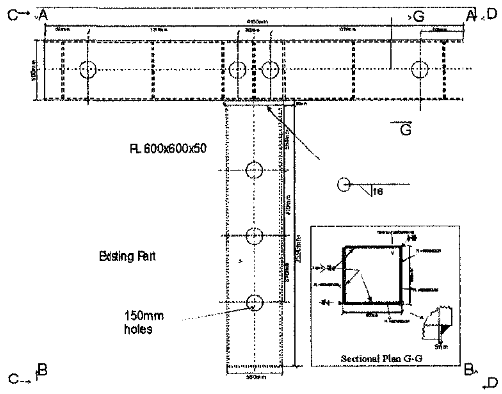

Fig. A2 Top View

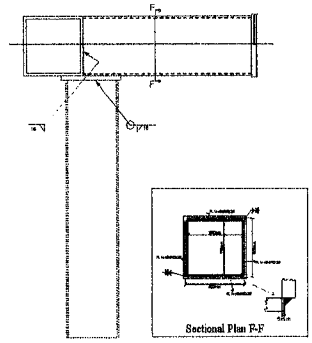

Fig A 3 Side View D-D

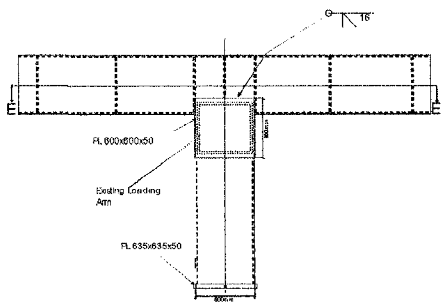

Fig. A6 Front View B-B

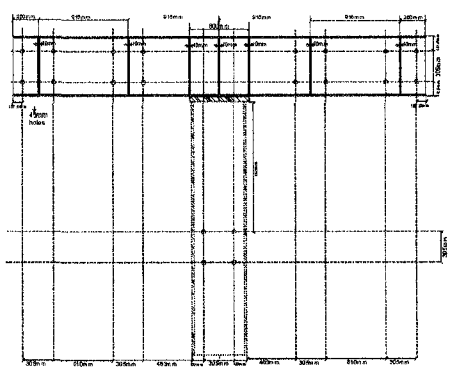

Fig. A7 Sectional Plan E-E

Fig. A1 Loading Arm

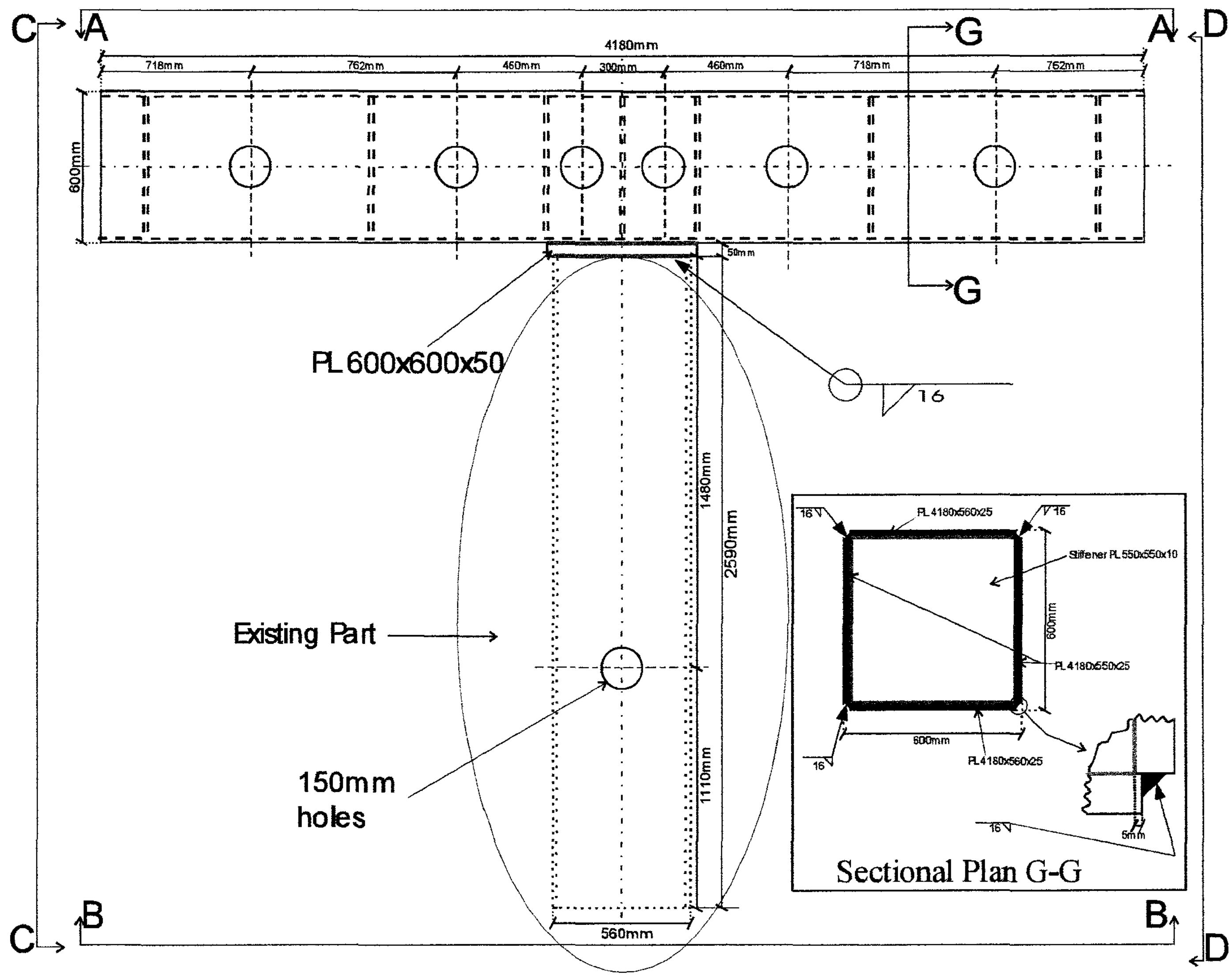

Fig. A2 Top View

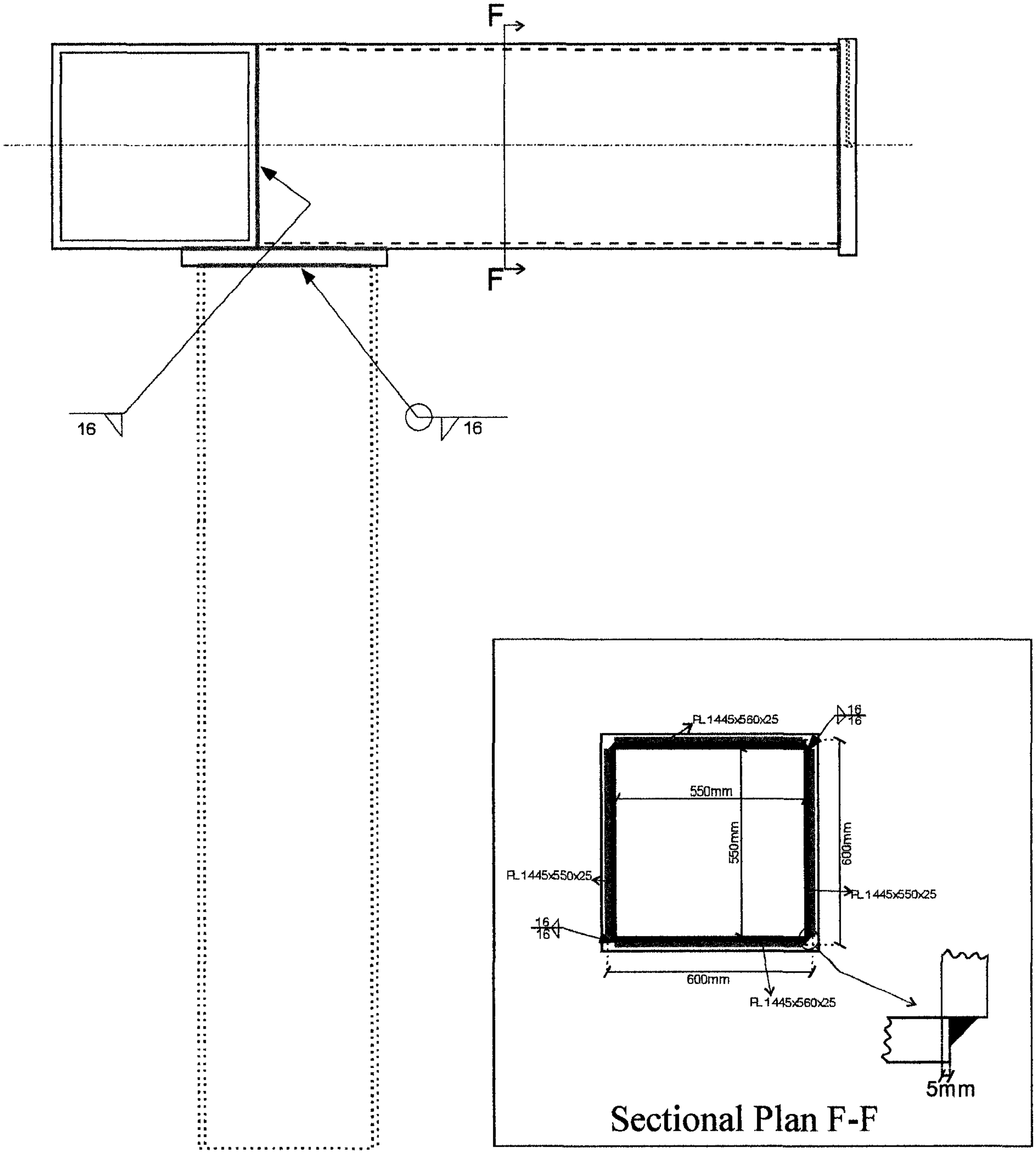

Fig. A3 Side View D-D

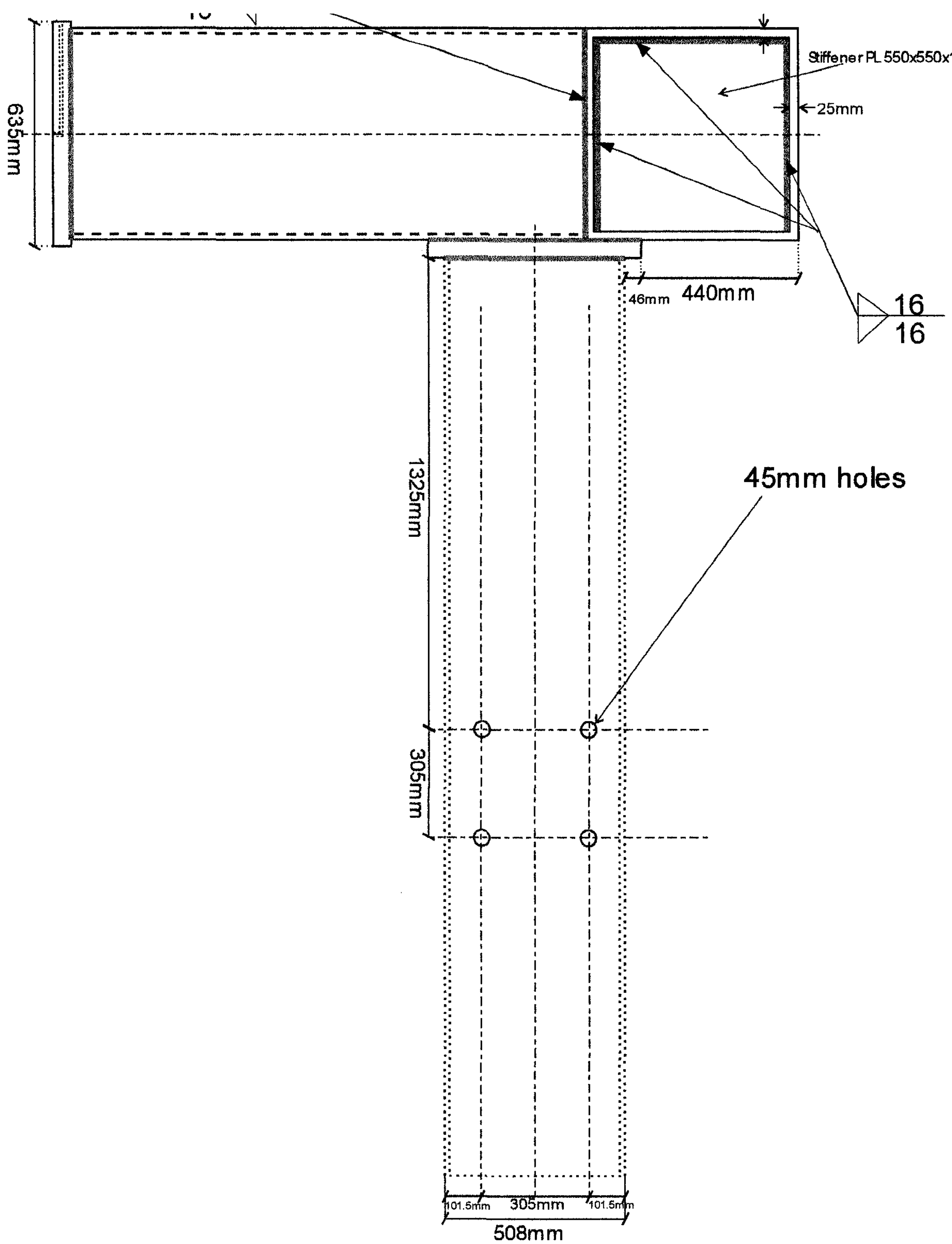

Fig. A4 Side View C-C

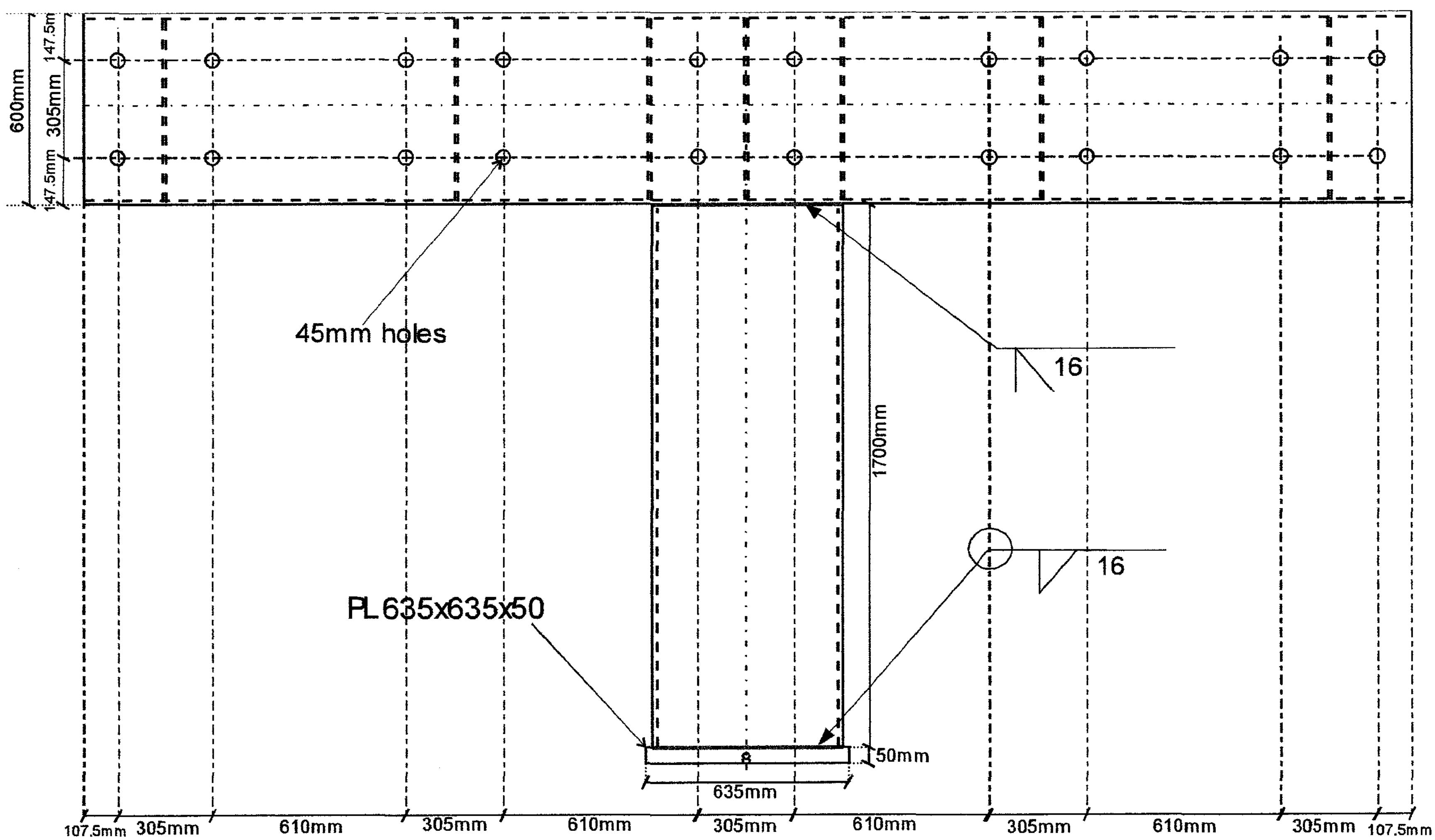

Fig. A5 Back View A-A

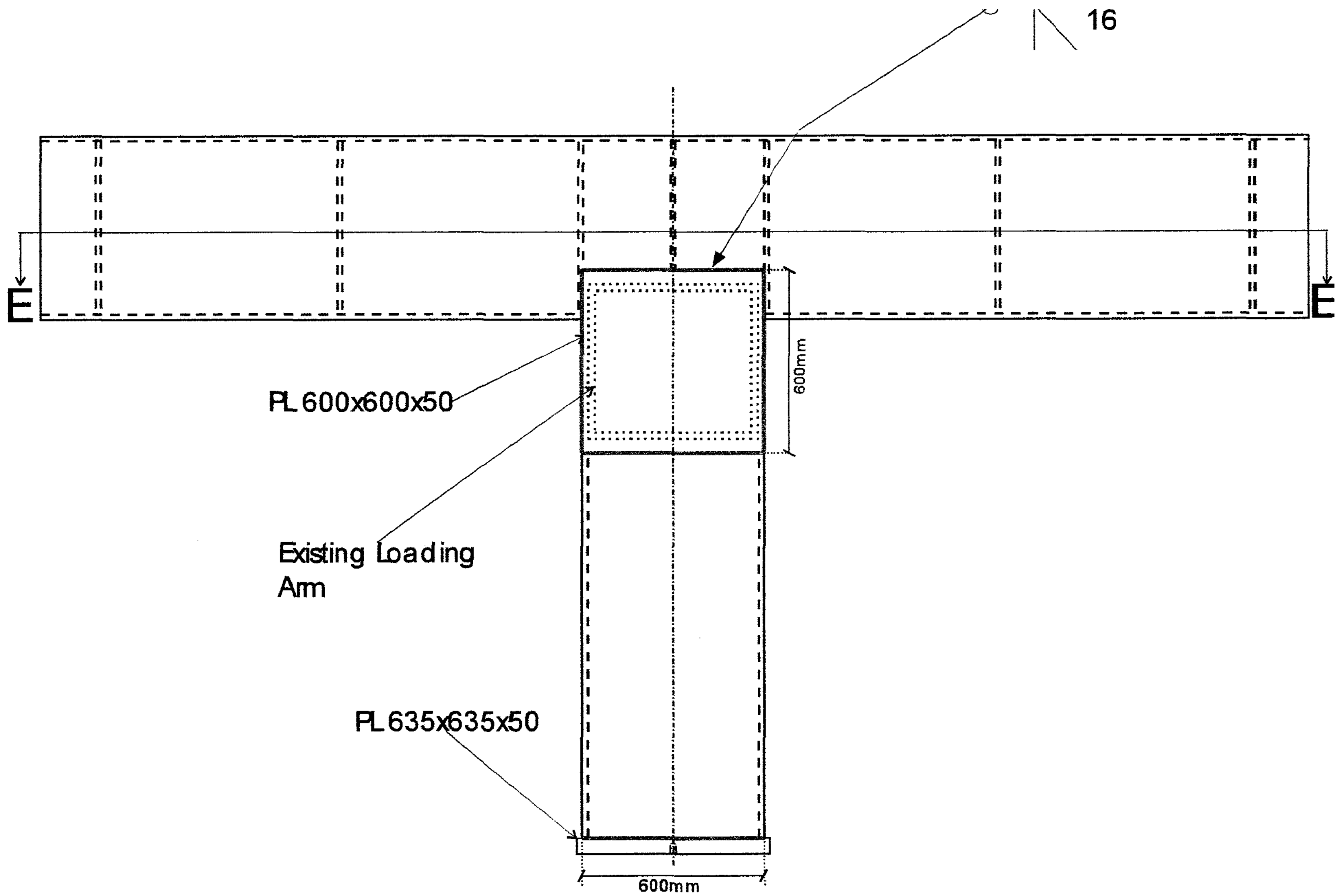

Fig. A6 Front View B-B

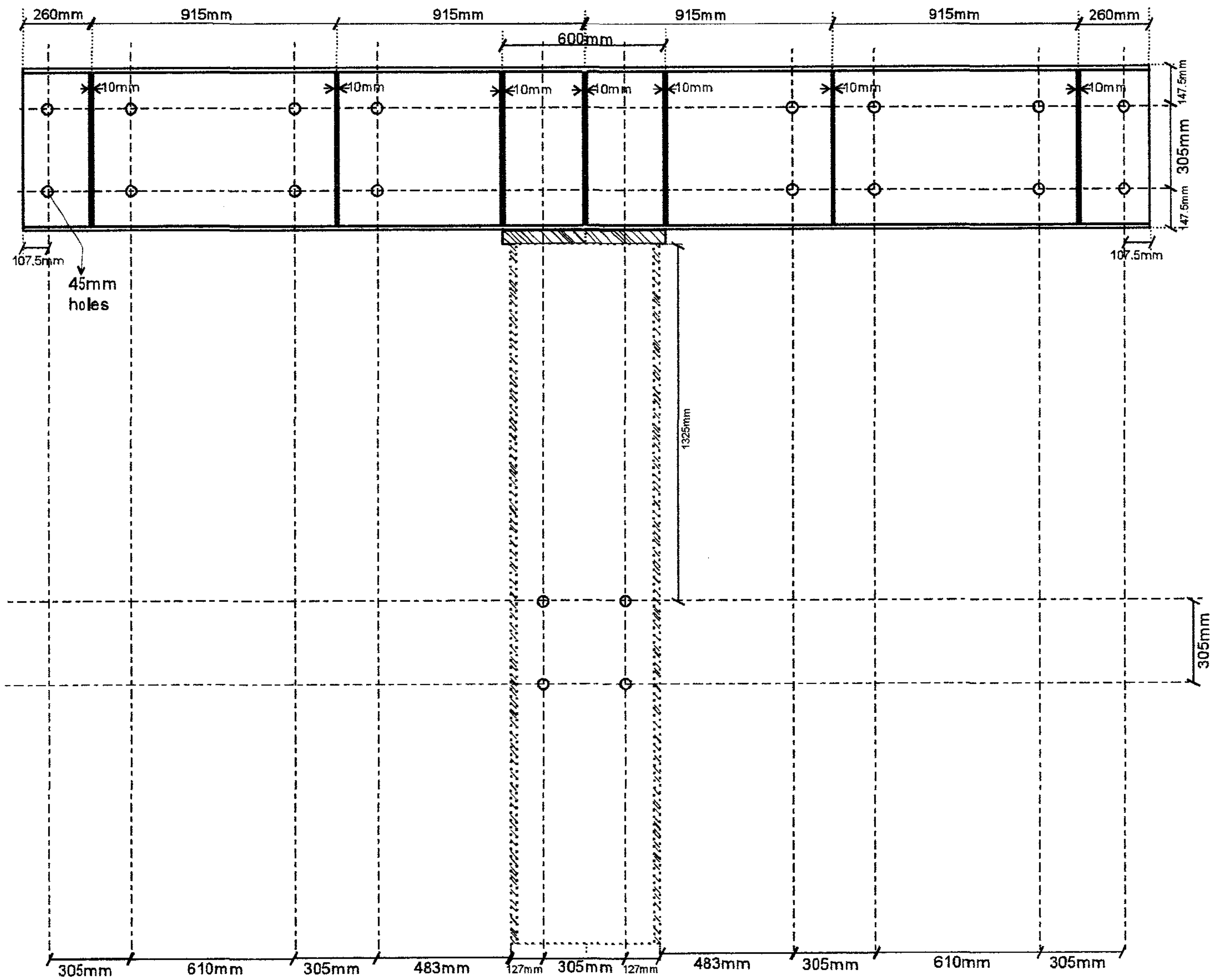

Fig. A7 Sectional Plan E-E

A2 Detailed Drawings for Bearing Frames and Bracing

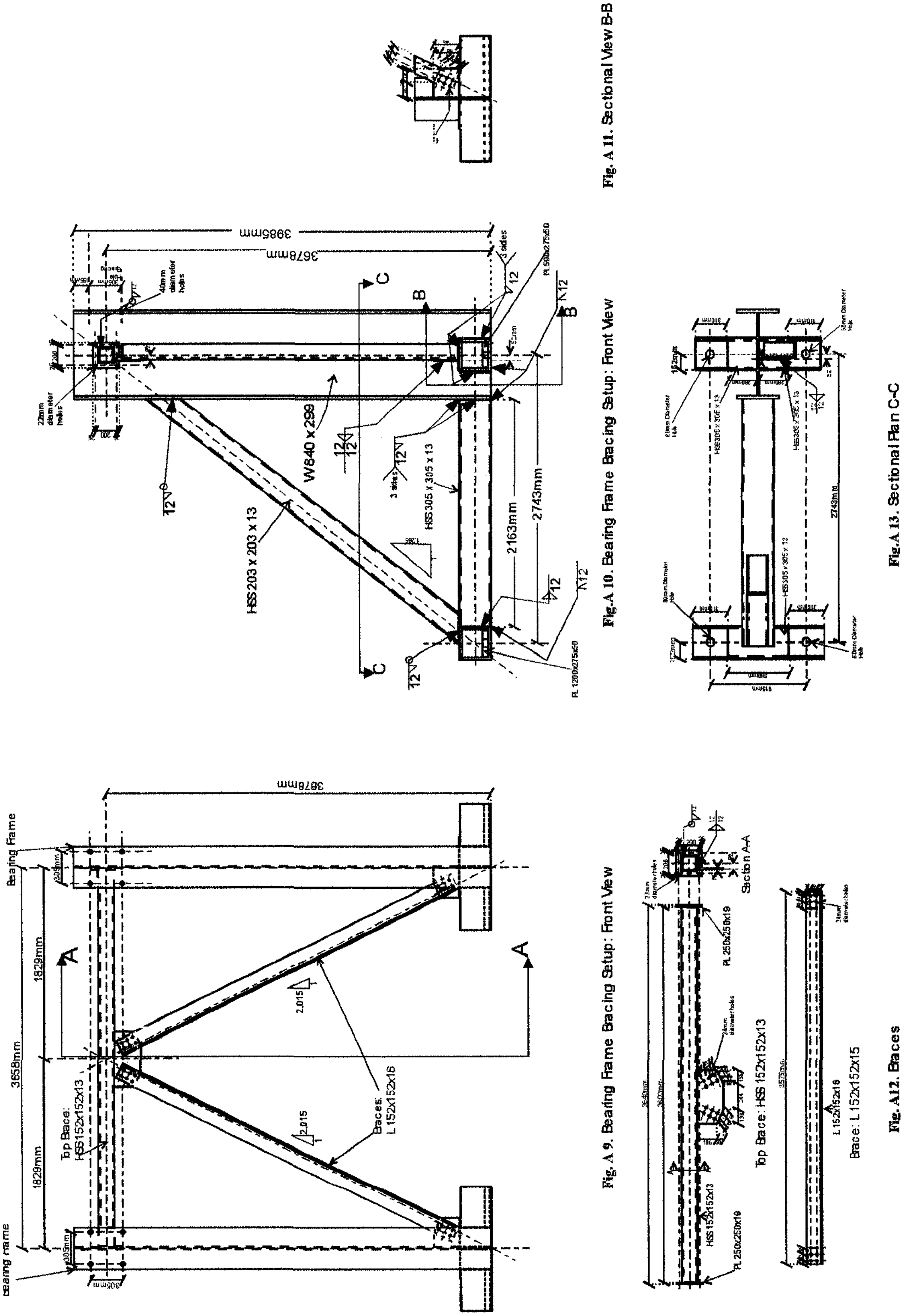

Fig. A8 Bearing Frame and Bracing System

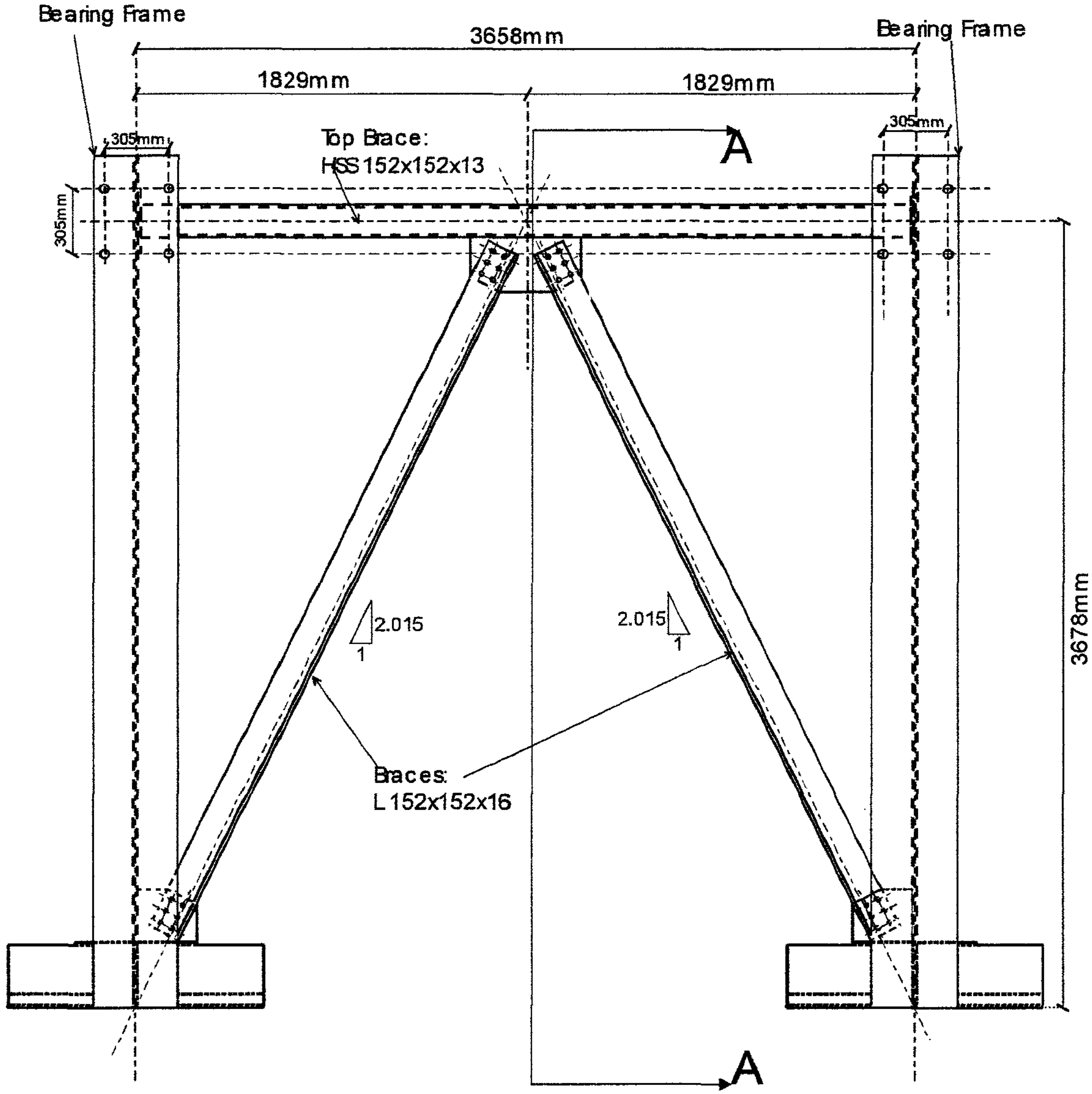

Fig. A9 Bearing Frame and Bracing Setup: Front View

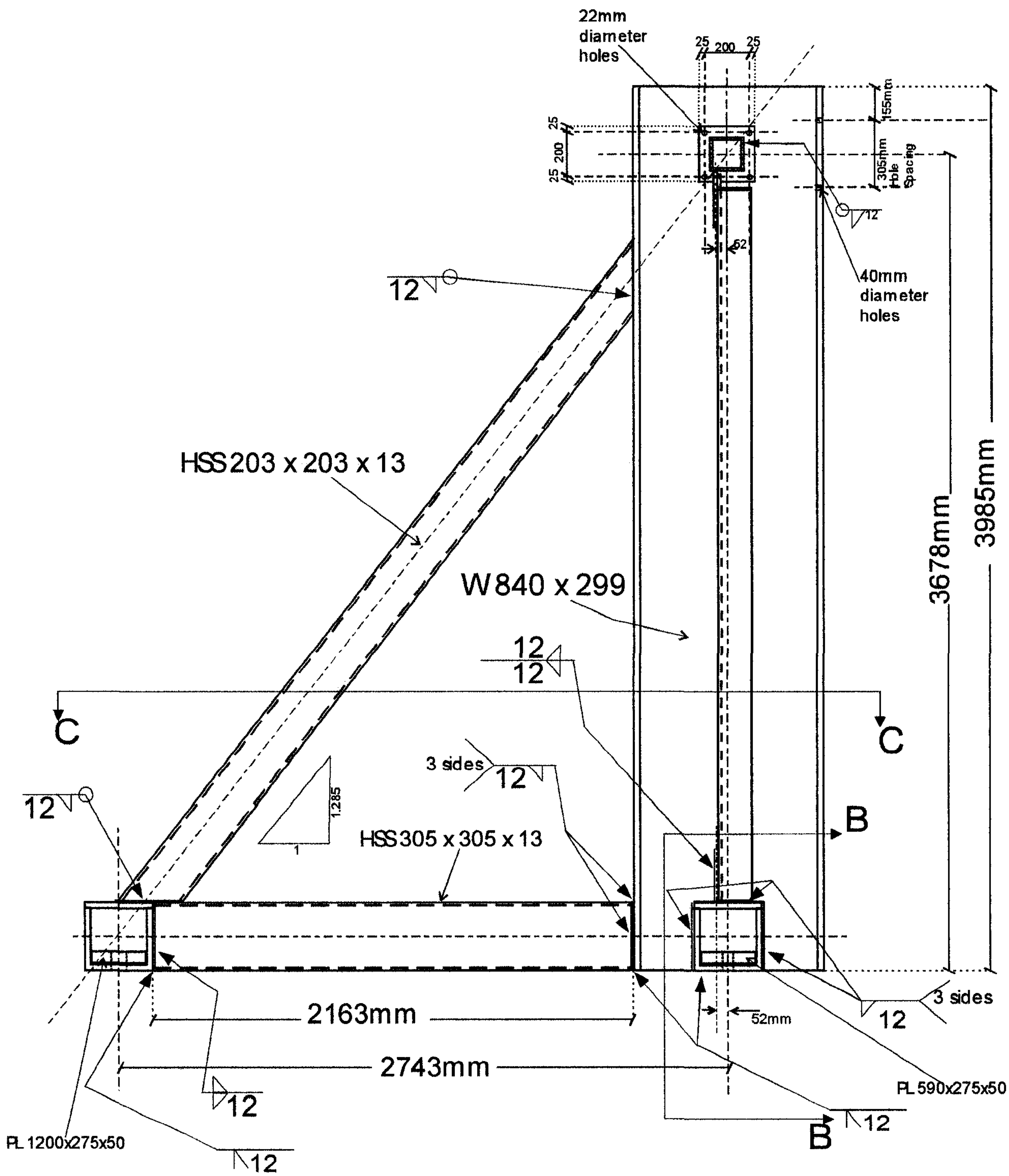

Fig, A10 Side View: Section A-A

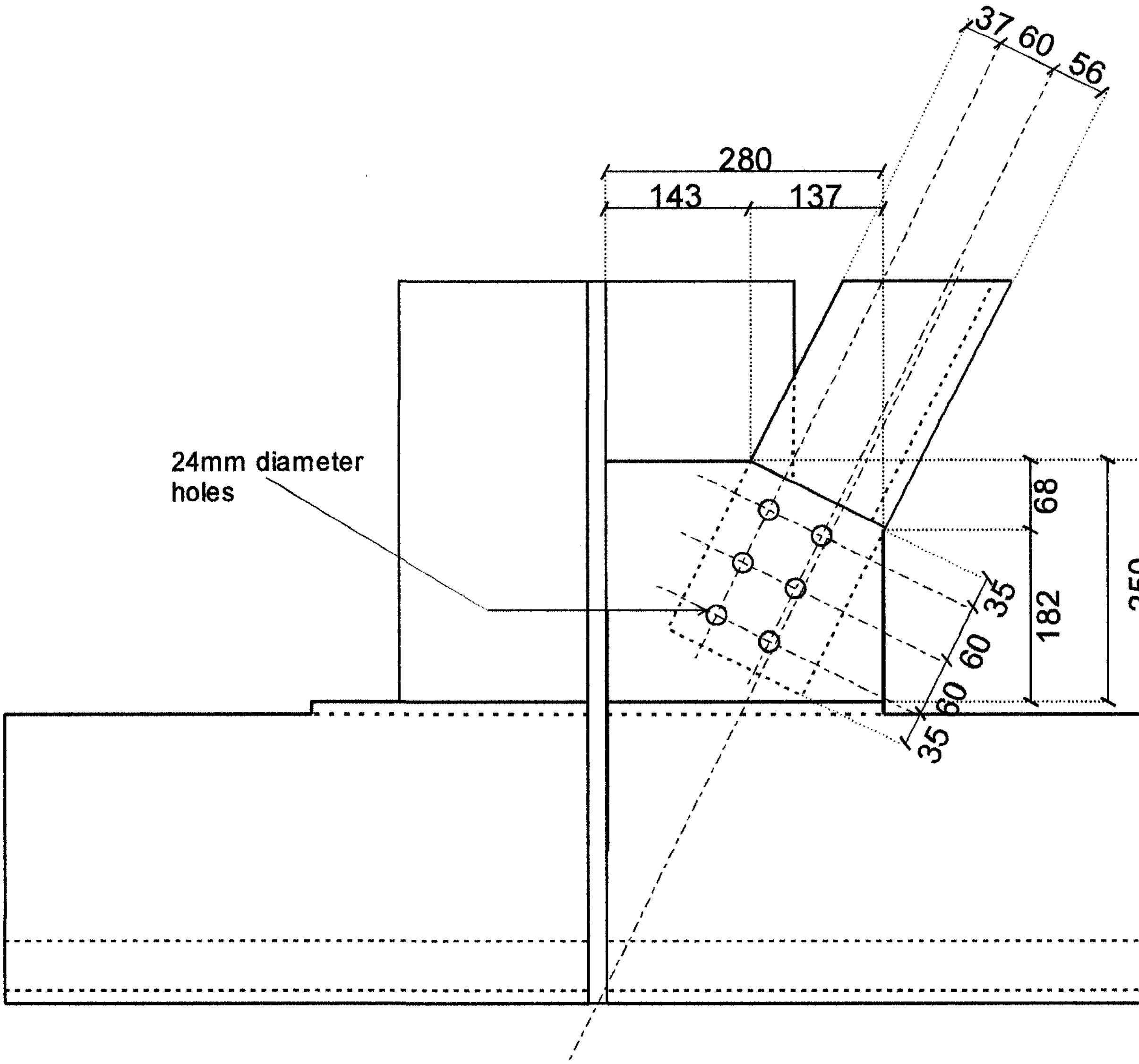

Fig A11 Sectional View B-B

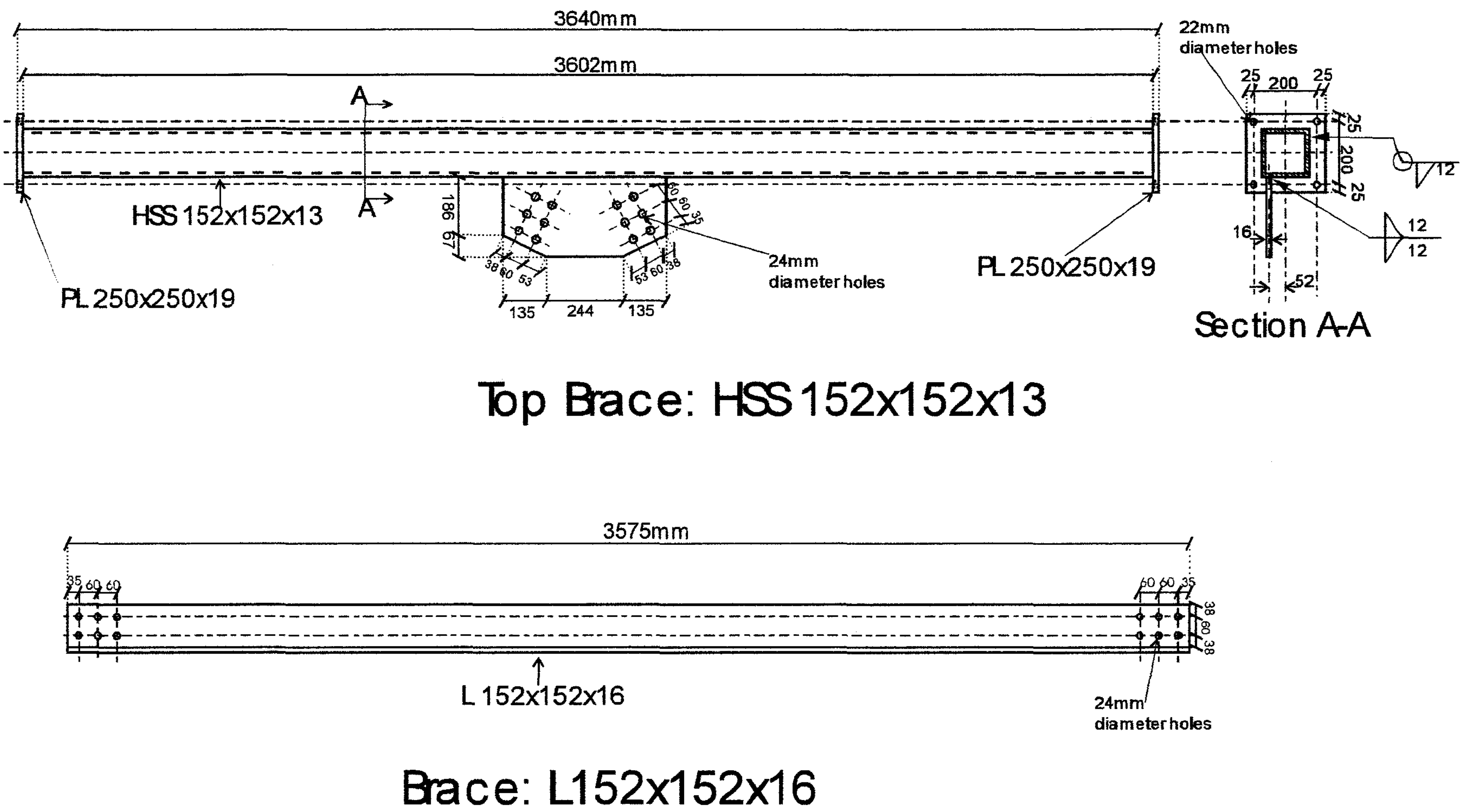

Fig. A12 Brace Details

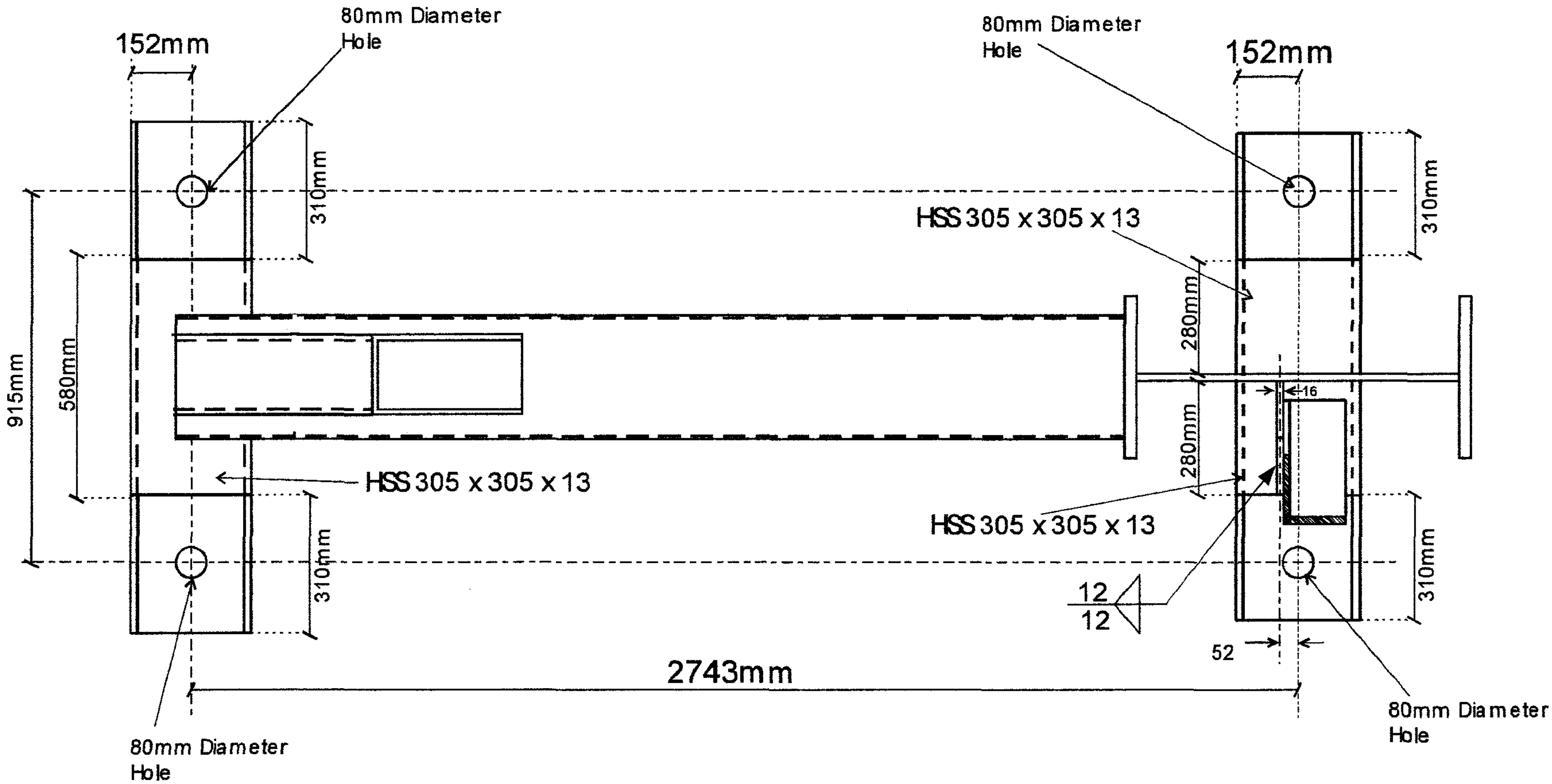

Fig. A13 Sectional Plan C-C

A3 Detailed Drawings for Fittings

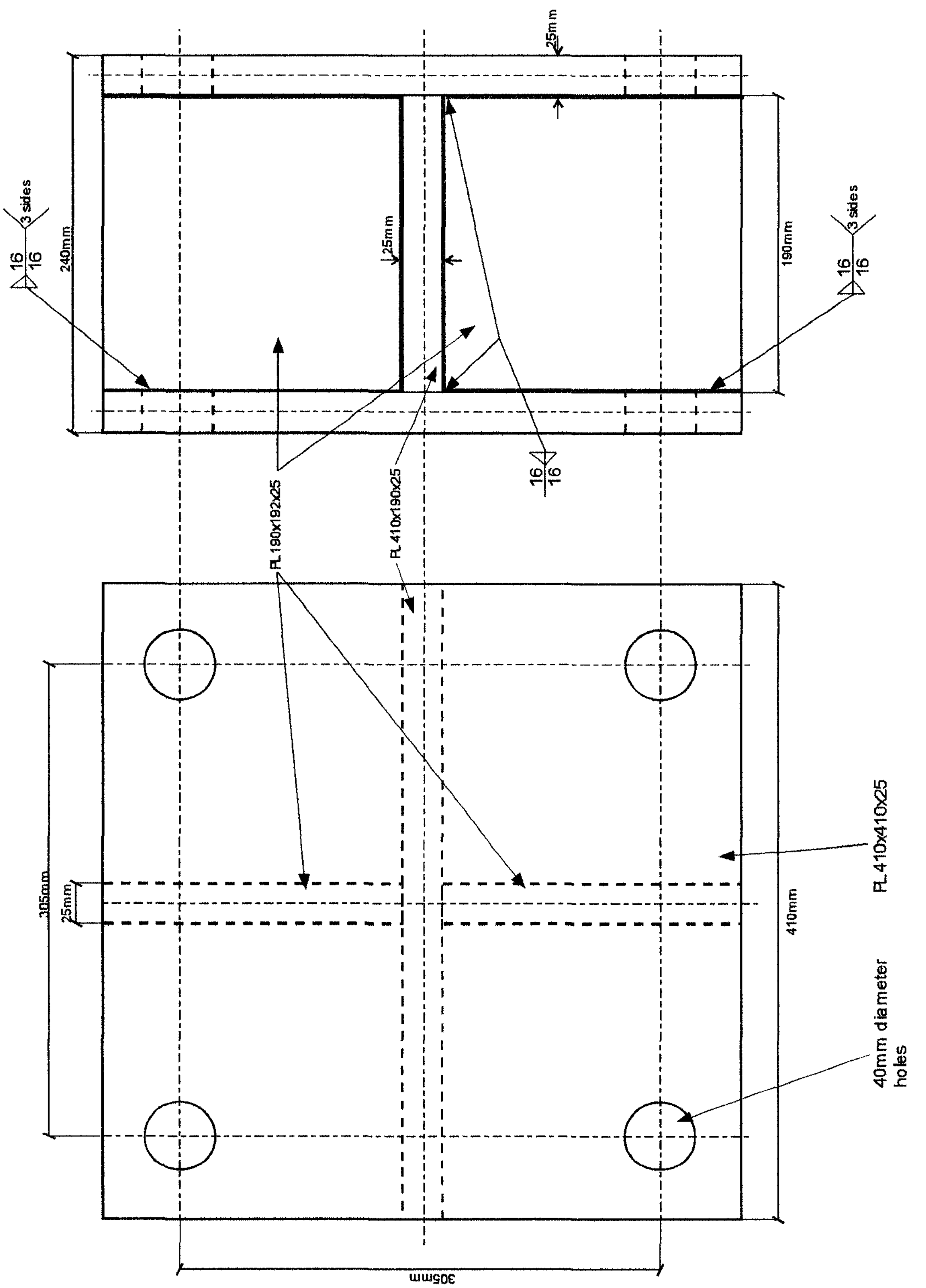

Fig. A14 Spacer (Type A)

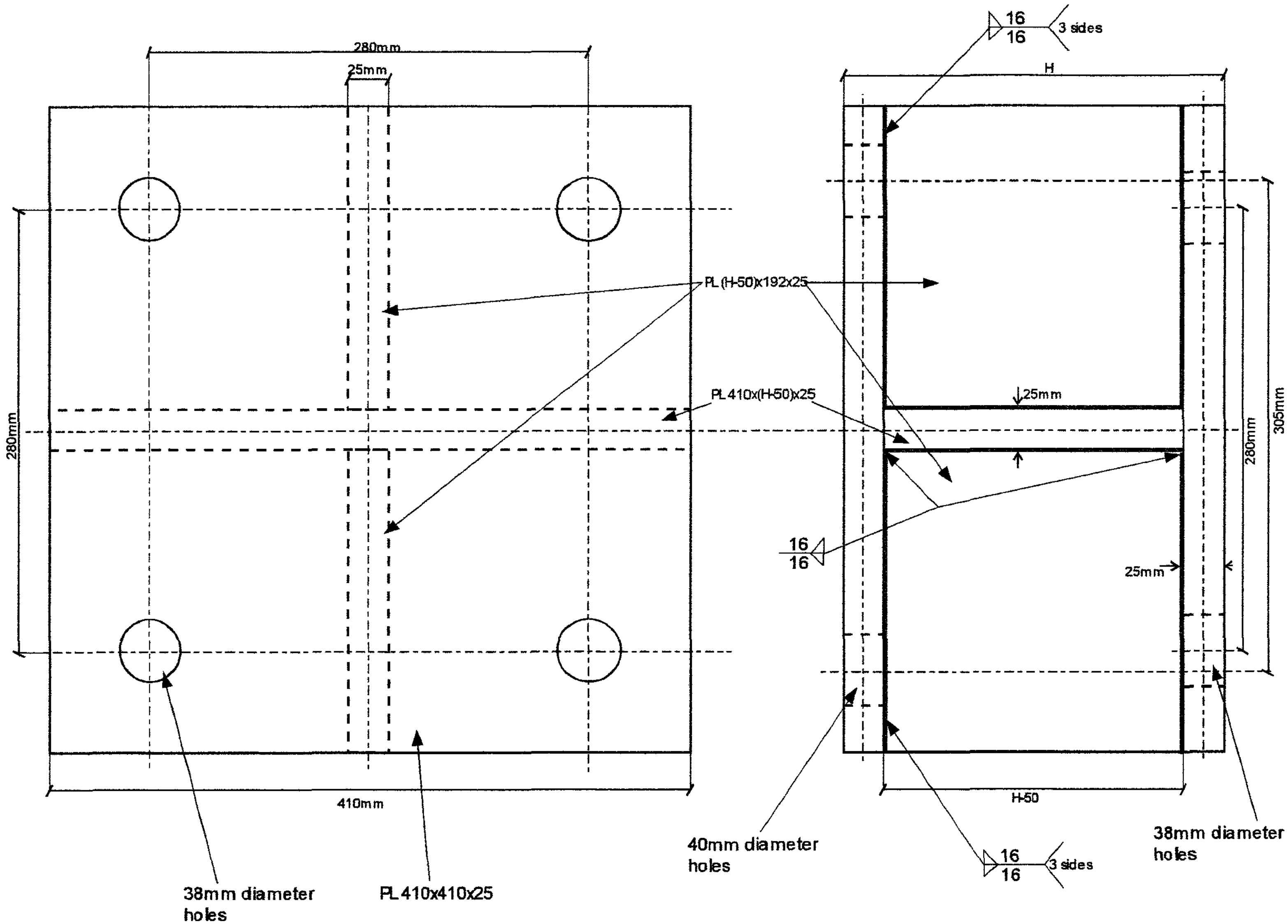

Fig A15 Spacer (Type B)

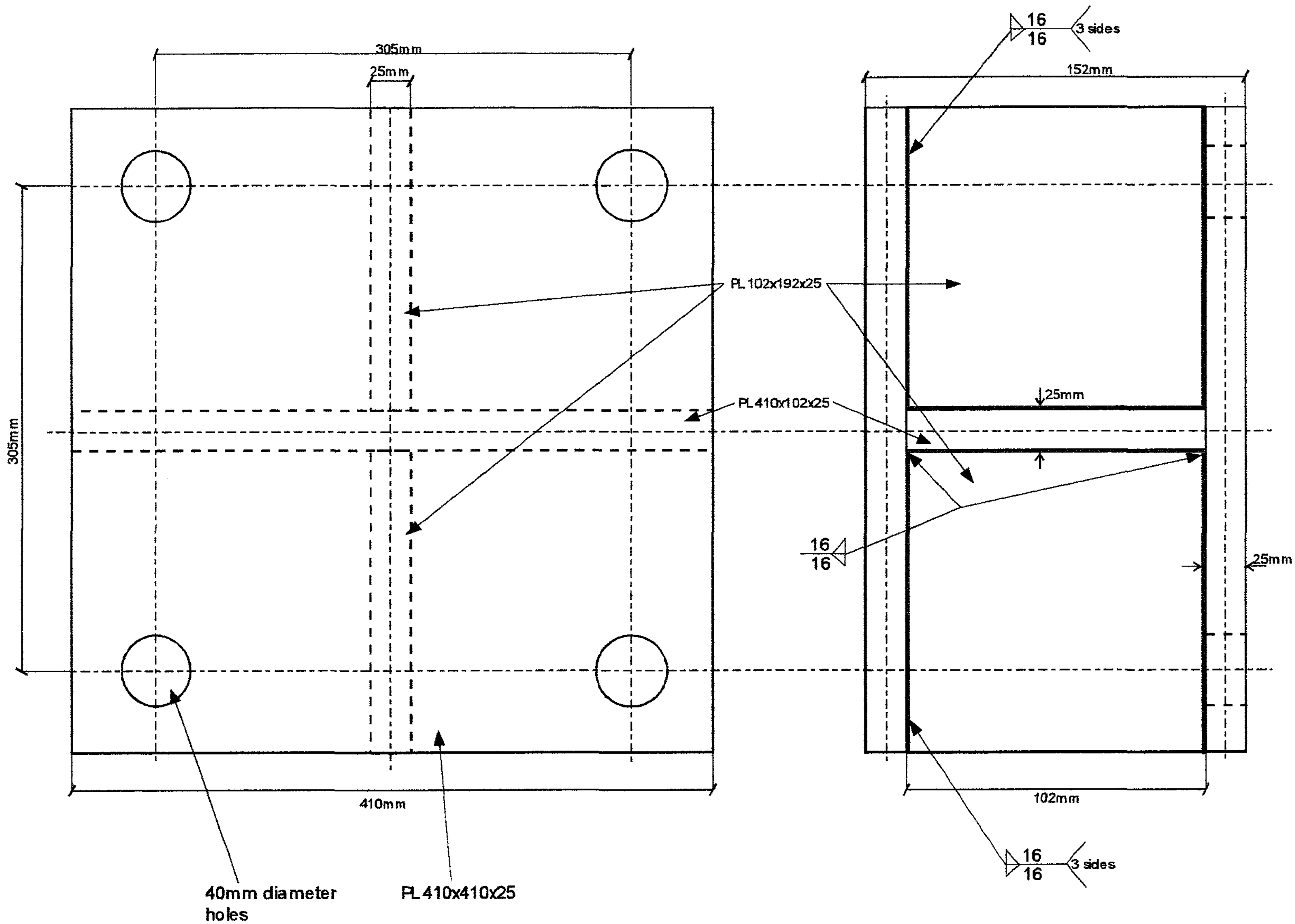

Fig A16 Spacer (Type C)

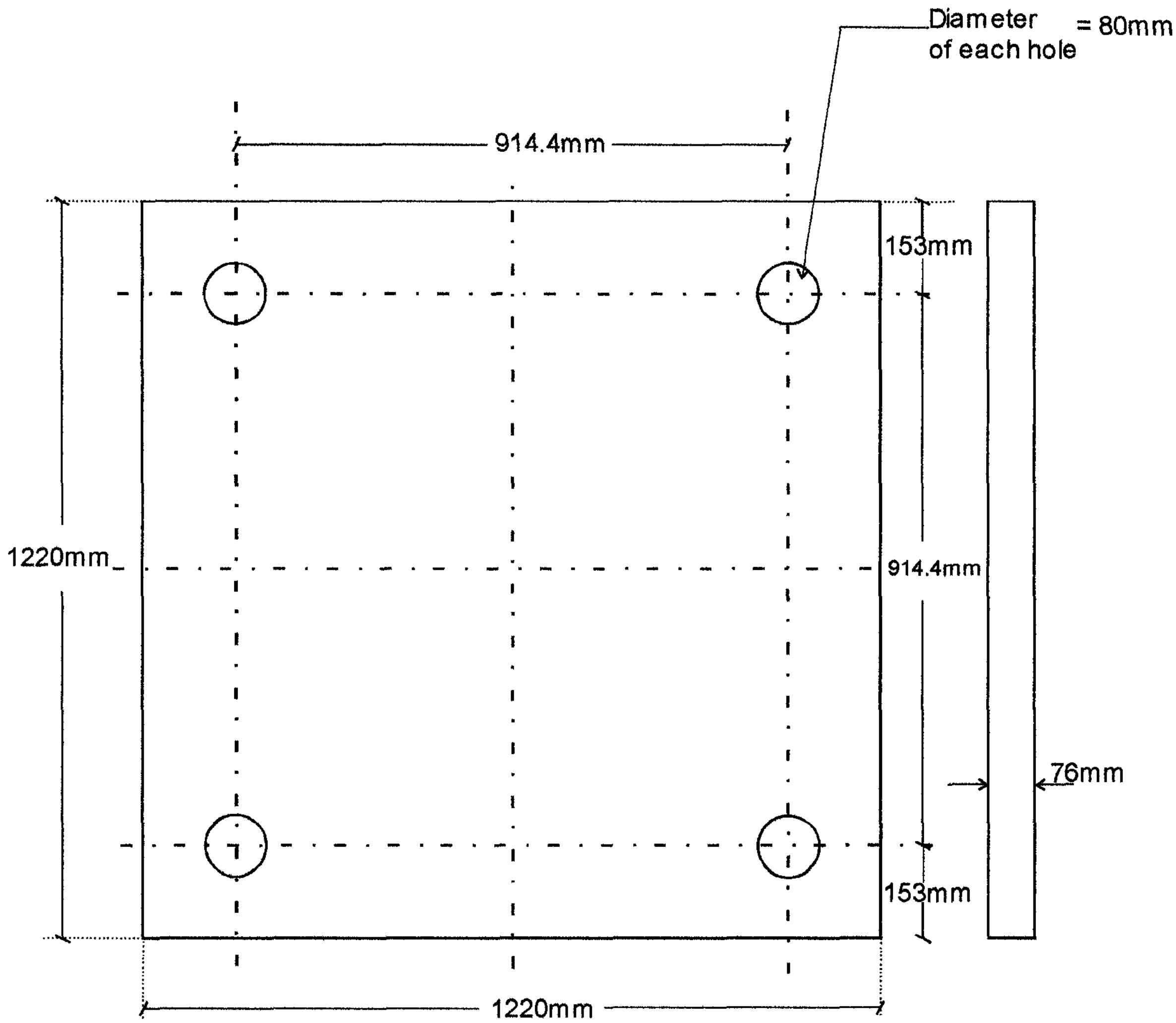

Fig A17 Base Plate

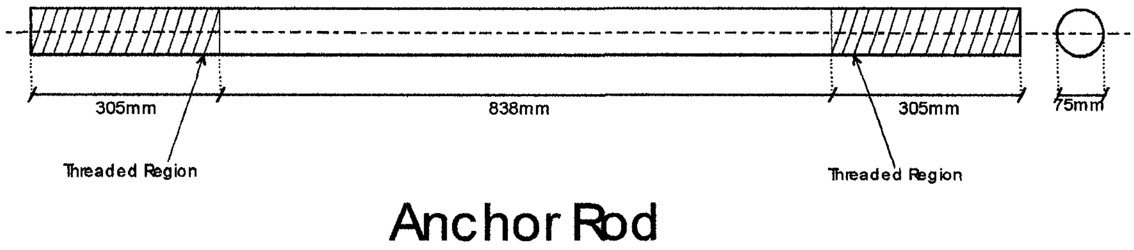

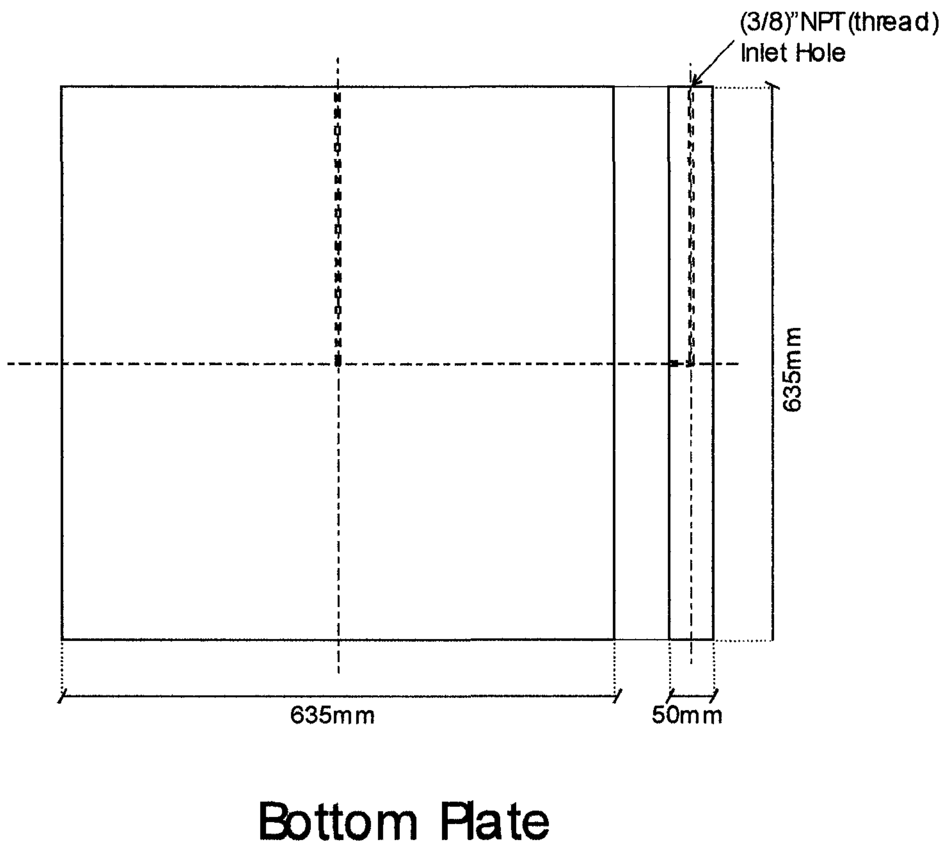

Fig. A18 Anchor Rod and Bottom Plate

Appendix B-Material Properties

B1 Stress vs. Strain data based on Tension Coupon Tests

The stress vs. strain data obtained from 14 tension coupon tests are presented in Table B1.

Table B1 Stress vs. Strain data from Tension Coupon Tests taken from the pipe material of specimens in Chapter 5

Strain	Specimen 1 Stress (MPa)	Specimen 2 Stress (MPa)	Specimen 3 Stress (MPa)	Specimen 4 Stress (MPa)	Specimen 5 Stress (MPa)	Specimen 6 Stress (MPa)	Specimen 7 Stress (MPa)
0.00000	0.0	0.0	0.0	0.0	0.0	0.0	0.0
0.00025	54.2	55.0	55.7	60.3	59.6	53.7	53.1
0.00050	109.3	108.0	110.5	109.6	119.3	106.8	106.0
0.00080	170.7	171.5	175.3	173.9	190.1	169.5	169.7
0.00096	204.4	204.3	209.8	207.8	225.4	203.0	204.3
0.00112	238.0	237.0	244.0	241.8	261.6	236.4	238.6
0.00128	269.3	268.5	277.0	275.6	298.7	270.3	271.6
0.00144	299.6	298.7	311.1	310.8	333.5	301.6	302.3
0.00160	328.6	325.8	343.4	344.4	365.4	331.4	332.9
0.00176	356.7	353.9	372.7	378.5	387.5	360.6	361.3
0.00192	381.7	382.0	398.5	411.6	408.9	389.1	387.3
0.00208	403.1	405.9	420.8	443.4	429.3	413.7	411.8
0.00224	424.5	427.9	439.4	473.3	449.2	436.6	434.4
0.00240	436.5		455.2	502.9	468.3	452.9	452.4
0.00300	497.5		490.7	538.0	511.5	502.8	498.3
0.00350	508.2		510.8	542.7	526.6	517.6	521.3
0.00400	519.0		531.0	542.7	541.3	532.3	536.0
0.00450	529.7		534.5	538.6	543.9	545.3	539.5
0.00500	540.4		537.7	538.6	546.6	545.9	543.0
0.00600	545.3		540.4	539.4	542.2	547.2	549.9
0.00800	549.4		538.3	543.0	542.3	549.7	553.9
0.01200	555.5		536.5	543.9	541.9	553.5	552.6
0.01400	557.0		536.0	547.2	541.9	554.6	551.9
0.02000	563.7		543.8	559.2	544.9	559.1	563.4
0.02800	573.6		554.5	560.9	551.6	568.4	571.3
0.03000	576.0		557.2	565.2	553.7	569.8	571.3
0.04000	580.9		568.0	569.5	564.2	576.7	572.6
0.06000	590.7		578.7	579.8	579.6	585.2	588.0
0.08704	592.2		583.8	584.7	584.4	587.8	590.5
0.13457			582.5				
0.17825			567.5				
0.22644			496.0				
0.23405			471.7				
0.25319			394.9				

Table B1 Continued

Strain	Specimen 8 Stress (MPa)	Specimen 9 Stress (MPa)	Specimen 10 Stress (MPa)	Specimen 11 Stress (MPa)	Specimen 12 Stress (MPa)	Specimen 13 Stress (MPa)	Specimen 14 Stress (MPa)
0.00000	0.0	0.0	0.0	0.0	0.0	0.0	0.0
0.00025	61.8	62.4	53.6	56.1	55.7	56.9	54.5
0.00050	122.0	120.3	107.1	113.2	111.1	112.1	108.4
0.00080	181.2	193.8	173.1	181.3	175.9	177.4	173.2
0.00096	213.4	218.6	209.1	216.2	209.5	212.2	207.0
0.00112	246.5	251.7	244.0	250.2	241.3	246.6	239.2
0.00128	283.0	284.8	276.4	283.3	275.4	280.0	270.0
0.00144	318.0	317.9	309.9	316.5	309.1	313.4	299.3
0.00160	351.1	349.1	342.8	347.2	339.5	344.4	327.2
0.00176	379.7	377.6	370.6	373.9	368.3	374.4	354.0
0.00192	404.6	403.6	396.6	398.6	396.1	402.2	376.6
0.00208	427.0	425.0	421.0	420.9	416.6	425.7	398.1
0.00224	449.3	444.9	441.7	440.7	437.1	447.2	416.6
0.00240	468.1	460.1	460.5	458.1	451.1	462.1	434.2
0.00300	508.1	498.0	508.4	506.8	489.3	501.9	470.0
0.00350	528.5	522.5	521.5	525.1	501.1	519.9	491.5
0.00400	541.4	539.8	534.5	537.8	512.8	538.1	501.1
0.00450	545.7	543.1	547.1	541.6	524.6	539.0	510.6
0.00500	550.0	546.4	546.4	545.5	536.3	539.9	520.1
0.00600	550.3	550.2	545.1	550.1	539.2	541.6	541.1
0.00800	550.3	550.2	545.1	550.6	539.8	545.1	537.8
0.01200	551.8	550.2	545.1	550.7	541.1	550.2	540.0
0.01400	552.7	552.0	545.1	550.7	543.1	551.9	541.4
0.02000	555.6	557.2	545.1	552.3	555.9	557.3	545.5
0.02800	561.2	565.0	555.6	559.7	565.8	567.0	554.5
0.03000	562.6	567.0	557.4	561.6	567.3	568.8	557.4
0.04000	569.6	577.2	566.5	570.8	574.9	577.6	568.7
0.06000	583.5	586.5	581.6	582.3	584.5	586.6	578.9
0.08704	588.2	591.3	586.5	587.5	586.4	583.4	590.7

Figure B1 illustrates engineering stress vs. engineering strain relationships up to initiation of necking as obtained from tension coupon tests generated by the data in Table B1.1.

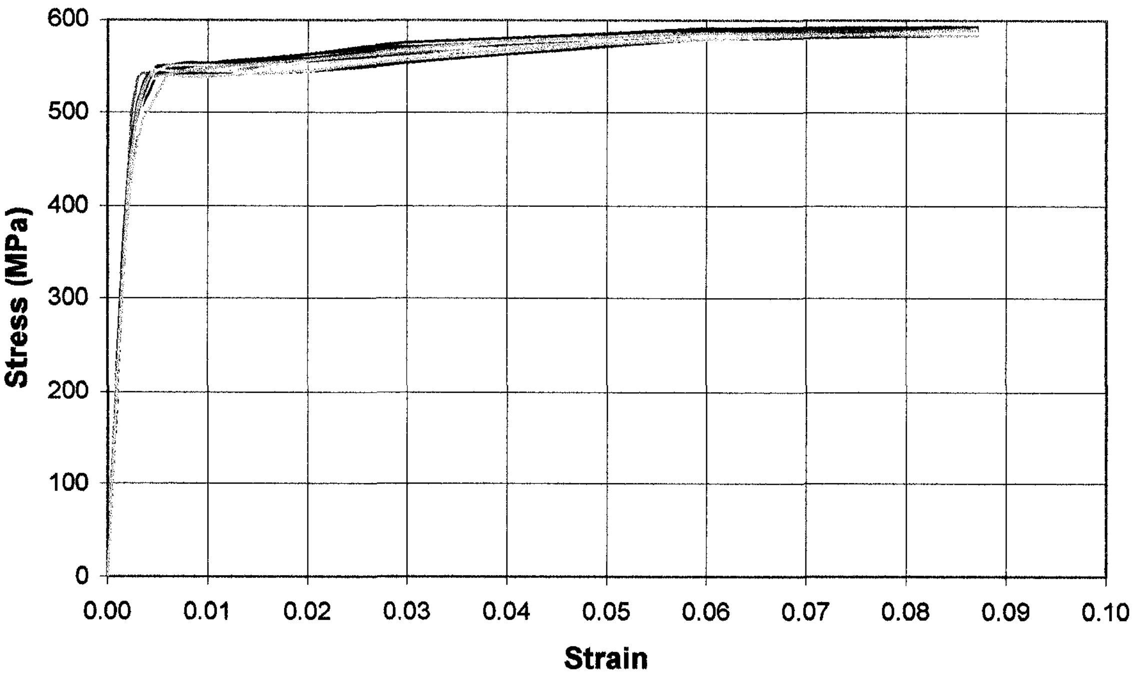

Fig. B1 Stress vs. Strain Relationships as obtained from 14 Tension Coupon Tests

Stress vs. strain relationships presented in Fig. B1 shows little variability in stress vs. strain properties of tension coupons taken around the circumference of the specimens. As was mentioned in Section 5.1.6, material properties of the specimens used in Test Series 1 were represented by selecting a stress strain data within the boundaries of the curves presented in Fig. B1 (Table 5.2). The Engineering Stress vs. Engineering Strain and True Stress vs. Logarithmic Strain curves generated by the data presented in Table 5.2 are provided in Fig. B2. It is noted that after the peak stress is attained, the strain field within the specimen is no longer uniform. Thus, the post-peak branch of the stress-strain relationship becomes dependent on the gauge length chosen, and thus looses its significance as a measure of the material behavior

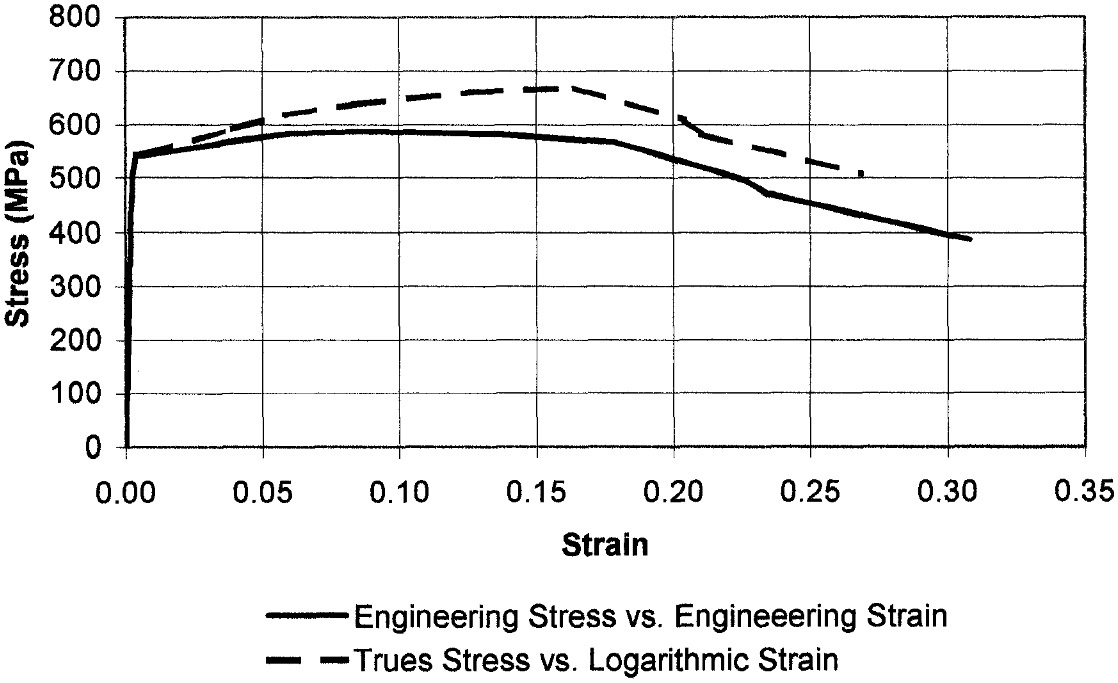

Fig. B2 Stress vs. Strain Relationship used in the Finite Element Model

Appendix C-Local vs. Global Curvatures

Figure C1 illustrates the local curvature vs. global curvature relations for the specimens tested in Chapter 5 for different pressure levels. The points where the slope of the curves changes (Initiation of buckling) are also shown. As can be seen in figures, curvature values corresponding to the initiation of buckling for the specimens tested under higher axial tensile force are higher than the specimens tested under lower levels of axial tension.

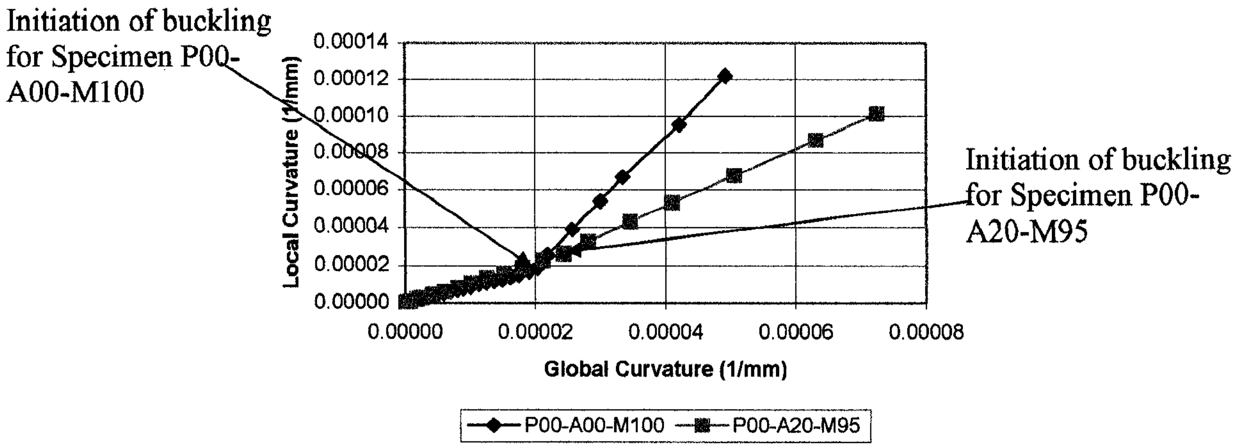

(a) p_r=0.0

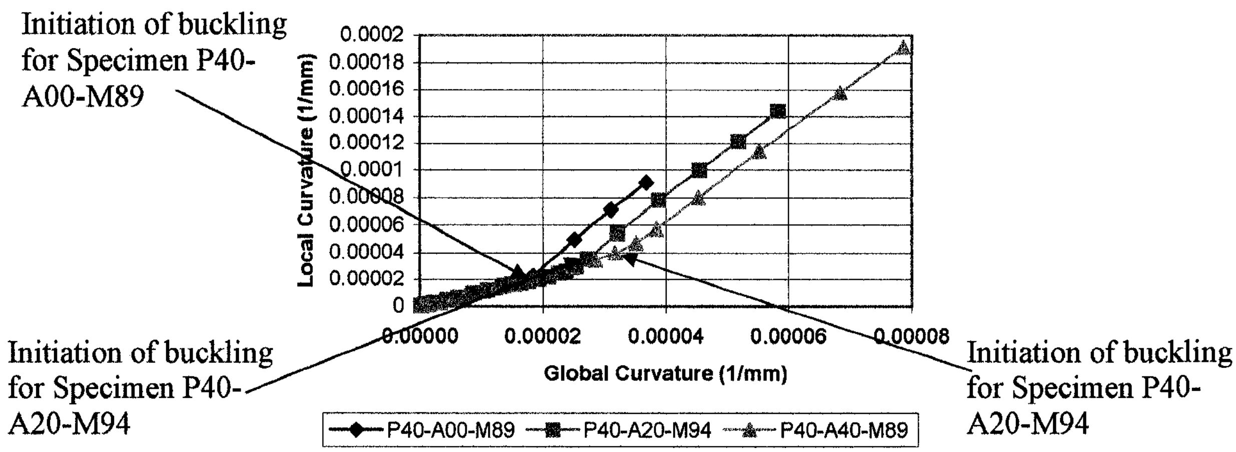

(b) p_r=0.4

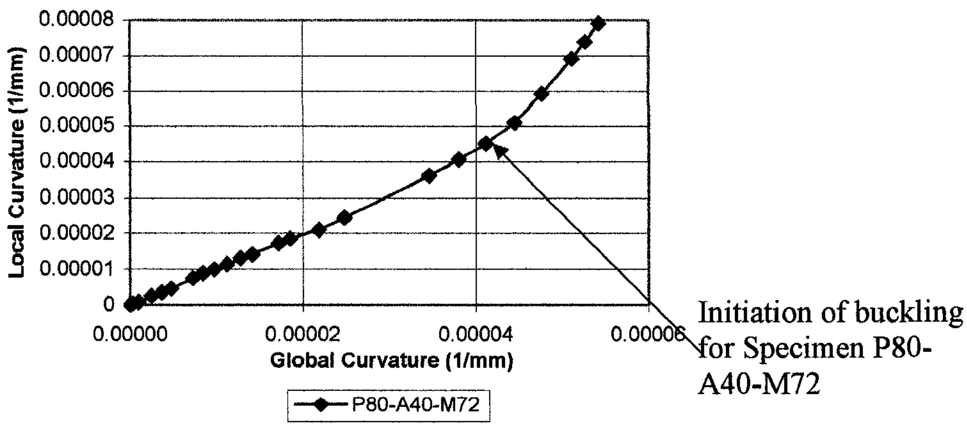

(c) p_r=0.8

Fig. C1 Local vs. Global Curvatures

Appendix D - Elastic Interaction Relations

D1 Statement of the Problem

Interaction relations for pipe sections based on the elastic resistance of the pipes subject to combined action of bending, torsion, axial force, and internal pressure are sought. Consider a pipe section with a mean diameter $D=2r$, thickness t, and yield strength F_y. (Fig. D1) subjected to axial force A, twisting moment T, internal pressure p, and bending moment M which initiates yielding either at the extreme fiber 1 or fibre 2.

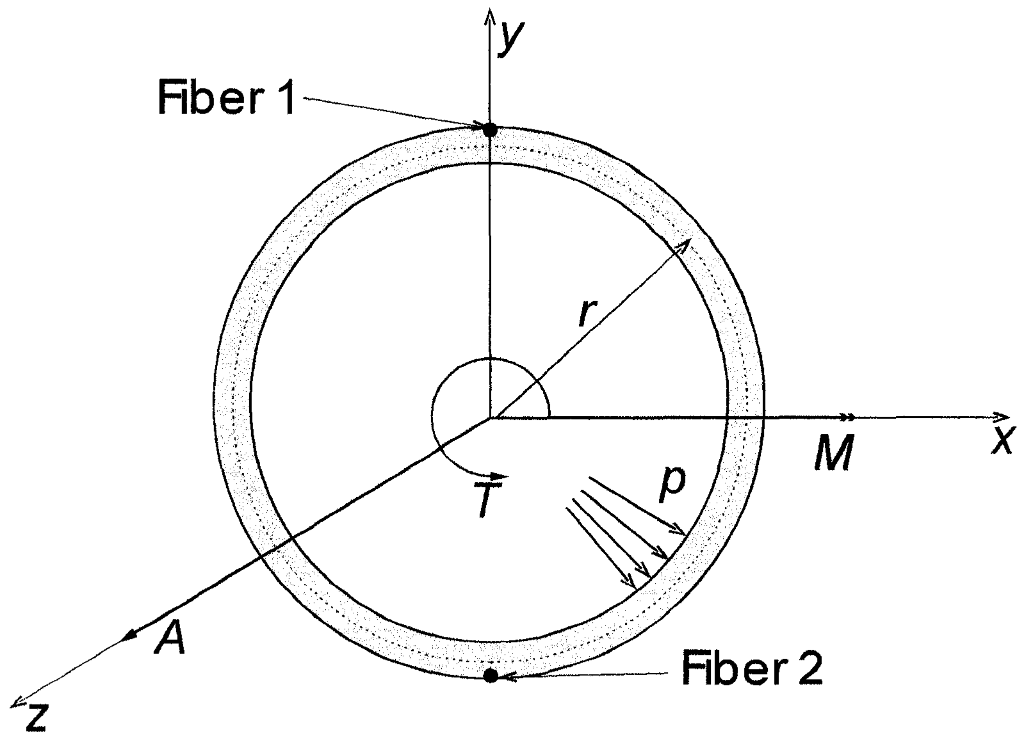

Fig. D.1 Internal Forces acting on Pipe Cross-section

It is required to develop two piecewise interaction relations of the form $f_i(A_r, M/M_e, T_r, p_r) \le 0$ for fibers i=1,2) in which $A_r = A/A_p$ ($A_p = F_y A_{pipe}$ in which $A_{pipe} = 2\pi rt$ is the area of the pipe cross-section), $M_e = F_y I/(r+0.5t) = SF_y$ is the elastic moment resistance calculated in the absence of other forces (I is the moment of inertia and S is the section elastic modulus of the pipe cross-section),

$T_r = T/T_p$, is the ratio of the applied torsion to the elastic torsional resistance and $p_r = p/p_y$ is the ratio of the applied internal pressure to the internal pressure corresponding to the yield hoop stress. The condition $f_1 \leq 0$ signifies that fibre 1 does not exceed yield and the condition $f_2 \leq 0$ signifies that fibre 2 does not exceed yield and the condition. For an admissible internal force state, both conditions ($f_1 \leq 0$, $f_2 \leq 0$) have to be satisfied. A limiting internal force state is attained either when ($f_1 = 0$, $f_2 \leq 0$) or when ($f_1 \leq 0$, $f_2 = 0$)

D2 Assumptions

- It is assumed that pipe cross-section can fully develop its modified elastic capacity prior the occurrence of local buckling on the compression side of the section (i.e., section meets Class 3 requirements according to CAN/CSA S16-01).
- The longitudinal stresses of the pipe are calculated from the Euler-Bernouilli beam theory.
- The shearing stress of the pipe are obtained from the St. Venant torsion theory for closed sections
- Pipe steel is assumed to yield in accordance with maximum distortional energy yield criterion (Boresi and Sidebottom 1985). For an element of pipe wall of thickness t of length dl along the pipe length and of length $rd\theta$ along the circumference (Fig. D2), the relevant non-zero stress components are normal stress σ_z due to axial force (A) and bending moment (M), the tangential shearing stress τ due to torsion (T), and the hoop stress σ_h due to internal pressure (p).

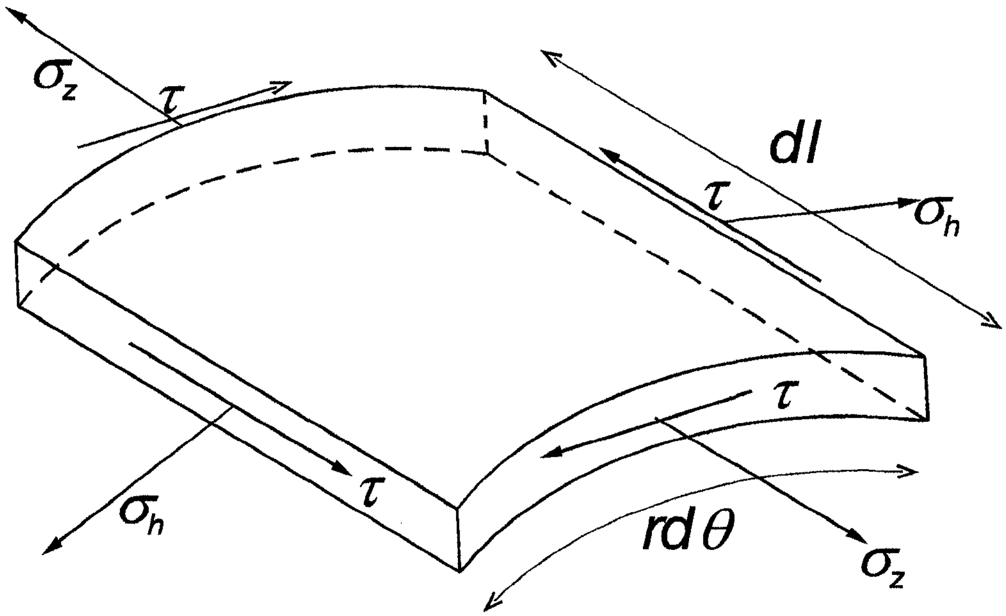

Fig. D2 Stress Components acting on Pipe Element

D3 Yield Criterion

For the above stress combination, an admissible state of stress based on the maximum distortional energy density yield criterion can be expressed as.

$$\sigma_h^2 - \sigma_h\sigma_l + \sigma_l^2 + 3\tau^2 \le F_y^2 \tag{D1}$$

By dividing both sides by the yield stress F_y, one obtains,

$$\left(\frac{\sigma_h}{F_y}\right)^2 - \left(\frac{\sigma_h}{F_y}\right)\left(\frac{\sigma_l}{F_y}\right) + \left(\frac{\sigma_l}{F_y}\right)^2 + \left(\frac{\tau}{F_y/\sqrt{3}}\right)^2 \le 1 \tag{D2}$$

D4 Relating Hoop Stress to Internal Pressure

With reference to Fig. D3a, the hoop stress is related to the applied internal pressure through

$$\sigma_h = \frac{p}{t}\left(r - 0.5t\right) \tag{D3}$$

The pressure p_y that causes the hoop stresses to attain the yield strength F_y of the pipe material in the absence of other internal forces is

$$F_y = \frac{p_y}{t}(r - 0.5t) \tag{D4}$$

By dividing Eq. D3 by Eq. D4, one obtains

$$\frac{\sigma_h}{F_y} = \frac{p}{p_y} = p_r \tag{D5}$$

D5 Relating Twisting Moment to shear Stress

With reference to Fig. D3b, the St. Venant torsion theory relates the twisting moment T to the shear stress τ

$$T = 2\pi r^2 t\tau \tag{D6}$$

The twisting moment T_p, which causes the pipe material to attain yielding in the absence of other internal forces, is

$$T_p = 2\pi r^2 t\left(\frac{F_y}{\sqrt{3}}\right) \tag{D7}$$

By dividing Eq. D6 by Eq. D7, one obtains

$$\frac{T}{T_p} = \frac{\tau}{\left(F_y/\sqrt{3}\right)} = T_r \tag{D8}$$

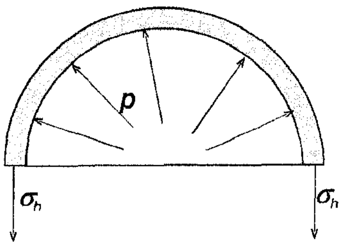

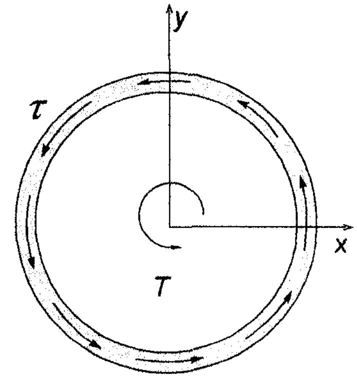

(a) Hoop Stress **(b)** Shear Stress Distribution

Fig. D3 Shear and Hoop Stresses

D6 Relating Bending Moments and Axial Force to Normal Stress

According to the Euler-Benoulli beam theory, a pipe section subject to normal force A and bending moment M (positive directions are shown in Fig. D1), the longitudinal stresses σ_1, σ_2 at fibers 1 and 2 respectively, are

$$\sigma_1 = \frac{A}{A_{pipe}} + \frac{M}{S} \tag{D9}$$

$$\sigma_2 = \frac{A}{A_{pipe}} - \frac{M}{S} \tag{D10}$$

in which A_{pipe} is the cross-section of the pipe, $S = I/(r + 0.5t)$ is the elastic modulus of pipe cross-section, and I is the moment of inertia. Stresses σ_1, σ_2 are positive when tensile. By dividing both sides of Eqs. D9 and D10 by F_y, one obtains

$$\frac{\sigma_1}{F_y} = \frac{A}{A_y} + \frac{M}{M_e} = A_r + \frac{M}{M_e} \tag{D11}$$

$$\frac{\sigma_2}{F_y} = \frac{A}{A_y} - \frac{M}{M_e} = A_r - \frac{M}{M_e} \tag{D12}$$

In Eqs. D11 and D12, A_y is the yield tensile resistance and M_e is the elastic moment resistance

D7 Expressing Yield Criterion in terms of Internal Forces

From Eqs. D5, D8, D11, by substituting into Eq. D2 and setting $\sigma_l = \sigma_1$, one recovers the interaction relation based on the yield of fiber 1.

$$f_1(A_r, M/M_e, T_r, p_r) = p_r^2 - p_r\left(A_r + \frac{M}{M_e}\right) + \left[A_r + \left(\frac{M}{M_e}\right)\right]^2 + T_r^2 \leq 1 \tag{D13}$$

Similar substitution of Eqs. D5, D8, D12 into Eq. D2 while setting $\sigma_l = \sigma_2$, yields

$$f_2(A_r, M/M_e, T_r, p_r) = p_r^2 - p_r\left(A_r - \frac{M}{M_e}\right) + \left[A_r - \left(\frac{M}{M_e}\right)\right]^2 + T_r^2 \leq 1 \tag{D14}$$

which is the interaction relation based on the yield of fibre 2.

The equation $f_1(A_r, M/M_e, T_r, p_r) = 1$ is quadratic in M. The two roots $M_{em,1,1}$ and $M_{em,1,2}$ of Eq. D13 have opposite signs. Only one of the two roots, say $M_{em,1,1}$, will meet the interaction condition at fibre 2.

$$p_r^2 - p_r\left(A_r - \frac{M_{em,1,1}}{M_e}\right) + \left[A_r - \left(\frac{M_{em,1,1}}{M_e}\right)\right]^2 + T_r^2 \leq 1 \tag{D15}$$

while the other root $M_{em,1,2}$ will violate the interaction relation, i..e.,

$$p_r^2 - p_r\left(A_r - \frac{M_{em,1,2}}{M_e}\right) + \left[A_r - \left(\frac{M_{em,1,2}}{M_e}\right)\right]^2 + T_r^2 > 1 \tag{D16}$$

Thus, the root $M_{em,1,2}$ has to be discarded for an admissible internal force state, and the modified elastic moment solution sought is $M_{em} = M_{em,1,1}$. It is observed that if $M_{em,1,1}$ is a root of Eq. D13, $M_{em,2,1} = -M_{em,1,1}$ is always a root of the interaction relation $f_2\left(A_r, M/M_e, T_r, p_r\right) = 1$.

D8 Summary

In summary, the two possible solutions for the modified elastic moment are $M_{em} = \pm M_{em,1,1}$ where $M_{em1,1}$ is obtained by satisfying the conditions

$$p_r^2 - p_r\left(A_r + \frac{M_{em,1,1}}{M_e}\right) + \left[A_r + \left(\frac{M_{em,1,1}}{M_e}\right)\right]^2 + T_r^2 = 1 \tag{D17}$$

And

$$p_r^2 - p_r\left(A_r - \frac{M_{em,1,1}}{M_e}\right) + \left[A_r - \left(\frac{M_{em,1,1}}{M_e}\right)\right]^2 + T_r^2 \le 1 \tag{D18}$$